Preparation, Characterization and Applications of Ionic Liquids with Perfluorinated Alkyl Groups

Dissertation
zur Erlangung des Grades
des Doktors der Naturwissenschaften
der Naturwissenschaftlich-Technischen Fakultät
der Universität des Saarlandes

von
Daniel Rauber

Saarbrücken
2019

Tag des Kolloquiums:	01.07.2019
Dekan:	Prof. Dr. Guido Kickelbick
Berichterstatter:	Prof. Dr. Rolf Hempelmann Prof. Dr. David Scheschkewitz Prof. Dr. Ralf Ludwig
Vorsitz:	Prof. Dr. Michael Springborg
Akad. Mitarbeiter:	Dr. Dan Durneata

'There is probably no other topic in pure and applied chemistry that is now dealt within so many different contexts.'

- Hermann Weingärtner on ionic liquids[1]

Acknowledgements

At first, I would like to give my honest gratitude to my supervisor ('Doktorvater') *Prof. Dr. Dr. h. c. Rolf Hempelmann* for giving me the opportunity to perform my research on an interdisciplinary, very interesting and current subject. I highly value his interest in the progress of the work, his appreciation and the continuous support through all the time. He was always a motivating, pleasant guide who left me the freedom to develop own ideas and create networks with many researchers form other adjacent fields.

I would also like to thank my scientific advisor ('wissenschaftlicher Begleiter') *Prof. Dr. Michael Springborg* for his interest and the pleasant scientific discussions during the time of my PhD studies.

Further thanks go to *PD Dr. Harald Natter* and *Prof. Dr. Christopher Kay* for the opportunity to continue my work in their group and all the helpful, intelligent and inspiring talks that I had with them.

Other thanks go to my appreciated and experienced collaborates from whom I was really able to learn a lot and earned a deeper understanding for associated fields of science. Without their ongoing assistance, help and complementary knowledge, this work would not have been possible in this way. First of all, I want to mention *Dr. Florian Heib* and *Dr. Michael Schmitt*, two very talented, capable physicochemists who developed the 'High precision Drop Shape Analysis' used in parts of this work and were open minded towards various collaborations. Moreover, I want to express my thanks to *Prof. Dr. Tobias Kraus* and *Dr. Peng Zhang* from the INM Leibniz Institute for New Materials for their interest in the interconnection of our researches and the time they spent therefore. Further thanks are addressed to *Dr. Josef Zapp* from the Department of Pharmaceutical Biology who always had an open ear towards the different problems regarding non-routine NMR measurements and spent a lot of time for the help with calibration of the devices and setting up the experiments. Gratitude is also owed to *Prof. Dr. Dietrich Volmer*, *Dr. Klaus Hollemeyer* and *Dr. Tobias Dier* from the Department of Bioanalytical Chemistry for the possibility to work at a highly interesting topic besides my main work that contained both practical applications and advanced analytical techniques. I would furthermore like to thank *Dr. Jan Embs*, *Dr. Tatsiana Burankova, Juan Cardozo* and *Dr. Antonio Benedetto* from the Paul Scherer Institute in Switzerland for the nice, uncomplicated contacts and for considering me as their collaborator of choice. Last but not least, I want to thank *Frederik Philippi*, a young, highly talented and competent chemist for his continuous support and the very inspiring talks we had and the much appreciated friendship that grew through the time.

I would also like to acknowledge all the past and current colleagues from the research groups and the Department of Physical Chemistry for the very pleasant and supporting working environment. This includes *Silvia Kuhn*, *Dr. Dan Durneata*, *Angelo Stephan*, *Nils Schumacher*, *Dina Klippert*, *Jan Geiser*, *Konstantin Weißhaar*, *Galina Skorikova Dr. Ruiyong Chen*, *Dr. Stefan Keck, Stefan Ruloff* and *Anna Quinten*. I really enjoyed the talks and exchange with you all a lot.

Further thanks go to my colleagues from the chemistry didactics field that helped me a lot in the understanding of the science of teaching that was indispensable for my work in developing new, exiting ionic liquid based experiments that could be carried out with the equipment and in the time frame of schools. Especially appreciated are *Dr. Johannes Huwer*, *Johann Seibert*, *Matthias Marquardt*, *Dr. Sabine Fey*, *Heike Luxenburger-Becker* and *Dr. Angela Munnia-Scholl* for the interesting talks and the view beyond the horizon of specialized science.

Additional thanks go to *Rainer Wintringer*, the best analytical technician you could have, for his ongoing assistance and fast response on an uncountable amount of different tasks. Your passing away is a great loss for all of us.

Furthermore I want to thank *Thomas Scherer* for his fast and straightforward help regarding problems with the NMR spectrometer. Thanks for the help regarding all technical, engineering and construction problems are addressed to our engineer *Rudolf Richter* and our precision mechanics *Norbert Ochs* and *Jens Wiegert.* Additional thanks are also addressed to our system administrator *Nicolas 'Supernico' Louis* for the fast and non-complicated help with hard- and software problems, the access to the cluster and all the other support we experienced from him throughout the years.

And last but not least I want to express my very deep gratitude to my wife *Natascha* for her love, continuous support, motivating words and appreciation throughout all the past and coming years.

Table of contents

I. Kurzzusammenfassung

Ionische Flüssigkeiten (ILs) sind eine vielseitig abstimmbare neue Materialklasse, die eine einzigartige Eigenschaftskombination für ein großes Spektrum an Anwendungen bietet. Die immense Anzahl an möglichen ILs für die Einbindung in fortgeschrittene Technologien erfordert ein detailliertes Wissen über deren Synthese, physikochemische Eigenschaften und mikroskopische Wechselwirkungen, die das makroskopische Verhalten bestimmen. Die Einführung fluorierter Alkylgruppen kann die Eigenschaften von ILs auf verschiedene, vorteilhafte Weisen ändern.

Die Ziele dieser Arbeit waren die systematische Untersuchung der Synthese von neuen ILs mit perfluorierten Gruppen, die daraus resultierenden makro- und mikroskopischen Eigenschaften (Transportgrößen, Benetzungsverhalten und Flüssigstruktur) sowie möglichen Anwendungen, die von der Verwendung dieser fluorierten ILs (FILs) profitieren.

Die Einführung langer Perfluorokohlenstoff-Ketten in Kation oder Anion von ILs führte zu höheren Schmelzpunkten und Viskositäten sowie einer veränderten Nanostruktur durch die ausgeprägtere Bulk-Strukturierung. Darüber hinaus zeigten die FILs ein deutlich verändertes Benetzungsverhalten auf verschiedenen Oberflächen und es wurde demonstriert, dass ein hochfluorierter Vertreter zur Immobilisierung eines Palladium-Katalysators in einer thermoregulierten fluorigen Zweiphasenkatalyse genutzt werden kann. Im Gegensatz dazu zeigten Anionen mit Trifluormethylgruppen verbesserte Transporteigenschaften durch stärkere Ladungsdelokalisation.

II. Abstract

Ionic liquids (ILs) constitute a highly tunable class of novel materials that offers a unique property combination for a large variety of high-performance applications. As there are a vast number of possible ILs accessible for the implementation in advanced technologies, the knowledge about their synthesis, physicochemical properties and microscopic interactions that determine the macroscopic behavior is of vital interest. The introduction of fluorinated alkyl groups in ILs significantly alters their properties depending on the chain length in different beneficial ways.

The aim of this thesis was the systematic investigation of the synthesis of novel ILs with perfluorinated alkyl groups, the resulting macro- and microscopic properties (transport characteristics, wetting behavior and bulk structuring) as well as possible applications that could benefit from these fluorinated ILs (FILs).

The introduction of elongated perfluorocarbon segments in the ILs' cation or anion resulted in increased melting points and viscosities as well as an altered nanostructure through pronounced structuring in the bulk liquid. Furthermore, the FILs showed a significantly altered wetting behavior on different surfaces and it was demonstrated that a highly fluorinated representative could be used in thermoregulated fluorous biphasic catalysis for the retention of a palladium catalyst. In contrast to this, anions containing trifluoromethyl groups showed improved transport properties due to increased charge delocalization.

III. Motivation and aim of the thesis

The fascinating material class of ionic liquids was already discovered more than one hundred years ago. However, they had fallen into oblivion and remained a curiosity until the mid of the 1990s with the discovery of low viscous, air and water stable ILs. As low temperature molten salts they show an interesting property spectrum that combines the characteristics of molecular solvents and conventional fused salts. This unique property combination and customizability offer a vast number of new possibilities for chemists, material scientists, physicists and other scientists for many advanced applications. Indeed, ILs have been implemented in many technical applications for instance as special solvents, electrolytes, working fluids, additives or reactive phases. Very promising IL-applications are in fields where their special characteristic profile can be fully exploited to increase efficiency, performance or safety for instance of reactions, processes, materials as well as technical devices. As there are a very large number of possible IL-constituting cation-anion-combinations a detailed understanding of their structure-property combination is essential for designing and tuning IL properties towards desired applications.

This thesis aims at a better understanding of ILs that incorporate perfluorinated alkyl groups in either the cation or the anion. The highly nonpolar molecular fragments are known to change the ILs' physicochemical characteristics, such as thermal transitions, solvent and transport properties, as well as their structuration in the bulk and at surfaces depending on their attaching positions and lengths. Furthermore, the ILs of highest electrochemical stability and performance for electrochemical devices usually include fluorine-containing anions. Although it is known that attaching perfluorocarbon moieties to ILs can alter their properties in beneficial ways for many special applications, such as gas-separation, solvent behavior or composite materials, only a very limited number of fluorinated ILs have been investigated so far. In addition, a systematic investigation of their properties is often lacking.

To achieve this aim, synthesis protocols for many novel ILs were developed and their most important physicochemical properties were determined. In many cases their characteristics were compared to the non-fluorinated hydrocarbon analogues for direct demonstration of the influence resulting from fluorination. Besides the general characteristics of the novel ILs, some special features of the fluorinated ILs, such as wetting behavior, bulk structuration and ionicity, should be analyzed. Also, a practical application of a highly fluorinated IL as substitute for volatile organic compounds should be demonstrated.

VI. Abbreviations

[A]	Anion
[BETI]	Bis(pentafluoroethanesulfonyl)imide anion
$[B((CF_2)_xF)(CN)_3]$	Perfluoroalkyltricyanoborate anion
$[B((CF_2)_xF)(CN)_yF_z]$	Perfluoroalkylcyanofluoroborate anion ($x \geq 1$; $y+z = 3$)
$[B((CF_2)_xF)F_3]$	Perfluorotrifluoroborate anion ($x \geq 1$)
$[B(CN)_4]$	Tetracyanoborate anion
$[BF_4]$	Tetrafluoroborate anion
$[C(CN)_3]$	Tricyanomethanide anion
[Cl]	Chloride anion
$[ClO_4]$	Perchlorate anion
$[CO_2(CH_2)_xH]$	Carboxylate anion ($x \geq 0$)
$[CO_2CF_3]$	Trifluoroacetate anion
$[CO_2(CF_2)_xF]$	Perfluoroalkylcarboxylate anion ($x \geq 1$)
$[C_xC_yIM]$	1-alkyl-3-alkyl-imidazolium cation (x,y: number of carbon atoms in alkyl side chain)
$[C(Tf)_3]$	Tris(trifluoromethanesulfonyl)methanide anion
[FAP]	Tris(pentafluoroethyl)trifluorophosphate anion
$[N(CN)_2]$	Dicyanamide anion
$[NO_3]$	Nitrate anion
$[N(PO((CF_2)_2F)_2)_2]$	Bis[bis(pentafluoroethyl)phosphinyl]imide anion
$[N(SO_2CF_3)(CN)])$	Trifluoromethanesulfonyl-N-cyanoamide anion
$[N(SO_2CF_3)(COCF_3)]$	Trifluoro-N-(trifluoromethanesulfonyl)acetamide anion
$[N(SO_2CF_3)_2]$	Bis(trifluoromethanesulfonyl)imide anion
$[N(SO_2(CF_2)_2F)]$	Bis(pentafluoroethanesulfonyl)imide anion
$[N(SO_2(CF_2)_xF)_2]$	Bis(perfluoroalkylsulfonyl)imide anion
$[OC(CF_3)_3]$	Perfluoro-*tert*-butoxide anion
[OMs]	Methanesulfonate anion
[OTf]	Trifluoromethanesulfonate anion
$[P(CF_2)_2F)_3F_3]$	Tris(pentafluoroethyl)trifluorophosphate anion
$[PF_6]$	Hexafluorophosphate anion
$[PO_2(O(CH_2)_xH)(CH_2)_yH]$	Alkylphosphonate anion ($x \geq 1$, $y \geq 0$)
$[PO_2(O(CH_2)_xH)_2]$	Dialkylphosphate anion ($x \geq 1$)
$[PO_2(CF_3)_2]$	Bis(trifluoromethyl)phosphinate
[SCN]	Thiocyanate anion
$[SO_3(CH_2)_xH]$	Alkylsulfonate anion ($x \geq 1$)
$[SO_3CF_3]$	Trifluoromethanesulfonate anion
$[SO_3(CF_2)_4F]$	Nonafluorobutanesulfonate anion

$[SO_4(CH_2)_xH]$	Alkylsulfate anion ($x \geq 1$)
[TFA]	Trifluoroacetate

AIL	Aprotic ionic liquid
API	Active pharmaceutical ingredient
BASIL	Biphasic acid scavenging utilizing ionic liquids
DSSC	Dye-sensitized solar cell
DMF	Dimethylformamide
EDLC	Electrochemical double-layer capacitors
ESI-MS	Electrospray ionization - mass spectrometry
EWG	Electron withdrawing group
FIL	Fluorinated ionic liquid
GC	Gas chromatography
GPIM	Green propellant infusion mission
HPDSA	High-precision drop shape analysis
HPLC	High-performance liquid chromatography
IL	Ionic liquid
ILC	Ionic liquid crystal
LC	Liquid crystal
MALDI-MS	Matrix-assisted laser desorption/ ionization - mass spectrometry
MD	Molecular dynamics
MILs	Metal-containing ionic liquids
NP	Nanoparticle
NTf_2	Bis(trifluoromethanesulfonyl)imide
OTf	Triflate
PEMFC	Proton exchange membrane fuel cell
pK_a	Negative logarithmic acid dissociation constant
PIL	Protic ionic liquid
RTIL	Room temperature ionic liquid
SAXS	Small-angle X-ray scattering
SILP	Supported ionic liquid phase
TGA	Thermogravimetric analysis
Tf	Triflyl/ trifluoromethanesulfonyl
VOC	Volatile organic compound

1. Introduction

1.1 General aspects of ionic liquids – advanced liquid materials

Ionic liquids (ILs) are a comparably modern class of tunable liquid materials with a unique combination of characteristics. Their peerless features make them highly attractive for a very wide range of applications throughout the fields of science and technology. This substance class consists of organic salts with very low melting points that are, per arbitrary and widely accepted definition, below 100°C. This criterion was introduced to distinguish them from classical molten salts that typically have highly diverging properties, such as high melting points, low viscosities (in their liquid state) and corrosive behavior. Due to practical reasons the subclass of room temperature ionic liquids (RTILs), which is composed of ionic melts that are in the liquid state at ambient temperature, is of highest interest. ILs conflate the properties of organic liquids and molten salts which itself makes this class intrinsically attractive even for physicists as dense ionic fluids that are low temperature analogues of plasma.[2] As there is a virtually unlimited number of synthetically available ILs, one outstanding characteristic is their task specific adjustability towards desired applications. Many limitations set by common organic and inorganic solvents can thus be overcome. While the conventionally used solvents are restricted in their number to only a few hundred representatives, the amount of possible IL-forming anions and cations is estimated to be several orders of magnitude larger.[3] Due to this remarkable adaptability, they are frequently referred to as 'designer solvents'[4,5] or 'task-specific liquids'.[6] As ILs are composed solely of ions, the coulombic forces are the dominating intermolecular interactions.[7] This is in contrast to conventional molecular liquids, where the van der Waals interactions are decisive as intermolecular force. As a direct result of the stronger molecular interactions, ILs show distinctly altered properties compared to molecular compounds that are an exceptional characteristic feature of the low temperature molten salts. ILs have, for example, extremely high enthalpies of vaporization (ΔH_v) resulting in a negligible vapor pressure, insignificant volatility and non-flammability.[8,9] This prevents operators and the environment from exposition through the gas phase and ensures an increased safety in processing compared to conventional volatile and inflammable organic solvents. Because of their ionic constitution ILs exhibit an intrinsic conductivity which is determined by their viscosity (see the Walden relation discussed in section 1.7), making them promising electrolytes for electrochemical devices. Furthermore, they possess in most cases a wide liquid range as well as high thermal, chemical and electrochemical stability. These beneficial characteristics make them candidates with high potential for a broad range of technologies (see section 1.4 for more details). *Table 1* summarizes the general properties of ionic liquids in comparison to molecular organic solvents.

Table 1: Generalized comparison of conventional organic solvents and ionic liquids.[3]

Property	Organic solvents	Ionic liquids
Number of representatives	≈ 10^3	> 10^8
Adjustability	Limited range of solvents available	Functionalizable in a very wide range
Vapor pressure	Obeys Clausius-Clapeyron equation	Negligible under ambient conditions
Flammability	Often flammable	Non-flammable
Viscosity at 25°C	Low to moderate (≈ 0.2-200 mPa s)	Moderate to very high (≈ 15-10^4 mPa s)
Density	0.6-1.6 g cm^{-3}	0.8-3.3 g cm^{-3}
Functionality	Usually monofunctional	Often multifunctional
Catalytic activity	Rare	Common and tunable
Structuration in bulk and at surfaces	Usually poorly pronounced	Often highly structured on different length scales
Magnetic properties	Nonmagnetic	Intrinsic paramagnetism in metal-containing ionic liquids
Chirality	Very rare	Large variety of chiral ILs
Market price	Usually cheap	2-100 times the cost of molecular solvents
Recyclability	Sustainable impetus	Economic impetus

As already mentioned, the most particular feature of ILs are the highly customizable qualities through the choice of anion and cation or the attachment of functional groups that can be varied in nearly infinite ways. Thus, ILs can incorporate a large variety of different properties as single component that are either uncommon or impossible in the case of conventional molecular liquids. These features can include for instance luminescent,[10–13] magnetic[14–19] or chiral[20–23] properties to name only a few that are exotic or completely unknown for conventional molecular liquids.

The incredibly large number of possible ILs demands sophisticated knowledge about the underlying structure-property relationships to evaluate which purpose can be complied best with which ionic fluid. ILs were found to show distinct structuring on different length and time scales as there are more different competing molecular interactions present than in usual molecular liquids.[24] In the latter, usually dipolar as well as higher order multipolar electrostatic interactions (van der Waals interaction composed of Keesom, Debye and London forces) and sometimes hydrogen bonds are dominating. For the IL class the intermolecular forces range from the weak, isotropic and non-specific

van der Waals to the strong Coulombic interactions and often include specific, anisotropic forces, such as hydrogen bonding and dipole-dipole interactions.[25] Although there are more intermolecular interactions present in ILs than in molecular solvents, the Coulomb interaction plays the most dominant role.[26] The interactions and resulting structuration present in this special type of liquid salts will be discussed more detailed in section 1.5. Due to the inherent charge, ionic liquids are usually regarded as polar yet noncoordinating solvents[27] with polarity values[28] ranging from slightly less polar than water, for example found for ethylammonium nitrate $[EtNH_3][NO_3]$,[29] to highly nonpolar representatives that are even completely miscible with mineral oils (*e.g.* phosphonium ILs with long alkyl chains).[30–32] The extraordinarily low melting points of ILs are the result of their molecular structure which is designed to destabilize the crystalline state, leading to a thermodynamically favored liquid state at comparably low temperatures.[33] The structural formulae of commonly used cations and anions are sketched in *Figure 1.*

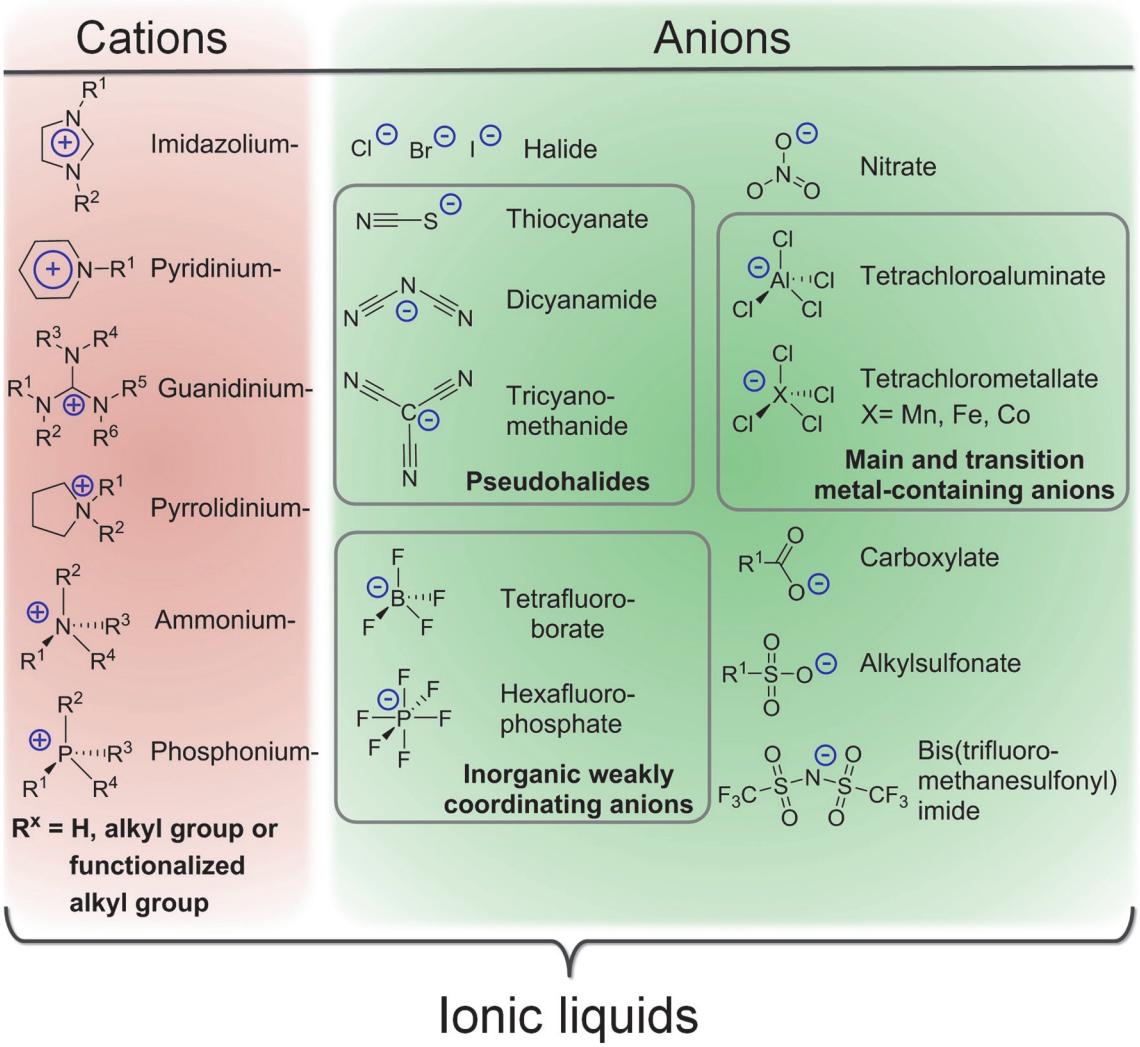

Figure 1: Molecular structures of typical cations and anions used for ionic liquids.

There are three main strategies to achieve low lattice enthalpies and large entropy changes upon melting for bulk ILs in order to obtain the usually desired RTILs, nominal

asymmetry, *charge delocalization* and *flexibility*.[34,35] In most cases the different types of this 'anti-crystal engineering approach'[36] are combined to obtain the most pronounced effects.

The first concept uses *asymmetric substitution patterns* to lower the symmetry and is mainly implemented in the organic cations. The reduction of ion symmetry lowers the energy of the crystal lattice energy by inhibiting more efficient ion packing as it is possible for ions with symmetric substitutions.[37] This leads to much lower melting temperatures for ILs with asymmetric substitution patterns compared to the symmetric ones. Lowering the symmetry of the alkyl tags can also be realized by long unsaturated or branched hydrocarbon fragments.[38]

A further strategy for melting point depression is *charge delocalization* in either cation, anion or both resulting in more dispersed charges over larger volumes along with reduced electrostatic interactions. For cations, a low charge density can be achieved using nitrogen-containing delocalized π-electron systems, such as the aromatic imidazolium and pyridinium or the cross-conjugated guanidinium cation. The charge delocalized aromatic cations were also found to possess lower relative interaction strength values than the saturated cyclic counterparts.[39] Efficient charge delocalization to reduce the ion-ion interactions can also be achieved by anions with a large number of contributing resonance structures. This is for instance realized in nitrate, alkyl sulfonate, alkyl sulfate anions as well as in the bis(trifluoromethanesulfonyl)imide ([NTf_2]) and similar imides. Strong electron withdrawing groups (EWGs) to reduce the charge localization in the anions are also widely used. EWGs such as fluorine atoms in the tetrafluoroborate [BF_4] or hexafluorophosphate [PF_6], cyano-groups[40] in the dicyanamide [$N(CN)_2$] or tricyanomethanide [$C(CN)_3$], chlorine atoms in metal-containing anions as well as fluorinated alkyl groups for instance realized in the [NTf_2] or the trifluoromethanesulfonate ([OTf])[41] are some widespread examples.

The third strategy utilizes conformational *flexibility* via the incorporation of elongated, bulky alkyl groups and is mainly used in organic cations. Long hydrocarbon chains have a high degree of conformational flexibility and thus increase the entropy of the liquid state.[42] Furthermore, these flexible alkyl chains reduce the contribution of the Coulombic interaction to the crystal lattice energy by increasing the dominance of the ions' covalent part.[43] Additionally, the flexibility can be increased by ether functionalities in the side chains that have an even higher degree of rotational freedom, thus further reducing the lattice energy along with the melting temperatures.[44–47]

Due to the frustrated lattice packing, only glass transition temperatures T_g are observed for many ILs.[48,49] The thermal behavior of these good glass-formers is characterized by absence of first order phase transitions, such as crystallization and melting, resulting in the formation of amorphous glasses upon cooling.[50] Similar thermal behaviors are also often observed in eutectic mixtures of ILs[51] or ILs with inorganic salts.[52] Another related result of the low lattice energy is the phenomenon of pronounced supercooling that is often observed for ionic liquids in the absence of seed crystals.[53–55] The influence of the

attached alkyl chain on the liquefaction temperatures for the widely used 1-alkyl-3-methyl-imidazolium ILs [C_xC_1IM][A] is shown in *Figure 2*.

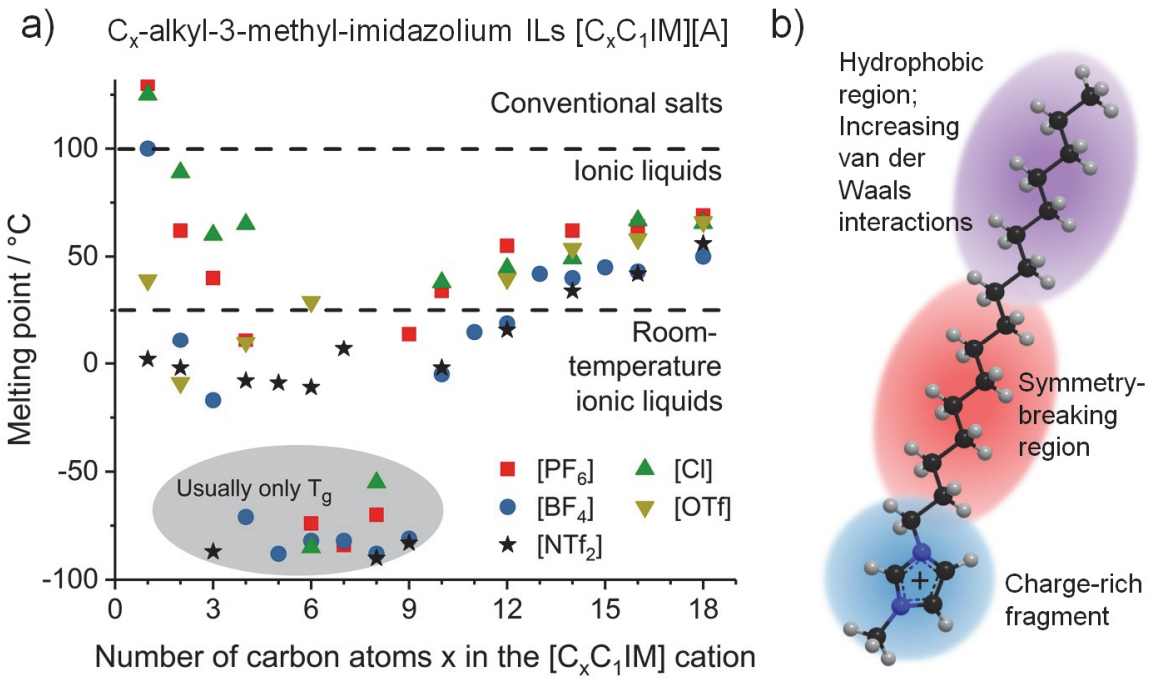

Figure 2: a) Melting point (T_m) progression in dependence of the attached side chain length in 1-alkyl-3-methyl-imidazolium [C_xC_1IM][A] ILs with different commonly used anions [A] from literature values.[37,56–61] The dashed lines show the boundaries between the conventional molten salts (T_m > 100°C), ionic liquids (T_m ≤ 100°C) and room temperature ionic liquids (T_m ≤ 25°C). For some examples, solely glass transitions T_g are observed. Commonly observed values for T_g are in the range of -100°C to -50°C. b) Sketch of the [$C_{16}C_1IM$] cation showing the structural regions relevant for the melting point progression.[3] The charge-rich fragment of the aromatic imidazolium core has a higher symmetry than the one with elongated hydrocarbon chains which leads to the experimentally observed higher melting points for short hydrocarbon chains (x = 1-3). The increase of the hydrocarbon chain length reduces the symmetry and Coulombic attraction, thus resulting in lower melting points or even the occurrence of only glass transitions. Further increasing of the side chain length leads to more pronounced van der Waals interactions between the hydrophobic sections. This in term stabilizes crystalline structures, resulting in increasing melting points similar to molecular compounds such as linear alkanes. However, the [C_xC_1IM][A] ILs with long alkyl chains (x ≥ 14) often show also liquid crystalline features so that additional thermal transitions of the liquid crystalline phases are present.

Creating low melting ILs demands a balance of the ion-ion interactions, the van der Waals forces of the hydrocarbon segments as well as symmetry that is generally observed best for butyl (x = 4) to decyl (x = 10) chains in the case of this imidazolium ILs. The attachment of longer nonpolar leads to intensified lipophilic interactions that stabilize the nonpolar region of the crystal and in turn increase the melting points again.

Another direct result of this molecular design consisting of charged fragments with attached organic groups is the occurrence of nanostructures and the widespread ability to support self-assembly of amphiphiles.[62] As a general rule related to the nature of ions and solvent microstructure, the ionic liquid class combines properties similar to polar molecular liquids, molten salts and bicontinuous microemulsions.[25] This also means that

their properties are fairly different from atomic and molecular fluids as well as from conventional molten salts. The physicochemical properties of typical representatives for molecular liquids, ionic liquids as well as a molten inorganic salt and a metallic fluid are given in *Table 2* for comparison.

Table 2: Physicochemical properties of typical representatives for molecular solvents, ionic liquids, conventional molten salts and metallic fluids.[a)]

Property	Fluid Class	Molecular liquid		Ionic liquid		Molten salt	Liquid metal
	Example	Water	n-Hexane	$[C_4C_1IM][NTf_2]$	$[P_{66614}][Cl]$	Molten NaCl[b)]	Hg
Appearance		Clear, Colorless	Clear, Colorless	Clear, Colorless	Clear, Colorless	Clear, Colorless	Silvery
M / g mol^{-1}		18.02	86.18	419.36	519.31	58,33	200.59
T_m / °C		0	-95	-4[63]	-66[64]	801	-39
T_b / °C		100	69	439[c) 65]	320[c) 66]	1465	356.65
ρ / g cm^{-3}		0.997	0.661	1.437[67]	0.893[68]	1.556	13.534
η / mPa s		0.890	0.300	51.22[69]	1683[68]	1.029[70]	1.526
ΔH_v / kJ mol^{-1}		40.66	28.85	139.15[71]	-	226.4[72]	59.11
P / Pa		3169	17600	Negligible	Negligible	59.7[73]	0.261
n_D		1.3334	1.3727	1.4267[74]	1.4831[75]	1.413[76]	-
γ_{LV} / mN m^{-1}		72.7	18.4	30.7[77]	29.6[78]	110.2[79]	485.5
C_m / J mol^{-1} K^{-1}		75.375	265.2	595[80]	772.4[81]	67.2[82]	28.0
λ / W m^{-1} K^{-1}		0.607	0.1167	0.126[83]	0.161[84]	0.497[85]	8.514
E_T^N		1.000[86]	0.009[86]	0.552[87]	0.444[88]	-	-

a) Data values from standard literature compendium[89] unless stated otherwise; physical properties of the liquid state are given at 25°C unless stated otherwise; property abbreviations are the following: M: molar mass; T_m: melting point; T_b: boiling point; ρ: density; η viscosity; ΔH_v: enthalpy of vaporization; P: vapor pressure; n_D: refractive index; γ_{LV}: surface tension of liquid-vapor interface; C_m: molar heat capacity; λ: thermal conductivity; E_T^N: normalized solvent polarity measured with the Reichardt's dye (2,6-Diphenyl-4-(2,4,6-triphenylpyridin-1-ium-1-yl)phenolate), the most often used solvatochromic dye; b) Data given for liquid sodium chloride at its melting point; c) Thermal decomposition temperature as determined by dynamic thermogravimetric analysis (TGA) under inert gas.

The amphipilic behavior and tunable balance of the molecular interactions in ionic liquids make them powerful solvents for a broad range of inorganic and organic compounds including polymeric species. This extraordinary solvent behavior also includes a suprisingly large number of cases where the activity of enzymes could be retained or even improved in IL media.[90]

The directed control over structure-property relationships towards a desired application can be attained by modification of the molecular structure of ILs. These ionic fluids can therefore be customized to special reactions or processes by reverse design of the molecular structure. This targeted methodology is in strong contrast to empirical approaches for the selection of conventional solvents. However, on the contrary also an advanced knowledge about the connection of micro- and macroscopic properties is essential for tailoring towards specific goals. The scientific paradigm for the IL research with the complementary approaches is sketched in *Figure 3*.

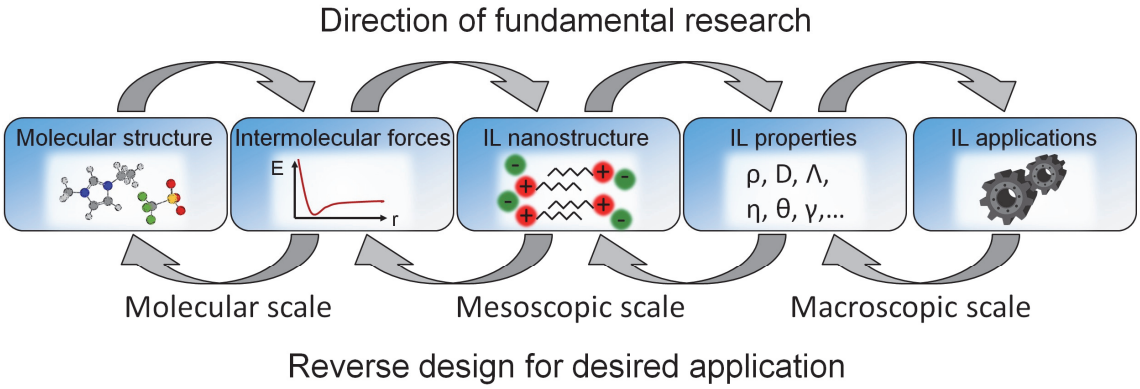

Figure 3: Complementary approaches in the field of IL research. The direction of fundamental research aims to gain detailed insight in the structure-property-relationship that in term allows the integration ILs in certain applications. The reverse design approach on the other hand tries to choose the best molecular composition starting from a certain task. The reverse design allows the purposeful tailoring of the ionic fluids if the connections between the micro- and macroscopic properties are known. This 'designer' proceeding is hardly possible for conventional solvents, where the choice of a system relies on empirical approaches.

One branch of more fundamental research is pursuing the investigation of ionic liquid properties as a function of the molecular design to enhance existing techniques or open paths to novel ones. The other reverse design manner focuses on the choice and design of anions and cations that can be manipulated in various ways for a desired practical application.[91] However, such innovative efforts in turn demand a multiscale thinking about the different spatial and temporal connections from molecular to macroscopic scales.[92] ILs have found widespread and highly diverse applications in both fundamental research and practical applications due to the virtually endless possible combinations of cations and anions as well as includable chemical functionalities and adjustable physicochemical properties. Therefore, the ionic fluids are currently entering the marketplace more and more[3,93,94] and are already implemented in some large scale production sites for instance in the case of the BASIL (acronym for 'Biphasic Acid Scavenging utilizing

Ionic Liquids') process of the BASF.[95,96] Some important uses of ILs will be discussed more detailed in section 1.4.

1.2. Ionic liquid subclasses – as diverse as chemistry?

A definite classification of ionic liquids themselves in comparison to other known substance classes is quite tough since there are a lot of different approaches according to analogies in their properties and the substance class itself is highly diverse. Literature suggestions span the range from similarities to liquid crystals,[26] fragile glass-formers[97] over supramolecular fluids[98] with heterogeneous structures and dynamics[99] (related to the existence of different microdomains in ILs) to the conjunction between molecular solvents and conventional molten salts.[100,101]

Compounds included in the ionic liquid class can be classified according to various criterions depending on the diversification desired. By this way a single ionic liquid is characterized by different attributes according to its physicochemical properties and structural features. An overview of frequently applied multifaceted classifications used in the literature is shown in *Figure 4*.

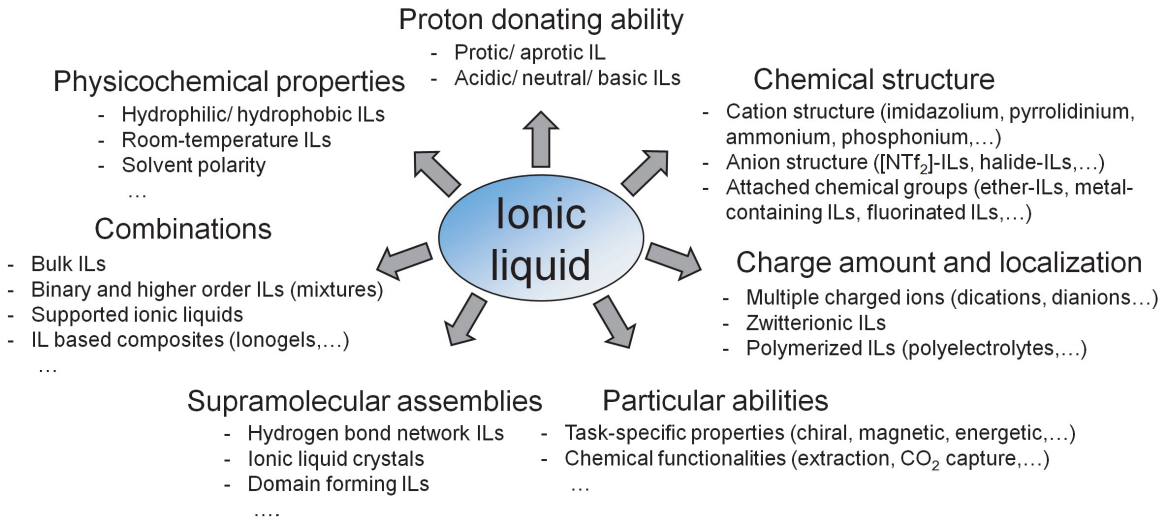

Figure 4: Classifications of an ionic liquid according to different criteria used in the literature.

Besides the already mentioned differentiation between the general chemical composition of cation and anion or by attached side chains, ILs can also be grouped following their proton donation ability. The consequence is a distinction in either acidic, neutral or basic ILs[102] relevant to catalytic properties[103] or in the two big subclasses of protic and aprotic ILs.[104,105] Protic ILs (PILs) are proton donating solvents, whereas the non-proton-donating ILs are classified as aprotic in analogy to the terms established for molecular solvents. PILs are synthesized via proton-transfer from a Brønsted acid to a Brønsted base. The first RTIL ever described was the PIL ethylammonium nitrate $[EtNH_3][NO_3]$[106] which melts at 12°C.[107] It was discovered as early as 1914 by the German-Latvian-Rus-

sian chemist Paul Walden.[108] This was preceded by the first report on the PIL ethanolammonium nitrate [HO-$(CH_2)_2$-NH_3][NO_3] melting at 52°C[107] in 1888.[109] An outstanding feature of some PILs is the existence of H-bond donor and acceptor sides that can result in hydrogen bonded networks[110] due to the presence of strong, directional interactions.[111] The occurence of these interactions influences properties, such as thermal conductivity,[112] thermal stability[113] or solvation characteristics.[114–116] This leads to inherent diverse properties of PILs compared to aprotic ILs (AILs) since there is always a reversible proton transfer possible,[117] opening an evaporation or decomposition pathway and leading to an equilibrium of ionic and neutral species[118] especially if the pK_a difference of the precursors is comparably small.[119] The consequences of the equilibrium between ionic and non-ionic species are altered properties, especially in the case of volatility and conductivity.[120] In contrast to that, AILs are usually prepared by alkylation of nucleophiles to obtain the IL cations. The subsequent anion metathesis or addition of Lewis acids often required makes the synthetic process more tedious, complicated and less atom efficient (see also section 1.3).[121,122] The first detailed research on AILs was conducted from the 1950s to the late 1980s by the U.S. Air Force.[3,123] The low temperature molten salts investigated there consisted of substituted organic aromatic cations, such as pyridinium and imidazolium, combined with the Lewis acidic aluminum chloride to yield chloroaluminate ILs.[124,125] The examined anions were inherently sensitive to moisture and oxygen as well as corrosive in their nature. These undesirable features prevented a widespread breakthrough of ionic fluids as solvents or functional fluids. Yet, a niche use of the chloroaluminate ILs remained: the application as electrochemical solvents.[126] In the early and mid-1990s, the discovery of AILs that are stable towards air and humidity marked a turning point in the history of ILs since they brought the field from a curiosity to the mainstream of the scientific community. Suddenly, pathways to a vast amount of new applications were opened through this novel findings.[123,127–129] The AILs in general have the benefits of more extensive chemical possibilities, higher thermal and chemical stability combined with lower melting points as result of the absence of directed hydrogen bonds (in most cases) and the often higher degree of asymmetry achievable. Furthermore, they show different solvation characteristics than PILs and usually behave more similar to strongly dissociating molecular solvents.[130]

Another possibility to distinguish ILs is by their physicochemical properties, mainly applied with their applications as solvents in mind. The subdivision of RTILs that is of the highest interest for most practical uses was already mentioned. The phase behavior of ILs towards water may also be used for differentiation, *i.e.* into hydrophobic and hydrophilic ones.[65,131,132] This classification is particularly of interest for their use in extractions,[133] IL separation or recovery,[134,135] biphasic systems including water[136,137] or applications where moisture uptake needs to be avoided.[138] Comparable considerations hold true for the classification by solvent polarity[139–141] that is important to control the miscibility of fluids for instance in extractions[142] or multiphasic reactions.[143,144] Despite the practicality of these attempts, it should be noted that the mentioned classifications to evaluate the phase and solvent behavior are ambiguous since the phase behavior of

fluid-mixtures are mostly sensitive to temperature and include often critical solution temperatures.[145]

Besides investigation of the IL as bulk phase, there is also an emerging interest in confined ILs, since they show significant changes in their physicochemical properties due to the spatial restriction and interactions with a solid surface.[146,147] Although this is not strictly a classification for ILs they are often listed as a subclass since they utilize the beneficial properties of ILs and allow applications that are hardly possible with molecular liquids. These confined ionic liquids are a novel class of solid-liquid composite materials that combine the characteristics of ILs and their solid support. These hybrids enable completely new materials, such as ionogels[148] made from ILs and polymers. Also the immobilization on solid supports, either with or without covalent anchoring groups, leads to interesting new processes, such as the SILP (acronym for 'supported ionic liquid phase') catalysis[149,150] or the removal of contaminants.[151] This allows the usage of low levels of both catalyst and IL, facile product separation, interface controlled dynamics and continuous reaction processes.[152] Binary or ternary composites including confined ILs are also of great interest for energy applications including supercapacitors,[153] fuel cells[154] or batteries.[155]

A famous classification frequently applied by physicochemists is the subdivision by solvent structures and spatial extent adopted in bulk state since it is of fundamental importance for deviated macroscopic behavior.[25] The already discussed hydrogen bonding (that is also present to some extend in several aprotic ILs[156]) is also relevant to the formation of networks[157] and related phenomena, such as reaction kinetics and dissolution of biomass compounds.[158] The formation of polar ionic and nonpolar hydrocarbon domains, which is driven by solvophobic interactions if the attached hydrocarbon chains are sufficiently long, was reported for a large spectrum of ILs.[159,160] The formation of this nanostructured aggregates has also a great influence on the macroscopic properties. The interactions and resulting structures in ILs will be discussed in more detail in section 1.5. Ionic liquids with orientation on larger scales are referred to as ionic liquid crystals (ILCs), bridging the field of ILs and conventional liquid crystals.[161] The thermotropic ILCs combine the self-assembly and anisotropic physical properties of liquid crystals with the tenability, conductivity and strong electrostatic interactions as structure determining factors of ILs.[162] For ILs with hydrocarbon chains longer than tetradecyl, smectic mesophases similar to conventional liquid crystals are often found.[163]

As ionic liquids can incorporate a large variety of functionalities uncommon in pure molecular liquids, they are often denoted as task-specific or functional ionic liquids. In these cases, the tailored fluids are classified according to the unique properties included or processes where they are designed to be used. These special, beyond solvent attributes[164] encompass for example chiral ILs,[22,165] photon-upconversion,[166] redoxactivity,[167] energetic ILs (ILs that have a large amount of chemical energy stored),[168,169] magnetism[170] or luminescence.[171,172] Also, ILs tailored for specific purposes, such as CO_2 capture[173] or biological activity,[174] are in the focus of current research.

Another possible distinction often used is by the charge amount and distribution if no longer simple, single charged cations and anions species are considered. This includes mainly dicationic ILs[175,176] that show higher melting temperatures, densities and viscosities compared to the monocharged ones,[177,178] while there are only little reports of dianionic ILs.[179] The two opposite charges may also be connected by covalent linkers forming the so called zwitterionic liquids that find some uses for instance in electrochemical applications[180,181] or as surface active compounds.[182] Polymerized ILs, polymeric ILs or poly(ionic liquids),[183] all terms describing the same class, are the macromolecular analogues of conventional ILs. They are a subgroup of ionic polymers and transfer common IL properties, such as glass-forming tendency, thermal stability and high ionic conductivity, to polymers.[184] They can either be synthesized from ionic monomers with polymerizable groups or by modifying polymeric structures with ionic groups.[185] Research on the polymerized ILs focuses mainly on the use in catalysis,[184] electrochemical energy conversion[186] or the use as stimuli-responsive substances[184] as well as separation and absorption materials.[187,188]

Beside the various classifications in the field of single component ILs, there is also an emerging interest in mixtures of ILs,[189] leading to new systems with altered characteristics,[190] although the IL blends are in general only sparsely investigated. However, there is growing evidence that these multicomponent systems behave almost ideal if the ionic species are of comparable ionic size.[191] On the contrary, the deviation from ideal behavior is more significant if there are more complex interactions and the ion sizes are quite different.[191]

1.3 Synthesis of ionic liquids – toolbox and key rolled into one

As only a small part of the immense number of synthetically available ILs is also commercially available, their tailored synthesis is essential for developments incorporating ILs. As a consequence of the high variety and different IL properties, their synthesis is also not straightforward and has to be adapted to the needs. The synthetic pathways to the general types of ILs are sketched in *Figure 5*.

Especially the purity of ILs is of concern for a range of applications such as electrochemistry, catalysis or spectroscopy.[192] A particular problem in the purification of ILs is the intrinsic restriction of purification methods as conventional practices like crystallization or distillation are only applicable in rare cases. Also, column chromatography is often difficult if larger quantities are needed. Therefore, it is vital to choose synthesis pathways with facile purification techniques and to limit the number of inter stages to a minimum. The reduction of energy-intensive purifications and multiple step reactions is obviously important to decrease their overall cost which in turn limits their distribution. This is of especial concern when they act as substitute for volatile organic compounds (VOCs) that are commonly low in price.[193] In practice, the purification of low temperature molten salts is conventionally achieved via filtration of the intermediate organic salts, solvent

extraction strategies as well as the removal of volatile impurities and excess precursors under reduced pressure.

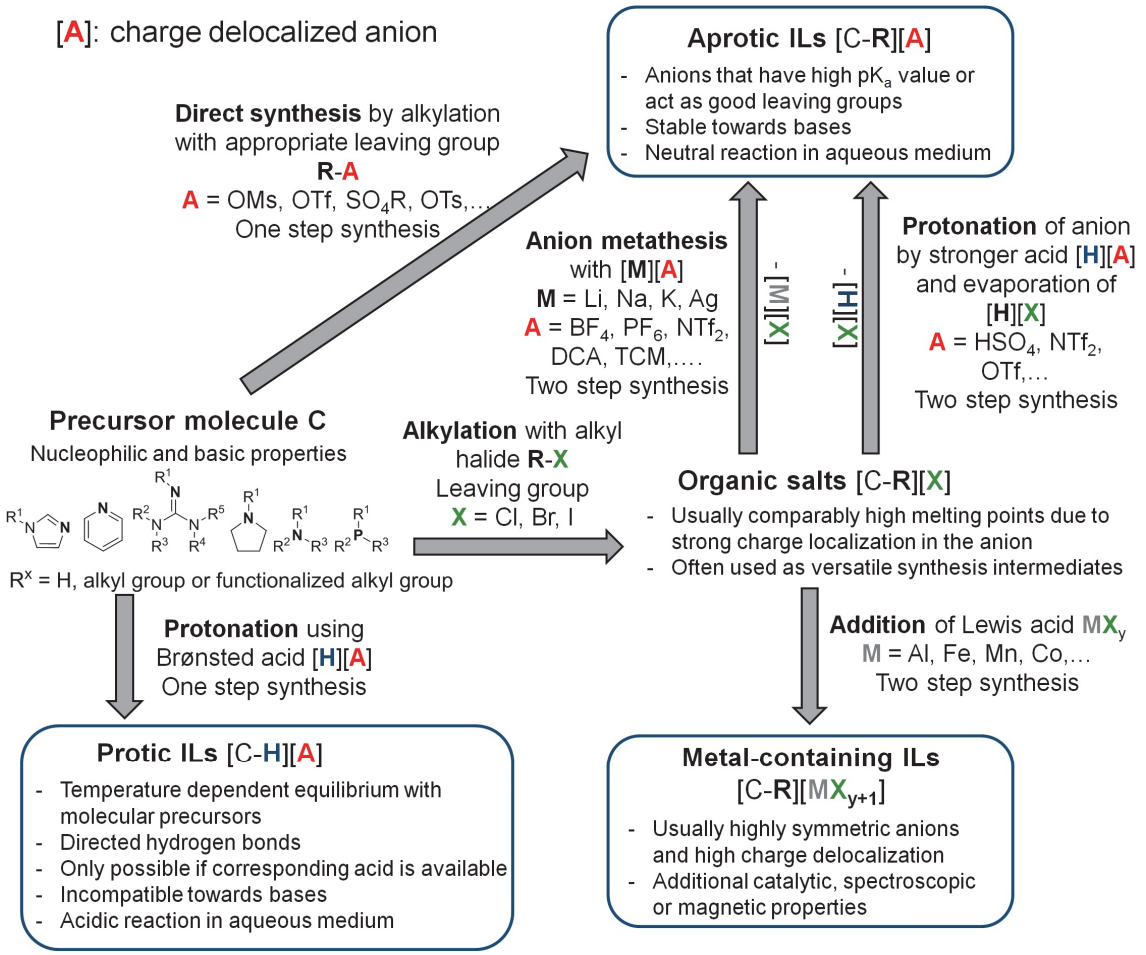

Figure 5: General synthesis pathways to different classes of ionic liquids from nucleophilic, basic precursor molecules and some general properties of the obtained IL subclasses.

The syntheses of ILs usually start with a Lewis basic precursor that can either act as Brønsted base or nucleophile forming the cationic part during the neutralization or nucleophilic substitution.[194] Frequently used precursors are the aromatic N-substituted imidazoles, pyrrolidines or piperidines, pyridines, mono-, di- and tri-substituted amines as well as tri-substituted phosphines.[127] Although there are a large variety of applicable precursors commercially available, the synthesis of more complex substitution patterns often demands additional reaction steps. Furthermore, proper purification of the precursor and the alkylation reagents are required, especially if spectroscopically pure compounds are indispensable.[195]

The formation of PILs is achieved by direct protonation of the precursor in an acid-base-neutralization, if the related acid is available. Due to the nature of this reaction types the synthesis is usually rapid, atom-efficient and quantitative making the PILs attractive in the context of greener chemistry, especially from a synthetic point of view.[196] The ILs

obtained this way share the characteristics of incompatibility towards bases and an acidic reaction in aqueous medium.

AILs, on the other hand, can be prepared either by direct alkylation in a one-step reaction, if an organic compound with appropriate leaving group is available, or by a two-step protocol including alkylation and subsequent anion metathesis. Regarding atom economy and waste prevention in accordance with Green Chemistry principles,[197] the direct synthesis is obviously favorable.[198] The direct alkylation also ensures a halide-free pathway to IL applications, such as electrochemistry, where even very small amounts of halides can have a disturbing effect. Applicable anions for this procedure are for example the alkylsulfates $[SO_4(CH_2)_xH]$,[199] alkylsulfonates $[SO_3(CH_2)_xH]$,[200] tosylates [OTos],[201] trifluoromethanesulfonate [OTf],[202] dialkylphosphates $[PO_2(O(CH_2)_xH)_2]$,[203,204] alkylphosphonates $[PO_2(O(CH_2)_xH)(CH_2)_yH]$[205] or the fluorinated bis(perfluoroalkylsulfonyl)imides $[N(SO_2(CF_2)_xF)_2]$.[206] The Meerwein's salt derivatives based on the trialkyloxonium $[O((CH_2)_xH)_3]$ cation with the tetrafluoroborate $[BF_4]$ or hexafluorophosphate $[PF_6]$ anion can also act as strong alkylation agents for the direct synthesis of aprotic ILs, but are comparably expensive.[207] The direct synthesis of 1-alkyl-3-methyl-imidazolium nitrates $[C_xC_1IM][NO_3]$ by alkylation with alkyl nitrates is also feasible, but requires explosive starting materials.[208] As most of the direct alkylation reagents are highly sensitive to nucleophiles and moisture, the syntheses of ILs are often conducted under inert gas atmosphere. Especially the reaction of the nucleophilic water with the reactive compounds used for the direct alkylation can lead to contamination with the free acid of the corresponding anion. These acids often have high boiling points and are therefore hard to remove by evaporation. Even the presence of acidic proton in trace amounts can have a significant disturbing effect in many cases and also catalyzes the decomposition of the $[PF_6]$ anion.[209] Therefore proper reaction control and appropriate purification are indispensable to obtain ionic fluids in high purity by these reactions.

Due to the disadvantages discussed above, the more frequently applied procedure for the synthesis of ILs utilizes the preparation of the halide salts by alkylation with a haloalkane to the quaternary species as an intermediate step.[210] Choosing this preparative pathway has the further advantage of easier processing due to the stability of the reagents towards moisture and less exothermic reactions. Also, there is a large spectrum of inexpensive, often functionalized, representatives available which offers a high degree of synthetic flexibility. The products obtained in this way are often comparably high melting organic salts rather than ionic liquids thus additionally allowing further purification by crystallization. However, in some rare cases even RTILs with halide ion can be obtained, but they always form highly viscous compounds. Both the high melting point and the high viscosity have their origin in the charge localizations of the halide anions that stabilizes their crystalline structures and induces strong intermolecular interactions. The halide salts obtained by the quarternization reaction can subsequently be converted by anion metathesis reactions to yield molten salts with the desired anions, thus offering a highly adaptable platform for the synthesis of AILs. Conventionally used for the anion exchange are alkali metal salts[211,212] or silver salts.[123,213] Also, the preparation by addition of the conjugate acid of the desired anion is feasible in some cases.[122,214] This pathway

demands a sufficiently high pK_a value of the acid to protonate the halide followed by removal of the hydrogen halide over the gas phase or separation via solvent extraction processes. The two step synthesis using the alkyl halides has the disadvantage that alkali metal or silver cations as well as halide anions or silver particles may remain in the final product.[215] Especially the halide residues can have significant influence, for example in transition metal catalysis,[216] or on the physicochemical[217] and electrochemical properties.[218] It is therefore necessary to reduce the concentration of these contaminants as far as possible. Applying appropriate purification methods or the change to direct alkylation procedures are therefore critical to avoid these problems. Nevertheless, the preparation of ILs via the intermediate halide salt is for some IL subclasses the only possible reaction pathway. Exemplary anions for the molten salts that are not accessible by direct alkylation are carboxylates [$CO_2(CH_2)_xH$], perfluoroalkylcarboxylates [$CO_2(CF_2)_xF$], tetracyanoborate [$B(CN)_4$], the pseudohalides thiocyanate [SCN], dicyanamide [$N(CN)_2$], tricyanomethanide [$C(CN)_3$] as well as perchlorates [ClO_4] or metal-containing anions. Additionally, anion exchangers can be an efficient tool for the preparations of AILs.[219] The AILs without functional groups show a greater alkaline stability and form neutral solutions in aqueous media. As already discussed, their thermal[220] and electrochemical stability[221] is usually higher and directed hydrogen bonds are only present to minor extent,[222] making them effectively a special class of polar, aprotic solvents.

The halide salts are also commonly used precursors for the preparation of metal-containing ILs (MILs). They are usually synthesized by adding a stoichiometric portion of the metal chloride to the halide either in bulk[223] or solution.[224] The MILs have typically highly symmetric anions that usually adapt tetrahedral[224] or octahedral[225] geometries in their complexes. Often applied is also a combination of anion metathesis and metal complex formation by suitable ligands such as [SCN].[226] Besides the already mentioned chloroaluminate ionic liquids, there are also some other reports on MILs containing main group metals such as indium and gallium.[227] For these ILs, an equilibrium of different anionic species/complexes is often observed if the Lewis acids are added in non-stoichiometric amount.[4,228,229] Many more representatives of transition[18,170,230] and rare earth metal[17,231,232] containing ILs that are in liquid state at ambient temperature are known.

As ILs are frequently considered as 'greener' substitutes for volatile organic solvents a more environmental friendly synthesis of the ionic liquids themselves is demanded.[233] For the overall assessment of sustainability in a certain task, the whole production cycle of the ILs has to be considered. This has to be taken into account to judge whether they can be more sustainable alternatives to VOCs.[193] More environmentally friendly alternatives utilize, for example, solvent free, sonochemical[234] or microwave assisted[233] methods. Nevertheless, the synthesis of most ionic liquids is based on petroleum-derived chemicals making their replacement by bio-based ones very interesting from ecological perspectives.[235] Furthermore, the environmental persistence and toxicity of many ILs are still subject to controversy.[93,236–238]

1.4 Applications of ionic liquids – from curiosity to universality

As diverse as the structures and properties of ILs are, so are their possible implementations, covering areas from specialized niche applications in science to large scale processes in the chemical industry.[3] As the knowledge about the syntheses, physicochemical properties and structure-property relationships of ILs is becoming more sophisticated, the low temperature molten salts are currently spreading to wider marketplaces,[93,239] along with a dropping of their price due to increased commercial requests (economy of scale). *Figure 6* gives an overview about a selection of important and promising fields for which their beneficial influences were reported in the literature.

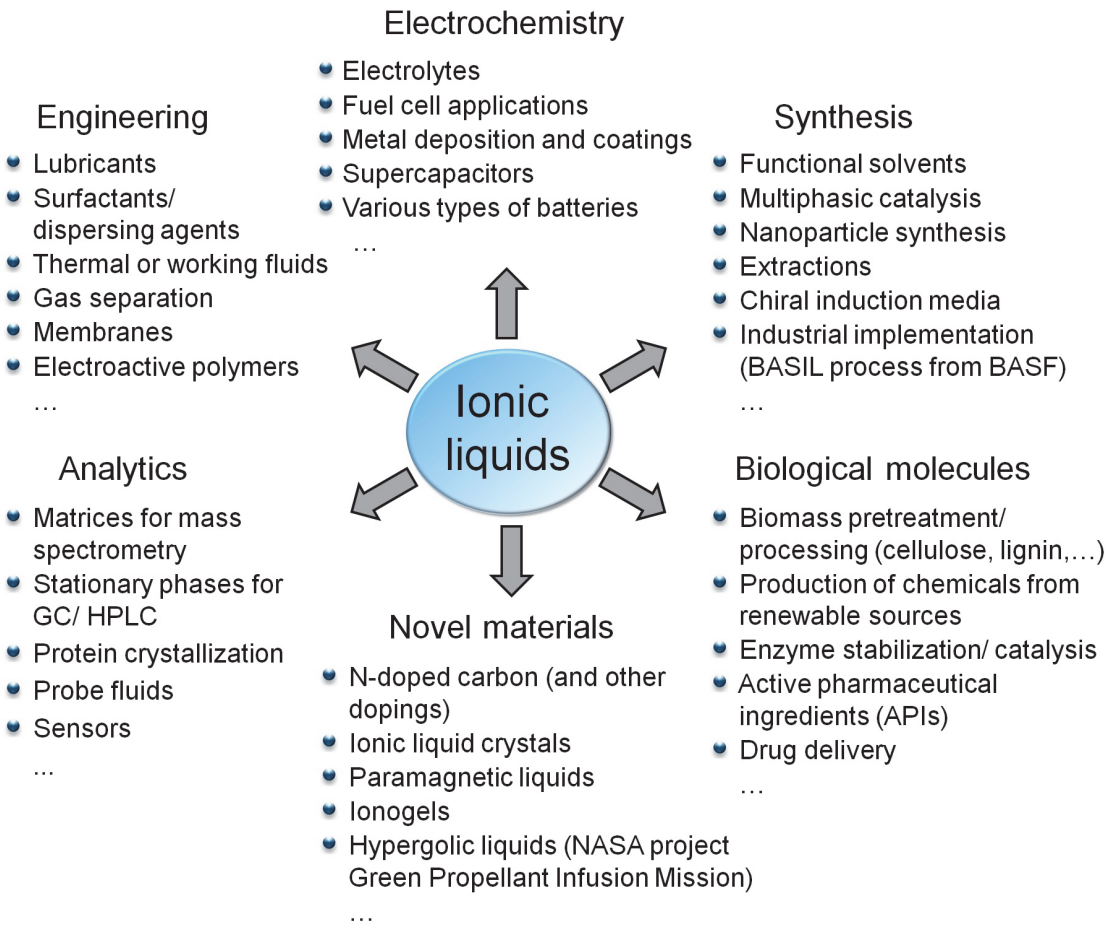

Figure 6: A selected range of important applications of ionic liquids divided into larger subcategories. Note that the fields and applications are often overlapping.

As there are an immense number of IL applications, only an excerpt of the most intensively investigated fields will be reviewed here to demonstrate the wide scope of their diverse implementations.

One of the most promising fields for ionic liquids is *electrochemistry*,[240] for the implementation in which the initial research on low temperature molten salts was also carried out. The ILs used in this field act as solvent-free and safe electrolytes that incorporate chemical stability, intrinsic conductivity and non-volatility along with wide electrochemical

windows and applicable temperature ranges that markedly exceed those of organic electrolytes. Due to this property combination, their applicability has been successfully demonstrated for nearly every electrochemical device in the area of energy storage and conversion. The usage of ILs for the storage of energy includes mainly capacitors and the highly diverse field of battery technology. Besides the already mentioned favorable property-combination, the high concentration of ions is usually beneficial for electrochemical double-layer capacitors (EDLCs).[241] This leads to large capacitance values and increasing energy density due to the formation of large double-layers that yield high performance EDLCs. However, the structure of the electrochemical double-layer formation and voltage dependence of the capacitance at electrified interfaces appears to be altered for ILs ('bell' or 'camel' shapes) compared to the one obtained for conventional electrolytes (U-shapes as predicted by Gouy-Chapman theory).[242] For advanced battery technology, ILs[243,244] can perform different additional duties besides the use as safe and highly stable, solvent-free electrolytes.[245] This includes for example the use as conductive plasticizer in ternary gel-electrolytes,[155] improvement of lithium diffusion in electrolytes bases on polymerized ionic liquids[246] or the suppression of lithium dendrite formation.[247] The various battery types in which the low temperature molten salts are applied span the range from lithium-based ones, such as Li-metal,[248] Li-ion[249,250], Li/air[251] or Li/S[252] batteries, over cells that are based on sodium/sodium-ion[253,254] or magnesium[255,256] to redox-flow batteries.[257,258] In the area of energy conversion, ILs are applied in fuel cells and dye-sensitized solar cells (DSSC). In high and intermediate temperature fuel cells under non-humidified conditions, PILs are regarded as stable proton conductors when immobilized in membranes.[259–261] For the polymer electrolyte membrane fuel cells (PEMFC), working at low temperature, the coating of the electrocatalyst with hydrophobic ILs was shown to increase the electrocatalytic activity and catalyst stability.[262] This was believed to be a combined result of an increased amount of catalytically active sites, higher oxygen concentration in the IL and electrostatic stabilization of the nanoparticles.[263] Using ILs in this way could help to reduce the cost of PEMFCs and improve the lifetime of the catalysts. For DSSCs, the ultra-low volatility of ILs paired with their thermal stability and comparably high polarity is beneficial to minimize the problems of their long-term stability due to micro-cracks as a result of thermal stress and often insufficient encapsulation.[264]

In the area of *engineering*, ILs are employed as working [265,266] or thermal fluids,[267,268] as neat lubricants[269] or lubricant additives.[30] Their remarkable protective effect against wear and the significantly reduced friction coefficients are believed to be the result of structured tribofilms[270,271] with structures comparable to those in bulk ILs. Furthermore, they include other properties necessary for advanced lubrication such as adaptable viscosity, non-volatility, high thermal, chemical and tribochemical stability along with applicability to a wide range of temperatures.[272,273] The latter properties are also closely connected to the wetting behavior of ILs[274] which's analysis is necessary to judge the interfacial behavior of ILs for applications in heterogeneous systems.[275] Other attractive operational areas of ILs are in the separation and storage of gases. This can, for example, be realized by selective absorption and desorption of particular gases in bulk ILs[276] by

either physical[277] or chemical mechanisms[278] as well as by IL-supported or IL-derived membranes.[279] Carbon capture processes utilizing ILs as substitute for volatile amine solutions are also widely investigated.[173,280] These auspicious technologies aim for an improvement of the economic efficiency over the amine-based ones currently used for CO_2 separations on industrial scale.[281] The neoteric solvents are also interesting for the use in ionic electroactive polymer actuators that are capable of large deformations even at comparably low voltages (< 5 V).[282] The developing fields of electro-mechanical actuators benefit from the broader potential windows, high concentration of ions and non-volatility of ILs, making these devices more efficient and durable.[283,284] In combination with the deployed elastomers, ILs often provide the additional function as plastiziser.[285] Furthermore, they are applicable under more extreme conditions such as reduced pressure or elevated temperature, broadening the range of possible implementations.[286] As a result of the improved safety compared to VOCs, favorable extraction behavior and stability against radiolysis, ILs have even been suggested for an advanced nuclear fuel cycle.[287]

The use of ionic liquids in *synthesis* is one of the oldest research topics.[127] In the progress of research, it became clear that ILs can take highly diverse and often beneficial roles in organic and inorganic reactions as either solvent or 'beyond solvent'.[288] They offer, for instance, the possibility to act as functional solvents[289] or polar, but weakly coordinating solvents[290,291] which is of special interest in transition metal catalysis.[4] It was also shown that the use of certain ILs as reaction media can have a drastic influence on the outcome of some reactions by favoring certain reaction pathways.[292] Due to the coexistence of polar and apolar, micro-segregated domains, the low temperature molten salts mimic the solution behavior of emulsions and have often a high solubility for both organic (usually nonpolar) and inorganic (often polar) compounds.[293] The phase behavior of ILs towards organic solvents and water can be used to create a large variety of novel, easily adjustable multiphasic systems for reactions[294] or liquid-liquid extractions.[295] Using thermoregulated mixing in liquid multiphasic systems, the advantages of homogeneous catalysis, such as improved kinetics and selectivity, can be combined with those of heterogeneous catalysis offering facile catalyst recycling.[145,296] The roles that ILs play in catalysis are also very diverse and range from the use as catalyst itself, over the function as co-catalyst, catalyst activator or ligand for catalytically active metal centers, to the use as simple solvent.[35] Despite the vast majority of publications utilizing ILs as solvents, it should be kept in mind that their practical implementation in this way is very unlikely unless the ILs have significant benefits over conventional liquids.[297] This means that for a successful industrial implementation the ionic liquids should not just act as 'simple solvents' but rather 'functional liquid reaction media'. Using ILs in this manner can, for example, be put into practice by using ILs with catalytic activity. This can be realized by the use of Brønsted-[298,299] or Lewis-acidic[300] as well as Lewis-basic[301] representatives. ILs acting as co-catalyst can, for instance, reduce the reduction potential of certain electrochemical reactions[302–304] or increase reaction efficiency and economy.[305,306] Also, the activation and immobilization of catalytically active (nano-)particles is an efficient tool to boost selectivity and yield of catalytic reactions, enable catalyst recycling and reduce overall cost.[307] Additionally, the low temperature ionic fluids efficiently stabilize metal

nanoparticles (NPs) and hence avoid loss of catalytic activity due to Ostwald-ripening.[308] As the interactions of ILs with NPs are governed by a combination of diverse effects, including van der Waals, electrostatic, steric, solvophobic and structural interactions as well as hydrogen bonds, various self-organized structures are synthetically accessible.[309] Therefore, the molten salts can also act as flexible platform that may serve as reaction medium, stabilizer, ligand or support for NPs.[310] These IL-NP systems, combining the characteristics of both substance classes, are of particular relevance for advanced catalysis and electrochemical applications.[311] Besides the usage of ILs in nanoparticle dispersions, they are also attractive for NP synthesis due to their ability to operate as electronic and steric stabilizers.[312,313] The low surface tension of many ILs often leads to high nucleation rates and consequently small particles that are generally desired.[314] The inherent and complex solvent structure of the ILs has also a strong effect on the obtained particle morphology allowing a tailoring of well-defined nanoscale structures with enhanced ordering.[315] The low temperature molten salts are furthermore successfully used as reaction media for an exhaustive amount of organic reactions. The interested reader is referred to reviews concerning this topic.[4,35,122,127,300,316–318] Many of the reactions given in the literature show advantages when carried out in low temperature molten salts that can be either enhanced reaction kinetics or selectivity due to energetic changes in the reaction pathways or more facile catalyst reuse.[319] In some cases it was also observed that the reaction mechanism of a certain catalyst changes drastically when used in IL media.[320] Another highly interesting possibility offered by the task-specific fluids is the use as chiral induction media when chirality is inherently present in the IL. By this way, chirality can be transferred directly from the reaction media[165] rather than from chiral ligands as is common in transition metal catalysis. Especially ILs derived from amino acids are thereby of interest as rather cheap, chiral solvents obtainable from renewable resouces.[321,322] The amino acid precursors can thereby be converted into either the ILs' cation or anion, thus offering synthetic flexibility and adaptability. In some syntheses, certain ionic liquids can also act both as solvent and reagent. This was demonstrated, for instance, when an IL acts as a save and easy to handle fluorine source in the synthesis of fluoridosilicate NPs.[323] By this way the usage of highly dangerous and hard to handle hydrogen fluoride is avoided.

Although the striking advantages of ILs in diverse fields are well known, little information about the industrial applications of ionic liquids is distributed in the scientific community.[324] However, there is evidence from the rapidly increasing number of patents dealing with ILs and the shift in emphasis towards practical applications that their commercialization will further continue and expand.[325,326]

The most widely known and recognized industrial realization of IL usage is probably the BASIL-process developed by the BASF.[327] The process uses 1-methylimidazole as base for the acid scavenging in the production of alkoxyphenylphosphines that are precursors for the production of photoinitiators applied in UV curing resins.[324] The PIL 1-methyl-imidazolium chloride formed by the neutralization has a quite low melting point for a chloride salt (T_m[C_0C_1IM][Cl] = 75°C) and forms a biphasic liquid system in the reaction vessel. The discrete IL phase is easy to remove by simple gravity separation

and no thick, dense slurry is formed as it was the case in the former process where triethylamine was employed as base.[95] After separation of the IL-phase, the initial base is regenerated with sodium hydroxide and recycled. The improvements made using ILs in this procedure are manifold. The process becomes amenable to small jet stream reactor vessels improving the reaction rate and space-time yield by several orders of magnitude.[324] In addition, it was found that the generated IL has a catalytic activity that further improved the efficiency of the process. Another successful industrial application of ILs was achieved by Degussa (now Evonik Industries) to improve the efficiency of hydrosilylation reactions by recovering the platinum catalyst in a liquid-liquid biphasic system.[324,328] In the process the platinum catalyst is dispersed in an ionic liquid phase while the pure reaction product is separated in a second phase formed in the reaction. This allows easy separation and reuse of the catalyst with ultralow leaching and only minor loss in catalytic activity for several cycles.[328] Evonik Industries has also demonstrated a SILP (acronym for '<u>s</u>upported <u>i</u>onic <u>l</u>iquid <u>p</u>hase') process on pilot scale for the hydroformylation of olefins by syngas.[324] Their SILP technique immobilizes precious metal catalysts dissolved in an IL thin film on the surface of porous material by physisorption.[296,329] The advantage of this approach lies in the low amounts of ILs needed, the often high catalyst activity and improved or altered kinetics as well as in the reduction of mass transfer effects.[324] The process management thus combines the advantage of heterogeneous and homogeneous reactions as discussed above with considerable extended operation time making the process more economic and ecological.[330]

Another field of high potential for ILs is the area of *biological* resources and bioactive compounds. The further development of biological, carbon-neutral sources is one of the main domains of IL research aiming at a more sustainable, 'greener' chemistry. These efforts are often targeting a synergistic combination of the environmentally friendly properties of ILs with the utilization of renewable resources and more sustainable processing methods.[331] Similar to the other application fields described above, strategies for the advantageous usage of ILs with biological compounds are also very versatile. As already mentioned, the exceptional and tunable dissolution behavior of ILs allows for the dissolution and processing of biopolymers that are insoluble or hardly soluble in conventional organic solvents and water.[332,333] For example chitin,[334,335] keratin,[336] suberin[337] as well as the main components of hardwood, lignin[338] and cellulose, belong to these poorly soluble biocompounds for which a dissolution in ILs was proven.[339] Even the complete dissolution of wood in ILs was reported.[340,341] The exceptionally high dissolution ability of some ILs for biomass compounds is attributed to their usually high polarity and H-bond basicity.[342,343] These attributes make the ILs capable of breaking hydrogen bonds and other intra- and intermolecular interactions that are present in the matrices of the macromolecular biomass compounds. With these powerful and adaptable solvents for biopolymers, the separation or purification of individual compounds such as the pretreatment of lignocellulosic biomass,[344–346] the separation of cellulose and lignin[196,347,348] or the saccharification of polysaccharides becomes also feasible in or with the aid of ILs.[349–351] Similar to these strategies is the more environmentally friendly and expanded production of biofuels and -chemicals[352,353] from renewable sources with the

aid of ILs. For example cellulosic ethanol,[353–355] furfural,[356,357] sugars,[358–360] biodiesel[361,362] or fine chemicals[363,364] are attractive candidates for the production of which ionic liquids were applied. Besides the cracking into useful chemicals also novel materials based on renewable sources, composite materials[365,366] and processes[367] are also enabled by the powerful biomass solvents.[368–370] These biopolymer derived materials can have beneficial mechanical properties and are biodegradable, which allows for substitution of synthetic materials based on non-renewable sources, especially polymers.[371,372] By using carbon neutral sources, the anthropogenic climate change could be attenuated and the problem of persistent plastics in the maritime habitats reduced. Furthermore, ILs offer a homogeneous reaction medium for the conversion of otherwise hard to handle biopolymers.[373,374] An alternative to the exploitation of macromolecular biocompounds is the extraction of bioactive compounds with the aid of ionic fluids. In this way ILs offer a valuable tool for the isolation and purification of various classes of bioactive molecules with diverse functions.[133,375] This is of particular concern as a source of high-value pharmaceutical molecules[376] or enzymes.[377] For the latter ones, aqueous biphasic systems (ABSs), which consist of two water-rich phases, are suggested for efficient extractions without organic solvents. The phase behavior of these ABSs can be fine-tuned by the amount and concentration of the applied ILs[378] and are often found to maintain enzyme activity.[379,380] Enzymatic reactions in ionic liquid media are benefiting from the high tunability and unconventional solvent characteristics enabling conditions and reactions that are not feasible in molecular organic solvents.[381,382] ILs allow for example the altering of enzyme structures, activity or enantioselectivity depending on biocatalyst and solution environment.[383] Another important benefit of the molten salt media is that enzyme stabilization[384] and activity can be retained up to temperatures higher than their usual degradation temperature in other media.[385,386] Besides the attractive chemical and physical properties of ILs, their biological activity has recently become the focus of many researchers' attention, since they offer novel drug designs and alternative drug delivery systems.[387] Strategies with ionic liquids can take advantage of their dual nature due to their two discrete ions to achieve tunable active pharmaceutical ingredients (APIs) that can be liquid under physiological conditions.[388] In this way it would be possible to face a range of challenges in drug delivery of solid-state APIs, for instance low solubility, bioavailability and stability or undesired polymorphic forms as well as non-uniform particle distribution leading to hardly controllable drug release kinetics.[389] The selection of the ion pair constituting a potential drug can have a significant influence on the pharmacokinetic and -dynamic properties, thus profiting from the tuning offered by the IL toolbox.[390] Besides the options of APIs being liquids under pharmacological condition or having even dual-active species, the ionic compounds can, for example, also be used as prodrug API-ILs or for the solubilization of drugs that are poorly soluble under physiological conditions.[391,392]

The usage of ILs in *analytical chemistry* has also developed in recent years together with the field of ionic liquids itself, yielding multiple uses of great diversity in the techniques of both sample preparation and analysis.[393,394] Due to the low-temperature molten salts' negligible vapor pressure, high ionization efficiency, more homogeneous matrix-analyte

dissolution as well as high and adaptable solvation efficiency, they are good candidates for the use as liquid matrices in matrix-assisted laser desorption/ ionization mass spectrometry (MALDI-MS).[395] Applying IL-based matrix substances also reduces the formation of hot spots compared to the crystalline low molecular weight compounds usually used in MALDI-MS and allows for both qualitative as well as quantitative measurements.[396,397] The ILs' interactions with analytes are usually more versatile than those of most stationary phases, enabling better resolution in chromatographic methods. Combined with their adjustable selectivity and thermal stability, the ionic fluids can be used as novel stationary phases in gas chromatography (GC) for the separation, detection and identification of volatile analytes.[398] The multiple interactions of ionic liquids are also the reason for their widespread investigation in capillary electrophoresis[399] or in liquid-chromatography for example as mobile phase additives,[400] liquid-liquid chromatography[401] or in attachment to mobile phases.[402] In addition to the direct use of ionic fluids in analytical methods they are also examined for the crystallization of proteins.[403] An efficient crystallization method for proteins is an essential prerequisite to acquire structural information by X-ray or neutron diffraction methods that are highly important in structural biology.[404] As a result of their controllable surface tension, high thermal stability, chemical inertness and negligible vapor pressure, the neoteric solvents are also frequently suggested as versatile probe fluids for surface analysis methods.[405] A further field of interest for the usage of low temperature molten salts in analytical chemistry is their implementation in sensors for instance in the detection of gases,[406,407] biomolecules,[408,409] or ions.[410]

The last highlighted field where the low temperature ionic fluids have a strong influence is novel, *advanced materials* enabled by the use of ILs.[411,412] For instance, they offer a new liquid medium for material production even under vacuum.[413] Another notable area of IL usage are functional carbon-based materials resulting from thermal treatment of IL precursors.[414] The combined ionic and fluid nature of ILs enables a simple processing, high control over the obtained structures, incorporated heteroatoms and higher yields than obtained from thermal pyrolysis of polymer precursors.[415,416] The heteroatom- containing carbon materials resulting from the carbonization of ILs often show superior properties compared to the pure carbons, which includes higher conductivity, catalytic activity and oxidation stability.[417] Applications including electrocatalysis or new electrode materials for supercapacitors, batteries and fuel cells were shown to benefit from these novel IL-derived carbon materials.[243] New highly functional materials based on ionic liquids can also be designed by combination of ILs (or their structural motifs in polymerized ILs) with other material classes. One of these examples are thermotropic ionic liquid crystals (ILCs) that combine the characteristics of liquid crystals (LCs), for instance anisotropic physical properties and self-assembled structures, with those of ILs (conductivity, stability, adjustable interactions etc.).[163] The obtained structural motifs and transitions exhibited by the wide range of examined molecular compositions of the ILCs are highly diverse and somewhat similar to the molecular LCs.[418] Targeted applications of the ionic mesogens are mainly anisotropically conductive materials, for in-

stance realized for the conduction of protons,[419] ions[420] or via delocalized electron hopping.[421] A further class of hybrid materials enabled by ionic liquids are ionogels that consist of ILs confined in a host network. These matrices can be either of organic (such as a low molecular weight gelators and polymers) or of inorganic (for instance carbon nanotubes or silica particles) origin.[148] By this combination, the main features of the fluids like molecular mobility and ionic conductivity are retained while the confinement modifies the phase transition behavior, allows for stable shaping and avoids outflow.[422] The resulting virtually unlimited possibilities are of particular interest for the use in solid state electrolytes,[423,424] optical devices,[421] catalyst retention[425] and sensing.[426] Low-temperature molten salts based on transition metal complexes are a further interesting class of new liquid materials. Most of these MILs show an inherent paramagnetism and allow the manipulation of these compounds by an external magnetic field.[427] Attractive applications of these materials that do not suffer from sedimentation, demixing or flammability when compared to ferrofluids, can be found in the field of magnetic and magnetorheological fluids[224] or the use as extraction agents[428] as well as catalysts.[19] Although the high thermal and chemical stability of ILs is often highlighted and exploited in many uses, there are also researchers that design energetic materials based on ionic liquids that can be applied as explosives or propellants. These molten salts are specially designed to release the large amount of chemically stored energy when a specific trigger, such as heat, shock or friction, is applied.[168] These energetic ILs show a captivating property combination compared to conventional energetic materials, for instance low melting temperature, broad liquid range, thermal stability and often more environmentally friendly properties.[168] The usually reduced sensitivity to triggers, *e.g.* heat, shock etc., also makes handling, transport and storage safer compared to conventional energetic materials. In addition, the problem of polymorphism and shock sensitivity present in solid energetic materials is inherently avoided if they can be kept in liquid state.[429] The volatile hydrazine and its derivatives are often used as hypergolic liquids in rocket propellant systems despite many concerns about safety, difficulty in handling as well as their acute toxicity and cancerogenity.[430,431] An alternative to the propulsion with hydrazine that avoids these drawbacks is the use of energetic ILs which were reported to additionally show high stability, ultra-fast ignition times and good ignition performance.[432] They can be either combined with an appropriate oxidizer as bipropellant (hypergolic ILs) or used as single-compound, monopropellant energetic ILs (realized by oxygen balance compounds).[169,433] Using salt propellants instead of liquid hydrazine also increases the energetic density, thus providing benefits for satellites such as longer mission durations, increased payload and simplified processing of the launch. The demonstration of a monopropellant based on the ionic liquid hydroxylammonium nitrate as fuel/ oxidizer is implemented in the NASA project called 'Green propellant infusion mission' (GPIM).[434] The mission is aimed to prove the decreased toxicity due to the combustion to nontoxic gases combined with higher performance of the energetic IL propellant in practice. The launch of a satellite bus utilizing the GPIM is planned for March 2019 and is aimed to show that energetic ionic liquids might be an alternative propellant of choice for next generation launch vehicles or space crafts.

To sum this chapter up and to give a retrospective justification of the initial quote[1] given by Prof. Dr. Hermann Weingärtner, the applications of ILs are extremely diverse, making a rational design and tuning of their molecular structure indispensable. Therefore, an advanced knowledge about the synthesis, structure-property-relations and macroscopic properties of ILs is crucial for the optimization of performance due to the nearly infinite possibilities offered by the ionic liquids toolbox.

1.5 Structural organization in ionic liquids – microscopic effects with macroscopic impact

Liquids are essential in modern technologies and involved in the most different fields that include fabrication and production (*e.g.* pharmaceutics, food, polymers and chemicals), processing (*e.g.* extractions, analytics, energy storage and surface modifications) and transportation processes (*e.g.* heat, propellants, fuels and lubricants). Yet the description of the molecular organization in liquids remains a challenge since they form an intermediate state of matter between solid and gaseous which still lacks a unified theoretical description.[86] Since the underlying molecular interactions and structuring of a liquid phase determines the macroscopic behavior, a detailed understanding of their effects, manifestations and interrelations is important. This holds true for both basic science and practical implementations. The underlying molecular design has therefore a large impact on the physical and chemical properties of the liquid phase and allows the tuning of micro- and macroscopic properties in a desired way. This holds especially true for the case of ILs as there is distinct evidence for their pronounced structuring on different time and length scales by theoretical, computational and experimental results.[25,435] However, at the beginning of the research on ILs they were first believed to possess a time-averaged homogeneous, irregular structure with the ions undergoing Brownian motion in the absence of pronounced structural features.

Compared to molecular liquids or high temperature molten salts, the low temperature molten salts show additional molecular interactions with the Coulomb interactions being the dominating ones for the macroscopic properties. Nevertheless, the contribution of other molecular interactions can also have a significant influence on the ILs' properties and liquid structure, both in the bulk and near to interfaces. The molecular interactions in ILs range from weak, isotropic and nonspecific forces, such as van der Waals forces, over solvophobic and dispersion forces to specific and anisotropic ones like, *e.g.* hydrogen or halogen bonding as well as dipole-dipole or electron donor-acceptor interactions.[25] Overall, the combined strength and diversity of the intermolecular interactions existent in ILs are responsible for their behavior differing from conventional molecular liquids and the formation of higher order arrangements in the bulk ionic fluids. For the case of simple, non-functionalized ILs, a liquid structure with nanoscale ordering of near ions and disorder on longer scales is usually observed.[43] The near-order arrangement is thereby the result of the balance between charge-charge attraction as a result of the Coulombic forces against the translational, rotational and vibrational motions of the constituting ions. However, for most ILs investigated from a structural point of view so far,

the situation seems to be more complicated. Furthermore, the structure is, as already mentioned, sensitive to other interactions so that slight changes in molecular structure can have a significant influence on the structuring. The structural motifs reported in ILs on different length- and time-scales are shown in *Figure 7* as an overview. These structures range from supramolecular aggregates (ion pairs[436] and ion clusters[437]) over mesoscopic structures (hydrogen bond networks, multicontinuous networks, formation of micelle-like structures) to ILs forming different kinds of mesophases (ionic liquid crystals). Usually the structural motifs found in the liquid state (preferred ion-arrangements, H-bonds, domain formation,...) are also often present in the crystalline state, *nota bene* with much higher spatial order.[438] This makes the determination of the single crystal structure helpful to get insights in the organization in the liquid state where similar structuring is present but with a lot more disorganization. Initial hints on the unique structuring and solvent behavior of ILs were observed quite early when they were found to dissolve both polar and nonpolar compounds. These findings were in contradiction with the established models of solvents with uniform polarity that preferably dissolve either polar or nonpolar materials according to the 'like dissolves like' principle. The different, complex interactions and structures present in ILs with polar and nonpolar parts could later be attributed to be the cause for this mixing and dissolution behavior.[439]

As the structural features are very diverse and sensitive to modifications of the molecular structure,[440] only a general overview of the liquid state structures and trends will be given in this section. Likewise, the discussion of the ionic liquid crystal phases that resemble the diversity of conventional liquid crystals[162,163] are excluded. Furthermore, it should be noted that external triggers as the presence of solutes may influence the structuring of the liquid phase.[25,441]

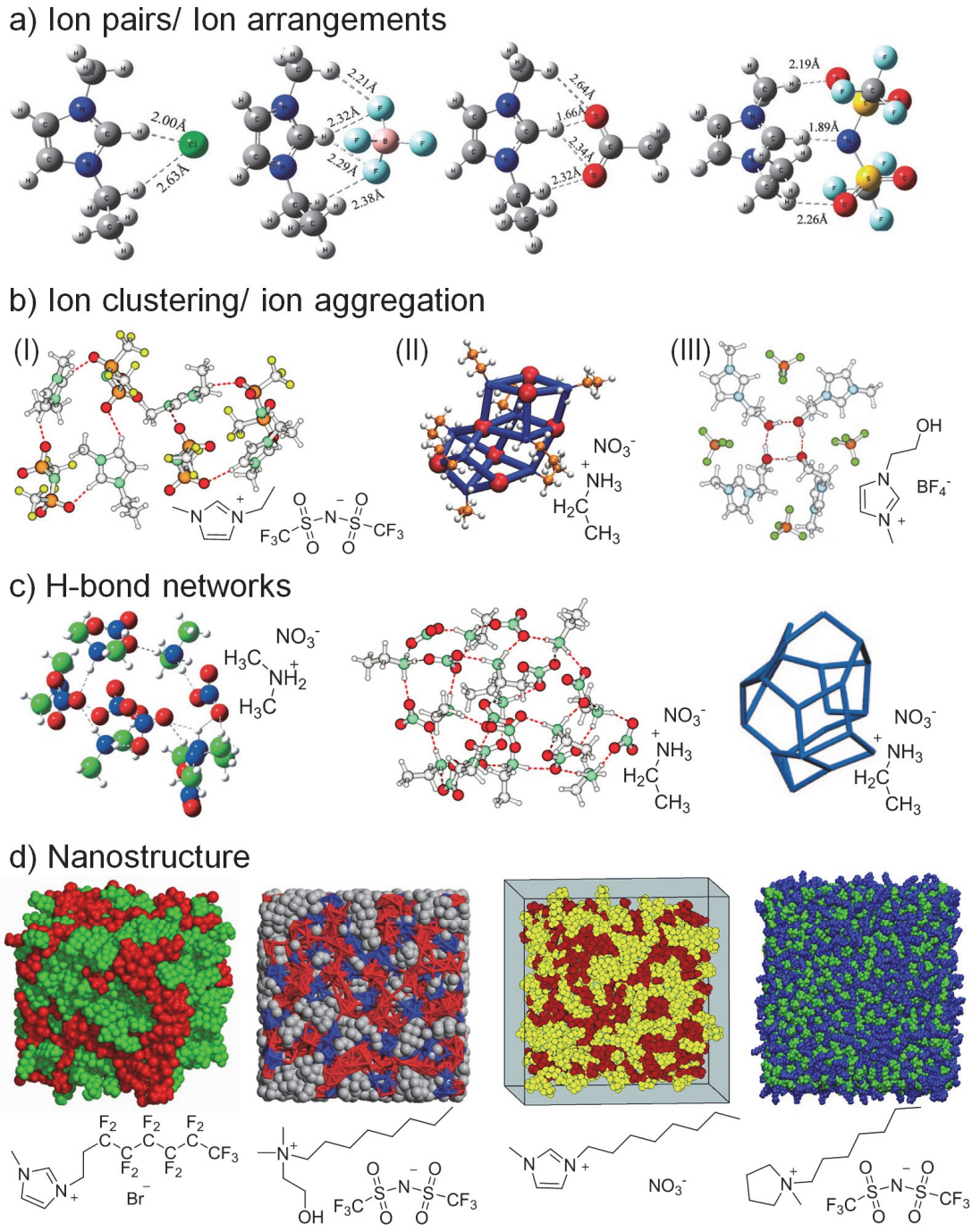

Figure 7: Overview of the different levels of structural organization in ionic liquids with increasing spatial and time scale from top to bottom. a) ion pairs as simplest repeating unit in ILs with calculated energetically favorable distances leading to preferred arrangements of ions and hydrogen bonding in aprotic ILs. A series of 1-ethyl-3-methyl-imidazolium cations with the anions being chloride, tetrafluoroborate, acetate and bis(trifluoromethanesulfonyl)imide is shown (adapted from ref.[158]). b) exemplary formation of ion clusters or aggregates in a common aprotic IL (I), a common protic IL (II) and a hydrogen bonding aprotic IL (III) with corresponding molecular structures (adapted from ref.[442–444]). c) hydrogen bonding networks for ILs with multiple hydrogen bond donor and acceptors (adapted from ref.[110,442,445]). The right hand side graphic shows the connections of anion and cation nitrogen in ethylammonium nitrate that build up the network. d) self-assembled liquid structures of various ILs (adapted from ref.[446–449]). Polar and apolar domains are labelled by different colors.

Pairs of cations and anions are the smallest building blocks in ionic liquids and their interactions and preferred orientation[450] is therefore of special concern for the description of the liquid structure of the neoteric solvents. This is somewhat in analogy to conventional high temperature salt melts although there are more diverse interactions present in the case of ionic liquids. The type and extent of the interactions between ion pairs is also of interest for the rationalization and prediction of key physical properties such as melting point and viscosity, for instance.[446] Many researchers have tried to describe the ionic liquid structure by a heuristic approach in terms of ion pairs with additional 'free' ions.[451] Some low temperature molten salts are also reported to evaporate as ion pairs[452,453] under more extreme conditions, which is a hint that ion pairs might also be present in the bulk liquid state. Ion pairing is also well known and described for diluted electrolyte solutions[454] so that this phenomena of spatially tight, persistent ion pairs can be expected to occur also in the concentrated ionic media. Up to date, there are remaining controversies about the existence or absence of ion pair or ion aggregates in bulk IL as there are experimental and computational results both in favor and against this hypothesis.[25,455] Some results by dielectric[456] and FTIR-spectroscopy[457] as well as multinuclear NMR[458], NMR dispersion[459] and surface force measurements[460] support this picture. However, the majority of recent scientific results find no evidence for the formation of long-lived ion pairs.[25] Dielectric spectroscopy measurements that are capable to reveal the pico- to nanosecond dynamics in liquid state find no verification for ion pairs on this time scale for both protic[461] and aprotic[462,463] ILs. Similar conclusions were drawn from solute phenomena associated with dissolution[464] or kinetics induced by the reaction media.[465] A variety of computational results also contradicts the assumption of persistent ion pairs by finding no evidences for correlated motions on longer timescales.[466–468] The MD trajectories reveal that each ion in bulk ILs is surrounded by a counter ion solvation shell with charge ordering shells over large distances making an interpretation of neutral ion pairs hardly justifiable.[466] For the exemplary IL $[C_4C_1IM][PF_6]$, the ion interactions could be described by an ionic atmosphere rather than dynamics coupled to a particular counterion.[467] Contrary to the situation found in undiluted ILs, there are many reports about the formation of close ion pairs in IL solutions[469–471] or upon dilution with molecular solvents.[457]

Similar to molecular liquids and the quantum cluster equilibrium approach,[472] the ionic liquid state was often modelled by fluctuating clusters of different amount, life-times and sizes.[25,473] In analogy to the description by 'ion pairs' and 'free ions', the IL bulk structure was attributed to be the sum of different populations of overall neutral and charged clusters.[438,474] There are indeed analogies in the experimental results, for instance the formation of binary mixtures with molecular liquids.[475–477] It should also be noted that the interpretation of clusters in ILs' neat state should be treated with care since there are no clear definition criteria of ion clusters. Most of the experimental results that point towards the existence of ion aggregates are from electrospray ionization - mass spectrometry (ESI-MS).[443,478–480] The findings indicate fluctuating polydisperse aggregates with the formula $[C]_x[A]_y^{x-y}$ in the bulk with a series of postulations drawn, for instance the occurrence of certain 'magic' numbers[479] or empirical descriptions for the

association of ions.[480] Some researchers pointed out that the violent nature of fragmentation by ESI-MS may have a contribution to the detection of ion clusters and that the obtained results require additional proof.[25] The observation of shear thinning in rheological measurements in some ionic liquids also indicates larger persistent aggregates that are reduced in size upon shearing or increasing temperature.[481] Further evidence for ion clustering is provided from vibrational[482] and NMR[483] spectroscopy and quantum chemical calculations that were capable of reproducing experimentally determined IR spectra of multiple ion clusters.[484] Particular clusters of like-charged ions can also be formed by hydrogen bonds if hydroxyl groups are attached to the cations.[157,437,444,485,486] Comparable formation of aggregates at the gas-liquid interface has also been reported for both PILs[487] and AILs.[488] In these systems, the hydrophobic alkyl groups were found to shield the charged moieties by their alignment towards the gas phase. Additional evidence for clustering is revealed by computational and neutron scattering methods that find a sub-diffusive behavior of ILs in molecular cages on the picosecond time scale.[435,489–491] The diffusion coefficients on this short time scale are reported to be significantly higher than the ones measured or computed for higher time scales, similar to the diffusion in polymeric networks or supercooled liquids.

The strength of hydrogen bonds between cation to anion in PILs were detected to be commonly in the range of 50 kJ mol^{-1}.[492–495] Therefore, the H-bonds in PILs can be classified as moderate to strong bonds that have a significant contribution to the total interaction energies and to the observed liquid structure.[492–495] Furthermore, the time scales on which hydrogen bonds exist have a significant contribution to the mobility of ILs.[496] It is therefore not surprising that there are a variety of reports on ILs forming three dimensional networks via hydrogen bonds that can hence be classified as associated fluids. The discovery of three dimensional hydrogen-interconnected ions in ILs was as early as 1982 by a study on the gas solubilities in ethylammonium nitrate.[497] Most of the first reports about hydrogen bond interconnected structures were on PILs with two or more H-bond donors and acceptors, such as mono-[497] or dialkylammonium[110] nitrates. Later results also confirmed the existence of this structural motive for AILs, especially the ones based on imidazolium cations.[498–500] In these cations, the three hydrogens attached to the carbon atoms in the aromatic ring participate in hydrogen bonding although with different contributions.[501] The manifestation of the H-bond network in the imidazolium AILs is more pronounced when good hydrogen bond acceptors, like halides,[502,503] chlorometallates[504] or tetrafluoroborates,[498] are used.

The existence of mesoscopic structures that represent an intermediate between molecular liquids and liquid crystals is nowadays well established and deciphered for a large number of low temperature molten salts.[25] Regardless of the scientific consensus about the presence of this structural motif, there are various terms to designate this higher order structure such as micro-,[505,506] nano-[25,62] or mesoscopic[507,508] structure without clear distinction. The understanding of this particular solvent structural feature is regarded as a key in understanding their physicochemical properties needed for a focused control and tuning of their bulk properties.[509] Most of the ILs investigated have a distinct degree

of order in the liquid state with heterogeneities on the spatial scales of about a few nanometers.[26,509] The sophisticated understanding of this phenomenon and its consequences is mainly the result of the synergy between molecular dynamics simulations and experimental results based on diffraction methods.[508] The unique spatial heterogeneity[510] is the result of the amphiphilic structure consisting of polar, ionic moieties and nonpolar fragments usually comprising of alkyl side chains present in ILs.[62,191] This effects of unfavored interactions of molecular fragments with different polarizabilities are often attributed as hydrophobic or lipophobic interactions similar to the macroscopic effect of demixing found for solvents with sufficiently large polarity differences. A more general term that is also often used is the so called 'solvophobic effect'. The thermodynamic origin of the aggregate formation on nanoscale is the minimization of the system's free energy. This amphiphilic nature of most IL ions is also reported to support the self-assembly of other amphiphiles.[62]

A general trend in the bulk structure for 1-alkyl-3-methyl-imidazolium [C_xC_1IM] ILs is the pronounced nanosegregation into polar and nonpolar domains with increasing length of the attached alkyl chain, relatively independent of the anion.[511] The occurrence of nanosegregation in IL with the [C_xC_1IM] cation was proven for halides,[512] [BF_4],[160] [PF_6],[513,514] [NTf_2],[515] anions as well as for symmetrical [C_xC_xIM][NTf_2] ILs.[516,517] For most of these imidazolium systems an incorporated butyl side group was sufficiently long to induce a mesostructure rather than a globular, uniform distribution of the hydrocarbon side chains. This solvophobic effect and the resulting change of liquid morphology with increasing nonpolar moieties are visualized by snapshots from molecular simulations in *Figure 8*. For the [C_xC_1IM] ILs, the change in solvent morphology is also adaptable to explain the progression of the melting temperatures with increasing x.[160] While short alkyl chains (x = 1-3) lead to salts with comparable strong interactions, intermediate chain lengths (x = 4-10) show wide liquid ranges and high tendencies to form glasses as a result of the more disordered liquid state.[160] At higher chain lengths (x > 10) the ionic liquids often show a more complex crystalline behavior being the consequence of a more stabilized nonpolar nanostructure. Besides the incorporation of elongated alkyl groups in the cations which is more commonly applied, it is also possible to obtain the structural heterogeneity of polar and nonpolar domains by attaching hydrocarbon moieties of sufficient length to the anion.[518]

The presence of mesostructured aggregates is most widely investigated for AILs consisting of imidazolium cations. Similar structural heterogeneities and trends upon increasing the alkyl chain lengths were also found for pyridinium,[519] piperidinium,[440,520] pyrrolidinium,[521–523] ammonium[521,524,525] or phosphonium[526,527] based cations without further functionalization. The segregation in nonpolar hydrocarbon domains is suppressed if more polar or flexible groups, such as hydroxyls or ethers, are present in the side chains.[157,528,529] The occurrence of a pronounced nanostructure is not only limited to aprotic ILs but also found in a variety of protic ILs where even shorter chains are sufficient for domain formation.[159] A reason for this finding may be the presence of directional hydrogen bonds that stabilize certain anion-cation geometries. In the case of ethylammonium nitrate, the solvophobic separation induced by the ethyl groups was reported to

be strong enough to yield long-range structures similar to those of bicontinous microemulsions or L_3-sponge phases.[157]

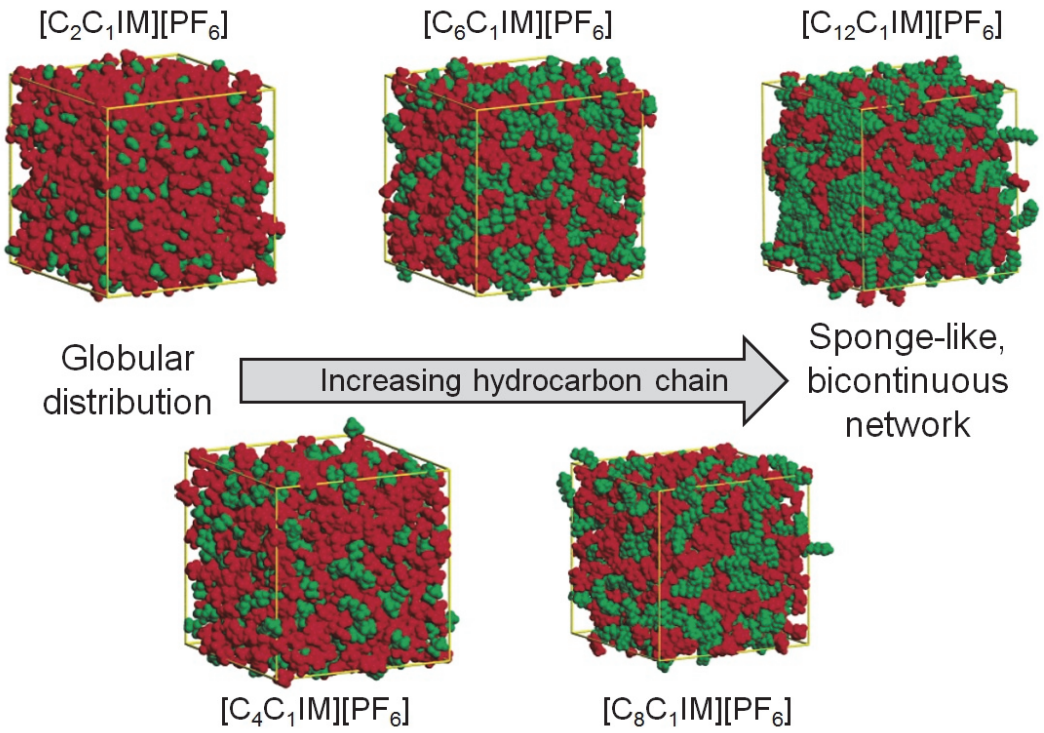

Figure 8: Snapshots of molecular simulations of 1-alkyl-3-methyl-imidazolium hexafluorophosphate ILs $[C_xC_1IM][PF_6]$ (x = number of carbons in the hydrocarbon fragment) with increasing alkyl chain length. Each box contains 700 ions at equilibrium. Polar domains (imidazolium core of the cation and anion) are colored in red while the nonpolar moieties (hydrocarbon chain attached to the cation) are shown green. The bulk structure shows a gradual transition from globular distribution of ethyl groups in a polar network ($[C_2C_1IM][PF_6]$) with increasing domain size ($[C_4C_1IM][PF_6]$ to $[C_8C_1IM][PF_6]$) to sponge-like structures with a bicontinuous three-dimensional network of polar and nonpolar domains. Boxes are not equal in size due to different cations sizes and liquid densities. Figure was adapted from ref.[513]. Similar structure evolution was also reported when the $[NTf_2]$ anion is used.[530]

Most of the reports about the bulk mesoscopic nanostructure mentioned above are the combined results of experimental scattering data from either X-ray or neutron diffraction methods as well as computational results that generally complement each other.[25,526,531,532] A common finding of the ILs' diffraction patterns from small-angle scattering techniques is the occurrence of two or three peaks. The three characteristic peaks found for ILs are a result of atomic environment (adjacency peak, high values of the scattering vector q), the charge alternation of cation and anion (charge peak, intermediate q values) and the mesoscopic organization (polarity peak, low q values).[515,533] The first two features were found for all types of ILs unless the peaks and antipeaks do not cancel each other due to the same spatial periodicity but phase offset.[522,526] The polarity peak at low q values (thus larger real space distances) is only found if sufficiently long alkyl groups are present in either the anion or cation.[25,160,515,531,534] This polarity peak was

shown to be the result of the segregation into polar and nonpolar domains with different polarity on molecular scale.[533] Exemplary small-angle X-ray diffraction patterns and computational results are shown in *Figure 9*.

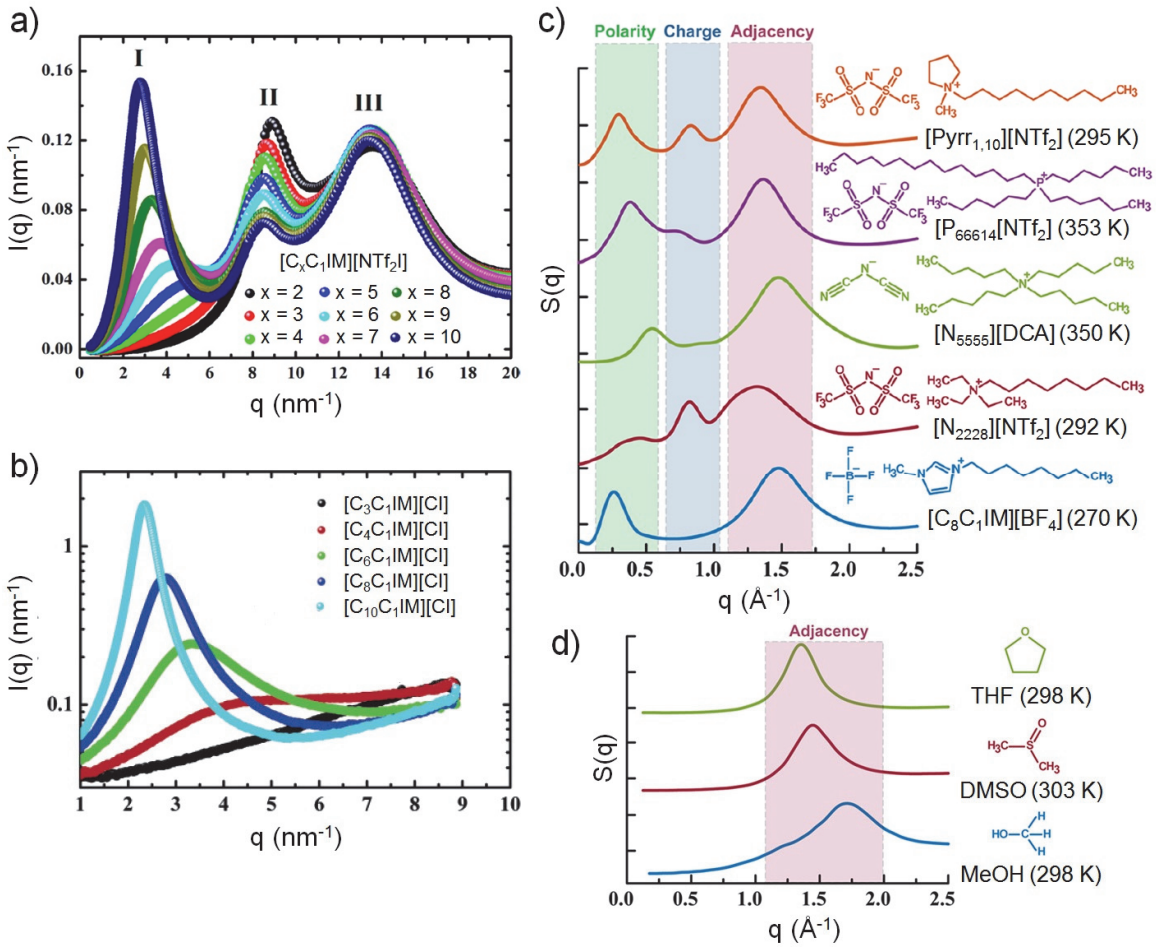

Figure 9: Experimental small-angle X-Ray diffraction patterns of a) $[C_xC_1IM][NTf_2]$ ILs and b) $[C_xC_1IM][Cl]$ with increasing carbon numbers x in the alkyl tail at 298 K. The patterns show a peak at low values of the scattering vector q as an indicator for the formation of hydrocarbon domains leading to nanoscale segregation (adapted from ref.[515] and [160]). Roman numerals in a) indicate the three characteristic peaks found in the diffraction patterns of ILs (I: polarity peak; II: charge peak; III: adjacency peak). The occurrence of the polarity peak in b) for the butyl side chains shows that hydrocarbon tails equal to and larger than butyl induce a nanostructure with polar and nonpolar domains. Furthermore, it can be seen that the structure becomes more pronounced with increasing length of the hydrocarbon fragment. The resulting structure function S(q) for c) a series of ionic liquids and d) conventional molecular liquids (adapted from ref.[533]). In the case of ILs, three peaks are observable in reciprocal space: The peak at high q values is associated with adjacency correlations of neighboring atoms (adjacency peak) whereas the one at intermediate q is the result of the charge alternation inherently present in ILs (charge peak). The peaks at the lowest q values are assigned to the polarity alternation as a cause of the microsegregation present in the bulk state (polarity peak). In contrast to that, the molecular solvents only show an adjacency peak. Note that the absence of the peak at intermediate q values for the imidazolium $[BF_4]$ IL is the result of the peaks and antipeaks that cancel each other out and does not mean that this structural feature is absent.

Besides these methods for the direct detection of the domain size by scattering methods, there is also a large variety of other experimental techniques that confirm the existence of nanoscale aggregation. This includes spectroscopic methods such as NMR,[535,536] EPR,[537] Raman,[538] or dielectric relaxation,[539] as well as optical Kerr effect studies.[539] A direct consequence of the non-uniform nanoscale structure is the observation of dynamic heterogeneities in ILs[483,540,541] that lead to altered relaxation dynamics.[542] The addition of perfluorocarbon groups either to the anion or cation leads to another solvophobic interaction in addition to the ones usually present in bulk ionic liquids which in consequence alters the nanostructure. These triphilic ionic liquids,[543] consisting of polar-ionic, nonpolar hydrocarbon and nonpolar fluorocarbon domains, will be discussed in more detail in the following section.

1.6 Ionic liquids with fluorinated alkyl groups – synergy from extremes?

The replacement of hydrocarbon moieties with perfluorinated groups is a long used method in chemistry for selective modification of the structure and properties of molecules, complexes or active pharmaceutical ingredients.[544,545] The special characteristics of the carbon-fluorine bond are the underlying reason for the altered properties of the fluorocarbon groups compared to the hydrocarbon analogues. With an average binding energy of 480 kJ mol^{-1} the covalent bond between carbon and fluorine is one of the strongest single bonds in organic chemisty.[544] This leads to the high thermal stability and chemical inertness of fluorocarbon compounds. With bond lengths around 1.4 Å the C-F bond is also relatively short. Due to the small van der Waals radius of the fluorine substituent (R_{VdW}(F) = 1.47 Å[89]), which is shorter than any other substituent and close the one of hydrogen (R_{VdW}(H) = 1.10 Å[89]), there is no strain in perfluorinated carbon chains. This is a further reason for the high thermal stability of fluorous groups on the one hand and leads to a shielding of the carbon atoms from reactive species on the other hand. As a result of the comparably large difference in the electron negativity of carbon (χ(C) = 2.55 by Pauling scale[89]) and fluorine (χ(F) = 3.98 by Pauling scale[89]), the C-F bond has a high dipole moment of 1.41 D.[544] As the polarizability of the fluorine atom in the ground state is the lowest of all elements with a value of 0.56 × 10^{-24} cm^3,[89] the dispersion forces between perfluorinated molecules are very weak. This usually leads to lower boiling points than observed for the analogous hydrocarbons as well as simultaneous hydro- and lipophobicity, often referred to as fluorophilicity.[546]

By increasing the amount and length of perfluoro groups, the fluorophilicity of a molecule, complex etc. can thus be selectively adjusted. The incorporation of these so called fluorous tags or ponytails in the periphery usually does not change the reactivity of a particular compound. This enables a liquid phase chemistry orthogonal to the one in conventional hydrocarbon-based solvents. The fluorophilicity of the perfluoro-segments leads to miscibility gaps in the binary phase diagrams of perfluoro and hydrocarbon solvents with upper critical solution temperatures as a common finding.[547] Therefore, biphasic systems that form a homogeneous single phase at elevated temperatures are

commonly observed when fluorous solvents and conventional organic solvents are combined.[548] This temperature regulated mixing behavior can for example be exploited for catalyst retention in biphasic reactions (often termed 'fluorous biphasic catalysis'[549]) or for selective extractions. Observations similar to the thermoregulated macroscopic mixing and demixing behavior of fluorous liquids with other liquids can be made on the molecular scale. For example, mixtures of short-chain perfluorinated alcohols and water have been shown to segregate strongly into highly lipophilic perfluoroalkyl domains and into highly hydrophilic domains consisting of water clusters, a finding not observed for small hydrocarbon alcohols.[550]

Perfluorinated compounds are of high technical relevance in spite of environmental problems associated with the use of some representatives.[551] This mainly includes the ozone depletion potential of volatile fluorous liquids and the persistence of ionic representatives, such as salts of the perfluorooctane sulfonic acid, that were widely used as surfactants until being listed in Annex B of the Stockholm Convention on persistent organic pollutants.[552] Properties, interactions and phase behavior similar to the ones observed for molecular species with fluorinated parts mentioned above are also found for ionic liquids either in bulk (chemical and thermal stability, strong electron withdrawing character of fluorine substituents, fluorophilic interactions, inertness of perfluorinated groups) or in mixtures with other compounds (interactions with and structuring at surfaces, mixing/demixing behavior towards other liquids).

Ionic liquids that contain fluorinated alkyl groups can be divided into two large subclasses according to the influence of fluorous segments on the structure and physicochemical properties. The first class consists of ILs with short fluorocarbon segments of the general formula $-(CF_2)_nF$ with $n \leq 3$ while the other group contains perfluorinated moieties with longer perfluorocarbon chains ($n \geq 4$).[553] The latter group is often denoted as fluorinated ionic liquids (FILs),[553] whereas for very high amounts of fluorine the term fluorous ILs[554] is occasionally used, however without clear differentiation criteria. It should be noted that although the distinction is somewhat arbitrary, it is nevertheless quite helpful to distinguish from a physicochemical property point of view. The difference between the two classes is mainly in the pronounced structuring due to solvophobic/fluorophilic interactions if chains of four or more fluorinated carbons are present. This generally leads to stable microscopic structures along with increased melting points,[555] surface activity[556] and viscosities[557] as well as to high gas solubilities[558] and densities.[553]

Short perfluorocarbon groups, the trifluoromethyl moiety being the most frequent, are commonly applied in a wide range of IL-forming anions, as the obtained low temperature molten salts show in general beneficial properties. The resulting ILs do not show any marked characteristics associated with fluorous behavior (besides the fact that they are usually hydrophobic) which distinguishes them from the FILs discussed in the next paragraph. Often used perfluorinated anions are, for instance bis(trifluoromethanesulfonyl)imide ([NTf_2] or [$N(SO_2CF_3)_2$]), trifluoromethanesulfonate ([OTf] or [SO_3CF_3]), trifluoroacetate ([TFA] or [CO_2CF_3]). The similar structural motifs are also frequently ap-

plied in asymmetric combinations such as the trifluoro-N-(trifluoromethanesulfonyl)acetamide[559] ([$N(SO_2CF_3)(COCF_3)$]) or trifluoromethanesulfonyl-N-cyanoamide[560] ([$N(SO_2CF_3)(CN)$]) as well as homologues with elongated fluorinated chains, for instance the bis(pentafluoroethanesulfonyl)imide[561] ([BETI] or [$N(SO_2(CF_2)_2F)$]), bis(perfluorobutanesulfonyl)imide[562] ([NNf_2] or [$N(SO_2(CF_2)_4F$]), nonafluorobutanesulfonate,[557] ([$SO_3(CF_2)_4F$]) and perfluoroalkylcarboxylate[558,563] anions ([$CO_2(CF_2)_xF$]). Less frequently used are anions like the tris(pentafluoroethyl)trifluorophosphate[564] ([FAP] or [$P((CF_2)_2F)_3F_3$]), bis[bis(pentafluoroethyl)phosphinyl]imide[565] ([$N(PO((CF_2)_2F)_2)_2$]), bis(trifluoromethyl)phosphinate[560] ([$PO_2(CF_3)_2$]), perfluorotrifluoroborates[566,567] ([$B((CF_2)_xF)F_3$]), perfluoroalkyltricyanoborates[568] ([$B((CF_2)_xF)(CN)_3$]), perfluoroalkylcyanofluoroborates[568] ([$B((CF_2)_xF)(CN)_yF_z$] with $x \geq 1$ and $y+z = 3$) and tris(trifluoromethanesulfonyl)methanide[569,570] ([$C(Tf)_3$]). The very strong electron withdrawing character of the perfluoroalkyl groups also makes stable hydrophobic ILs with perfluoroalkoxides, such as the perfluoro-*tert*-butoxide anion[571] ([$OC(CF_3)_3$]), accessible.[571] These anions utilize the high electronegativity of the fluorine atoms to achieve a diffuse negative charge and poor participation in hydrogen bonding.[572] A direct result of the very low polarizability of the fluorinated groups and the absence of H-bonds in ILs with these anions is that they are usually hydrophobic. The formation of a biphasic mixture in combination with water is therefore a common finding although the measured polarities of these ILs are relatively high compared to hydrophobic molecular solvents.[28] The incorporation of the small trifluoromethyl group yields small anions with a comparably low degree of symmetry. Therefore ILs based on these anions tend to have beneficial properties such as low melting points or only glass transitions, along with low viscosity and high conductivity.[573] In general the utilization of slightly longer perfluorinated segments in the anions has a negative effect on the transport properties[568] but may nevertheless be beneficial to decrease melting points or increase hydrophobicity. Furthermore, ILs with these anions generally show high chemical, electrochemical and thermal stability as a result of the inertness and electron withdrawing character of the perfluorocarbons.[572,574] Hydrolysis is also not reported for anions with perfluorocarbon segments, as it was found for other fluorine containing anions such as [BF_4] and [PF_6].[575] As a consequence of this favorable combination of properties, the trifluoromethyl group is present in many ILs with high performance, especially in those used for electrochemical applications.

Notwithstanding the widespread presence of short fluorinated alkyl groups in the anion, these structural motifs are seldom utilized in the cations. The reason for this is the strong electron withdrawing character of the fluorine atoms that increases the localization of the positive central charge leading to a negative impact on their properties. In particular this holds true when compared to the nonfluorinated hydrocarbon analogues. For example the melting point of 1-methyl-(3,3,3-trifluoropropyl)-imidazolium hexafluorophosphate was found to be 75°C[576] and by that notably larger than the one for 1-methyl-3-propyl-imidazolium hexafluorophosphate (T_m([C_3C_1IM][PF_6]) = 38°C),[577] although the perfluoro functionalization is spaced by two methylene units. However, the influence on other physicochemical properties is only sparsely studied and only selective investi-

gations are given in the literature. One example is the viscosity of 1-methyl-3-(2,2,2-trifluoroethyl)-imidazolium [NTf_2] ($\eta^{35\,°C}$([$(F_3CCH_2)C_1IM$][NTf_2]) = 55.1 mPa s)[578] that is nearly twice as high as the one of the comparable alkyl IL ($\eta^{35\,°C}$([C_2C_1IM][NTf_2]) = 23.7 mPa s)[579] while at the same time the conductivity of the fluorinated IL ($\sigma^{35\,°C}$([$(F_3CCH_2)C_1IM$][NTf_2]) = 1.92 mS cm^{-1}) is significantly lower than for the alkyl one ($\sigma^{35\,°C}$([C_2C_1IM][NTf_2]) = 11.9 mS cm^{-1}).[580]

Contrary to the ILs mentioned above, the attachment of perfluorocarbon tags leads to pronounced nanostructural organization that is the reason for the highly altered macroscopic properties of FILs.[581] The resulting compounds combine IL-specific characteristics as well as properties that stem from their partial fluorous nature, making them an outstanding class of new liquid materials.[553,557,581] Similar to the attachment of sufficiently large alkyl segments, the incorporation of perfluorinated moieties induces segregation into polar and nonpolar nanodomains, as a result of solvophobic interactions.[582] As the fluorous groups are even more lipophilic and show enhanced chain stiffness than the hydrocarbon analogues, this structuring is more pronounced in the case of the FILs,[25] which was attributed to increased dispersion interactions.[583] However, this does not necessarily lead to a stabilized crystal structure as the symmetry of cations might be decreased by introduction of both fluorocarbon and hydrocarbon chains.[584] If both alkyl and fluorous groups of sufficient length scales are present, some ILs were found to yield self-assembled nanostructures consisting of polar-ionic, nonpolar hydrocarbon and nonpolar flurorocarbon domains.[585] Accordingly, the FILs show an advanced tunability and highly controllable solvent properties that are defined by the size of the three nanodomains and the contribution of the different interactions.[586] As a result of the segregation into three domains, the FILs are also frequently termed triphilic materials.[543]

The domain formation, for example, was proven for a series of PILs with perfluorocarboxylate anions, whereas a similar structuring was not found for the corresponding nonfluorinated hydrocarbon carboxylates.[587] The nanosegregation of FILs in bulk was proven by MD-simulations,[532,581,582,585,588] X-ray[543,581,587–589] and neutron scattering experiments[581,588,589] as well as NMR spectroscopy[190,543,581] for both protic and aprotic IL representatives. Exemplary experimental scattering patterns and snapshots of simulation boxes are shown in *Figure 10*. The nanostructural organization into polar, hydrogenated apolar and fluorinated apolar domains was also reported for mixtures of FILs with alkyl alcohols in dependence on their ratio.[590] These unique structural features of FILs are also believed to be the reason for the rich phase behavior of some representatives that show different solid-solid transitions.[582,585]

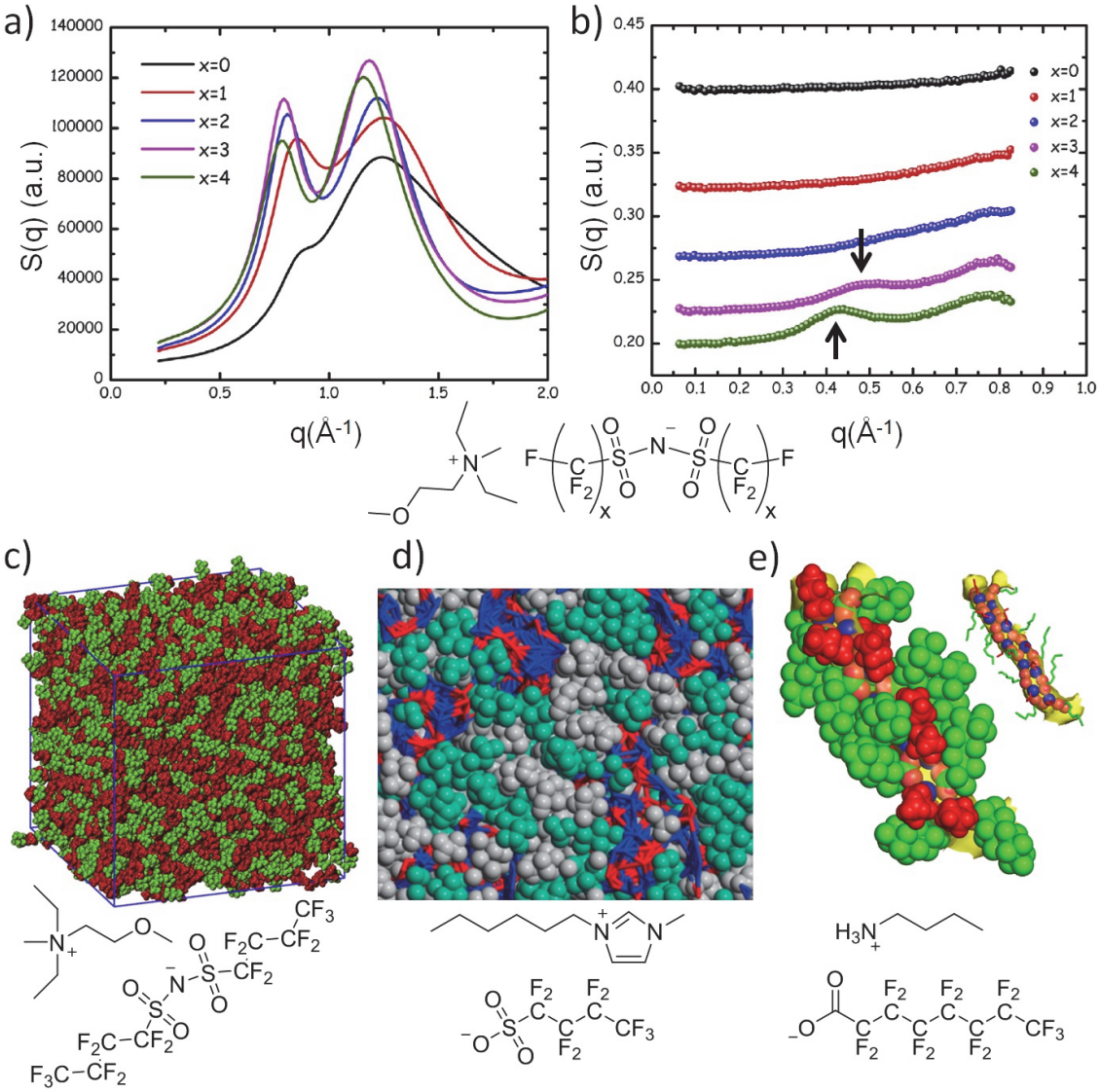

Figure 10: Scattering patterns of the diethylmethyl(2-methoxyethyl)ammonium ([DEME]) cation paired with imide anions of the composition $[N(SO_2(CF_2)_xF)_2]$ ($0 \le x \le 4$) obtained by a) medium angle X-ray and b) small-angle neutron scattering experiments at ambient conditions (adapted from ref.[581] and [589]). The indicated low q-peak is emerging in the neutron scattering patterns for x being equal or greater than 3. This peak at low q-position is a fingerprint for the fluorous domains that are only formed if the perfluorinated chains are long enough. It is therefore absent for $x \le 2$. c) Snapshot of a simulation box for [DEME][$[N(SO_2(CF_2)_4F)_2]$].[589] Perfluorinated segments are colored in green whereas all other molecular fragments are red. d) Molecular dynamics (MD) simulation snapshot of 1-hexyl-3-methyl-imidazolium nonafluorobutanesulfonate.[585] Ionic subunits are given in red (negative charge) and blue (positive charge) and represent the polar network. Grey spheres are the hydrogenated nonpolar domains, while green spheres correspond to the fluorinated nonpolar domains. e) Single filament of butylammonium pentadecafluorooctanoate from MD simulations.[532] The hydrogen bonded filaments are a section of a continuous triphilic network (see the insert). Cationic alkyl tails are colored in red and fluorous tails in the anion in green.

The FILs were also demonstrated to reduce the impact of the addition of water to the ILs' ability for hydrogen bond acceptance compared to conventional ILs, yielding task-

specific materials with enhanced solvent quality and tunability.[586] As a result, the FILs were suggested for the dissolution of biomolecules, extractions or material design.[586] In addition, the unique interactions of FILs can also be used in combination with carbohydrates to create aqueous biphasic systems as benign alternatives for extractions.[591] FILs were also investigated for drug delivery of the protein lysozyme since they had no negative effect on its stability and were able to retain the enzyme's hydrolytic activity.[592] As a result of the inherent amphiphilicity through the presence of both an ionic and a highly apolar part in one ion, the FILs are often highly active surfactants.[556,593,594] This allows for example the emulsification of molecular perfluorinated compounds in conventional non-fluorinated ILs.[593] In addition, it was shown that FILs with fluorinated groups in both anion and cation reduce the surface tension of water to a much greater extent than a single perfluoro fragment in either the cation or the anion.[595] A general trend found for the FILs is the comparably high gas solubility[596] similar to the gas-philic properties of molecular fluorinated compounds.[597,598] This has been mainly investigated for oxygen,[558] but also for other gases to some extent.[599,600] Consequently, the FILs were proposed as electrolytes in metal-air-batteries[558] or oxygen therapeutic emulsions.[553,601] The high gas solubility of the FILs also can be applied for gas separation in FIL-polymer membrane composites.[602,603] If enough and sufficiently long perfluorocarbon segments are introduced into the molecular structure, the resulting ILs show a high fluorophilicity with some properties similar to perfluorinated solvents.[604,605] These highly fluorophilic ILs can, for instance, be utilized in biphasic catalysis to form a non-volatile fluorous phase[554] or for the preparation of composite materials with PTFE that do not suffer from bleeding out of the FIL plasticiser.[605] Other possible applications of fluorinated ILs are the use as coatings to achieve superhydrophobic surfaces by either covalent[606] or non-covalent bonding.[607,608]

1.7 Correlation of transport properties in ionic liquids – reminiscence of electrolyte solutions

The determination of transport properties of fluids is an important field in science dating back to the works of Isaac Newton in 1687.[609] The measurement of transport properties is a routine method to gain understanding of molecular motion, momentum, charge, mass and heat transfer as well as the underlining molecular interactions.[610] For fluids, the transport properties of highest interest cover the physical quantities of self-diffusion coefficient D_s (molecular motion), viscosity η (momentum transport), electrical conductivity κ (charge transport), chemical diffusion coefficient D (mass transport) and thermal conductivity λ (heat transport). The detailed knowledge about the transport properties of fluids is essential for their successful implementation in processes and products.[611] In the case of ionic liquids, the first three quantities are the most interesting for the determination of liquid association that in turn is desired to be minimized to achieve high conductivities. The electrical conductivity of ILs is conventionally determined by impedance spectroscopy while viscosities are measured by various rheological techniques. The

self-diffusion coefficients of cation and anion are generally determined by NMR measurements either using pulsed[612] or steady field[613] gradient experiments. They can also be determined by quasi-elastic neutron scattering[614,615] and potentially by tracer-diffusion. However, the obtained self-diffusion coefficients differ depending on the measurement method which is believed to be a result of scale-dependence.[435] It is reported that ILs show a sub-diffusive behavior on short timescales (picosecond range) that are investigated by computational chemistry and neutron scattering techniques while on larger time scales a linear relationship (regular diffusion – the mean squared displacement of the diffusing species is a linear function of time) is found.[433,487–48]

The usage of ILs in advanced electrochemical devices is one of the most promising and developing fields and requires the optimization of conductivity by tuning the intermolecular interactions.[243] The benefits of ILs in electrochemical applications have already been discussed in section 1.4. Changes of the ILs' conductivity without impacts on other transport properties are not feasible since these are correlated by different empirical relations. A scheme of the correlations between the transport properties of low temperature molten salts is shown in *Figure 11*. It should be noted that these empirical interrelations were initially derived for electrolyte solution and molecular liquids but are also applicable to ILs and therefore seem to be quasi-universal.[610]

The most important transport property relations applied in the field of ionic liquids are the Walden, Nernst-Einstein and Stokes-Einstein-Sutherland (SES) relation. The Walden relation (1) links the molar conductivity Λ_M of an electrolyte solution to its inverse viscosity η (fluidity) at a given temperature T and can be written as:

$$\Lambda_M \propto (\eta^{-1})^t \tag{1}$$

With t being a fractional exponent necessary to fit the data for both molecular electrolyte solutions and ionic liquids. The SES equation (2), that is more commonly written in the non-fractional version (3) (valid for particles with a diffusion coefficient D that are significantly larger than the solvent molecules), connects the self-diffusion D_S with the temperature depended viscosity of fluids.

$$\frac{D_S}{T} \propto (\eta^{-1})^t \tag{2}$$

$$D = \frac{kT}{n\pi\eta r} \tag{3}$$

With t being a fractional exponent necessary to fit the data for real solvents that do not meet the assumptions of the simple SES model of particles moving in a nonmolecular medium,[617] k the Boltzmann constant, n being either 4 (β = 0: no slip boundary conditions) or 6 (β = ∞; slip boundary conditions) in dependence of the Stokes frictional parameter β limits and r the hydrodynamic radius of the diffusing particle.[610] The Nernst-Einstein equation (4) on the other hand relates the conductivity of a fluid to the self-diffusion coefficients of the charge carriers i and was derived for dilute, non-interacting electrolyte solutions that are regarded as an 'ideal behaving electrolytes'.

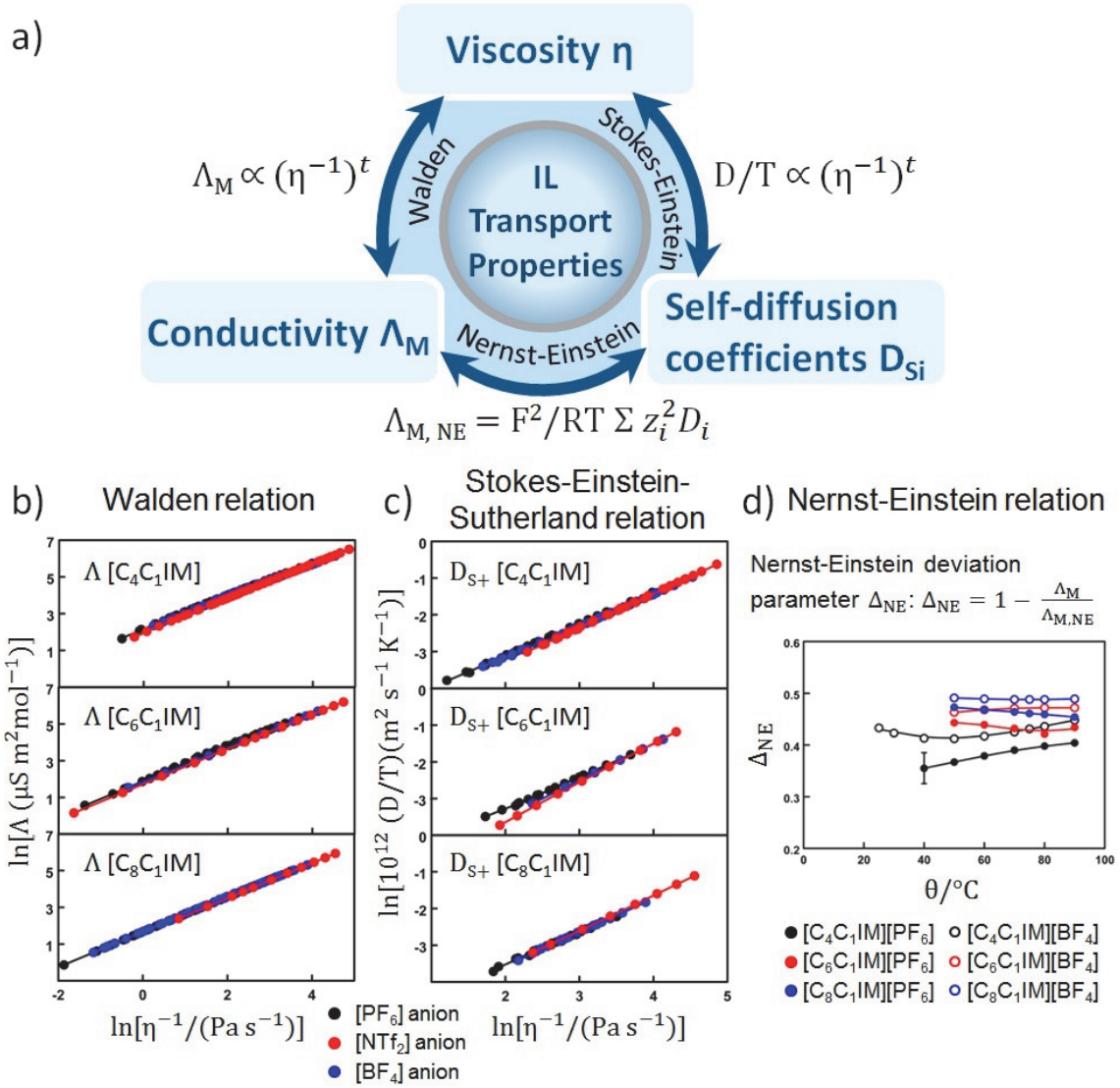

Figure 11: a) Scheme of the relations for important IL transport properties. Representative graphs of b) Walden relation, c) Stokes-Einstein-Sutherland relation and d) deviation parameter of the Nernst-Einstein relation that is frequently interpreted as an indicator for ion pairing in ILs. (Graphs of the transport property relations are adapted from ref.[616]).

$$\Lambda_{M,} = \frac{F^2}{RT} \sum_{i=1}^{n} \nu_i\, z_i^2\, D_{Si} \qquad (4)$$

Where F is the Faraday constant, R the gas constant, v the stoichiometric coefficient, z the charge and D_S the self-diffusion coefficients of the species i. For every investigation of the ILs' transport properties, there are deviations found when the experimental conductivity $\Lambda_{M,Exp}$ is compared to the one calculated from the Nernst-Einstein relation (therefore denoted as $\Lambda_{M,NE}$ in the following section). This difference between the diffusive and electrical mobilities can be quantified with either the Haven ratio H_R (5),[612,618–621] the Nernst-Einstein deviation parameter Δ_{NE} (6)[616,617,622] or the ionicity I_{HR} (7) that is the reciprocal Haven ratio and quantifies the amount of 'free', non-aggregated ions.

$$H_R = \frac{\Lambda_{M,NE}}{\Lambda_{M,Exp}} \quad (5)$$

$$\Delta_{NE} = 1 - {H_R}^{-1} \quad (6)$$

$$I_{HR} = {H_R}^{-1} = \frac{\Lambda_{M,Exp}}{\Lambda_{M,NE}} \quad (7)$$

Both the deviation from Walden and Nernst-Einstein behavior were used in the literature to quantify the deviation of ILs from an ideally behaving electrolyte which is often termed 'ionicity'. In the Walden plot, the deviation from the so called 'ideal KCl line' is regarded. This line was obtained from the temperature dependent conductivity and viscosity of a 0.01 M aqueous KCl solution where the ionic interactions are regarded as negligible. The discrepancy from ideality can be quantified by the fractional Walden approach (8) that relates conductivity and fluidity by the introduction of an additional parameter α.[623,624] This parameter describes the deviation from the relation proposed by Walden in which t is equal to unity (C being a fitting constant).

$$\log\frac{\Lambda_M \text{ mol}}{\text{S cm}^2} = \log C + t\log\frac{0.1 \text{ Pa s}}{\eta} \quad (8)$$

The ionicity based on the Walden relation is obtained from the vertical difference of the measured conductivity Λ_M^{exp} to the one of the 'ideal KCl line' Λ_M^0.[625] In this way the ionicity from the Walden plot I_W at a certain temperature is obtained according to equation (9).

$$I_W(T) = \frac{\Lambda_M}{\Lambda_M^0} = \frac{\Lambda_T^{exp}(T) \text{ mol}}{\text{S cm}^2} \; \frac{\eta^{exp}(T)}{0.1 \text{ Pa s}} \quad (9)$$

Based on the degree of deviation, the Walden plot is also commonly used to group ILs into 'good' (high ionicity – usually obtained for AILs) and 'poor' (low ionicity – often obtained for PILs with low pK_a difference between the IL constituting acid and base).[120] The origin of this deviation from an ideally behaving electrolyte is still a matter of debate in the scientific literature.[626] Some research groups postulate that the reason for this phenomena is the formation of 'ion pairs' or 'ion aggregates' that are overall neutral units and therefore do not contribute to the conductivity.[623] This effect is assumed to be similar to the investigated and well-known formation of ion pairs in solution.[454] There are opposing evidences for and against the hypothesis of ion aggregation.[626,627] Results from dispersion NMR[459] and electrophoretic NMR[619] as well as MD simulations[628] for instance point towards some sort of aggregated species. On the contrary, Harris argues that there are no hints for ion aggregation in the vast majority of low temperature molten salts when the Laity resistance coefficients are considered.[622] Other groups concluded from theoretical studies that the lifetimes of ion-ion contacts as well as their correlated motions are too low to justify the existence of neutral subunits in ionic liquids.[627] Further approaches rationalize the experimentally observed deviation of calculated and measured electrical conductivity with the assumption of charge transfer (CT) between cation and anion. This CT would lead to fractional charges that are lower than the integer charges in the Nernst-Einstein equation (4) and would also suppress the aggregation of

oppositely charged ions.[629] It should be noted that for protic ILs, the presence of neutral subunits as a result of proton back transfer to the molecular precursors is a common finding, leading to a comparable description in terms of 'ionicity'.[630–632]

Further rationalizations for the deviation of ILs from an ideally behaving electrolyte and a standalone interpretation of IL transport properties are anticorrelated motions of ions.[633] This description has its origin in momentum conservation that is different for diluted electrolytes and ILs or molten salts since the momentum is distributed among solvent molecules in the former case.[634] The distinct diffusion coefficients (DDC) D_{ij}^{d} (i,j = + in case of the cation or – for the anion; eq. (10-12)) or equally the velocity cross-correlations (VCC) f_{ij} (eq. (13)) are calculated from the same experimental quantities as needed for the calculation of the Haven ratio or Nernst-Einstein deviation parameter. For ILs with single charged ions, the DDC in the mass-fixed[635] or barycentric reference frame are given by:[636]

$$D_{+-}^{d} = -\frac{2RT\,\Lambda_M}{F^2}\,\frac{M_+\,M_-}{M^2} \tag{10}$$

$$D_{++}^{d} = \frac{2RT\,\Lambda_M}{F^2}\,\frac{M_-^2}{M^2} - 2D_{S+} \tag{11}$$

$$D_{--}^{d} = \frac{2RT\,\Lambda_M}{F^2}\,\frac{M_+^2}{M^2} - 2D_{S-} \tag{12}$$

$$f_{ij} = \frac{D_{ij}^{d}\,M}{2\rho} \tag{13}$$

with M_+ the molar mass of the cation, M_- the molar mass of the anion, M the molar mass of the ionic liquid and D_{Si} the self-diffusion coefficient of either cation (i = +) or anion (i = i).These equations for the DDC deviate from the McCall-Douglas-Hertz VCCs[637,638] that are time and ensemble averages of the Kubo VCCs.[617,635] For the unlike ions, the DDC D_{+-}^{d} are proportional to the molar conductivity whereas for the like-charged anions (D_{++}^{d} and D_{--}^{d}) they contain conductive and diffusive terms. Both DDC and VCC are negative quantities in pure ILs as a result of momentum conservation.[616]

In order to determine if there is ion association present in conventional molten salts or ionic liquids, the Laity resistance coefficients[639] (LRC) r_{ij} are occasionally applied.[613,640] The LRC are phenomenological coefficients obtained from non-equilibrium thermodynamics describing the flow of the ions. They are functions (eq. (14-16)) of the ionic charges and stoichiometry as well as the transport quantities. For an ionic system consisting of only one component one obtains:

$$r_{+-} = \frac{z_+ \nu_+ (z_+ + |z_-|) F^2}{\Lambda_M} \quad (14)$$

$$r_{++} = \frac{1}{|z_-|} \frac{(z_+ + |z_-|)RT}{D_{S+}} - |z_+| r_{+-} \quad (15)$$

$$r_{--} = \frac{1}{|z_+|} \frac{(z_+ + |z_-|)RT}{D_{S-}} - |z_-| r_{+-} \quad (16)$$

The values for the unlike LRCs r_{+-} are necessary positive whereas r_{++} and r_{--} might have both positive and negative values. Negative values in molten salts and ionic liquids are thereby regarded as indicator for ion association.[622]

Even though the origin of the ILs' deviation from ideal electrolyte behavior is still a matter of debate in scientific literature, the quantification is of high importance especially for the design of optimized electrolytes with maximum conductivity.

2. Main Part

This cumulative thesis is based on the following seven publications in peer-reviewed journals, with me as first author or equally contributing first author.

Publication A: Daniel Rauber, Frederik Philippi, Josef Zapp, Guido Kickelbick, Harald Natter, Rolf Hempelmann, Transport properties of protic and aprotic guanidinium ionic liquids, *RSC Adv.*, **2018**, 8, 41639-41650.

Publication B: Frederik Philippi, Daniel Rauber, Josef Zapp, Rolf Hempelmann, Transport properties and ionicity of phosphonium ionic liquids, *PCCP*, **2017**, 19, 23015-23023. (Daniel Rauber as equally contributing first author).

Publication C: Daniel Rauber, Peng Zhang, Volker Huch, Tobias Kraus, Rolf Hempelmann, Lamellar structures in fluorinated phosphonium ionic liquids: the roles of fluorination and chain length, *PCCP*, **2017**, 19, 27251-27258. (Peng Zhang as equally contributing first author).

Publication D: Daniel Rauber, Frederik Philippi, Rolf Hempelmann, Catalyst retention utilizing a novel fluorinated phosphonium ionic liquid in Heck reactions under fluorous biphasic conditions, *J. Fluor. Chem.*, **2017**, 299, 115-122.

Publication E: Daniel Rauber, Florian Heib, Michael Schmitt, Rolf Hempelmann, Trioctylphosphonium room temperature ionic liquids with perfluorinated groups – Physical properties and surface behavior in comparison with the nonfluorinated analogues, *Colloids Surf. A*, **2018**, 537, 116-125.

Publication F: Daniel Rauber, Florian Heib, Tobias Dier, Dietrich A. Volmer, Michael Schmitt, Rolf Hempelmann, On the physicochemical and surface properties of 1-alkyl 3-methylimidazolium bis(nonafluorobutylsulfonyl)imide ionic liquids, *Colloids Surf. A*, **2017**, 529, 169-177.

Publication G: Daniel Rauber, Florian Heib, Michael Schmitt, Rolf Hempelmann, Influence of perfluoroalkyl-chains on the surface properties of 1-methylimidazolium bis(trifluoromethanesulfonyl)imide ionic liquids, *J. Mol. Liq.*, **2016**, 216, 246-258.

In Publication A and B the thermal behavior and important transport properties of novel ILs with less frequently used, but promising cation subclasses were investigated.

In Publication A the focus was on the synthesis and characterization of protic and aprotic cations that are derivates of the superbase tetramethylguanidine. ILs originating from superbases are of particular interest for practical applications since they usually show

higher thermal, electrochemical and chemical stability. Different cation substitution patterns and anions from acids with broadly varied pK_a values were investigated. The obtained transport quantities (viscosity, conductivity and self-diffusion coefficients) were analyzed according to different models for their correlation such as the Nernst-Einstein, Walden and Stokes-Einstein-Sutherland relation. The deviation from fully dissociated, 'ideal behaving' electrolytes was quantified in terms of the ionicity as reciprocal Haven ratio or as obtained from the Walden plot. Both the protic and aprotic guanidinium ILs were found to have transport properties values similar to other IL cations with comparable molecular weight and high ionicity values, especially in the case of the protic ILs. The most promising transport properties and ionicity values were found for the anions with small perfluorinated groups. Elongated perfluorocarbon segments that are present for instance in the bis(pentafluoroethanesulfonyl)imide anion or nonfluorinated anions, such as the methanesulfonate, show a more pronounced undesirable transport behavior when compared to anions with trifluoromethylgroups, such as the bis(trifluoromethanesulfonyl)imide [NTf_2] or trifluoromethanesulfonate [OTf].

In Publication B the transport properties for a series of mostly novel phosphonium-based ionic liquids in dependence on the cation substitution pattern or anion were measured. As model system the bis(trifluoromethanesulfonyl)imide was chosen since ILs containing this anion with perfluorinated groups usually show low melting points, good transport properties and high stabilities. These characteristics are the result of the high charge delocalization enabled by the strong electron withdrawing character of the perfluorinated moiety. Phosphonium ILs are of special interest for practical applications since they show some beneficial characteristics compared to other cation classes. For instance, they show higher chemical and electrochemical stability than imidazolium- or pyridiunium-based ILs and usually improved transport properties compared to ammonium analogues with the same substitution pattern. The [NTf_2]-ILs were found to have the highest ionicity values and the most favorable transport properties compared to other anions. Furthermore, short alkyl side chains and the utilization of ether groups in the cation had a beneficial influence on the ILs' transport behavior.

Publication C deals with the supramolecular structure and resulting macroscopic properties of phosphonium ILs with perfluorinated groups in the cation and compares the results to the nonfluorinated ones. For this purpose several novel ILs with varied length of perfluorinated or hydrocarbon side chain and the weakly coordinating dicyanamide anion were synthesized. Small-angle X-ray scattering (SAXS) revealed the formation of lamellar structures with long-range order in the liquid state for all fluorinated ILs while the alkylated ones only showed the general features found for most ILs that contain polar-ionic and nonpolar hydrocarbon domains. The long-range ordered structure is the result of fluorophilic interactions and therefore the more pronounced, the longer the perfluorinated moieties are. Furthermore, the effect of the micro-structuration on the macroscopic properties was investigated. The fluorinated ILs were found to have higher melting points and viscosities that are about one order of magnitude larger than the alkylated ILs. In addition the incorporation of perfluorocarbon segments leads to non-Newtonian shear thinning contrary to the hydrocarbon ones that showed only Newtonian flow behavior.

The application of a highly fluorous IL for the immobilization of a fluorous catalyst was the subject of Publication D. Highly fluorous ionic liquids combine the fluorophilic characteristics of perfluorocarbon solvents with non-volatility to avoid the problem of evaporation of fluorous compounds. Although the novel highly fluorinated IL had a melting point above room temperature, it remained in the liquid state to form a fluorous phase when combined with DMF in a thermoregulated biphasic system. This mixture could be exploited in fluorous biphasic catalysis for the immobilization and reuse of a perfluorotagged Pd-catalyst. As model system the Heck reaction as example for a widely used C-C coupling reaction was used. The reaction of iodobenzene and methyl acrylate gave 83% yield of coupling product after 20 runs with minimal loss of fluorous phase.

Publications E to G contain the investigations on the general physicochemical properties of novel or rarely investigated ILs with elongated perfluorinated chains in either the cation or anion. For these ILs the dynamic and static wetting behavior on different surfaces was investigated by the *High precision Drop Shape Analysis* (HPDSA).

As many practical applications of ILs include some sort of solid-liquid interfaces an advanced insight in their static and dynamic wetting behavior on different surfaces is highly demanded for tailored modifications. In Publication E the general properties of trioctylphosphonium cations with attached perfluorinated chains of different length and the low coordinating anions [$N(CN)_2$], [$C(CN)_3$] and [NTf_2] were measured. The results were compared to the alkylated ILs with similar side chain length to show the influence of the perfluorinated segments directly. The fluorinated ionic liquids were found to have diverse thermal transitions, anion-dependent decomposition temperatures, similar solvent polarities, higher overall viscosities and a shear dependent non-Newtonian thinning behavior. Furthermore, the fluorinated ILs showed an altered wetting behavior on a hydrophobic modified surface leading to higher static uphill and downhill contact angles and stronger pinning on the surface. The general physical properties of 1-alkyl-3-methyl-imidazolium-ILs with the highly fluorinated anion bis(nonafluorobutylsulfonyl)imide [NNf_2] and their wetting behavior on hydrophilic and hydrophobic surfaces was the subject of Publication F. The resulting properties of this fluorinated ILs were compared to the imidazolium-ILs with the widely used [NTf_2] anion. The [NNf_2]-ILs had melting points near ambient temperature, high decomposition temperatures and wide liquid ranges. Their polarities decreased with increasing side chain length and were slightly higher than the values of the [NTf_2]-ILs with similar alkyl chains. The viscosities of the [NNf_2] were significantly higher than the ones found for the [NTf_2]-ILs and the crystal structure of 1-decyl-3-methyl-imidazolium [NNf2] revealed the formation of three different domains (polar ionic, nonpolar-hydrocarbon and nonpolar-perfluorocarbon; see also chapter 1.6) by favored homogeneous interactions. Analysis of the wetting characteristics by the high-precision drop shape analysis (HPDSA) approach revealed only minor differences in the *static* wetting behavior of the [NNf_2] and [NTf_2] samples on hydrophobic and hydrophilic surfaces. However, the two anion classes showed noticeable differences in their *dynamic* wetting properties on both types of surfaces leading to a stronger pinning on the surface in case of the [NNf_2]-ILs. Publication G deals with the important physicochemical properties and wetting properties of a series of 1-(1*H*,1*H*,2*H*,2*H*-perfluoroalkyl)-3-methyl-imidazolium [NTf_2] ILs in comparison with the 1-alkyl-3-methyl-imidazolium [NTf_2] analogues. The fluorinated ILs were found to have an altered phase transition behavior compared to the nonfluorinated cations, high

decomposition temperatures and wide liquid ranges. The viscosity o the FILs was about one order of magnitude higher and showed a much stronger dependence on the side chain length than the alkyl-imidazoles, which is the result of the higher degree of charge localization in the cation, as indicated by the increased solvatochromic polarity, combined with the increased stiffness and solvophobic interactions of the perfluoroalkyl moieties. The solvophobic interactions were also observable in the crystal structure of 1-(1*H*,1*H*,2*H*,2*H*-perfluorodecyl)-3-methyl-imidazolium [NTf_2] that revealed an ionic and a fluorous domain. The HPDSA was applied to investigate the wetting behavior on different surfaces. While the alkylated ILs showed wetting characteristics similar to conventional organic test liquids with small surface tension the fluorinated ionic liquids had a strong pinning and higher wetting of all investigated surfaces. In applications as electrolyte in electrochemical devices the wetting of the ionic liquid electrolyte on the electrode material is of great importance for the charge transfer process and thus for the operation of the electrochemical device.

2.1 Publication A

Transport properties of protic and aprotic guanidinium ionic liquids

Daniel Rauber, Frederik Philippi, Josef Zapp, Guido Kickelbick, Harald Natter, Rolf Hempelmann.

RSC Adv., **2018**, 8, 41639-41650.

RSC Advances

PAPER

View Article Online
View Journal | View Issue

Cite this: *RSC Adv.*, 2018, **8**, 41639

Transport properties of protic and aprotic guanidinium ionic liquids†

Daniel Rauber,[ab] Frederik Philippi,[a] Josef Zapp,[c] Guido Kickelbick,[d] Harald Natter[ab] and Rolf Hempelmann*[ab]

Ionic liquids (ILs) are a promising class of solvents, functional fluids and electrolytes that are of high interest for both basic as well as applied research. For further fundamental understanding of ILs and a successful implementation in technical processes, a deeper insight into transport properties and their interrelations is of particular importance. In this contribution we synthesised a series of mostly novel protic and aprotic ILs based on the tetramethylguanidinium (TMG) cation that is a derivative of the superbase guanidine. Different substitution patterns and anions from acids with broadly varied pK_a values were investigated. We measured general properties, such as thermal transitions and densities of these ILs, as well as their transport quantities by means of rheology, impedance spectroscopy and NMR diffusometry. Different models for the correlation of the transport properties, namely the Nernst–Einstein, Walden and Stokes–Einstein–Sutherland relations were applied. The deviation from ideal behaviour of fully dissociated electrolytes, often termed as ionicity, was quantified by the reciprocal Haven ratio, fractional Walden rule and ionicity obtained from the Walden plot. Velocity cross-correlation coefficients were calculated to gain further insight into the correlation between ion movements. Both protic and aprotic TMG ILs show transport properties comparable to other ILs with similar molecular weight and high ionicity values especially in contrast to other protic ILs. Lowest ionicity values were found for the protic ILs with smallest ΔpK_a values between constituting acid and base. This can either be explained by stronger hydrogen bonding between cation and anion or lower anti-correlations between the oppositely charged ions. These results aim to provide insight into the properties of this interesting cations class and a deeper understanding of the transport properties of ILs and their interrelations in general.

Received 5th September 2018
Accepted 16th November 2018

DOI: 10.1039/c8ra07412g

rsc.li/rsc-advances

Introduction

Ionic liquids (ILs) are a very diverse and promising class of advanced functional fluids which show a unique property combination beneficial for a number of practical applications. These include synthesis,[1] electrochemistry and energy conversion[2] or engineering and processing.[2,3] For implementation in existing or new technologies the detailed knowledge about their transport properties is of essential importance[4,5] since they limit the achievable performance. The immense number of possible ILs and functionalisations makes deeper understanding of their physicochemical properties, the correlation between these properties and their molecular structure essential. Insights into structure–property-relations are the foundation for further optimisation of their transport properties along with the design of novel ILs with tailored characteristics. The Coulomb interactions inherently present in these low temperature molten salts are the dominant intermolecular force, however the contribution of other intermolecular interactions such as solvophobic interactions[6] or hydrogen bonding[7] are reported to have significant impact on the liquid mesostructure and therefore on the macroscopic quantities. Systematic investigations on structural modifications are crucial, especially due to contradictions in the scientific community.[8]

In this contribution, we report the synthesis of a series of ILs based on the tetramethylguanidinium (TMG) cation paired with anions from acids covering a wide range of pK_a values. To the best of our knowledge most of these ILs have never been reported before. Molecular structures and nomenclature of cations and anions investigated in this work are shown in Scheme 1. We synthesised both protic (PILs) and aprotic (AILs) species to investigate the influence of hydrogen bonds on their

[a]*Physical Chemistry, Saarland University, Campus B 2 2, 66123 Saarbrücken, Germany. E-mail: r.hempelmann@mx.uni-saarland.de*

[b]*Transfercenter Sustainable Electrochemistry, Saarland University and KIST Europe, Am Markt, Zeile 3, 66125 Saarbrücken, Germany*

[c]*Pharmaceutical Biology, Saarland University, Campus B 2 3, 66123 Saarbrücken, Germany*

[d]*Inorganic Solid State Chemistry, Saarland University, Campus C 4 1, 66123 Saarbrücken, Germany*

† Electronic supplementary information (ESI) available: Syntheses of the ionic liquids and intermediates as well as the corresponding NMR spectra; experimental parameters, obtained data and fit results. See DOI: 10.1039/c8ra07412g

physicochemical properties. The literature often distinguishes between these two large IL subclasses due to significant differences in synthesis and characteristics.[9] Since the acid–base neutralisation reactions used in the preparation of PIL systems are reversible, neutral species and more or less acidic protons are present.[10] The latter can act as H-bond donors, often resulting in expanded hydrogen bond networks.[11] Contrary to this, AILs are formed by nucleophilic substitution reactions and subsequent anion exchange, making the synthesis less atom-efficient and more time-consuming. It was shown by Watanabe *et al.* that the difference in pK_a values (ΔpK_a) in PILs has a significant influence on the strength of hydrogen bonds between cation and anion.[12] They found that for higher ΔpK_a values a stronger bond between the precursor base and the acid proton is formed as confirmed by ^{1}H-NMR and FT-IR spectroscopy. The TMG cations are derivatives of the organic superbase tetramethylguanidine (pK_a[HHTMG] = 13.6 in aqueous solution[13]), ensuring comparably large ΔpK_a values between the IL constituting cation and anion (pK_a for the conjugate acids of the anions:[14] pK_a[HNTf$_2$] = −10.0; pK_a[HOTf] = −7.0; pK_a[HOMs] = −2.0; pK_a[HTFA] = 0.5). Large ΔpK_a values between the Brønsted acids and bases forming the PILs are reported to result in a complete proton transfer and suppress reverse proton transfer to the molecular species at elevated temperatures thus leading to increased thermal stabilities.[12] For the AILs equilibria of ionic and neutral species as well as strong, directional hydrogen bonds are absent. This makes a comparison of the PILs physicochemical properties with those of their AIL counterparts interesting for fundamental investigations. The TMG cation has a delocalised π-electron system similar to the intensively investigated imidazolium and pyridinium cations. The difference is that the resonant system is in Y-shape in the former and cyclic in the latter. Furthermore, the guanidinium cation has more substituents at the core allowing for a larger degree of synthetic possibilities for modification or functionalisation.[15] Guanidinium-based ILs were reported to have promising properties as reaction media,[16] high electrochemical and thermal stability,[17] as well as high gas absorption capacities.[18] In contrast to imidazolium and pyridinium cations, the central moiety in guanidinium cations is more easily distorted from planarity.[19] This bears the potential to induce axial chirality when side chains of high sterical demand are used.

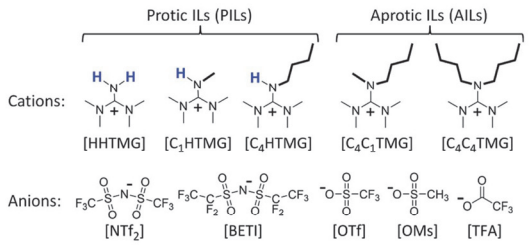

Scheme 1 Molecular structures of the IL cations and anions investigated in this work. C_x denotes the number of carbons in the attached alkyl side chains (x = 1: methyl; x = 4: butyl).

The focus in this work is put on small cations with side chain lengths not larger than butyl. Elongated alkyl-chains were found to generally increase the viscosity of ILs[20] making these representatives less attractive for most technical implementations. For these mostly novel ILs, determination of thermal transitions revealed that most of them are liquid or supercooled at ambient temperature. For these samples, the most important transport properties were determined by stress-controlled rheology (momentum transport/viscosity), impedance spectroscopy (charge transport/conductivity) and NMR-diffusometry (mass flux/self-diffusion). The obtained results were analysed using different models to investigate correlation of transport properties such as the Walden (1), Nernst–Einstein (2) and Stokes–Einstein–Sutherland (3) relations that can be written as:

$$\Lambda_M \propto (1/\eta)^t \quad (1)$$

$$\Lambda_{NE} = \left(\frac{F^2}{RT}\right)\sum_i z_i^2 D_{Si} \quad \text{and} \quad \Lambda_M = \Lambda_{NE} H_R^{-1} = \Lambda_{NE}(1 - \Delta_{NE}) \quad (2)$$

$$D_{Si}/T \propto (1/\eta)^t \quad (3)$$

where Λ_M is the molar conductivity directly obtained from experiment, η the viscosity, Λ_{NE} the molar conductivity calculated by the Nernst–Einstein equation, F is the Faraday constant, R the gas constant, T the absolute temperature, z_i the charge number of a particular ion and D_{Si} (cation: i = +; anion: i = −) are the self-diffusion coefficients of the cation and anion. The Nernst–Einstein parameter Δ_{NE} and the Haven ratio H_R are deviation parameters introduced as a correction between the molar conductivities obtained from diffusive and electrical mobilities. Note that Δ_{NE} is not present in the simple Nernst–Einstein equation since the model was derived for infinitely diluted electrolyte solutions. The fractional exponents t were found to be necessary for the fitting of molecular solvents and ionic liquids.[21] The first two relations are established methods in the literature to quantify the deviation of ILs from ideally behaving electrolytes, although they lack an underlying theory.[22–24] This 'deviation from ideality' or 'ionicity I' is often attributed to ion-pairing or ion aggregation in the bulk liquid leading to decreased measured conductivities since the overall neutral species are assumed to not contribute to charge transport.[23] For the quantification of this discrepancy from ideal behaviour with temperature the fractional Walden approach (4) was also applied.[23,25] This method relates molar conductivity to fluidity by means of introducing an additional parameter α that accounts for deviation from the relation initially proposed by Walden in which α is equal to unity.

$$\log\frac{\Lambda_M\ \text{mol}}{\text{S cm}^2} = \log C + \alpha \log\frac{0.1\ \text{Pa s}}{\eta} \quad (4)$$

The vertical difference of the measured conductivity data to the 'ideal' KCl-line (Λ_M^0), that is regarded an ideal behaving, fully dissociated electrolyte, can also serve as a measure for

Table 1 Thermal transitions of the investigated ionic liquids including densities and molar volumes of the RTILs

Ionic liquid	T_c[a]/°C	T_g[b]/°C	T_{cc}/°C[c]	T_{ss}/°C[d]	T_m/°C[e]	$\rho^{25\ °C}$/g mL^{-1}	$V_M^{25\ °C}$/mL mol^{-1}
[HHTMG][NTf_2]	−1	—	—	—	49	—	—
[HHTMG][BETI]	—	−71	−40	18	25	1.569	316
[HHTMG][OTf]	−17	—	—	—	43	—	—
[HHTMG][OMs]	—	−44	1	—	117	—	—
[HHTMG][TFA]	17	—	—	15	39	—	—
[C_1HTMG][NTf_2]	−47	—	—	—	17	1.452	283
[C_1HTMG][BETI]	−58	—	—	—	−13	1.530	334
[C_1HTMG][OTf]	−22	—	—	—	32	1.312[f]	213
[C_1HTMG][OMs]	30	—	—	—	68	—	—
[C_1HTMG][TFA]	−4	—	—	—	28	1.220[f]	199
[C_4HTMG][NTf_2]	—	−83	—	—	—	1.354	334
[C_4HTMG][BETI]	−29	—	—	—	31	1.429[f]	387
[C_4HTMG][OTf]	—	−70	−17	—	10	1.218	264
[C_4HTMG][OMs]	—	−53	—	—	—	1.109	241
[C_4HTMG][TFA]	—	−76	−17	—	10	1.138	251
[C_4C_1TMG][NTf_2]	—	−86	—	—	—	1.338	349
[C_4C_1TMG][BETI]	−21	—	—	—	28	1.416[f]	400
[C_4C_1TMG][OTf]	20	—	—	—	52	—	—
[C_4C_1TMG][OMs]	56	—	—	—	113	—	—
[C_4C_1TMG][TFA]	22	—	—	—	39	—	—
[C_4C_4TMG][NTf_2]	—	−75	—	—	—	1.276	398
[C_4C_4TMG][BETI]	—	−70	−8	—	23	1.351	451
[C_4C_4TMG][OTf]	—	−58	−7	−18	19	1.160	325
[C_4C_4TMG][OMs]	—	−40	—	—	—	1.063	304
[C_4C_4TMG][TFA]	15	—	—	—	44	—	—

[a] Crystallisation temperature at −1 °C min^{-1} cooling rate. [b] Glass transition temperature. [c] Cold crystallisation temperature in the heating step. [d] Solid–solid transition. [e] Melting point. [f] Measured in supercooled state.

ionicity. In this way the ionicity I_W from the Walden plot at a particular temperature is obtained according to eqn (5).[22]

$$I_W(T) = \frac{\Lambda_M}{\Lambda_M^0} = \frac{\Lambda_M^{exp}(T)\ \text{mol}}{\text{S cm}^2} \times \frac{\eta^{exp}(T)}{0.1\ \text{Pa s}} \quad (5)$$

Another quantification parameter frequently applied in the framework of this ion aggregation assumption is that the ionicity I_{HR} as defined by Watanabe *et al.*[26] (6) is the reciprocal of the Haven ratio H_R. It describes the amount of unpaired/dissociated ions similar to the Nernst–Einstein parameter Δ_{NE} used for the degree of aggregated species.[27]

$$I_{HR} = \frac{\Lambda_M}{\Lambda_{NE}} = {H_R}^{-1} \text{ and } \Delta_{NE} = 1 - \frac{1}{H_R} \quad (6)$$

Whether the assumption of paired or clustered ions in ionic liquids is valid for ILs is still the subject of ongoing discussions. There are contrary experimental and theoretical results for and against this hypothesis.[8,28] For example NMR dispersion[29] or electrophoretic NMR[30] show evidence for certain types of ion clustering while Harris[31] argues that for the large majority of ILs there are no hints for ion association when the Laity resistance coefficients are considered. Other authors report nearly quantitative ionicity values for chloride ILs based on measurements of the $^{35}Cl^-$ quadrupolar coupling constants.[31] Based on theoretical studies, Kirchner *et al.* concluded that the lifetimes of ion–ion contacts and their collective motions are far too low for a verification of neutral ion pairs in ionic liquids.[28] Other approaches rationalise the experimentally proven deviation of IL conductivities from those calculated by the simple Nernst–Einstein equation with the assumption of charge transfer (CT) between cation and anion. The CT leads to fractional charges lower than the integer charges in the Nernst–Einstein equation and suppresses association of oppositely charged ions.[32] Another possible explanation given in the literature for the discrepancy between diffusive and electrical mobilities are anticorrelated motions of ions due to momentum conservations. The momentum conservation law is satisfied for diluted electrolytes by solvent and ions which is significantly different to the situation of ILs or molten salts where the conservation law must be satisfied solely by the constituting ions.[33] The distinct diffusion coefficients (DDC), D_{ij}^d (i,j = + or −) can be calculated from experimentally available quantities by equations deviated from the McCall–Douglas–Hertz velocity cross-correlation coefficients (VCC).[34,35] For the unlike ions (D_{+-}^d) they are proportional to the molar conductivity while for the like ions the DDCs (D_{++}^d and D_{--}^d) contain conductive and self-diffusive terms. The VCC are time and ensemble averages of the Kubo cross-correlation functions.[36] The DDC/VCC approach is based on statistical mechanics and thus produces clearly defined quantities that can be calculated using molecular dynamics. In the case of a pure ionic liquid with single charged ions one obtains eqn (7)–(9) for the three distinct diffusion coefficients D_{ij}^d in the mass-fixed or barycentric reference frame[37] and the VCC f_{ij} according to eqn (10).[38]

$$D^{d}_{+-} = -\frac{2RT\Lambda_M}{F^2}\frac{M_+M_-}{M^2} \quad (7)$$

$$D^{d}_{++} = \frac{2RT\Lambda_M}{F^2}\frac{M_-^2}{M^2} - 2D_{S+} \quad (8)$$

$$D^{d}_{--} = \frac{2RT\Lambda_M}{F^2}\frac{M_+^2}{M^2} - 2D_{S-} \quad (9)$$

$$f_{ij} = \frac{D^{d}_{ij}M}{2\rho} \quad (10)$$

Here, M_i is the molar mass of a certain ion, M the molar mass of the IL. Regardless of the current debate detailed knowledge about the transport properties is important for the utilisation and optimisation of these advanced materials in technical applications. The same applies to the deviation from ideal behaviour and quantification of this.

In this contribution we want to categorize the TMG ILs based on their transport properties in comparison to other PIL and AIL classes and show that the PILs derived from small superbases behave as 'pseudo alkylated' ILs.

Experimental

Additional details on the experimental methods, measured data and applied fittings as well as the syntheses of the investigated ILs, NMR spectra and parameters are given in the ESI†. Products were identified by multinuclear NMR spectroscopy. Prior to each physicochemical measurement the samples were dried in high vacuum at elevated temperatures for about 24 h and further handled in a glove box. Absence of halides was checked by testing the bulk samples with $AgNO_3$ solution and ion chromatography. Water content as determined by Karl Fischer titration was found to be below 100 ppm. Temperature dependent values for the viscosity, molar conductivity and self-diffusion coefficients were fitted following the Vogel–Fulcher–Tammann equation[39,40] (11) and the Litovitz equation[41] (12) that were both found in the literature to be suitable for IL transport properties[42–44] since deviations from Arrhenius type behaviour are usually found.

$$Y = A_0 \exp\left(\frac{B}{T - T_0}\right) \quad (11)$$

$$Y = A \exp\left(\frac{B'}{R\,T^3}\right) \quad (12)$$

The variable Y can either be the dynamic viscosity η, the molar conductivity Λ_M or the self-diffusion coefficients D_{Si} (i = +, −) while A_0, B and T_0 (Vogel temperature) as well as A and B' are material dependent parameters (B, $B' > 0$ for η; B, $B' < 0$ for Λ_M and D_{Si}). Since the VFT fitting is more frequently used for ILs only the VFT parameters are included in the main manuscript.

Thermal transitions

Thermal behaviour of the samples was analysed using differential scanning calorimetry on a DSC 1 STARe (Mettler Toledo, Gießen, Germany) equipped with a liquid nitrogen cooling system. Slow scan rates of ±1 °C min^{-1} were applied to ensure correct determination of the thermal transitions and to suppress supercooling observed for high scanning rates.[45] Each DSC trace was recorded on samples of about 10 mg mass that were hermetically sealed in aluminium crucibles under inert atmosphere. The applied temperature program started with +10 °C min^{-1} heating from 25 °C to 150 °C with isothermal treatment at this temperature for 10 min. Afterwards the samples were cooled at −1 °C min^{-1} to −125 °C followed by a 10 min isothermal period. The samples were then subjected to dynamic heating with a heating rate of +1 °C min^{-1} to 150 °C, held at this temperature for 10 min and cooled again to 25 °C. Thermal transitions are given as extrapolated onset temperatures beside glass transitions that were obtained by the midpoint method.

Density measurements

Densities were measured with a Reischauer-type pycnometer (Neubert Glas, Geschwenda, Germany) of 5 mL nominal volume. Volume calibration in the investigated temperature range was performed using octane; the volume calibration was confirmed with purified water. The largest deviation from literature values for water densities obtained was 0.1%.[46] The pycnometer was rinsed several times with acetone and dried in vacuum prior to weighing before the measurement. For each density measurement the IL sample was carefully placed in the pycnometer with a cannula at ambient temperature until the liquid level was slightly above the mark. The pycnometer was then sealed, placed in a thermostat bath (max. temperature deviation ±0.01 °C) at 25 °C and allowed to equilibrate for at least 20 min. The liquid level was adjusted to the mark with Pasteur pipettes and the pycnometer weighted after cooling to ambient temperature. The procedure was repeated in 10 °C steps up to 75 °C.

Table 2 Viscosity at 25 °C of the RTILs and VFT fitting parameters

Ionic liquid	$\eta^{25\ °C}$/mPa s	η_0/mPa s	B/K	T_0/K
[HHTMG][BETI]	206.5	0.390	549.1	210.6
[C_1HTMG][NTf_2]	66.4	0.277	636.6	182.0
[C_1HTMG][BETI]	155.4	0.116	829.4	182.9
[C_1HTMG][OTf]	171.4	0.207	724.6	190.3
[C_1HTMG][TFA]	116.7	0.832	357.6	225.8
[C_4HTMG][NTf_2]	82.8	0.203	705.0	180.8
[C_4HTMG][BETI]	174.2	0.116	829.4	182.9
[C_4HTMG][OTf]	233.9	0.172	793.6	188.2
[C_4HTMG][OMs]	1237	0.974	376.8	227.8
[C_4HTMG][TFA]	163.9	0.472	513.7	210.3
[C_4C_1TMG][NTf_2]	93.1	0.430	567.0	192.7
[C_4C_1TMG][BETI]	175.1	0.283	674.4	193.2
[C_4C_1TMG][TFA]	—	0.117	770.7	197.7
[C_4C_4TMG][NTf_2]	135.3	0.131	885.6	170.6
[C_4C_4TMG][BETI]	250.1	0.106	932.2	178.2
[C_4C_4TMG][OTf]	433.0	0.131	891.5	188.1
[C_4C_4TMG][OMs]	1454	0.333	584.7	228.4
[C_4C_4TMG][TFA]	—	0.230	636.4	209.2

Dynamic viscosity

Temperature dependent viscosities were determined on a stress-controlled MCR 301 Rheometer (Anton Paar, Graz, Austria) using cone-plate geometry with CP50-1 cone (49.95 mm diameter, cone angle 1°) and 0.101 mm gap size. All measurements were conducted under dry N_2 atmosphere applying shear rates from 5–150 s^{-1} in linear steps with 30 data points measured overall. Since there were no shear rate or time dependent effects visible, *i.e.* only Newtonian behaviour was observed, the data points were averaged. Before each measurement the temperature was allowed to equilibrate for at least 15 min. The first measurement was performed at 25 °C and the temperature raised in 10 °C steps to 95 °C. Maximum temperature deviation was ±0.1 °C. Estimated uncertainty is ±3% as judged by commercial viscosity standards.

Specific and molar conductivity

Specific conductivities of the samples were measured by means of impedance spectroscopy in a closed electrochemical cell using a SP-150 potentiostat (BioLogic, Seysinnet-Pariset, France). The conductivity probe (WTW, Weilheim, Germany) consisted of two platinised platinum electrodes of rectangular geometry fixed in glass with a nominal cell constant of 0.5 cm^{-1}. The cell constant was determined using commercial standards. Temperature was controlled with a Proline RP 1845 thermostat (LAUDA, Lauda-Königshofen, Germany) with a maximum deviation of ±0.01 °C. Before each measurement the temperature was allowed to equilibrate at least 30 min. Conductivity measurements were performed in 10 °C steps from 25 °C to 75 °C. Impedance spectra were recorded at applied voltage amplitudes of 5, 10 and 15 mV and frequencies from 200 kHz to 1 Hz in 50 logarithmic steps. Determined resistances used for the calculation of the specific conductivity κ were averaged with deviations of max. ±1.0%. The molar conductivities can then be calculated with eqn (13) if the specific conductivities and the densities are known.

$$\Lambda_M = \frac{\kappa}{c} = \frac{\kappa M}{\rho} \quad (13)$$

Estimated uncertainty for the specific conductivity is ±2% as judged by commercial conductivity standards.

Self-diffusion coefficients

Self-diffusion coefficients were determined using a NMR pulse sequence based on the pulsed field-gradient stimulated echo (PFGSTE) as developed by Wu *et al.*[47] incorporating bipolar field gradients g and an additional longitudinal eddy current delay T_e. The simpler pulsed field gradient spin echo (PFGSE) is unsuitable for more viscous systems such as ILs since it has some drawbacks and artefacts.[48,49] The PFGSTE experiment minimises eddy currents that are the consequence of the currents used to generate the magnetic field gradients.[47,50,51] In the periods when the macroscopic magnetisation is stored in the direction of the magnetic field, spoiler gradient pulses are used to remove transverse magnetisation. This method minimises effects like inaccurate pulses or undesired coherence pathways.[48,50,52] Further experimental details and the visualisation of the pulse program are reported in a former publication.[27] NMR spectra for the determination of the individual self-diffusion coefficients of the bulk ILs were recorded in argon-filled, sealed NMR tubes on an AVANCE II 400 NMR spectrometer (Bruker, Billerica, USA) with 5 mm BBFO probe. The gradient was calibrated using pure water since this self-diffusion coefficient is well known from other techniques.[53–55] Self-diffusion coefficients were determined using the ^1H nucleus for cations and the ^{19}F nucleus for the anion with the exception of the methanesulfonate anion which was also measured by ^1H NMR utilising the separated signal of the anion protons. Temperature was allowed to equilibrate for at least 1 h. The probe was tuned and shimmed manually after every change of sample, nucleus or temperature. Gradient pulse durations for sufficient signal attenuation as well as a rough estimation of the longitudinal relaxation time T_1 were determined manually.

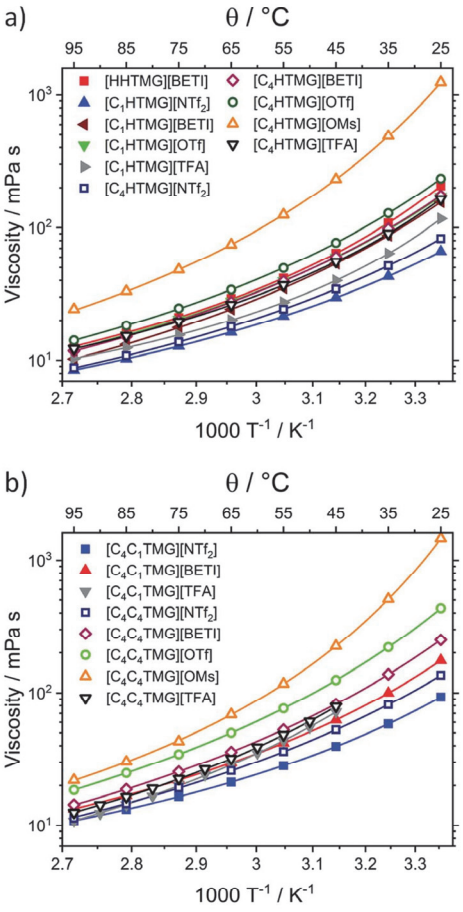

Fig. 1 Temperature dependent viscosities of (a) the protic TMG ILs and (b) the aprotic, hexaalkylated guanidinium salts. Solid lines are the fits using the VFT eqn (11).

Table 3 VFT fit parameters of the TMG IL's molar conductivity and value at 25 °C

Ionic liquid	$\Lambda_M^{25\ °C}$/S cm^2 mol^{-1}	$\Lambda_{M,0}$/S cm^2 mol^{-1}	B/K	T_0/K
[HHTMG][BETI]	0.247	250.2	−772.4	186.1
[C_1HTMG][NTf_2]	1.01	213.8	−686.3	170.1
[C_1HTMG][BETI]	0.344	165.1	−643.0	194.0
[C_1HTMG][OTf]	0.378	165.3	−644.5	192.1
[C_1HTMG][TFA]	0.394	144.2	−643.3	189.1
[C_4HTMG][NTf_2]	0.721	360.7	−846.7	161.6
[C_4HTMG][BETI]	0.310	230.9	−765.3	182.5
[C_1HTMG][OTf]	0.240	183.6	−735.0	187.8
[C_4HTMG][OMs]	0.039	277.5	−866.6	200.4
[C_4HTMG][TFA]	0.192	106.6	−696.8	187.9
[C_4C_1TMG][NTf_2]	0.690	341.5	−873.3	157.5
[C_4C_1TMG][BETI]	0.294	198.5	−741.8	184.2
[C_4C_1TMG][TFA]	—	85.5	−422.4	230.3
[C_4C_4TMG][NTf_2]	0.421	339.4	−895.6	164.3
[C_4C_4TMG][BETI]	0.201	229.4	−813.5	182.6
[C_4C_4TMG][OTf]	0.119	491.7	−1014.7	176.4
[C_4C_4TMG][OMs]	0.034	303.5	−781.0	212.1
[C_4C_4TMG][TFA]	—	237.5	−762.3	191.3

Relaxation delay together with the acquisition time was chosen as 5 to 7 times the value obtained for T_1. For each single self-diffusion coefficient determination 16 spectra were recorded in total with 16 scans each. The raw spectra were subjected to manual phase an automatic baseline correction followed by integration. Plotting $\ln(I/I_0)$ *versus* Q following the Stejskal–Tanner eqn (14) then results in a straight line from which the self-diffusion coefficient D_{Si} can be obtained as the slope.

$$\ln\frac{I}{I_0} = -D_{Si}\gamma^2\delta^2 g^2\left(\Delta - \frac{\delta}{3} - \frac{\tau}{2}\right) = D_{Si}Q \qquad (14)$$

where I is the signal intensity with gradient applied, I_0 the initial signal intensity, γ the gyromagnetic ratio of the investigated nucleus, δ the overall gradient duration, g the applied gradient strength, Δ the diffusion time and τ the gradient interspacing. It should be noted that the gradient interspacing due to the bipolar gradients does not appear in the original equation.[50,51] Estimated uncertainty for the self-diffusion coefficients is ±5% by comparison to viscous calibration liquids suggested in literature.[56]

Results and discussion

Thermal transitions and densities

Knowledge about the thermal transitions of ILs is important since the solidification point puts limits on many applications. Thermal transitions of the samples were determined by means of DSC yielding a broad range of different thermal behaviours. The determined crystallisation T_c, glass transition T_g, cold crystallisation T_{cc}, solid–solid T_{ss} and melting T_m temperatures along with the densities ρ and molar volumes V_M at 25 °C are reported in Table 1. The obtained DSC traces include the three types of IL thermal behaviour commonly found in the literature.[45] These are (a) only glass formation, for example found in all [NTf_2] salts with butyl chain; (b) crystallisation upon cooling and melting transition with often wide temperature ranges where the IL remains in supercooled state, as found for all investigated ILs with [C_1HTMG] cation; (c) no crystallisation upon cooling and crystallisation upon reheating (cold crystallisation) followed by melting transition, for example found in [C_4C_4TMG][BETI]. Furthermore some samples were also found to have additional solid–solid transitions. Most of the samples were room temperature ionic liquids (RTILs) or could be obtained in supercooled state at ambient temperature. All ILs with the [HHTMG] cation with the exception of [HHTM][BETI] were solids at 25 °C. The methanesulfonate ILs with [HHTMG] and [C_4C_1TMG] cation even have melting points exceeding 100 °C. As for many other classes of ILs there are no clear trends regarding the phase transition behaviour as these are complex and sensitive interplays of symmetry, lattice effects and molecular interactions.[57] This also makes the comparison with other cation classes rather difficult. The IL densities showed a decrease with molecular weight and an increase with fluorine and sulphur content. With temperature the decrease in density showed a linear behaviour (Fig. S1 and S2†). For the ILs with the [C_4HTMG] cation the densities decreased in the anion order [BETI] > [NTf_2] > [OTf] > [TFA] > [OMs].

Viscosity

The viscosity of ionic liquids is of high concern for the potential applications in a large number of processes. This quantity puts limits on procedures like separation and mixing as well as the demands for the equipment, for example, of heat exchangers or pipelines. Compared to conventional molecular solvents, ILs are moderate to highly viscous liquids with viscosity values at least about an order of magnitude larger. The temperature dependence of the viscosities can be describe by the Vogel–Fulcher–Tammann eqn (11); the obtained fitting parameters for TMG ILs and the viscosities η at 25 °C are given in Table 2. The temperature dependent viscosities are plotted in Fig. 1. The lowest viscosity at ambient temperature was found for [C_1HTMG][NTf_2].

For $[NTf_2]$ ILs the viscosity correlates with the cation size in the order $[C_1HTMG] < [C_4HTMG] < [C_4C_1TMG] < [C_4C_4TMG]$. This is believed to be a combination of the increase in cation size and van der Waals interaction[20] that lead to the manifestation of a mesostructure with polar-ionic and nonpolar-hydrocarbon domains in the bulk ILs.[6] This structuration is the result of solvophobic interactions and becomes the more pronounced the longer the alkyl chains attached to the anion or cation are.[58] For the $[C_4HTMG]$ cation the viscosity increases in the order $[NTf_2] < [TFA] < [BETI] < [OTf] < [OMs]$. For the $[C_4HTMG]$ cation the viscosity increases in the order $[NTf_2] < [TFA] < [BETI] < [OTf] < [OMs]$. All [OMs] ILs that were liquid at ambient temperature had viscosity values approximately one order of magnitude higher than those with other anions. The viscosities seem to depend primarily on the size of the ions; there is hardly any distinct effect of H-bonding on the viscosity in the PILs visible. This is believed to be the result of the very high ΔpK_a between the IL forming acid and base leading to highly localised protons on the cation. The resulting PILs behave as 'pseudo-AILs'. Similar trends were also reported for viscosities of PILs with the organic superbase 1,8-diazabicyclo-[5,4,0]-undec-7-ene (DBU)[12] and AILs with phosphonium cations.[27] Besides the [OMs] ILs the TMG ILs can be classified as moderately viscous ILs, making them equivalent candidates to other IL cations for applications. The viscosity values of the AIL $[C_4C_1TMG][NTf_2]$ compared with other ILs consisting of aromatic cations such as the 1-methyl-3-octyl-imidazolium $[C_8C_1Im]$ and octyl-pyridinium $[C_8Py]$ of similar weight are in the same range ($\eta^{25\ °C}([C_8C_1Im][NTf_2]) = 92.5$ mPa s[59] and $\eta^{25\ °C}([C_8Py][NTf_2]) = 104.1$ mPa s[60]). The IL $[C_4C_1Pyrr][NTf_2]$ based on the 1-butyl-1-methyl-pyrrolidinium cation is between $[C_1HTMG][NTf_2]$ and $[C_4C_1TMG][NTf_2]$ in both molecular weight and viscosity ($\eta^{25\ °C}([C_4C_1Pyrr][NTf_2]) = 76.5$ mPa s[61]). The phosphonium IL triethylpentylphosphonium $[NTf_2]$ with similar molecular weight is also in the same viscosity range as $[C_4C_1TMG][NTf_2]$ ($\eta^{25\ °C}([P_{2225}][NTf_2]) = 98.0$ mPa s[27]). Triethylammonium $[NTf_2]$ as a representative of PILs is reported to have a comparable viscosity ($\eta^{25\ °C}([Et_3NH][NTf_2]) = 63$ mPa s)[62] to the PIL $[C_1HTMG][NTf_2]$ although the molecular weight of the latter is higher.

Conductivity

Another property of interest is the conductivity of ILs since it is an intrinsic property of this material class. A vast amount of proposed implementations are in the field of electrochemistry and electronic devices[2] where often high charge transport is desired. Therefore, overall conductivity as well as the connection of an ILs' conductivity to its structure in accordance with deviation from ideal behaviour is essential for optimisations when used as electrolyte. The parameters for the VFTs fit of the TMG ILs' molar conductivity Λ_M and their values at 25 °C are listed in Table 3.

Usually the VFT fitting is applied to the specific conductivity[63] (see ESI†) but can also be applied to the molar conductivity as there are only minor, linear changes in density with temperature. The resulting plots of Λ_M against temperature are shown in Fig. 2. All examined ILs show moderate to good conductivities with exception of the [OMs] anion where the values are one order of magnitude lower. The highest molar conductivity value was found for $[C_1HTMG][NTf_2]$. For this anion the molar conductivity shows the opposite trend to the viscosity and is related to the molecular weight where $[C_1HTMG] > [C_4HTMG] > [C_4C_1TMG] > [C_4C_4TMG]$. The decreasing molar conductivity values with elongation of the attached alkyl chains of the TMG ILs is a trend found also for most other reported IL cations[64–66] although there are often no clear tendencies in the VFT fitting parameters visible.[67] Molar conductivities for the anions paired with the $[C_4HTMG]$ cation decrease in the order $[NTf_2] > [BETI] > [OTf] > [TFA] > [OMs]$ which is different from the trends observed for viscosity. The conductivity of the PIL $[C_1HTMG][NTf_2]$ is similar to an ammonium IL with comparable molecular weight ($\Lambda_M^{25\ °C}([Et_3NH][NTf_2]) = 1.05$ S cm^2 mol^{-1})[62]. Also the values for AILs with molecular weights comparable to the $[C_4C_1TMG]$ are

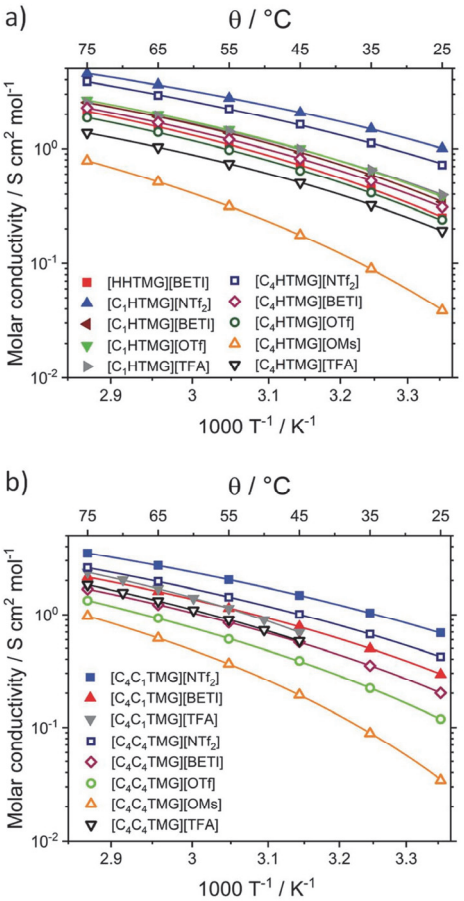

Fig. 2 Molar conductivities of the ILs at different temperatures for (a) protic ILs and (b) aprotic representatives. Drawn lines are the corresponding VFT fits (eqn (11)).

considerably lower underlining the interesting properties of the guanidinium ILs ($\Lambda_M^{25\ °C}$([C_8C_1Im][NTf_2]) = 0.49 S cm^2 mol^{-1};[68] $\Lambda_M^{25\ °C}$([C_8Py] [NTf_2]) = 0.35 S cm^2 mol^{-1};[60] $\Lambda_M^{25\ °C}$([P_{2225}][NTf_2]) = 0.63 S cm^2 mol^{-1})[27]. The molar conductivity and molecular weight of the IL [C_4C_1Pyrr][NTf_2], which often used in electrochemical applications, is between the values of [C_1HTMG][NTf_2] and [C_4C_1TMG][NTf_2] ($\Lambda_M^{25\ °C}$([C_4C_1Pyrr][NTf_2]) = 0.834 S cm^2 mol^{-1})[61] similar to its viscosity values.

NMR diffusometry

The individual self-diffusion coefficients D_{Si} of IL's anions and cations are a measure for the movement of molecular units of the species i in absence of external electric fields or concentrations gradients. The self-diffusion coefficients are inherently connected to the conductivity through linear response theory as both can be expressed in terms of velocity correlation functions. Conclusions about the microscopic structure can be drawn based on this connection. This allows for the control of the structure–property-relations that are required for desired properties. Studying the individual contributions and ratios of the conducting species (or the diffusion of dissolved compounds) reveals more detailed information than macroscopic measurements. The self-diffusion coefficients of the TMG ILs from single temperature measurements, their ratios, the calculated Nernst–Einstein parameters Δ_{NE} and ionicities I_{HR} as reciprocal Haven ratios along with the ionicities I_W obtained from Walden plot are summarised in Table 4. Due to experimental limitations and absence of pronounced supercooling, the values for the methanesulfonate ILs and aprotic trifluoroacetates were only accessible at elevated temperature (45 °C).

The deviations from ideal behaviour show only minor sensitivity in the investigated temperature range as discussed below so that these can be used for a rough comparison. The highest self-diffusion coefficients found were those for [C_1HTMG][NTf_2] in accordance with the lowest viscosity and highest conductivity at this temperature. For the [C_1HTMG] cations both the anion and cation's diffusion coefficients follow the order [NTf_2] > [TFA] > [OTf] > [BETI] similar to the molar conductivities at 25 °C. Upon elongation of the attached alkyl chain the order for the D_{S+} of the [C_4HTMG] cation is changed to [NTf_2] > [BETI] > [TFA] > [OTf] and to [NTf_2] > [TFA] > [BETI] > [OTf] for the case of D_{S-}. For the [NTf_2]-series both cation and anion self-diffusion coefficient show a decrease with increasing cations size in the order [C_1HTMG] > [C_4HTMG] > [C_4C_1TMG] > [C_4C_4TMG]. The ratio of the diffusion coefficients for the [C_1HTMG] and [C_4HTMG] ILs decreases by [BETI] > [NTf_2] > [OTf] > [TFA] corresponding to decreasing size of the anions. In most PILs the cation diffuses faster than the anion, whereas for the AILs, except [C_4C_1TMG][BETI], the anion has a higher self-diffusion coefficient. The self-diffusion coefficients of [C_4C_1TMG][NTf2] for both cation and anion are higher compared to an imidazolium IL with comparable molecular weight ($D_{S+}^{25\ °C}$([C_8C_1Im][NTf_2]) = 9.08 × 10^{-12} m^2 s^{-1}; $D_{S-}^{25\ °C}$([C_8C_1Im][NTf_2]) = 8.99 × 10^{-12} m^2 s^{-1})[66] which may be related to the known nanoscale structuring of IL with long alkyl chains.[6,69]

These results show the complicated interplay of intermolecular forces, molecular size and shape of the ions in bulk ILs. To gain a more detailed insight in the progression of the self-diffusion coefficients, temperature-dependent diffusion measurements for the PILs [C_1HTMG][NTf_2] and [C_1HTMG][TFA] as well as the AIL [C_4C_1TMG][NTf_2] were performed. These three samples were chosen to compare the influence of the anion in PILs as well as the PILs to the AILs. The temperature dependent D_{Si} could also be fitted with the VFT eqn (11). The resulting fit parameters are listed in Table 5 and the measured diffusion coefficients are shown in Fig. 3. The ratio of the self-diffusion coefficients (see Table S19†) does not change with temperature for the AIL and shows only a minor decrease with temperature for the PILs.

Table 4 Cation and anion self-diffusion coefficients D_{Si} of the ionic liquids, their ratio, D_{S+}/D_{S-} the Nernst–Einstein deviation parameter Δ_{NE}, ionicities I_{Hr} expressed as reciprocal Haven ratio and ionicity I_W according to the Walden plot

Ionic liquid	T/°C	$D_{S+}/10^{-12}$ m^2 s^{-1}	$D_{S-}/10^{-12}$ m^2 s^{-1}	D_{S+}/D_{S-}	Δ_{NE}	I_{HR}/H_R^{-1}	I_W
[HHTMG][BETI]	25	5.86	4.16	1.41	0.34	0.66	0.51
[C_1HTMG][NTf_2]	25	20.5	15.7	1.30	0.26	0.74	0.67
[C_1HTMG][BETI]	25	7.83	5.34	1.47	0.30	0.70	0.53
[C_1HTMG][OTf]	25	8.18	6.53	1.25	0.32	0.68	0.65
[C_1HTMG][TFA]	25	11.0	10.3	1.07	0.51	0.49	0.46
[C_4HTMG][NTf_2]	25	13.9	13.0	1.08	0.29	0.71	0.60
[C_4HTMG][BETI]	25	6.73	5.33	1.26	0.32	0.68	0.54
[C_4HTMG][OTf]	25	5.13	4.73	1.08	0.35	0.65	0.56
[C_4HTMG][OMs]	45	5.13	5.88	0.87	0.55	0.46	0.50
[C_4HTMG][TFA]	25	6.08	6.13	0.99	0.58	0.42	0.32
[C_4C_1TMG][NTf_2]	25	12.1	12.5	0.97	0.25	0.75	0.64
[C_4C_1TMG][BETI]	25	6.28	5.63	1.12	0.34	0.66	0.52
[C_4C_1TMG][TFA]	45	15.5	18.0	0.86	0.36	0.64	0.50
[C_4C_4TMG][NTf_2]	25	6.63	8.70	0.76	0.27	0.73	0.57
[C_4C_4TMG][BETI]	25	3.67	4.14	0.89	0.31	0.69	0.50
[C_4C_4TMG][OTf]	25	1.95	2.48	0.78	0.29	0.71	0.51
[C_4C_4TMG][OMs]	45	3.43	5.29	0.65	0.37	0.63	0.50
[C_4C_4TMG][TFA]	45	14.1	14.9	0.95	0.43	0.57	0.46

Table 5 VFT fit parameters of the self-diffusion coefficients D_{Si} (cation: $i = +$; anion: $i = -$)

Ionic liquid	i	$D_{Si,0}/10^{-7}$ m^2 mol^{-1}	B/K	T_0/K
[C_1HTMG][NTf_2]	+	1.05	−620.7	199.3
[C_1HTMG][NTf_2]	−	0.339	−409.0	223.0
[C_1HTMG][TFA]	+	30.4	−1647	136.3
[C_1HTMG][TFA]	−	18.9	−1446	150.3
[C_4C_1TMG][NTf_2]	+	0.337	−488.0	212.2
[C_4C_1TMG][NTf_2]	−	0.376	−504.0	210.4

Nernst–Einstein and Walden relation

As mentioned earlier, the Nernst–Einstein parameter Δ_{NE} and ionicity I_{HR} as reciprocal Haven ratio are important and simple quantities for the optimisation of ILs, although their interpretation is a matter of debate. The I_{HR} values obtained for all cations follow the order [NTf_2] > [BETI] > [OTf] > [OMs] > [TFA] (besides [C_4C_4TMG] where [BETI] and [OTf] are interchanged), corresponding to a decrease in the pK_a values of the anion's conjugate acids. For the anions [NTf_2], [BETI] and [OTf] the I_{HR} values are all in the same range, independent of being PILs or AILs. The I_{HR} values for the protic methanesulfonate and protic trifluoroacetate ILs are significantly lower than those of their aprotic counterparts. This might indicate a more pronounced hydrogen bond due to the lower difference in pK_a between the precursors, leading to a formally neutral species that does not contribute to the macroscopic conductivity. These findings are in accordance to literature findings that a high ΔpK_a is necessary to obtain ILs with high ionicities.[12,24] Watanabe *et al.* also found similar trends but lower ionicity values for ILs from the larger superbase DBU.[12] The observed reciprocal Haven ratios of the protic TMG ILs are also considerably higher than those of other PILs such as ammonium[70,71] or amidinium[12] underlining its correlation with the highly basic nature of the precursor.[12] To the best of our knowledge these are also the highest I_{HR} values reported for PILs so far. Compared to other classes of ILs, most of the TMG-based ILs show high values for the reciprocal Haven ratio making them very interesting for electrochemical applications.[72] The I_{HR} values reported for imidazolium, for instance, range from 0.52 to 0.76,[72] those of phosphonium ILs from 0.47 to 0.71 (ref. 27) and those of ammonium from 0.06 to 0.62.[71] Values reported for AILs consisting of aromatic cations with similar molecular weight to the [C_4C_1TMG] cation are significantly lower (I_{HR}([C_8C_1Im][NTf_2]) ≈ 0.32; 1-methyl-1-octylpyrrolidinium NTf_2: I_{HR}([C_8C_1Pyrr][NTf_2]) ≈ 0.41).[60]

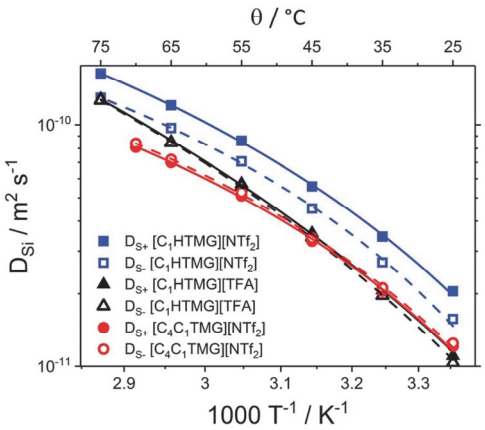

Fig. 3 Temperature-dependent individual self-diffusion coefficients of the TMG ILs. Solid lines are the VFT fits for the cations, dashed ones for the anions.

Due to its simplicity and easy interpretation, the Walden plots are also widely used in the literature.[22] The Walden plots of the investigated ILs are shown in Fig. 4. Analysis of the PILs and AILs according to the fractional Walden rule (4) yield straight lines with slopes approximately unity (values given in Table S20†). Although being quite a straightforward approach, the findings for the ionicity trends quantified by the reciprocal Haven ratio are well reproduced. The ILs with the highest ionicities show the highest values for the parameter log(C) and *vice versa*. Since the Walden plot uses macroscopic parameters it can be seen as a practical measure for overall performance in which the highest log(C) values belong to highly conductive and highly fluid ILs. From the ratio of the measured molar conductivity to the ideal conductivity, the ionicity I_W according to the Walden plot can be calculated (5). However this method remains a more qualitative approach. The obtained values for the single point measurements are listed in Table 3 and are in good agreement with the general trends of the ionicities I_{HR} but smaller in their overall values, with [C_4HTMG][OMs] being the only exception. The temperature dependent progression of the I_{HR} and I_W are shown in Fig. 5. Both show a slight decrease with temperature that is a bit more pronounced for the reciprocal Haven ratio. The highest overall I_{HR} value was found for the AIL followed by the protic [NTf_2] IL with minor interspacing. The protic [TFA] IL shows distinct lower reciprocal Haven ratios and I_W values than the [NTf_2] ones at all temperatures. Marginally decreasing or constant I_{HR} values with temperature and a strong dependence on the pK_a of the protonated anion are also found for a number of other IL systems such imidazolium,[66,73] phosphonium[27] and ammonium.[70]

Stokes–Einstein–Sutherland relation, velocity cross-correlation and distinct diffusion coefficients

The Stokes–Einstein–Sutherland (SES) plot is an empirical viscosity correlation that relates the diffusion coefficients to the reciprocal viscosity (fluidity).[21] The obtained SES-plot of the individual self-diffusion coefficients is shown in Fig. 6. All of the investigated ILs yield straight lines in the SES plot with slopes around unity (Table S21†). The exponents found for the cations were observed to be smaller than the ones for the anions in the same IL. Analogous plots can be performed for the viscosity scaling of the distinct diffusion coefficients D_{ij}^{d} calculated from the velocity cross-correlation coefficients (VCC) f_{ij} (7–10). These quantities are another interpretation of IL transport properties if self-diffusion and conductivity data are experimentally available. Contrary to the situation usually found in electrolyte

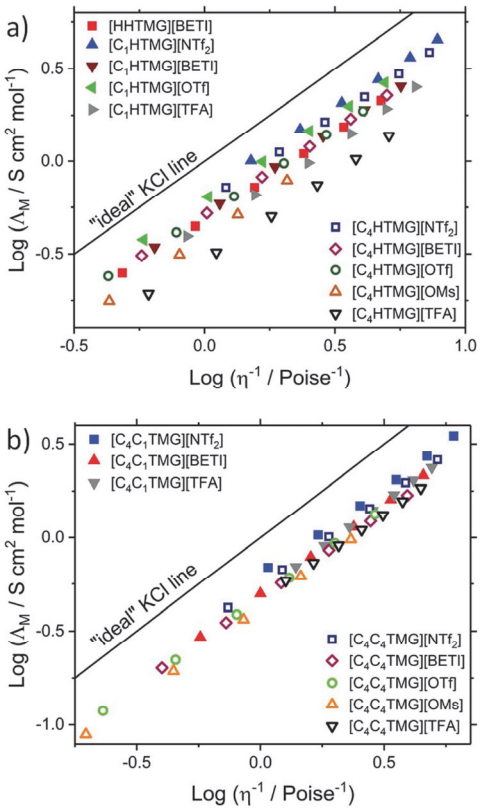

Fig. 4 Walden plots of (a) the protic and (b) aprotic TMG-ILs investigated in this study. Temperature of the data points increases from left to right.

solutions, the D_{ij}^{d} and VCC are all negative quantities in bulk ILs so that the velocities of the ions are anti-correlated in the ensemble as a result of the momentum conservation.[5] The SES

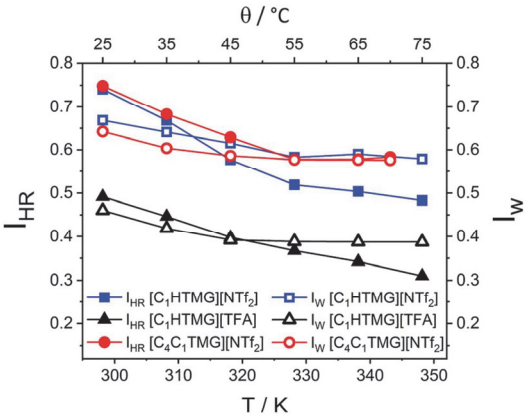

Fig. 5 Temperature dependent ionicity I_{HR} as reciprocal Haven ratio and ionicity I_W from Walden plot. Drawn lines are a guide to the eye.

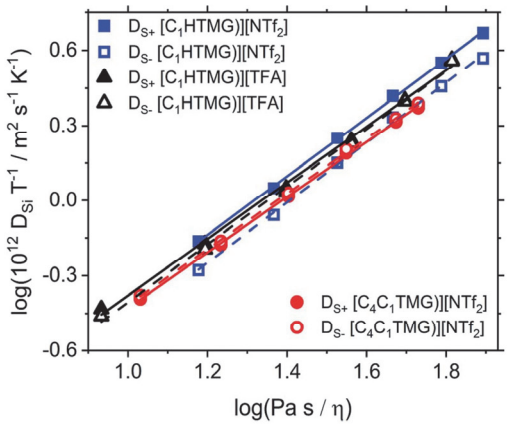

Fig. 6 Stokes–Einstein–Sutherland plot of the self-diffusion coefficients D_{Si} as a function of fluidity (inverse viscosity). Solid lines are the linear fits for the cations, dashed ones for the anions.

plot for the distinct diffusion coefficients is shown in Fig. 7 and their values could also be fitted linearly (see Table S22 and S23†). The VCC of the [NTf_2] ILs obey the order $f_{--} < f_{++} < f_{+-}$ consistent with the findings for a number of other [NTf_2] ILs investigated.[21,61] In the protic [TFA] IL the order of f_{--} and f_{++} is reversed with smaller difference between the two quantities at all viscosities. As the anion–anion VCCs are largest in magnitude and most negative for the [NTf_2] ILs, the anti-correlations of the ion velocities averaged over an ensemble are largest for these interactions. Then again for [C_1HTMG][TFA] the cation–cation VCC are dominant. At the same viscosity the unlike-charged ions VCC f_{+-} is the least negative in [C_1HTMG][TFA]. This means that the anti-correlation of cation and anion is less

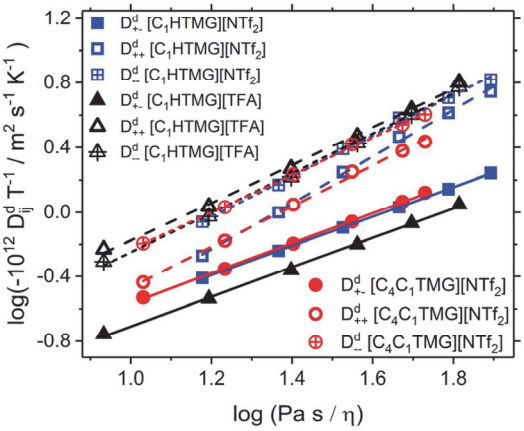

Fig. 7 Stokes–Einstein–Sutherland plot of the distinct self-diffusion coefficients D_{ij}^{d} as a function of fluidity (inverse viscosity). Note that all distinct diffusion coefficients are negative quantities so that $-D_{ij}^{d}$ is plotted and the order of the VCCs is reversed. Solid lines are the linear fits for the D_{+-}^{d}, dashed ones for the D_{++}^{d} and dotted for D_{--}^{d} lines are the linear fits for the D_{+-}^{d}, dashed ones for the D_{++}^{d} and dotted for D_{--}^{d}.

pronounced leading to a higher discrepancy between expected and measured conductivity. Harris reported that the order of the like-ion VCCs may be related to the ion size and liquid structure and that the magnitude of Δ_{NE} is proportional to the difference between f_{+-} and the arithmetic mean of the like-ionic VCCs f_{--} and f_{++}.[31] This large difference compared to both the protic and aprotic [NTf_2] IL is also found in [C_1HTMG][TFA]. It reproduces the findings and quantifications of the larger deviation from ideal behaviour found by other approaches above although there are other assumptions about their origin in literature. However the findings also show that the deviation is related to the anion–cation combination and not to the difference of protic and aprotic ILs *per se*.

Conclusions

We synthesised a series of protic and aprotic ILs based on the TMG cation. The used anions stem from a variety of acids with different pK_a values. Although this type of IL shows beneficial characteristics for several implementations it is has not been comprehensively investigated so far. The cations are derivatives of super strong bases and have a delocalised π-system like the intensively investigated and applied imidazolium and pyridinium cations. The length of the attached alkyl side chain was varied for the sake of a systematic investigation. Most of these ILs have, to the best of our knowledge, not been reported in the literature before. We measured important fundamental properties such as thermal transitions and densities as well as the transport quantities viscosity, conductivity and self-diffusion coefficients. The ILs show a wide range of diverse phase-transition behaviours and many of them are RTILs or exhibit supercooled states. Temperature dependence of viscosity, molar conductivity and self-diffusion coefficients are empirically well described by the VFT (11) or Litovitz eqn (12). Scaling of and correlation between the transport properties were analysed by the Nernst–Einstein, Walden and Stokes–Einstein–Sutherland relations. The discrepancy between ideal electrolyte behaviour and experimental quantities was quantified by means of the ionicity I_{HR} as reciprocal Haven ratio, fractional Walden approach and ionicity I_W from Walden plot. All the TMG ILs show transport properties comparable to other ILs subclasses together with high ionicities, especially when compared to other PILs with more acidic cation protons/lower pK_a values of the constituting base. Lower ionicity values were also found for the PILs that incorporate anions from acids with higher pK_a values. Also the velocity-cross-correlation coefficients of the unlike-ions in [C_1HTMG][TFA] exhibit less anticorrelation. This is the cause for its reduced conductivity in relation to the diffusive properties compared to the [NTf_2] ILs. The results show that smaller discrepancies between expected and measured conductivity can be achieved for PILs with high ΔpK_a between constituting acid and base. Furthermore the TMG PILs and AILs show comparable transport properties which are more related to the size of the cation rather than to the occurrence of an acidic proton in the PILs. These 'pseudo AILs' show characteristics similar to their alkylated analogues. This makes the TMG-based PILs promising candidates for practical applications that combine the advantages of PILs, such as economic synthesis and improved transport properties, due to lower molecular weight with the higher ionicity values usually found for AILs. These results provide a better understanding of guanidinium-based ILs, the difference between the PIL and AIL subclasses and the interrelations of their transport properties.

Conflicts of interest

There are no conflicts of interest to declare.

Acknowledgements

We gratefully acknowledge financial support by the German Research Foundation, DFG, grant number HE 2403/21-1.

References

1 J. P. Hallett and T. Welton, *Chem. Rev.*, 2011, **111**, 3508–3576.
2 M. Watanabe, M. L. Thomas, S. Zhang, K. Ueno, T. Yasuda and K. Dokko, *Chem. Rev.*, 2017, **117**, 7190–7239.
3 G. G. Eshetu, M. Armand, H. Ohno, B. Scrosati and S. Passerini, *Energy Environ. Sci.*, 2016, **9**, 49–61.
4 K. Dong, X. Liu, H. Dong, X. Zhang and S. Zhang, *Chem. Rev.*, 2017, **117**, 6636–6695.
5 K. R. Harris, T. Makino and M. Kanakubo, *Phys. Chem. Chem. Phys.*, 2014, **16**, 9161–9170.
6 R. Hayes, G. G. Warr and R. Atkin, *Chem. Rev.*, 2015, **115**, 6357–6426.
7 P. A. Hunt, C. R. Ashworth and R. P. Matthews, *Chem. Soc. Rev.*, 2015, **44**, 1257–1288.
8 T. Welton, *Biophys. Rev.*, 2018, **10**, 691–706.
9 C. A. Angell, N. Byrne and J.-P. Belieres, *Acc. Chem. Res.*, 2007, **40**, 1228–1236.
10 T. L. Greaves and C. J. Drummond, *Chem. Rev.*, 2015, **115**, 11379–11448.
11 K. Dong, S. Zhang and J. Wang, *Chem. Commun.*, 2016, **52**, 6744–6764.
12 M. S. Miran, H. Kinoshita, T. Yasuda, M. A. B. H. Susan and M. Watanabe, *Phys. Chem. Chem. Phys.*, 2012, **14**, 5178.
13 K. Abdur-Rashid, T. P. Fong, B. Greaves, D. G. Gusev, J. G. Hinman, S. E. Landau, A. J. Lough and R. H. Morris, *J. Am. Chem. Soc.*, 2000, **122**, 9155–9171.
14 M. S. Miran, H. Kinoshita, T. Yasuda, M. A. B. H. Susan and M. Watanabe, *Chem. Commun.*, 2011, **47**, 12676.
15 J. Nowicki, M. Muszyński and J.-P. Mikkola, *RSC Adv.*, 2016, **6**, 9194–9208.
16 S. Li, Y. Lin, H. Xie, S. Zhang and J. Xu, *Org. Lett.*, 2006, **8**, 391–394.
17 S. Fang, L. Yang, J. Wang, M. Li, K. Tachibana and K. Kamijima, *Electrochim. Acta*, 2009, **54**, 4269–4273.
18 X. Lu, J. Yu, J. Wu, Y. Guo, H. Xie and W. Fang, *J. Phys. Chem. B*, 2015, **119**, 8054–8062.
19 A. Castiglia, H. M. El Sehrawi, T. Orbegozo, D. Spitzner, B. Claasen, W. Frey, W. Kantlehner and V. Jäger, *Zeitschrift für Naturforsch. B*, 2012, **67**, 337–346.
20 G. Yu, D. Zhao, L. Wen, S. Yang and X. Chen, *AIChE J.*, 2012, **58**, 2885–2899.

21 K. R. Harris, *J. Mol. Liq.*, 2016, **222**, 520–534.
22 D. R. MacFarlane, M. Forsyth, E. I. Izgorodina, A. P. Abbott, G. Annat and K. Fraser, *Phys. Chem. Chem. Phys.*, 2009, **11**, 4962.
23 K. Ueno, H. Tokuda and M. Watanabe, *Phys. Chem. Chem. Phys.*, 2010, **12**, 1649–1658.
24 M. Yoshizawa, W. Xu and C. A. Angell, *J. Am. Chem. Soc.*, 2003, **125**, 15411–15419.
25 C. Schreiner, S. Zugmann, R. Hartl and H. J. Gores, *J. Chem. Eng. Data*, 2010, **55**, 4372–4377.
26 H. Tokuda, K. Hayamizu, K. Ishii, M. A. B. H. Susan and M. Watanabe, *J. Phys. Chem. B*, 2004, **108**, 16593–16600.
27 F. Philippi, D. Rauber, J. Zapp and R. Hempelmann, *Phys. Chem. Chem. Phys.*, 2017, **19**, 23015–23023.
28 B. Kirchner, F. Malberg, D. S. Firaha and O. Hollóczki, *J. Phys. Condens. Matter*, 2015, **27**, 463002.
29 G. W. Driver, Y. Huang, A. Laaksonen, T. Sparrman, Y.-L. Wang and P.-O. Westlund, *Phys. Chem. Chem. Phys.*, 2017, **19**, 4975–4988.
30 M. Gouverneur, J. Kopp, L. van Wüllen and M. Schönhoff, *Phys. Chem. Chem. Phys.*, 2015, **17**, 30680–30686.
31 K. R. Harris, *J. Phys. Chem. B*, 2016, **120**, 12135–12147.
32 O. Hollóczki, F. Malberg, T. Welton and B. Kirchner, *Phys. Chem. Chem. Phys.*, 2014, **16**, 16880–16890.
33 H. K. Kashyap, H. V. R. Annapureddy, F. O. Raineri and C. J. Margulis, *J. Phys. Chem. B*, 2011, **115**, 13212–13221.
34 D. W. McCall and D. C. Douglass, *J. Phys. Chem.*, 1967, **71**, 987–997.
35 H. G. Hertz, K. R. Harris, R. Mills and L. A. Woolf, *Berichte der Bunsengesellschaft für physikalische Chemie*, 1977, **81**, 664–670.
36 K. R. Harris, *J. Phys. Chem. B*, 2010, **114**, 9572–9577.
37 H. J. Schoenert, *J. Phys. Chem.*, 1984, **88**, 3359–3363.
38 T. Rüther, M. Kanakubo, A. S. Best and K. R. Harris, *Phys. Chem. Chem. Phys.*, 2017, **19**, 10527–10542.
39 H. Vogel, *Phys. Z.*, 1921, **22**, 645–646.
40 G. Tammann and W. Hesse, *Zeitschrift für anorganische und allgemeine Chemie*, 1926, **156**, 245–257.
41 T. A. Litovitz, *J. Chem. Phys.*, 1952, **20**, 1088–1089.
42 K. R. Harris and M. Kanakubo, *J. Phys. Chem. B*, 2016, **120**, 12937–12949.
43 K. R. Harris and M. Kanakubo, *J. Chem. Eng. Data*, 2016, **61**, 2399–2411.
44 K. R. Harris, M. Kanakubo, D. Kodama, T. Makino, Y. Mizuguchi, M. Watanabe and T. Watanabe, *J. Chem. Eng. Data*, 2018, **63**, 2015–2027.
45 E. Gómez, N. Calvar and Á. Domínguez, in *Ionic Liquids - Current State of the Art*, InTech, 2015.
46 *CRC Handbook of Chemistry and Physics*, ed. W. M. Haynes, Taylor & Francis Group, Boca Raton, 95th edn, 2014.
47 D. H. Wu, A. D. Chen and C. S. Johnson, *J. Magn. Reson. Ser. A*, 1995, **115**, 260–264.
48 G. Annat, D. R. MacFarlane and M. Forsyth, *J. Phys. Chem. B*, 2007, **111**, 9018–9024.
49 W. S. Price, P. Stilbs, B. Jönsson and O. Söderman, *J. Magn. Reson.*, 2001, **150**, 49–56.
50 G. H. Sørland, *Dynamic Pulsed-Field-Gradient NMR*, Springer Berlin Heidelberg, Berlin, Heidelberg, 2014, vol. 110.
51 C. S. Johnson, *Prog. Nucl. Magn. Reson. Spectrosc.*, 1999, **34**, 203–256.
52 S. J. Gibbs and C. S. Johnson, *J. Magn. Reson.*, 1991, **93**, 395–402.
53 R. Mills, *J. Phys. Chem.*, 1973, **77**, 685–688.
54 M. Holz, S. R. Heil and A. Sacco, *Phys. Chem. Chem. Phys.*, 2000, **2**, 4740–4742.
55 L. G. Longsworth, *J. Phys. Chem.*, 1960, **64**, 1914–1917.
56 K. R. Harris, B. Ganbold and W. S. Price, *J. Chem. Eng. Data*, 2015, **60**, 3506–3517.
57 A. Martinelli, M. Maréchal, Å. Östlund and J. Cambedouzou, *Phys. Chem. Chem. Phys.*, 2013, **15**, 5510.
58 J. N. A. Canongia Lopes and A. A. H. P. Pádua, *J. Phys. Chem. B*, 2006, **110**, 3330–3335.
59 A. E. Andreatta, A. Arce, E. Rodil and A. Soto, *J. Chem. Thermodyn.*, 2009, **41**, 1317–1323.
60 J.-M. Andanson, N. Papaiconomou, P.-A. Cable, M. Traïkia, I. Billard and P. Husson, *Phys. Chem. Chem. Phys.*, 2017, **19**, 28834–28840.
61 K. R. Harris, L. A. Woolf, M. Kanakubo and T. Rüther, *J. Chem. Eng. Data*, 2011, **56**, 4672–4685.
62 K. Tsunashima, M. Fukushima and M. Matsumiya, *Electrochemistry*, 2012, **80**, 904–906.
63 J. Vila, P. Ginés, J. M. Pico, C. Franjo, E. Jiménez, L. M. Varela and O. Cabeza, *Fluid Phase Equilib.*, 2006, **242**, 141–146.
64 O. Zech, A. Stoppa, R. Buchner and W. Kunz, *J. Chem. Eng. Data*, 2010, **55**, 1774–1778.
65 K. Tsunashima and M. Sugiya, *Electrochem. Commun.*, 2007, **9**, 2353–2358.
66 H. Tokuda, K. Hayamizu, K. Ishii, M. A. B. H. Susan and M. Watanabe, *J. Phys. Chem. B*, 2005, **109**, 6103–6110.
67 J. Vila, L. M. Varela and O. Cabeza, *Electrochim. Acta*, 2007, **52**, 7413–7417.
68 S. Papović, S. Gadžurić, M. Bešter-Rogač and M. Vraneš, *J. Chem. Thermodyn.*, 2016, **102**, 367–377.
69 J. Haddad, D. Pontoni, B. M. Murphy, S. Festersen, B. Runge, O. M. Magnussen, H.-G. Steinrück, H. Reichert, B. M. Ocko and M. Deutsch, *Proc. Natl. Acad. Sci. U. S. A.*, 2018, **115**, E1100–E1107.
70 M. Martinez, Y. Molmeret, L. Cointeaux, C. Iojoiu, J. C. Leprêtre, N. El Kissi, P. Judeinstein and J. Y. Sanchez, *J. Power Sources*, 2010, **195**, 5829–5839.
71 S. K. Davidowski, F. Thompson, W. Huang, M. Hasani, S. A. Amin, C. A. Angell and J. L. Yarger, *J. Phys. Chem. B*, 2016, **120**, 4279–4285.
72 H. Tokuda, S. Tsuzuki, M. A. B. H. Susan, K. Hayamizu and M. Watanabe, *J. Phys. Chem. B*, 2006, **110**, 19593–19600.
73 B. E. Mbondo Tsamba, S. Sarraute, M. Traïkia and P. Husson, *J. Chem. Eng. Data*, 2014, **59**, 1747–1754.

2.2 Publication B

Transport properties and ionicity of phosphonium ionic liquids

Frederik Philippi, Daniel Rauber, Josef Zapp, Rolf Hempelmann.

Phys. Chem. Chem. Phys., **2017**, 19, 23015-23023.

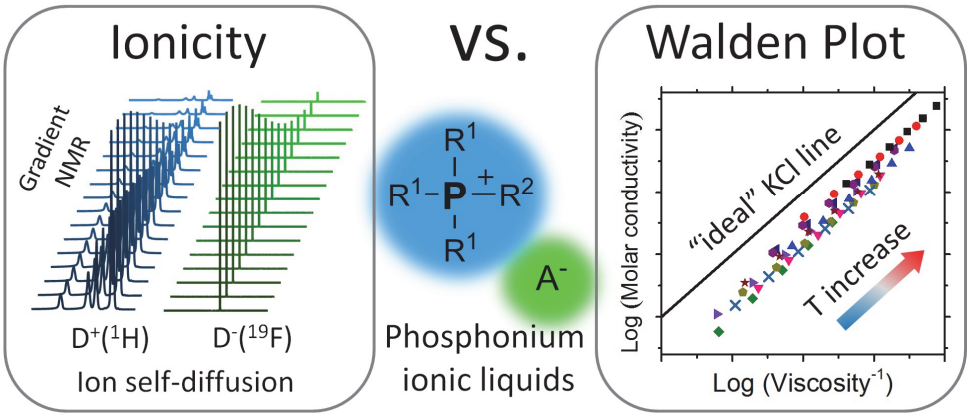

PCCP

PAPER

View Article Online
View Journal | View Issue

Cite this: *Phys. Chem. Chem. Phys.*, 2017, **19**, 23015

Transport properties and ionicity of phosphonium ionic liquids†

F. Philippi,‡[a] D. Rauber,‡[ab] J. Zapp[c] and R. Hempelmann *[ab]

Received 6th July 2017,
Accepted 2nd August 2017

DOI: 10.1039/c7cp04552b

rsc.li/pccp

Ionic liquids (ILs) are promising electrolytes and many efforts have been made in basic scientific research as well as in applied research. In this contribution, we synthesised a variety of partly novel phosphonium ILs with different anions as well as with different compositions and lengths of the side chains of the cations. We measured a variety of their important transport properties such as viscosity, conductivity and diffusivity by means of stress-controlled rheology, impedance spectroscopy and PFGSTE NMR diffusometry. The results are analysed with respect to different models for derivation from ideal behaviours such as the ionicity and the (fractional) Walden rule depending on their molecular structure. These models are well established in the literature and are herein applied to rarely investigated but promising phosphonium ILs, with a particular emphasis placed on the effect of ether side chains. In comparison, the models show a qualitative correlation but distinct deviation in the quantification especially in the temperature dependent values and with other IL systems. These results aim to facilitate a better understanding of the IL properties depending on the molecular composition and by this way help to choose the ILs with optimal properties for practical applications.

Introduction

Ionic liquids currently receive high attention throughout the fields of science because of their unique, enhanced properties and immense possibilities for tuning and optimisation.[1,2] The particular interest concerning applications in electrochemistry such as battery and capacitor technology is due to their relatively wide electrochemical windows, especially those based on phosphonium cations,[3,4] and a high concentration of free ions. Furthermore major advantages are their negligible vapour pressure together with low flammability resulting in an intrinsic gain in safety, even if the issue of toxicity is not yet fully resolved.[5,6] An enormous flexibility arises from the many available structural motifs and variations. They therefore have the potential to exhibit a better performance compared to many established systems, but it becomes challenging to "choose the best", *i.e.* the IL which shows the optimal behaviour for a desired application.[2]

The development of key strategies for systematic customisation and optimisation of ILs is therefore of high significance. For almost all practical applications, for example separation, synthesis or electrochemistry, the knowledge of the transport properties is of crucial importance. This especially holds true for ionic liquids, whose, in most cases, higher viscosities may limit their applicability. In addition to the impulse transport embodied by the viscosity η, the self-diffusion coefficient D is of interest as a measure for microscopic transport processes and therefore the ion mobility. In electrochemistry there is hence the need for ion combinations showing high mobility and conductivity (as a measure of charge transport) paired with electrochemical stability. For pure undiluted ILs deviations from the ideal charge transport are consistently found and consequently the knowledge about structure–property relationships is important to achieve maximum conductivity.[7,8]

All herein investigated ionic liquids are based on quaternary phosphonium cations and their structures are displayed in Scheme 1 together with the corresponding anions. The series was chosen to directly investigate the influence of molecular structure on the properties of this IL subclass in correlation with the choice of anion and incorporated side chain compositions as well as the asymmetric side chain length. Despite their sometimes superior properties, phosphonium-based ionic liquids are still much less commonly investigated compared to the very widely used imidazolium and ammonium ILs. Phosphonium-based ILs

[a] *Institute of Physical Chemistry, Saarland University, Campus B 2 2, 66123 Saarbrücken, Germany. E-mail: r.hempelmann@mx.uni-saarland.de*
[b] *Transfercenter Sustainable Electrochemistry, Saarland University and KIST Europe, Am Markt, Zeile 3, 66125 Saarbrücken, Germany*
[c] *Institute of Pharmaceutical Biology, Saarland University, Campus C 2 3, 66123 Saarbrücken, Germany*

† Electronic supplementary information (ESI) available: Experimental setup, detailed pulse sequence and parameters, further information about calibration and raw data processing. Experimental data for specific conductivity, molar conductivity, self-diffusion coefficients and densities together with the fit results. Detailed protocols for the synthesis of all compounds and the corresponding NMR spectra. See DOI: 10.1039/c7cp04552b

‡ Frederik Philippi and Daniel Rauber are equally contributing authors.

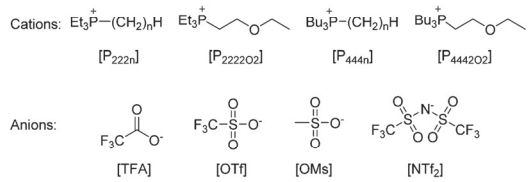

Scheme 1 Structure of ions investigated in this publication.

show for example a higher chemical stability compared to the imidazolium ILs that were found to react with certain bases, electro- and nucleophiles.[9] Surprisingly, they often exhibit good stability towards alkaline media, even as strong as Grignard compounds.[10] Furthermore phosphonium ILs are in general less viscous and slightly more stable towards electrochemical or thermal degradation than the ammonium based IL analogues.[11]

The introduction of ether groups is partly at the expense of (thermal) stability.[11] It nevertheless goes hand in hand with a higher mobility and allows for a fine adjustment of the properties.[12] The scientific discourse concerning the more controversial topics mainly focused on imidazolium based ionic liquids so far, although phosphonium ionic liquids are readily accessible in high purity as long as the initial phosphines are protected from oxygen.

The (industrial) synthesis proceeds *via* alkylation of tertiary phosphines in nearly quantitative yield with leaving groups being mostly halides but also others like tosylates.[13] With halides as leaving groups, the desired anion has to be introduced in another step, usually *via* salt metathesis. Problems may then arise from the residual halide content. Unlike quaternisation, which can be carried out in bulk, salt metathesis generally requires the use of molecular organic solvents. Avoidance of the latter, however, is one of the aims in using ionic liquids.[11] Solvent free methods to eliminate halides are described in the literature, we just mention the use of methyl triflate as a possible method at this point.[14] Attractive from an economical point of view is the introduction of an anion in the quaternisation.[15]

Diffusometry and ionicity

Self-diffusion coefficients presented in this work were obtained by means of NMR diffusometry. The measurements are not straightforward, but nevertheless feasible. Therefore some background information about the underlying principles and the obtained results is given here. For ionic liquids as rather viscous systems, the simple pulsed field-gradient spinecho experiment (PFGSE) is inappropriate due to several drawbacks and artifacts.[16,17] The pulse sequence shown in Fig. 1, which was developed by D. Wu *et al.*,[18] is more robust. It is based on a pulsed field-gradient stimulated echo (PFGSTE) experiment incorporating bipolar pulsed field gradients g and an additional longitudinal eddy current delay T_e. The purpose of the latter is to minimise disturbing eddy currents, which result from the large currents that have to be switched on and off to generate the required magnetic field gradients.[18,19] During the two periods

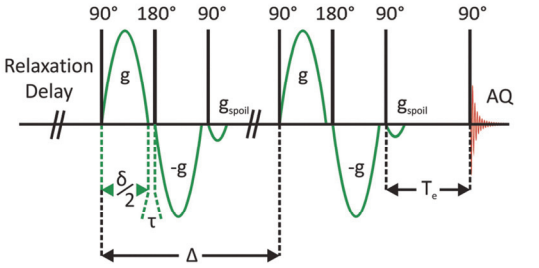

Fig. 1 PFGSTE pulse sequence used for self-diffusion measurement.

where the macroscopic magnetisation is stored along the direction of the static magnetic field, suitable gradient pulses g_{spoil} should be applied to wipe out any transverse magnetisation. These spoiler gradients are thus of great help in reducing the negative effects of inaccurate pulses or undesired coherence pathways.[16,19,20]

It is favourable to keep the total experiment time fixed throughout every separate measurement as in this case signal attenuation due to relaxation does not have to be taken into account. The signal intensity I then obeys the well-known Stejskal–Tanner equation shown below.[19,21,22]

$$\ln\frac{I}{I_0} = -D\gamma^2\delta^2 g^2\left(\Delta - \frac{\delta}{3} - \frac{\tau}{2}\right) = DQ \qquad (1)$$

Appropriate values for diffusion time Δ as well as for the overall gradient duration δ have to be determined prior to the actual measurement. It is worth mentioning that the gradient interspacing τ, which is due to the bipolar gradients, does not appear in the original equation.[19,21] Restrictions arise from the dependence of the gyromagnetic ratio γ as nuclei with rather small values of γ like ^{13}C require specialised equipment to produce sufficient gradient strengths. This poses no problem as the nuclei ^{1}H and ^{19}F are inherently present in most ILs and are accessible to high resolution NMR with a z-gradient probe.

Quantitative knowledge of self-diffusion coefficients together with the viscosity and conductivity of the system hence provides a good starting point for selective optimisation, for example regarding CO_2 capture.[23] While viscosity is measured directly using rheological experiments, the molar conductivity Λ_M is easily obtained from measurements of specific conductivity κ and density ρ as given by the following equation.[24,25]

$$\Lambda_M = \frac{\kappa}{c} = \frac{\kappa M}{\rho} \qquad (2)$$

Assuming that the motion of diluted spherical ions with charge z_i in the bulk is entirely uncorrelated, the theoretical molar conductivity Λ_{NMR} is expected to obey the familiar Nernst–Einstein equation:[26]

$$\Lambda_{NMR} = \frac{F^2}{RT}\sum_i z_i D_i \qquad (3)$$

Ionic liquids as neat salt melts are far from being diluted, and more than ever far from being ideally diluted. Considerable deviations owing to correlated motion and structuring are therefore

anticipated, and the molar conductivity is in most cases smaller than predicted from the Nernst–Einstein equation. In rather diluted solution, ion pair formation is believed to be the reason for this finding. Consequently the Haven ratio is frequently used to quantify "ionicity", similar to the Nernst–Einstein parameter Δ_{NE} for "aggregation":[26,27]

$$H_R = \frac{\Lambda_M}{\Lambda_{NMR}} \text{ and } \Delta_{NE} = 1 - H_R \quad (4)$$

Whether this holds true for ionic liquids is still lively discussed.[28] Kashyap *et al.* reported that anticorrelated motion of ions with the same charge should be regarded as a reason for the decrease of conductivity instead of associates or ion pairs.[29] In contrast to this, Hollóczki *et al.* suggested charge transfer as the reason for lowered conductivity rather than any sort of correlation or anticorrelation.[30] Another experimental approach using surface force measurements indicated a very dilute nature of ionic liquids, with the resulting ionicity being tremendously different from other models.[31] However recent considerations addressed several issues of the surface force measurements, implying a very short lifetime of ion pairs, if there are any at all.[32] To put it in a nutshell, the debate is far from settled. Countless contrary contributions to these topics have been published, all consistent in themselves. Nonetheless, properties like molar conductivity, viscosity or self-diffusion provide valuable information about the system of interest. The Haven ratio is in this context used as a criterion for ionicity or – less controversial – "deviation from ideality". Together with the other properties, it shall serve as the linchpin for further optimisations. Another established model is the Walden plot, which is appealing in its simplicity. It is derived from viscosity and molar conductivity and suits as another rough estimate for the deviation from ideality. Several more detailed models based on Walden's rule were proposed, such as the adjusted Walden plot and the fractional Walden rule.[33,34] In contrast to the adjusted Walden plot – which considers ionic radii and only contains C as a parameter – the fractional Walden rule used in this work is obtained from the original equation by introduction of α as an additional parameter:

$$\log \Lambda_M = \log C + \alpha \log \frac{1}{\eta} \quad (5)$$

This additional parameter shows the deviation from the original relation as found by Walden, in which α equals unity. From the vertical distance ΔW in the Walden plot, another measure of ionicity can be obtained comparing Λ_M to the conductivity at the ideal KCl line Λ_M^0:[34]

$$\frac{\Lambda_M}{\Lambda_M^0} = \frac{\Lambda_M}{1/\eta} = 10^{-\left(\log\frac{1}{\eta} - \log\Lambda\right)} = 10^{\Delta W} \quad (6)$$

Results and discussion

Thermal transitions and densities

Melting points T_M and glass transition temperatures T_G are important to know as they often become a limit for practical applications. Thermal transitions found *via* dynamic scanning calorimetry are listed in Table 1 together with their densities and molar volumes at 25 °C. All of the investigated ionic liquids are liquids at room temperature, two of them remain in a supercooled state for extended times with crystallisation temperatures T_c significantly below the respective melting points. For the cations without ether groups, melting points were found for short ($[P_{4442}][NTf_2]$) and long ($[P_{44410}][NTf_2]$) chains, whereas for intermediate chain lengths only glass transitions were found.

Table 1 Thermal transitions; densities and molar volumes at room temperature

	T_c/°C	T_G/°C	T_M/°C	$\rho^{25\,°C}$/g mL^{-1}	$V_M^{25\,°C}$/mL mol^{-1}
$[P_{2222O2}][NTf_2]$	−10	—	36	1.340	352
$[P_{2225}][NTf_2]$	−37	—	21	1.302	361
$[P_{2228}][NTf_2]$	—	−82	—	1.243	411
$[P_{4442O2}][TFA]$	—	−76	—	1.057	368
$[P_{4442O2}][OMs]$	—	−63	—	1.027	361
$[P_{4442O2}][NTf_2]$	—	−78	—	1.224	454
$[P_{4442O2}][OTf]^a$	—	−75	19	1.110	382
$[P_{4442}][NTf_2]$	9	—	31	1.244	411
$[P_{4446}][NTf_2]$	—	−81	—	1.183	480
$[P_{4448}][NTf_2]$	—	−80	—	1.162	513
$[P_{44410}][NTf_2]^b$	—	−81	18	1.141	546

[a] Cold crystallisation point at −41 °C. [b] Cold crystallisation point at −29 °C.

$[P_{4442O2}][OTf]$ was the only IL of those with $[P_{4442O2}]$ as a cation which exhibited a melting point. While having the same chain length as $[P_{2225}][NTf_2]$, the melting point of $[P_{2222O2}][NTf_2]$ was found to be 15 °C higher.

Molar volumes V_M and glass transition temperatures (if observed) are comparable to similar ammonium based ILs.[35] Densities exhibited a linear increase with temperature, with the parameters listed in the ESI.† It should be pointed out that the molarity of the ionic liquids is about 2 to 3 M, which is only half as much as that of over 5 M of saturated aqueous sodium chloride.[36] The ion concentration is therefore far below the one for conventional molten salts, although the solvent is of course replaced by the periphery of the ions.

Conductivity

As one of the fundamental transport properties, molar conductivity is especially relevant for electrochemical applications and is later on used for the calculation of the Haven ratios. The resulting fit parameters according to (6) for the molar conductivity and the values at 25 °C can be found in Table 2, whereas the corresponding plot is shown in Fig. 2. Apparently the curves deviate from the linear behaviour in the Arrhenius plot, which is why they were fitted with the Vogel–Fulcher–Tammann eqn (6). The latter was found to be applicable to several transport properties of a broad range of ionic liquids.[37] By far the highest value has been found for $[P_{2222O2}][NTf_2]$. It is followed by $[P_{2225}][NTf_2]$ as an IL of the same size but without the ether group. Lower conductivity values were found for $[P_{4448}][NTf_2]$, $[P_{4442O2}][NTf_2]$ and $[P_{2228}][NTf_2]$. High conductivity seems to be correlated with small cations containing ether groups. At least for the NTf_2 anion,

Table 2 VFT fit parameters of molar conductivity and the value at room temperature

	$\Lambda_M^{25°C}$/S cm^2 mol^{-1}	$\Lambda_{M,0}$/ S cm^2 mol^{-1}	B/K	T_0/K
$[P_{2222O2}][NTf_2]$	1.179	256.1	743.8	160.11
$[P_{2225}][NTf_2]$	0.630	531.2	−1012.2	147.81
$[P_{2228}][NTf_2]$	0.367	347.8	−947.9	159.79
$[P_{4442O2}][TFA]$	0.170	712.8	−1245.7	148.99
$[P_{4442O2}][OMs]$	0.038	1413	−1533.1	152.02
$[P_{4442O2}][NTf_2]$	0.347	411.0	−973.6	160.99
$[P_{4442O2}][OTf]$	0.105	488.0	−1147.4	162.20
$[P_{4442}][NTf_2]$	0.326	568.3	−1105.9	149.51
$[P_{4446}][NTf_2]$	0.188	1457	−1546.3	125.52
$[P_{4448}][NTf_2]$	0.157	6187	−2278.2	82.937
$[P_{44410}][NTf_2]$	0.123	1235	−1533.9	131.58

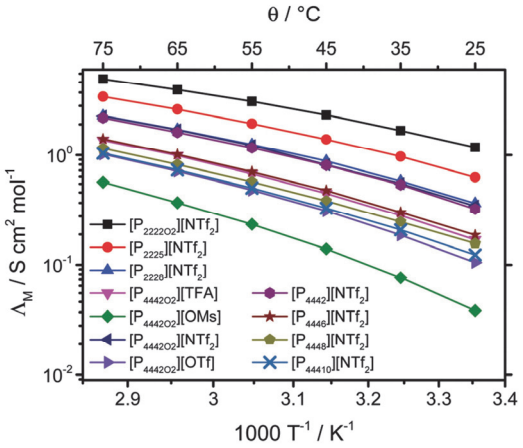

Fig. 2 Molar conductivity of the investigated phosphonium ionic liquids depending on temperature.

elongation of the side chain in the $[P_{444n}]$ series leads to reduced molar conductivities.

The remaining ILs with anions other than $[NTf_2]$ follow interspacing. The lowest molar conductivity was observed for $[P_{4442O2}][OMs]$ which is two orders of magnitude below the value for $[P_{2222O2}][NTf_2]$. Molar conductivity data for the ammonium based ionic liquids $[N_{2222O2}][NTf_2]$ and $[N_{4442O2}][NTf_2]$ have been reported in the literature.[38]

The values of molar conductivity of 0.87 S cm^2 mol^{-1} and 0.61 S cm^2 mol^{-1} at room temperature fall below and above the ones of their phosphonium analogues, so there is no clear benefit in either of the systems concerning conductivity.

Comparison with imidazolium systems is less reliable because of the vast structural difference. The positive charge in phosphonium ILs is more or less sterically shielded, while the much more accessible imidazolium cations naturally allow for more interactions. To name two examples, the molar conductivities found in the literature range from 1.15 S cm^2 mol^{-1} for $[C_2MIM][NTf_2]$ to 0.33 S cm^2 mol^{-1} for $[C_{10}MIM][NTf_2]$ and are therefore considerably smaller than those for phosphonium or ammonium ionic liquids of a similar molecular weight.

NMR diffusometry

Self-diffusion coefficients serve as a measure for molecular mass transport processes and ion mobility. However the information content is higher than for the fluidity/inverse viscosity because cations and anions (and even dissolved species) can be studied separately.

Since charge transport as the origin of conductivity is inherently connected to mass transport for ionic species, it is not surprising that the self-diffusion coefficients at room temperature presented in Table 3 show the same rank order as the respective molar conductivities. The data points for $[P_{4442O2}][TFA]$ and $[P_{4446}][NTf_2]$ are the sole exception and are interchanged. The highest self-diffusion coefficient is found to be 2.33×10^{-7} cm^2 s^{-1} for the cation in $[P_{2222O2}][NTf_2]$. Tabulated above are also the anion/cation ratios of the self-diffusion coefficients. This ratio is fairly equal to the one for $[P_{2222O2}][NTf_2]$, so both ions show comparable mobility. High ratios were found for the cations with more extensive alkyl chains, presumably due to the increased size or the nanosegregation discussed in the next subsection. The two causes cannot be distinguished at this point as they act in the same direction.

Among various anions, $[NTf_2]$ showed the highest self-diffusion coefficients although being the largest of the investigated anions. It is hence a good choice of anion to start with when optimising the transport properties. Similarly, ether groups should also be considered in this case as even a single ether group in the side chain substantially enhanced the self-diffusion coefficient. Unless nanosegregation is desired, long alkyl side chains should also be avoided when the self-diffusion is to be optimised.

Haven ratios

As already mentioned, the Haven ratio is still an important quantity especially for ILs, regardless of its nontrivial interpretation. Following (4), the Haven ratios shown in Table 4 were obtained in which certain trends become visible. These trends will be discussed in terms of ionicity, bearing in mind the difficulties that come with it.

Remarkably, the presence of ether groups leaves the ionicity mainly unaffected, allowing for the flexible and independent fine tuning of their transport properties. For the ILs with the $[P_{4442O2}]$ cation, the influence of several different anions was also investigated. The corresponding series is shown in the

Table 3 Self-diffusion coefficients at room temperature

	$D_{cation}^{25°C}$/cm^2 s^{-1}	$D_{anion}^{25°C}$/cm^2 s^{-1}	$D_{anion}^{25°C}/D_{cation}^{25°C}$
$[P_{2222O2}][NTf_2]$	2.33×10^{-7}	2.35×10^{-7}	1.01
$[P_{2225}][NTf_2]$	1.12×10^{-7}	1.21×10^{-7}	1.08
$[P_{2228}][NTf_2]$	7.54×10^{-8}	8.80×10^{-8}	1.17
$[P_{4442O2}][TFA]$	4.32×10^{-8}	5.32×10^{-8}	1.23
$[P_{4442O2}][OMs]$	0.98×10^{-8}	1.09×10^{-8}	1.12
$[P_{4442O2}][NTf_2]$	5.86×10^{-8}	8.07×10^{-8}	1.38
$[P_{4442O2}][OTf]$	2.27×10^{-8}	2.75×10^{-8}	1.21
$[P_{4442}][NTf_2]$	5.48×10^{-8}	6.93×10^{-8}	1.26
$[P_{4446}][NTf_2]$	3.30×10^{-8}	4.64×10^{-8}	1.40
$[P_{4448}][NTf_2]$	2.89×10^{-8}	4.06×10^{-8}	1.40
$[P_{44410}][NTf_2]$	2.48×10^{-8}	3.47×10^{-8}	1.40

Table 4 Haven ratios of the investigated ILs at 25 °C

	H_R		H_R		H_R
$[P_{2222O2}][NTf_2]$	66%	$[P_{4442O2}][TFA]$	47%	$[P_{4442}][NTf_2]$	71%
$[P_{2225}][NTf_2]$	68%	$[P_{4442O2}][OMs]$	51%	$[P_{4446}][NTf_2]$	63%
$[P_{2228}][NTf_2]$	60%	$[P_{4442O2}][NTf_2]$	65%	$[P_{4448}][NTf_2]$	60%
		$[P_{4442O2}][OTf]$	56%	$[P_{44410}][NTf_2]$	55%

middle column, where it can be seen that the ionicity increases with decreasing basicity of the anion. This behaviour has been reported for many systems and is considered generally valid.[8] It also meets the expectation that weak Lewis bases with widely delocalised charge are weakly coordinating not only towards protons. Counterintuitive at first sight is then again the decrease of ionicity for longer side chains evident in the last column. This may on the one hand be interpreted as the intrinsic limit of the model, where the term "ionicity" meets its borders. On the other hand one could also claim that the expected increased shielding of the charge – which would go along with an increase in ionicity – is overcompensated by an extended nanoscale structuring of the liquid phase. This so-called nanosegregation in polar, ionic and apolar alkyl domains is indeed well documented and known to play a decisive role in the case of ionic liquids.[39–41]

The second interpretation is furthermore supported by the Haven ratios for tributyl and triethyl based phosphonium ionic liquids with comparable side chains, which show virtually no difference. $[P_{2228}][NTf_2]$ and $[P_{4448}][NTf_2]$ may serve as an example, with the same haven ratio of 60%.

Temperature dependent measurements were performed for $[P_{4442O2}][NTf_2]$, $[P_{4442}][NTf_2]$ and $[P_{4448}][NTf_2]$, with the results for the three temperature dependent Haven ratios shown in Fig. 3. Surprisingly it is observed that the ionicity/deviation from ideality decreases with temperature, which is consistent with earlier findings for phosphonium ionic liquids.[42] The decrease of the haven ratio to about half its initial value despite increasing conductivity indicates that ion pairing has to be considered a relevant competing process. Imidazolium liquids contrarily show in general no or only little temperature dependence of the Haven ratio.[27,43] As an example, a constant Haven ratio of 0.66 with increasing temperature was reported for $[C_4MIM][PF_6]$.[28] The interpretation as ionicity again has to be treated with caution as using other methods like NMRD, decreasing ion pairing with increasing temperature was found for the same system.[28] The interpretation of temperature dependent Haven ratios as ionicities for phosphonium ILs at this point also contradicts intuition but is supported by the results obtained from X-ray scattering and computational investigations.[44] For practical applications the temperature dependence of IL ionicities therefore has to be taken into account to ensure optimal performance at the desired temperature.

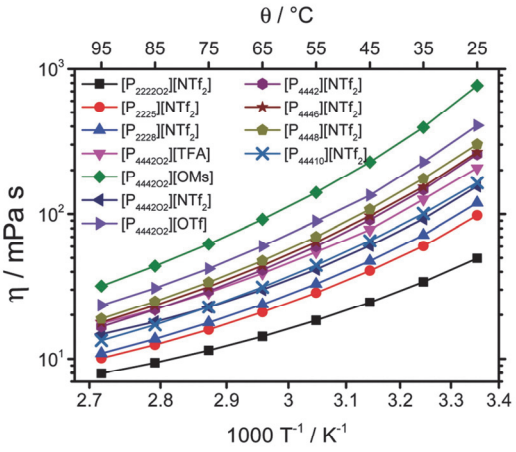

Fig. 3 Temperature dependent viscosities.

Rheological properties

In contrast to the majority of conventional molecular solvents, viscosity as a measure for momentum transport may narrow the applicability of ILs and is therefore of great importance. Experimental viscosities at room temperature are given in Table 5 together with the parameters obtained from the VFT fit and as a plot in Fig. 4. Comparative values taken from the literature for $[N_{2222O2}][NTf_2]$ and $[N_{4442O2}][NTf_2]$ are considerably higher with 71 mPa s and 315 mPa s.[38] Concerning fluidity, $[P_{2222O2}][NTf_2]$ is clearly superior to the other ionic liquids dealt with in this publication with the viscosity being as low as 49.7 mPa s. $[P_{2222O2}][NTf_2]$ is thus a promising electrolyte, together with several other similar ILs described in the literature.[12,45]

The performance of $[P_{4442O2}][OMs]$ is at the other extreme, with its viscosity so high that severe restrictions are put on processability and liquid handling. Remarkably the viscosity of $[P_{4442O2}][OTf]$ is only half of that of $[P_{4442O2}][OMs]$, even though the molecular structure of the anion remains unchanged, with hydrogen being replaced by fluorine.

For cations consisting only of alkyl chains, the viscosity increases with the size of the cation. Ether groups in the side chain drastically improve the fluidity, and $[P_{2222O2}][NTf_2]$ is only half as viscous as its alkyl analogue $[P_{2225}][NTf_2]$. From the group of ILs based on tributylphosphine, $[P_{4442O2}][NTf_2]$ has the lowest viscosity with 155 mPa s, which is even below the much smaller $[P_{4442}][NTf_2]$. Another advantage of the ether containing IL $[P_{4442O2}][NTf_2]$ is the very low T_G, while the melting point of $[P_{4442}][NTf_2]$ is above room temperature.

Table 5 VFT fit parameters of viscosity and the value at room temperature

	$\eta^{25\,°C}$/mPa s	η_0/mPa s	B/K	T_0/K
$[P_{2222O2}][NTf_2]$	49.7	0.29953	636.14	173.637
$[P_{2225}][NTf_2]$	98.0	0.23671	699.71	182.008
$[P_{2228}][NTf_2]$	119	0.20211	749.59	180.676
$[P_{4442O2}][TFA]$	207	0.17268	915.52	169.048
$[P_{4442O2}][OMs]$	767	0.18552	968.43	181.832
$[P_{4442O2}][NTf_2]$	155	0.36848	651.60	190.303
$[P_{4442O2}][OTf]$	405	0.12257	1046.73	168.990
$[P_{4442}][NTf_2]$	164	0.03708	1368.18	135.127
$[P_{4446}][NTf_2]$	257	0.10831	1006.06	168.714
$[P_{4448}][NTf_2]$	267	0.09290	1089.93	161.235
$[P_{44410}][NTf_2]$	301	0.04108	1366.32	144.627

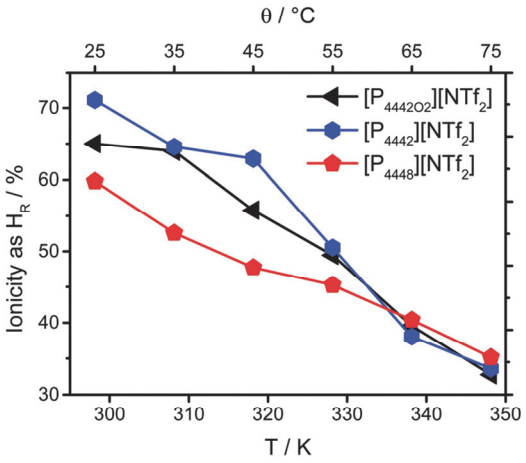

Fig. 4 Temperature dependent Haven ratios.

Walden plot

Notwithstanding its simplicity, the Walden approach often leads to reliable results and is hence widely spread.[8,34] The Walden plot of the phosphonium ionic liquids is shown in Fig. 5. It is possible to calculate a kind of "Walden plot ionicity" by taking the ratio of the observed molar conductivity and the one at the ideal line. The temperature dependent Walden plot ionicity thus obtained is presented in Fig. 6 for comparison with the already discussed Haven ratios in Fig. 3. In contrast to the latter, the Walden ionicity shows only minor changes with increasing temperature, so the ion pairing occurs differently. The direct comparison of the two evaluation methods for deviation from ideal conductivity is therefore hardly possible although both are valuable and applied tools for the categorisation according to general property trends and in accordance to optimisation of

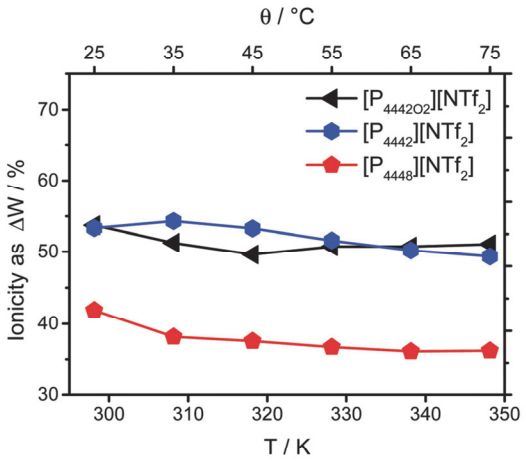

Fig. 5 Ionicity derived from the Walden plot.

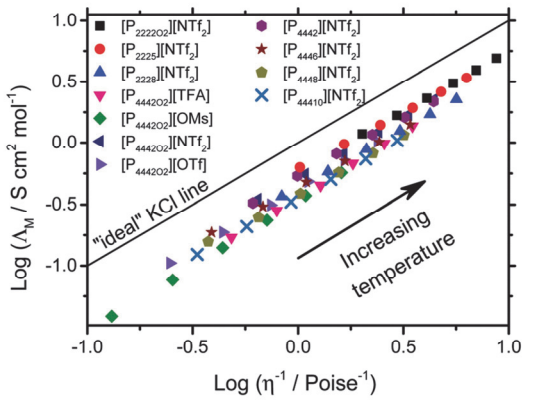

Fig. 6 Walden plot for the ionic liquids in this publication.

the IL structure according to special demands. The Walden approach attributes virtually the same ionicity to [P_{4442}][NTf_2] and [P_{4442O2}][NTf_2], which is consistent with them both exhibiting comparable conductivities, viscosities and self-diffusion coefficients. Extended side chains again result in decreased (Walden) ionicity apparent in Fig. 6 for the temperature dependent values of [P4448][NTf_2] and [P4442][NTf_2]. As the position of the ideal line is arbitrary, the vertical position and the exact course of the Walden plot ionicity may also be altered to some extent. This is achieved in the adjusted Walden plot by weighing with the effective ionic radii, which then have to be accessible somehow.[34] If the Stokes–Einstein equation is used to calculate the radii from the self-diffusion coefficients, the viscosity cancels in the calculation.

As a result essentially the same behaviour is then found as for the Haven ratios obtained from the Nernst–Einstein equation, only with a different factor.

Fit parameters according to the fractional Walden rule (5) are shown in Table 6. It is notable that the parameter α is always very close to unity, so the Walden rule is fulfilled to a high degree. Although being a very simple approach, the Walden plot largely reproduces the earlier findings. It is for example clearly seen that the values for the variable $\log C$ decrease with increasing side chain length as was found for the Haven ratios. However the Walden plot does not reproduce the exact

Table 6 Fit parameters for the fractional Walden rule

	$\log(C/\mathrm{S\ cm^2\ mol^{-1}})$	α
[P_{2222O2}][NTf_2]	$-0.2297 \pm 4.2 \times 10^{-3}$	$0.9741 \pm 6.3 \times 10^{-3}$
[P_{2225}][NTf_2]	$-0.2139 \pm 3.6 \times 10^{-3}$	$0.9262 \pm 7.0 \times 10^{-3}$
[P_{2228}][NTf_2]	$-0.3660 \pm 2.5 \times 10^{-3}$	$0.9570 \pm 5.3 \times 10^{-3}$
[P_{4442O2}][TFA]	$-0.4423 \pm 4.2 \times 10^{-3}$	$1.0560 \pm 1.3 \times 10^{-2}$
[P_{4442O2}][OMs]	$-0.4684 \pm 2.8 \times 10^{-3}$	$1.0779 \pm 5.9 \times 10^{-3}$
[P_{4442O2}][NTf_2]	$-0.2849 \pm 5.7 \times 10^{-3}$	$0.9778 \pm 1.5 \times 10^{-2}$
[P_{4442O2}][OTf]	$-0.3681 \pm 1.9 \times 10^{-3}$	$1.0060 \pm 5.6 \times 10^{-3}$
[P_{4442}][NTf_2]	$-0.2729 \pm 4.2 \times 10^{-3}$	$0.9538 \pm 1.1 \times 10^{-2}$
[P_{4446}][NTf_2]	$-0.3538 \pm 3.1 \times 10^{-3}$	$0.9293 \pm 9.1 \times 10^{-3}$
[P_{4448}][NTf_2]	$-0.4187 \pm 1.4 \times 10^{-2}$	$0.9362 \pm 1.4 \times 10^{-2}$
[P_{44410}][NTf_2]	$-0.4447 \pm 1.0 \times 10^{-3}$	$0.9717 \pm 3.1 \times 10^{-3}$

rank order as given from the Haven ratio. This can also be seen as advantage since desirable properties like high fluidity and conductivity are inherently also taken into account. Accordingly $[P_{4442O2}][OMs]$ has the lowest value for $\log C$, and the small ILs $[P_{2222O2}][NTf_2]$ and $[P_{2225}][NTf_2]$ the largest. Therefore the Walden plot can be considered a measure for "overall performance".

Experimental

Comprehensive details of experimental methods and parameters can be found in the ESI,† together with the raw data as well as additional information on fits and the NMR spectra of the ionic liquids.

Prior to every measurement, the respective ionic liquids were dried in a vacuum at a slightly elevated temperature (about 40 °C to 60 °C) for several days until the end pressure became of the order of 5×10^{-3} mbar.

Temperature dependent data for viscosity and molar conductivity were fitted with the commonly used Vogel–Fulcher–Tammann (VFT) equation shown below.[46,47]

$$A = A_0 \exp\left(\frac{B}{T - T_0}\right) \quad (7)$$

Variable A either replaced with η ($B > 0$) or Λ_M ($B < 0$).

Syntheses of the ionic liquids

The S_N2 reactions were performed in acetonitrile, based on the literature protocol for the synthesis of $[P_{4446}][Cl]$.[48] Salt metatheses in propanone are also based on a literature protocol, namely the preparation of $[P_{66614}][Cl]$.[49] To prevent oxidation and water uptake, reactions were performed and dry products were stored under argon as a protective atmosphere. Washing steps after metathesis were performed using Milli-Q water until no halides could be detected with aqueous $AgNO_3$. Solvents were dried with and stored over molecular sieves 3 Å or 4 Å as recommended in the literature.[50] Products were identified *via* multinuclear NMR Spectroscopy. NMR signals were assigned *via* chemical shift, integration and comparison of coupling constants/patterns with similar known compounds.[51]

General quaternisation procedure. A dried Schlenk flask was charged with the desired phosphine, 1.2 to 1.5 equivalents of the alkylating reagent and 1 mL acetonitrile per millimole phosphine under argon. The mixture was stirred at 45 to 50 °C until no remaining phosphine could be detected, which took up to several days depending on the system. Reaction monitoring was achieved *via* ^{31}P-NMR.

General procedure for salt metathesis to yield $[P_{RRRR'}][NTf_2]$. $[P_{RRRR'}][Cl]$ and 1.3 equivalents $LiNTf_2$ were stirred overnight together with 1–1.5 mL H_2O and 10 mL methylene chloride per millimole $[P_{RRRR'}][Cl]$. The organic phase was then separated, washed with 1–1.5 mL H_2O per millimole $[P_{RRRR'}][Cl]$ and dried over a small amount of MS 4 Å overnight. The solvent was removed by means of rotary evaporation. The remainder was dried for several days in a high vacuum and stored under argon.

Thermal transitions

Thermal transition points were measured by means of differential scanning calorimetry (DSC) on a DSC 1 STARe system (Mettler Toledo, Gießen, Germany) with liquid nitrogen cooling. Slow scan rates of ±1 °C min^{-1} were applied to ensure the correct determination of the transition points. For each measurement a vacuum dried sample of about 15 mg was hermetically sealed in an aluminium crucible. The temperature program started with dynamic heating of 10 °C min^{-1} from ambient temperature to 100 °C and was subsequently held at this temperature for 15 min to remove the thermal history of the sample. Afterwards a dynamic step with a cooling rate of −1 °C min^{-1} to −120 °C was applied with a subsequent isothermal step for 10 min and heating with 1 °C min^{-1} to 100 °C. Thermal transition points are given as onset temperatures.

Densities

Density measurements were conducted at temperatures ranging from 25 °C to 75 °C in steps of 10 °C using a Reischauer pycnometer (Neubert Glas, Thüringen, Germany), which essentially resembles a volumetric flask with very narrow neck. The pycnometer filled with the sample was carefully placed in a thermostated bath with the mark below the tempering fluid and allowed to equilibrate for 10 to 15 min. The filling height was then adjusted to the mark with the help of a Pasteur pipette, and the procedure was repeated until the filling height remained constant. The pycnometer was then allowed to cool down and weighted after drops in the neck were taken up. Prior to every measurement, the pycnometer was rinsed with methylene chloride, propanone, water and ethyl acetate and dried in a high vacuum. Similar to the regular density measurements of ionic liquid samples, the volume of the pycnometer at the target temperatures was determined by calibration with octane and checked with water. The largest deviation from the literature value for the density of water was as low as 0.1% with the octane calibration.[52]

Conductivity

Specific conductivities were measured in a cell purged with dry nitrogen to avoid contact with moist air. Temperature stability was assured through the external water circuit of a Proline RP 1845 thermostat (LAUDA, Lauda-Königshofen, Germany). Despite its low thermal conductivity, paraffin oil was chosen as an internal heat transfer medium to minimize water uptake. Immersed in the paraffin oil was a thick-walled test tube as a sample chamber containing the sample and the conductivity probe. The test tube was sealed with a viton ring. The conductivity probe LTA (WTW GmbH, Weilheim, Germany) consisted of two platinised platinum electrodes fused into a glass tube. The external Pt100 temperature sensor of the thermostat was placed in the paraffin oil in close proximity to the sample chamber. An electrode constant of 1.001 cm^{-1} given by the manufacturer was confirmed by the measurement of a conductivity standard. The conductivity of the ionic samples was measured by means of impedance spectroscopy, using a SP-150 Potentiostat (BioLogic, Seysinnet-Pariset, France). Impedance spectra were

recorded at 5, 10 and 15 mV from 200 kHz to 1 Hz in logarithmic spacing. The system was considered stable when consecutive measurements at different or equal amplitudes yielded comparable results without apparent drift. Measurements were performed from low to high temperatures, an additional downwards measurement performed for $[P_{4448}][NTf_2]$ showed no hysteresis.

NMR diffusometry

NMR spectra for the determination of self-diffusion coefficients were recorded in a pure substance without a deuterated solvent on an AVANCE II 400 routine spectrometer (Bruker, Billerica, USA) equipped with a 5 mm BBFO probe with a z gradient. The probe allowed for gradient strengths up to 53.5 g cm^{-1}, of which 34.1 g cm^{-1} were usable owing to the sinusoidal shape of the gradient pulses. Despite this loss of power, the sinusoidal shape was chosen because of the lower vulnerability towards distortions compared with rectangular pulse shapes. In contrast to conventional probes the outer coil can be tuned to ^{1}H as well as ^{19}F. The spectra of ^{19}F were thus measured without ^{1}H decoupling, which is anyhow advisable to avoid the unnecessary heat input into the (conductive) sample.[53] The spinner was also turned off because of the sensitivity towards vertical position changes.[21] During the measurements, the gas flow was set to 670 L h^{-1}. The probe was manually shimmed and tuned after every change of the sample, temperature or nucleus. Insufficient temperature stability helpfully shows up during the manual tuning in the form of a trembling wobble function. For less viscous samples convection can be problematic, and leads to scattered or bent appearance of the measurement points in the linear representation.[21,54] We hence recommend the use of the latter as given in (1) because deviations from the linear behaviour are then easy to spot, although the uncertainty given from the software is not as reliable as when fitting the Stejskal–Tanner eqn (1) in its ''natural'' exponential form. The pulse program is available in the bruker library as ''ledbpgp2s''. Pulse durations were determined manually, together with a rough estimate of the longitudinal relaxation time T_1.[55] The relaxation delay was subsequently chosen as 5 to 7 times T_1.

To validate the Stejskal–Tanner behaviour, spectra can be recorded with different pairs of Δ and δ which should yield the same diffusion coefficient (see the ESI†).

Manual phase and automatic baseline correction was applied to the raw spectra, which were then integrated. Plotting $\ln(I/I_0)$ *versus* Q following (1) results in a straight line, from which D is readily obtained as a slope.

Rheological properties

Temperature dependent viscosities were determined using a MCR 301 rheometer (Anton Paar, Graz, Austria) with a PP25 measuring plate of 25 mm and DD41 dishes of 41 mm. Samples were filled in the dishes and the temperature was allowed to equilibrate for 15 min before each measurement with a maximum deviation of ±0.1 °C. Temperature values started from 25 °C and were varied in 10 °C steps up to 95 °C. Shear rates were varied from 5 to 1000 s^{-1} in linear steps collecting 30 data points in order to detect any shear rate or time dependent effects. For all samples, shear rates and temperatures, solely Newtonian flow behavior was found. Therefore the collected viscosities for each temperature were averaged instead of extrapolating to zero-shear viscosity.

Conclusions

In this contribution we investigated the influence of the cation structure and the choice of an anion on the transport properties of phosphonium ionic liquids, especially the self-diffusion coefficient and derived quantities. The obtained properties of this important, but less commonly investigated IL subclass were analysed by means of different models established in the literature for derivation from ideal conductivity. The two models were found to result in similar trends but remarkable quantitative differences, especially for the temperature dependence. Contrary to the widely applied imidazolium-based ILs a decrease of the ionicity with increasing temperature was found for the investigated phosphonium ILs. Rather small cations were found to be preferable to achieve the highest conductivity and self-diffusion coefficients as well as lowest viscosities; however melting or glass transition points may place a lower limit to the size. Another aspect related to the size is the content of phosphorus and fluorine, which of course is high for the smallest ions.

From a more practical point of view, the experimental results showed the advantages of the introduction of ether groups into the side chain of the cation. Fluidity and conductivity were drastically improved with only a minor influence on the Haven ratio. This improvement does not depend on the cation size and makes possible the use of relatively large cations without loss of performance. Hence it provides a great opportunity to conserve important resources, *i.e.* fluorine and especially phosphorus.

The fact that even a small change in the side chain may alter the substantial properties is pleasant in terms of flexibility, but it also shows relentlessly that there is still a lot to be done in the field of ionic liquids.

Acknowledgements

The authors are very thankful to Thomas Scherer for his patient technical assistance. The authors declare no conflict of interest.

Notes and references

1 K. Dong, X. Liu, H. Dong, X. Zhang and S. Zhang, *Chem. Rev.*, 2017, **117**, 6636–6695.
2 N. V Plechkova and K. R. Seddon, *Chem. Soc. Rev.*, 2008, **37**, 123–150.
3 E. I. Rogers, B. šljukić, C. Hardacre and R. G. Compton, *J. Chem. Eng. Data*, 2009, **54**, 2049–2053.
4 N. De Vos, C. Maton and C. V Stevens, *ChemElectroChem*, 2014, **1**, 1258–1270.
5 J. Ranke, S. Stolte, R. Störmann, J. Arning and B. Jastorff, *Chem. Rev.*, 2007, **107**, 2183–2206.

6 K. R. Seddon, *J. Chem. Technol. Biotechnol.*, 1997, **68**, 351–356.
7 A. Rupp, N. Roznyatovskaya, H. Scherer, W. Beichel, P. Klose, C. Sturm, A. Hoffmann, J. Tübke, T. Koslowski and I. Krossing, *Chem. – Eur. J.*, 2014, **20**, 9794–9804.
8 K. Ueno, H. Tokuda and M. Watanabe, *Phys. Chem. Chem. Phys.*, 2010, **12**, 1649–1658.
9 B. Wang, L. Qin, T. Mu, Z. Xue and G. Gao, *Chem. Rev.*, 2017, **117**, 7113–7131.
10 S. Sowmiah, V. Srinivasadesikan, M.-C. Tseng and Y.-H. Chu, *Molecules*, 2009, **14**, 3780–3813.
11 K. J. Fraser and D. R. MacFarlane, *Aust. J. Chem.*, 2009, **62**, 309–321.
12 K. Tsunashima and M. Sugiya, *Electrochem. Commun.*, 2007, **9**, 2353–2358.
13 C. J. Bradaric, A. Downard, C. Kennedy, A. J. Robertson and Y. Zhou, *Green Chem.*, 2003, **5**, 143–152.
14 N. V. Ignat'ev, P. Barthen, A. Kucheryna, H. Willner and P. Sartori, *Molecules*, 2012, **17**, 5319–5338.
15 K. L. Luska and A. Moores, *Green Chem.*, 2012, **14**, 1736–1742.
16 G. Annat, D. R. MacFarlane and M. Forsyth, *J. Phys. Chem. B*, 2007, **111**, 9018–9024.
17 W. S. Price, P. Stilbs, B. Jönsson and O. Söderman, *J. Magn. Reson.*, 2001, **150**, 49–56.
18 D. H. Wu, A. D. Chen and C. S. Johnson, *J. Magn. Reson., Ser. A*, 1995, **115**, 260–264.
19 G. H. Sørland, *Dynamic Pulsed-Field-Gradient NMR*, Springer Berlin Heidelberg, Berlin, Heidelberg, 2014, vol. 110.
20 S. J. Gibbs and C. S. Johnson, *J. Magn. Reson.*, 1991, **93**, 395–402.
21 C. S. Johnson, *Prog. Nucl. Magn. Reson. Spectrosc.*, 1999, **34**, 203–256.
22 E. O. Stejskal and J. E. Tanner, *J. Chem. Phys.*, 1965, **42**, 288–292.
23 S. S. Moganty, P. S. Chinthamanipeta, V. K. Vendra, S. Krishnan and R. E. Baltus, *Chem. Eng. J.*, 2014, **250**, 377–389.
24 H. Ohno, M. Yoshizawa and T. Mizumo, *Electrochemical Aspects of Ionic Liquids*, John Wiley & Sons, Inc., Hoboken, NJ, USA, 2005, pp. 75–81.
25 J. O. Bockris and A. K. N. Reddy, *Modern Electrochemistry 1*, Kluwer Academic Publishers, Boston, 2nd edn, 2002.
26 M. A. B. H. Susan, A. Noda and M. Watanabe, *in Electrochemical Aspects of Ionic Liquids*, John Wiley & Sons, Inc., Hoboken, NJ, USA, 2005, pp. 55–74.
27 K. R. Harris and M. Kanakubo, *J. Chem. Eng. Data*, 2016, **61**, 2399–2411.
28 G. W. Driver, Y. Huang, A. Laaksonen, T. Sparrman, Y.-L. Wang and P.-O. Westlund, *Phys. Chem. Chem. Phys.*, 2017, **19**, 4975–4988.
29 H. K. Kashyap, H. V. R. Annapureddy, F. O. Raineri and C. J. Margulis, *J. Phys. Chem. B*, 2011, **115**, 13212–13221.
30 O. Hollóczki, F. Malberg, T. Welton and B. Kirchner, *Phys. Chem. Chem. Phys.*, 2014, **16**, 16880–16890.
31 M. A. Gebbie, M. Valtiner, X. Banquy, E. T. Fox, W. A. Henderson and J. N. Israelachvili, *Proc. Natl. Acad. Sci. U. S. A.*, 2013, **110**, 9674–9679.
32 A. A. Lee, D. Vella, S. Perkin and A. Goriely, *J. Phys. Chem. Lett.*, 2014, **6**, 159–163.
33 C. Schreiner, S. Zugmann, R. Hartl and H. J. Gores, *J. Chem. Eng. Data*, 2010, **55**, 1784–1788.
34 D. R. MacFarlane, M. Forsyth, E. I. Izgorodina, A. P. Abbott, G. Annat and K. Fraser, *Phys. Chem. Chem. Phys.*, 2009, **11**, 4962–4967.
35 C. A. Angell, N. Byrne and J.-P. Belieres, *Acc. Chem. Res.*, 2007, **40**, 1228–1236.
36 S. P. Pinho and E. A. Macedo, *J. Chem. Eng. Data*, 2005, **50**, 29–32.
37 M. A. Bin, H. Susan, A. Noda and M. Watanabe, *Electrochemical Aspects of Ionic Liquids*, John Wiley & Sons, Inc., Hoboken, NJ, USA, 2011, pp. 65–85.
38 M. Kärnä, M. Lahtinen, A. Kujala, P.-L. Hakkarainen and J. Valkonen, *J. Mol. Struct.*, 2010, **983**, 82–92.
39 A. Triolo, O. Russina, H.-J. Bleif and E. Di Cola, *J. Phys. Chem. B*, 2007, **111**, 4641–4644.
40 R. Hayes, G. G. Warr and R. Atkin, *Chem. Rev.*, 2015, **115**, 6357–6426.
41 J. N. A. Canongia Lopes and A. A. H. Pádua, *J. Phys. Chem. B*, 2006, **110**, 3330–3335.
42 S. Seki, K. Hayamizu, S. Tsuzuki, K. Fujii, Y. Umebayashi, T. Mitsugi, T. Kobayashi, Y. Ohno, Y. Kobayashi, Y. Mita, H. Miyashiro and S. Ishiguro, *Phys. Chem. Chem. Phys.*, 2009, **11**, 3509–3514.
43 H. Tokuda, K. Hayamizu, K. Ishii, M. A. B. H. Susan and M. Watanabe, *J. Phys. Chem. B*, 2004, **108**, 16593–16600.
44 J. J. Hettige, H. K. Kashyap and C. J. Margulis, *J. Chem. Phys.*, 2014, **140**, 111102.
45 A. Otani, Y. Zhang, T. Matsuki, E. Kamio, H. Matsuyama and E. J. Maginn, *Ind. Eng. Chem. Res.*, 2016, **55**, 2821–2830.
46 G. Tammann and W. Hesse, *Z. Anorg. Allg. Chem.*, 1926, **156**, 245–257.
47 G. S. Fulcher, *J. Am. Ceram. Soc.*, 1925, **8**, 339–355.
48 S. Dewilde, W. Dehaen and K. Binnemans, *Green Chem.*, 2016, **18**, 1639–1652.
49 A. Cieniecka-Rosłonkiewicz, J. Pernak, J. Kubis-Feder, A. Ramani, A. J. Robertson and K. R. Seddon, *Green Chem.*, 2005, **7**, 855–862.
50 C. Reichardt and T. Welton, *Solvents and Solvent Effects in Organic Chemistry*, Wiley-VCH Verlag GmbH & Co. KGaA, Weinheim, Germany, 4th edn, 2011.
51 M. Hesse, H. Meier and B. Zeeh, *Spektroskopische Methoden in der organischen Chemie*, Georg Thieme Verlag, Stuttgart, 8th edn, 2012.
52 *CRC Handbook of Chemistry and Physics*, ed. W. M. Haynes, D. R. Lide and T. J. Bruno, CRC Press, 95th edn, 2014.
53 D. S. McNair, *J. Magn. Reson.*, 1981, **45**, 490–502.
54 A. Jerschow and N. Müller, *J. Magn. Reson.*, 1998, **132**, 13–18.
55 S. Berger and S. Braun, *200 and More NMR Experiments*, Wiley-VCH Verlag GmbH & Co. KGaA, Weinheim, 2004.

2.3 Publication C

Lamellar structures in fluorinated phosphonium ionic liquids: the roles of fluorination and chain length

Daniel Rauber, Peng Zhang, Volker Huch, Tobias Kraus, Rolf Hempelmann.

Phys. Chem. Chem. Phys., **2017**, 19, 27251-27258.

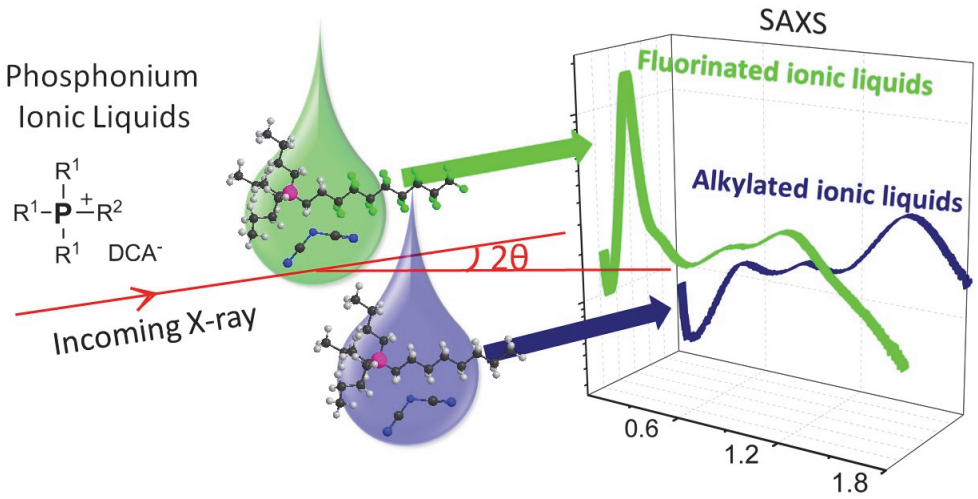

PCCP

PAPER

View Article Online
View Journal | View Issue

Cite this: *Phys. Chem. Chem. Phys.*, 2017, **19**, 27251

Lamellar structures in fluorinated phosphonium ionic liquids: the roles of fluorination and chain length†

Daniel Rauber,‡[a] Peng Zhang, ‡[b] Volker Huch,[a] Tobias Kraus*[bc] and Rolf Hempelmann [ad]

Received 17th July 2017,
Accepted 20th September 2017

DOI: 10.1039/c7cp04814a

rsc.li/pccp

Ionic liquids (ILs) exhibit tunable behaviour and properties that are due to their supramolecular structure. We synthesized a series of alkylated and fluorinated phosphonium dicyanamide ILs to study the relation between molecular structure and assembly with a focus on the roles of cation chain length and fluorination. Small angle X-ray scattering indicated a lamellar structure with long-range order for all fluorinated ILs, while alkylated ILs showed only the general structures of ILs, *i.e.*, alternating a polar ionic-zone and a nonpolar alkyl-zone. "Fluorophobic" interactions caused microphase segregation between perfluorinated and other molecular segments, "fluorophilic" interactions among the perfluorinated segments stabilized the microphase structure, and the coupling of "fluorophobic" and "fluorophilic" interactions resulted in a stable mesophase structure. The perfluorinated segments packed more densely than the alkylated analogues; the fluorinated versions (except for F2) liquefied at temperatures considerably above that of alkylated ILs. The lamellar structures strongly affected the rheology of the ILs. Fluorinated ILs had higher viscosities and exhibited non-Newtonian shear thinning; the alkylated ILs of the same length had an order of magnitude lower viscosities and were purely Newtonian. We propose that the disruption of lamellar structure in the shear flow causes the non-Newtonian flow behaviour.

1. Introduction

Ionic liquids (ILs) are a heterogeneous class of functional fluids with very low vapour pressures that enable new processes.[1] They have more persistent structures and dynamic heterogeneity[2] at different length scales[3,4] than other liquids due to the interplay of Coulomb interaction, hydrogen-bonding, and van der Waals interaction.[5] Their bulk structures at different length scales are affected by the coordination of ion pairs,[6] the formation of clusters[7,8] through hydrogen-bonding,[9] and the segregation of polar and nonpolar parts,[10,11] sometimes into ordered structures such as liquid crystals.[12] Segregation follows the rule of "like dissolves like"[12] and enables ILs to modify reaction kinetics,[13] dynamics,[14] and electrical conductivity.[15] Alkylated ILs, for example, are currently used as solvents/fluids in electrochemistry,[16] synthesis,[17] lubricants,[18] and in the preparation of advanced materials.[19]

The understanding of "structure–property" relationships is crucial in the molecular design of ILs for applications.[20] Adding new chemical functionalities is a method of tuning segregation, and thus bulk properties.[21] Here, we study the fluorination of the cation that affects the IL structure[22] *via* fluorophilic interactions.[23,24] Fluorinated molecules are hydro- and lipophobic at the same time.[25] Fluorinated ILs were reported to possess self-assembled domains of aggregated perfluoroalkyl-groups that occur in addition to the familiar ordered structures in the polar and nonpolar alkyl regions.[26] Fluorination generally lowers surface tension and enhances biochemical inertness compared to alkylated ILs,[27] which makes fluorinated ILs promising as surfactants,[28] as lubricants,[29,30] and for biomedical uses.[26]

So far, the effect of fluorination in alkylated ILs has not been systematically studied. We synthesized a homologous series of increasingly fluorinated ILs to assess the effect of perfluorinated molecular segments on the bulk structure of the IL and its effect on bulk properties such as liquefaction temperatures and viscosities of the ILs. Quaternary phosphonium as a cation provides high chemical,[31] electrochemical[32] and thermal stabilities.[33] The dicyanamide anion (DCA) was used for its relatively high charge delocalization and small size and most DCA-based ILs were found

[a] *Saarland University, Campus B2 2, 66123 Saarbrücken, Germany*
[b] *INM-Leibniz Institute for New Materials, Campus D2 2, 66123 Saarbrücken, Germany. E-mail: tobias.kraus@leibniz-inm.de*
[c] *Colloid and Interface Chemistry, Saarland University, Campus D2 2, 66123 Saarbrücken, Germany*
[d] *Transfercentre Sustainable Electrochemistry, Saarland University and KIST Europe, Campus Dudweiler Zeile 3, 66125 Saarbrücken, Germany*

† Electronic supplementary information (ESI) available: IL synthesis, NMR spectra, molecular interaction in ILs, TGA analysis, obtaining peak positions of SAXS data, F8 single crystal data, and rheological measurements. CCDC 1503513. For ESI and crystallographic data in CIF or other electronic format see DOI: 10.1039/c7cp04814a

‡ These authors contributed equally to this work.

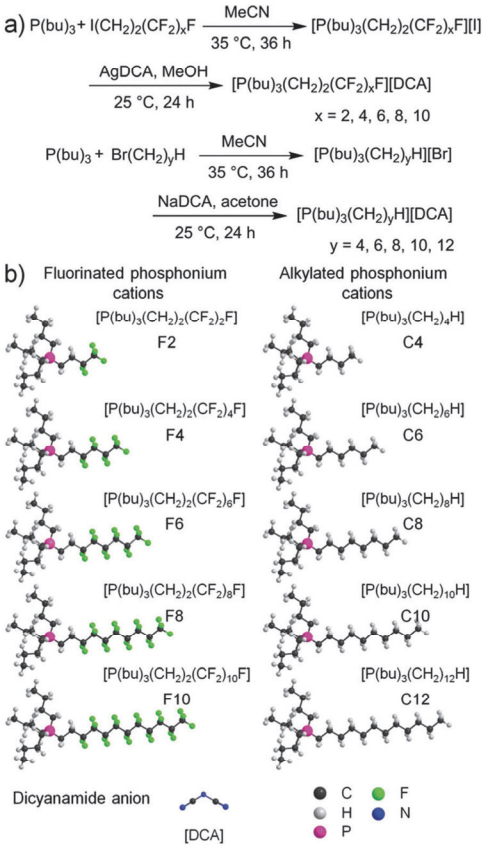

Fig. 1 (a) Reaction scheme for the synthesis of the fluorinated and alkylated tributylphosphonium dicyanamide ILs by quaternization reaction of the phosphine and subsequent anion metathesis. (b) Molecular structures and nomenclature of synthesized cations and anions.

to have low viscosities.[34] In addition, such ILs show no molecular interactions like hydrogen-bonds found in protic ILs[35,36] or π-interactions as found in ILs based on imidazolium or pyridinium systems.[37] A series of tributylphosphonium cations were prepared with 4 to 12 carbons and varying levels of fluorination in the longest alkyl chain. We were interested to see how fluorination of the alkyl chain changed bulk structure and properties.[38]

Using the designed IL series, we studied the dependence of liquid bulk structure of ILs on the chain-length and fluorination through small angle X-ray scattering, and the relationship between nanostructure and phase transitions, thermal stability, and rheological properties of the increasingly fluorinated ILs.

2. Experimental

2.1 Materials

Tributylphosphine (99%) was obtained from Strem Chemicals (Kehl, Germany) and distilled prior to use. 1*H*,1*H*,2*H*,2*H*-perfluorobutyl iodide (no further specification given), 1*H*,1*H*,2*H*,2*H*-perfluorohexyl iodide (95%) and 1*H*,1*H*,2*H*,2*H*-perfluorodecyl iodide (97%), 1*H*,1*H*,2*H*,2*H*-perfluorododecyl iodide (97%) were purchased from Apollo Scientific (Bredbury, UK) and distilled or sublimed prior to use. 1*H*,1*H*,2*H*,2*H*-perfluorooctyl iodide (95%) was obtained from Fluorochem (Hadfield, UK) and was distilled prior to use. The alkylbromides 1-bromobutane (99%) and 1-bromododecane (97%) from Sigma Aldrich (St. Louis, USA), 1-bromohexane (99%) and 1-bromooctane (98%+) from Alfa Aesar (Ward Hill, USA) and 1-bromodecane from Abcr (Karlsruhe, Germany) were distilled prior to use. Acetonitrile (>99.9%, Chromasolv, HPLC-Grad.), dichloromethane (≥99.9%) from Sigma Aldrich and acetone (Puriss. p.a. 99.9%) from Thermo Fisher Scientific (Waltham, USA) were dried over molecular sieves. Methanol (>99.8% HPLC-Grad.) was purchased from VWR International (Radnor, United Kingdom) and water was purified using a Milli-Q® Type 1 ultrapure water system from Merck (Darmstadt, Germany). Sodium dicyanamide (97%) from IoLiTec-Ionic Liquids Technologies (Heilbronn, Germany), silver nitrate (99.5%) from Carbolution Chemicals (Saarbrücken, Germany) and dry magnesium sulfate from Grüssing (Filsum, Germany) were used as received. $CDCl_3$ (99.8% D) from Sigma Aldrich was stored over molecular sieves.

2.2 Synthesis of ionic liquids

ILs were synthesized by quaternization of phosphine and subsequent anion metathesis (Fig. 1a). The synthesis of quaternary phosphonium salts was undertaken using Schlenk techniques in carefully dried glassware under an argon atmosphere to prevent the oxidation of tributylphosphine. Silver dicyanamide (freshly prepared and stored in the dark) in methanol was used for the anion exchange of iodides. Anion metathesis reactions of bromides were performed using sodium dicyanamide in acetone. To separate the ILs from the solution, we filtered off the precipitates (silver iodide and sodium bromide), removed the solvent by rotary evaporation, and dissolved the residues in dichloromethane. For further purification, the IL solution was washed four times with distilled water, dried over $MgSO_4$, filtered, and the organic solvent was removed by rotary evaporation. To remove the volatile substances from the IL samples, we treated them at 60 °C under oil-pump vacuum at 1×10^{-2} mbar for two days to obtain pure ILs in nearly quantitative yields. We checked the purities of the as-prepared ILs by multinuclear NMR-spectroscopy (AVANCE II 400, Bruker, Billerica, USA). More details for the synthesis process and NMR data are given in the ESI.†

Exemplary NMR resonances for F8:

^{1}H-NMR: (400 MHz, $CDCl_3$): δ [ppm] = 2.56–2.52 (m, 4H, P-(*CH*$_2$)$_2$-(CF$_2$)$_8$-F), 2.37–2.30 (m, 6H, P-*CH*$_2$-(CH$_2$)$_3$-H), 1.60–1.53 (m, 12H, P-CH$_2$-(*CH*$_2$)$_2$-CH$_3$), 1.00 (t, $^2J_{H/H}$ = 7.0 Hz, 9H, P-(CH$_2$)$_3$-*CH*$_3$).

^{13}C{^{1}H}-NMR (101 MHz, $CDCl_3$): δ [ppm] = 120.1 (s, N-(*CN*)$_2$), 24.0 (d, $^3J_{C/P}$ = 15.6 Hz, P-(CH$_2$)$_2$-*CH*$_2$-CH$_3$), 23.6 (d, $^2J_{C/P}$ = 4.9 Hz, P-CH$_2$-*CH*$_2$-(CH$_2$)$_2$-H), 18.7 (d, $^1J_{C/P}$ = 47.0 Hz, P-*CH*$_2$-(CH$_2$)$_3$-H), 13.4 (s, P-(CH$_2$)$_3$-*CH*$_3$).

^{19}F{^{1}H}-NMR (376 MHz, $CDCl_3$): δ [ppm] = −80.92 (3F, P-(CH$_2$)$_2$-(CF$_2$)$_7$-*CF*$_3$), −114.69 (2F, P-(CH$_2$)$_2$-*CF*$_2$-(CF$_2$)$_7$-F), −121.88 to −122.93

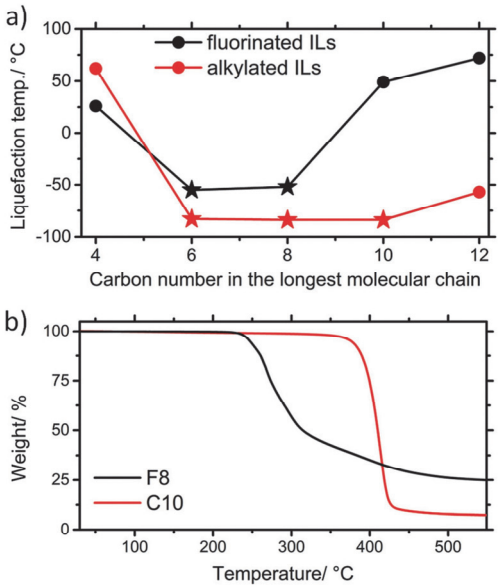

Fig. 2 (a) Liquefaction temperatures for fluorinated and alkylated phosphonium dicyanamide ILs of different chain lengths from DSC data. Dots denote melting points and stars glass transition temperatures; lines are merely used to guide the eye. (b) TGA data showing the thermal stability of F8 and C10.

(10F, P-$(CH_2)_2$-CF_2-$(CF_2)_5$-$(CF_2)_2$-F), −126.21 (2F, P-$(CH_2)_2$-$(CF_2)_6$-CF_2-CF_3).

$^{31}P\{^1H\}$-NMR (162 MHz, $CDCl_3$): δ [ppm] = 34.84 (s).

In the following, we refer to tributyl-alkyl-phosphonium dicyanamide ILs and tributyl(1*H*,1*H*,2*H*,2*H*-perfluoroalkyl)phosphonium dicyanamide ILs as C*y* and F*x*, where *y* and *x* indicate the numbers of alkyl- and perfluoro-carbons in the longest molecular chain. Note that the non-fluorinated linker carbons are not counted for F*x* (Fig. 1b).

2.3 Thermal properties

The differential scanning calorimetry (DSC) measurements were carried out in a DSC 1 setup (Mettler Toledo GmbH, Gießen, Germany) equipped with a liquid nitrogen cooling system. IL samples (about 15 mg) were sealed hermetically in aluminum crucibles with lids and dry nitrogen was used as a purge gas. For the DSC measurements, any IL sample was first heated from 25 °C to 120 °C at 5 °C min^{-1} and held for 30 min to remove its thermal history. The sample was then cooled to −120 °C at −1 °C min^{-1} and held at −120 °C for 30 min. Finally, the sample was heated to 100 °C at 1 °C min^{-1}. We repeated all DSC measurements for at least three times with fresh IL samples to confirm the extracted liquefaction temperatures (Fig. 2a). Thermogravimetric analysis (TGA) was performed using a TGA/DSC 1 setup (Mettler Toledo GmbH, Gießen, Germany). 10 mg of the IL sample sealed in an alumina crucible was heated from 30 °C to 550 °C at a rate of 10 °C min^{-1}, and purged with nitrogen.

2.4 Small angle X-ray scattering (SAXS)

We injected the bulk IL samples into the quartz capillary tubes (wall thickness 0.01 mm, Hilgenberg GmbH, Malsfeld, Germany) in the liquid state and sealed them with epoxy glue in an argon atmosphere. The samples that were crystallized at room temperature were melted at 90 °C in an oil bath to facilitate transfer.

Small angle X-ray scattering (SAXS) measurements were conducted using a Xeuss 2.0 set-up (Xenocs, Sassenage, France) equipped with a GeniX Low Divergence Cu-K_α source. The X-ray wavelength was 0.154 nm. A Pilatus 1M detector (Dectris Ltd, Switzerland) collected SAXS patterns and the integration time was 1800 seconds. The radial integrations of the 2D SAXS patterns were undertaken using Foxtrot (version 3.2.7, SOLEIL, France). The sample-to-detector distance was calibrated with silver behenate powder to be 335 mm. All the samples were measured in the liquid state; samples that were crystallized at room temperature were heated to 120 °C in an oven and investigated as a melt. A heating stage with the Xeuss 2.0 set-up was used to observe structural changes as a function of temperature in the range of −20 °C to 120 °C with a stability of ±1 °C.

2.5 Single-crystal X-ray diffraction

We prepared the single crystals of F8 by drying their dichloromethane/heptane (with vol/vol = 1/1) solution slowly at 25 °C, purged with a slight stream of dry nitrogen. The F8 single-crystals (colourless sheets) were measured at 142 K using an AXS X8 Apex II diffractometer (Bruker AXS, Karlsruhe, Germany) equipped with a Mo-Kα radiation source (λ = 0.71073 Å); 39 865 reflexes were collected in the Theta range from 0.840° to 26.722°. The acquired data were refined by the full-matrix least-squares on F^2 using anisotropic refinements for the hydrogen atoms resulting in 12 493 independent reflections, 257 restraints, 897 parameters, $R[F^2 > 2\sigma(F^2)]$ = 0.0593, w$R(F^2)$ = 0.1470, and the fitted crystal data are: empirical formula = $C_{24}H_{31}F_{17}N_3P$, M_r = 715.49, triclinic, $P\bar{1}$, a = 10.1936(7) Å, b = 12.6081(10) Å, c = 25.0746(17) Å, α = 102.184(4)°, β = 97.398(4)°, γ = 94.832(5)°, V = 3103.1(4) $Å^3$, Z = 4, and ρ_r = 1.531 g cm^{-3}. Complete F8 single-crystal data can be found in CCDC 1503513 ([P(bu)$_3$$(CH_2)_2$$(CF_2)_8$F][DCA]) published by us in the Cambridge Crystallographic Database.†

2.6 Rheological properties

We measured the rheological properties of the IL samples using a MCR 301 Rheometer (Anton Paar GmbH, Graz, Austria) equipped with a PP25 measuring plate (diameter: 25 mm) and a DD41 dish (diameter: 41 mm). We collected the rheological data at 25 °C and high temperature from 30 °C to 100 °C with a step of 10 °C. For each measurement, we first equilibrated the IL sample at set temperatures for at least 25 minutes to reach a stable temperature (maximum deviations of ±0.1 °C). The shear history was removed by applying a constant shear at 150 s^{-1} for 60 s, after which the shear rate was increased from 200 s^{-1} to 10 000 s^{-1} in linear steps. For each IL, 30 viscosity values were recorded. Zero-shear viscosities of the fluorinated ILs for the Vogel–Fulcher–Tammann (VFT) fit were obtained by extrapolation of the Newtonian flow region.[39]

3. Results and discussion

The synthesized series of ILs with increasing alkyl chain length and fluorination allowed us to study the balance between Coulomb and van der Waals interactions while avoiding other molecular interactions such as hydrogen-bonding in protic ILs[40,41] or the π–π-interactions of imidazolium and pyridinium ILs[42] (see the ESI†). We could thus isolate the effect of fluorination.

Fig. 2a shows liquefaction temperatures as a function of alkyl and fluorinated chain length. The fluorinated samples F2, F8, and F10, and the alkylated samples C4 and C12 had clear melting points, the others had only glass transitions. Fluorinated ILs melted at higher temperatures than their alkylated analogues except for C4 (T_m = 62 °C) and F2 (T_m = 26 °C). The lower liquefaction temperature of F2 may be due to the disruption of the symmetry of the tetrabutylphosphonium cation by fluorination as reported for other ILs.[43] The liquefaction behaviour of fluorinated ILs with a long chain such as F6 and F8 was dominated by fluorophilic interactions and the enhanced charge localization of the phosphonium-core indicated by a high-field shift in ^{31}P-NMR (see the ESI†). Alkylated ILs of similar lengths liquefied at far lower temperatures, indicating that fluorophilic interactions influenced strongly the structure formation and phase transitions in ILs.

All alkylated ILs showed good thermal stability (see the ESI†) with no significant decomposition below 400 °C (C10 in Fig. 2b); they were considerably more stable than other reported DCA-based ILs with imidazolium or pyrrolidinium cations[44] and were similar in stability to other DCA-based ILs with tetraalkylphosphonium cations.[45] The fluorinated ILs were far less stable with significant decomposition occurring already at 250 °C (F8 in Fig. 2b) independent of the number of perfluorinated carbons. This is in contrast to previous reports on fluorinated phosphonium ILs with NTf_2^-, OTf^-, or BF_4^- anions that had good thermal stabilities.[46,47] We believe that the poor thermal stabilities of our fluorinated ILs are due to electron withdrawal by the perfluorinated groups that destabilize the proton in the alpha position and makes it easy to be abstracted by a slightly basic anion, an effect also reported for imidazolium-based ILs.[48]

The homologous series of both alkylated and fluorinated ILs let us conveniently separate different structural features of the ILs simply by inspecting the change in X-ray scattering as a function of molecular chain length and fluorination. SAXS was used to analyse average cluster size, shape, and structural ordering.[3,4,49–53]

All alkylated ILs exhibited three peaks in SAXS (Fig. 3) that correspond to order from polarity, charge, and adjacency; they are frequently found in ILs.[53,54] The sizes of the corresponding real-space structures were calculated from peak positions (q) as $2\pi/q$ and are summarized in Table 1. The "prepeak" or "polarity peak" at lowest q indicates the structural heterogeneity from alternating polar ionic and non-polar alkyl zones. At higher q follows the charge peak that probes the alternation between cations and anions in the charged region as in a molten salt.[55] At highest q, the adjacency peak probes the intra- and intermolecular packing of adjacent atoms;[53] it was broad and strong for all alkylated-ILs as shown in Fig. 3a.

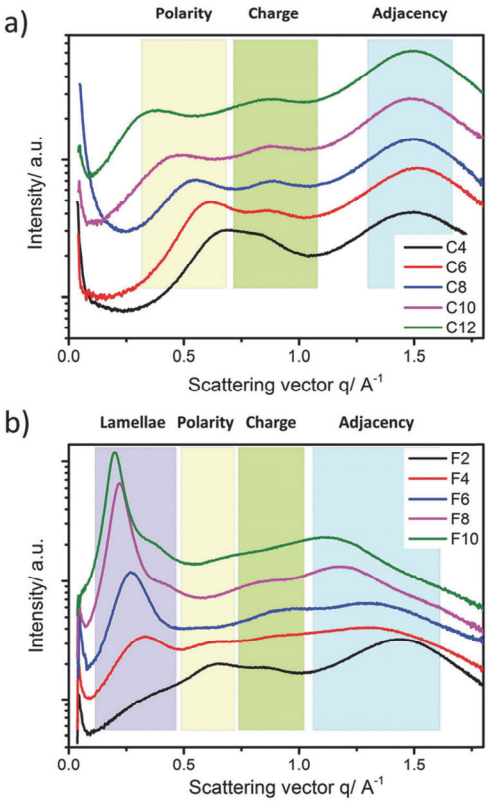

Fig. 3 Radially integrated SAXS data for (a) alkylated ILs and (b) fluorinated ILs in the liquid state. Typical scattering peaks attributed to lamellae, polarity, charge, and adjacency are marked with coloured boxes.

Table 1 Real-space length scales corresponding to the scattering peak positions[a] in Fig. 3

Sample	Peak 1 (Å)	Peak 2 (Å)	Peak 3 (Å)	Peak 4 (Å)	Peak 5 (Å)
C4	—	—	9.11	7.39	4.22
C6	—	—	9.97	7.39	4.16
C8	—	—	10.47	7.06	4.22
C10	—	—	12.57	7.06	4.22
C12	—	—	16.11	7.14	4.22
F2	16.98	—	9.52	7.66	4.39
F4	18.48	—	10.13	7.06	4.87
F6	24.17	—	—	7.06	4.87
F8	28.56	14.96	—	7.66	5.37
F10	31.42	16.98	—	7.48	5.66

[a] We obtained the peak positions by fitting the peaks with Gauss profiles or from the zero-crossing of the first derivative (see the ESI). Real-space length scales calculated with $2\pi/q$ from peaks in Fig. 3a and b. Peaks 1 and 2 refer to 1st and 2nd order scattering from the lamella formed by perfluorinated segments of adjacent ILs. Peak 3 is due to alternating polar and nonpolar zones. Peak 4 is due to cations and anions. Peak 5 is due to inter- and intra-molecular spacing.

The polarity peaks shifted to lower q values for increasing alkyl chain lengths, while the charge and adjacency peaks retained their positions. The shift indicates increased spacing

in the IL packing; small variations in the other peak positions indicates that the packing of charged ions or adjacent atoms remained constant. This implies that changing alkyl chain lengths mainly affects the structure of the nonpolar zone and merely shifts the positions of ionic regions and adjacent atoms.

Fluorination strongly changed the structure of the ILs and thus the scattering pattern. Two new peaks appeared at q below the usual "prepeak" (Fig. 3b). They were particularly strong for long perfluorinated chains, *e.g.*, F8 and F10. We believe that these two additional peaks are due to 1st and 2nd order scattering signals from ordered lamellar structures in the fluorinated ILs. The lamellar structures differ from the heterogeneity that has been reported for alkylated ILs in this work and elsewhere.[53,54] Lamellar structures with long-range correlations of this order have not been reported yet.

All fluorinated ILs had lamellar structures, even those with only two perfluorinated carbons. This is in striking contrast to similar ILs with alkyl chains. Lamellar structures and a smectic phase were previously found only for long alkyl chains.[56] A minimal carbon number (z) of 14 was required for the formation of a smectic phase in 1-alkyl-3-methylimidazolium [$C_z$mim][NO_3] ILs; the formation of a smectic phase was demonstrated to lower the free energy of long alkyl chains by forming a layered structure.[57] We are not aware of any report on the effect of fluorination on the formation of lamellae and their supramolecular structures in ILs.

Fluorination affected the polarity peaks, too. No polarity peak was discernible for F6 to F10. The presence of perfluorinated nanodomains is known to change the electron density contrast among different regions.[58] Perfluoroalkyl groups have been reported to aggregate and form fluorinated nanodomains in fluorinated ILs.[26,53] For polymers, Percec *et al.* reported that fluorination of the alkyl chains enhanced the stability of the mesophase structure by forming supramolecular columns in dendrimers.[59,60] A similar effect was found in fluorocarbon/hydrocarbon diblock amphilphiles, too.[61] We believe that the perfluorinated segments in our ILs segregate, too, and form a region with increased electron density. Segregation reduces the electron density contrast between the polar and nonpolar parts and the polarity peak becomes weaker. This is consistent with the solubility studies of Blesic *et al.* who found that fluorinated alkanes phase-segregated from tetraalkylphosphonium ILs while nonfluorinated alkanes were miscible with the ILs.[62]

The concept of Cohesive Energy Densities (CED) that quantify the strength of intra- and inter-molecular interactions of non-fluorinated and fluorinated alkanes can be used to provide a more detailed picture of structure formation. The CED of fluorinated alkanes at 298 K are below those of the alkane homologues (*e.g.*, 0.16 kJ cm^{-3} for C_8F_{18} and 0.24 kJ cm^{-3} for C_8H_{18}).[63] In the fluorinated ILs studied here, "fluorophobic" interactions cause strong microphase segregation between the longest (fluorinated) chain and the other (nonfluorinated) segments. "Fluorophilic" interactions that favour close packing of perfluorinated groups over heterogeneous packing support microphase segregation and assist in the formation of lamellae and crystalline supramolecular structures in ILs; typical examples are shown in Fig. 2a (F8 and F10).

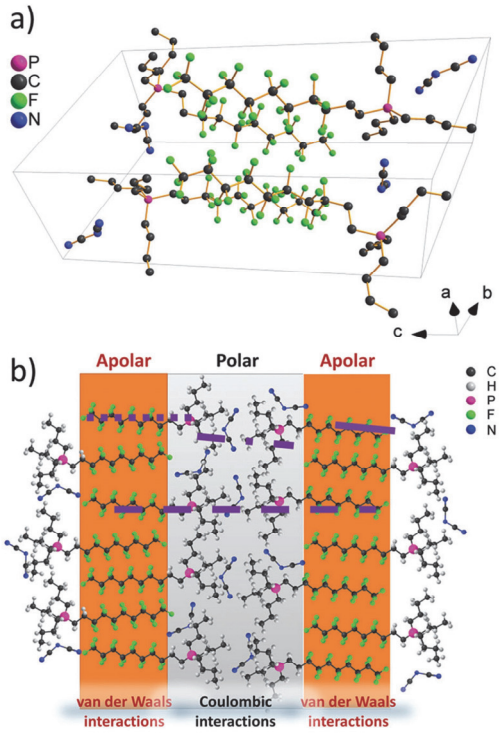

Fig. 4 (a) Illustration showing the single-crystal XRD data of F8. (b) Molecular scheme showing the molecular assemblies of the F8 melt in lamellar and smectic phases with regions dominated by Coulomb and fluorophilic interactions as marked. The length scales of molecular assemblies calculated from typical scattering peaks in Fig. 3 are marked with lines in panel b, *i.e.*, dashed line for lamellae, dotted line for polarity, dash-dotted line for charge and solid line for adjacency.

Future molecular dynamics simulation should provide more quantitative insights into the origin of a long-range ordered lamellae structure.

Single-crystal data on IL solids can be helpful to understand the ILs' liquid structure.[64] We compared the lamellar structure observed in the F8 melt to the structure of an F8 single crystal prepared by slow solvent evaporation. X-ray diffraction of the crystal at 142 K indicated a supramolecular structure with interdigitated fluorinated segments (Fig. 4a and single-crystal structural parameters in the ESI†). The lamellar periodicity along the c-axis was 25.07 Å, smaller than 28.56 Å in the liquid (Table 1, data from liquid phase SAXS). The difference is probably due to thermal expansion and the reduced packing density in the liquid. The sketch of the liquid structure in Fig. 4b is based on the following assumptions: (a) the ions' arrangement in the polar regions of the liquid is similar to that in the crystal; (b) the lamellar structure of the non-polar regions of the liquid has less positional (translational) and orientational order than that of the crystal.

The strong effects of perfluoroalkyl groups on the structure of the ILs, and in particular the emergence of a new ordered

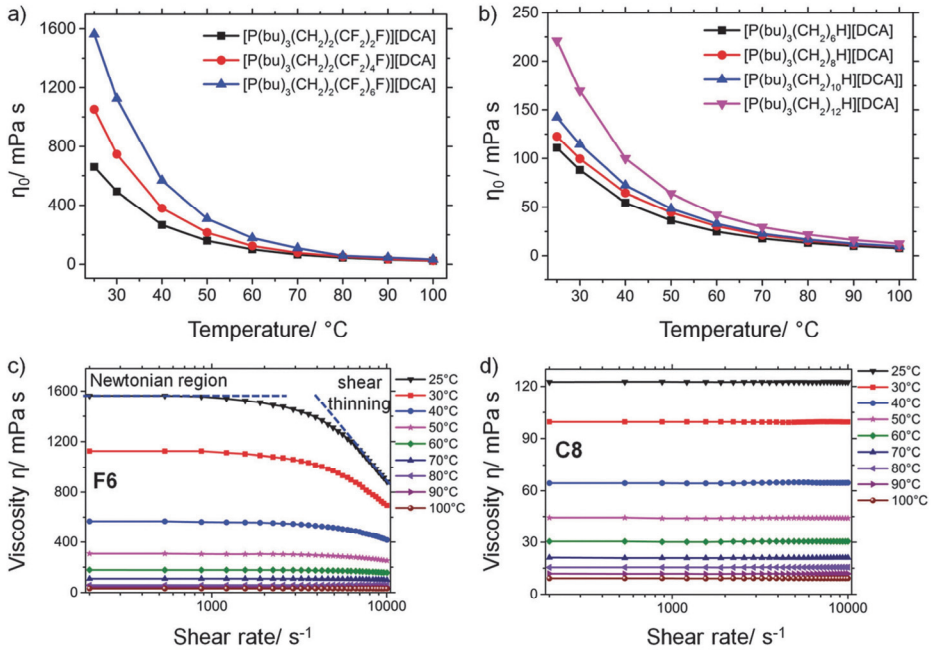

Fig. 5 Temperature dependent zero-shear viscosity, η_0, for (a) the fluorinated and (b) the alkylated phosphonium dicyanamide ILs. (c) Rheological behaviour of F6 at different temperatures and shear rates. A typical shear-thinning behaviour indicated by a remarkable change from Newtonian to shear-thinning regions (marked with dashed lines) is shown in the 25 °C curve. (d) Rheological properties of C8 at different temperatures and shear rates. Only Newtonian flow behaviour is observed at all investigated temperatures and shear rates.

lamellar structure, suggest that the flow behaviour of fluorinated ILs should deviate from that of the corresponding alkylated ILs. We studied the flow behaviour of F2 to F6 (Fig. 5a) and C6 to C12 (Fig. 5b) as functions of temperature and shear rate using rheometry. Zero-shear viscosities (η_0, extrapolated from the viscosity in the Newtonian region) for fluorinated and alkylated ILs are shown in Fig. 5a and b, respectively. All viscosities decreased exponentially with increasing temperature and followed the Vogel–Fulcher–Tammann (VFT) equation,[65–67]

$$\eta_0 = \eta_\infty \exp\left(\frac{B}{T - T_0}\right)$$

with temperature dependent material parameters η_∞ and B, and the Vogel temperature T_0 (see the ESI†) as expected for ILs.[68,69]

The viscosities of all fluorinated ILs were consistently above those of alkylated ILs (Fig. 5a and b); they were approximately one order of magnitude larger at 25 °C. The lamellar structure of fluorinated side chains apparently leads to larger cohesive aggregates in fluorinated ILs. We believe that the larger supramolecular structures formed in the fluorinated ILs affected momentum transfer, which led to increased viscosity. To verify our hypothesis, we studied the viscosities of ILs at shear rates from 200 to 10 000 s^{-1} at different temperatures (Fig. 5c and d). The viscosity of F6 was first constant and then decreased with increasing shear, consistence with the transition from Newtonian flow through a transition zone to linear shear thinning in accordance with the Ostwald-de Waele relationship,[70]

$$\tau = k(\partial v/\partial y)^n$$

with shear stress τ (Pa), consistency index k (Pa s^n), the shear rate $\partial v/\partial y$ (s^{-1}), and the dimensionless flow behaviour index n. The greatest deviation of F6 from Newtonian flow (n = 1) occurred at 25 °C, where n = 0.46. We believe that this strong shear thinning results from the disruption of the cohesive lamellar structure. In contrast, only Newtonian flows were observed for C8 at all temperatures. All other ILs showed similar trends – strong shear thinning for fluorinated and purely Newtonian flows for alkyl ILs. We also studied the flow behaviour of F6 at elevated temperatures because previous work on other fluorinated ILs reports that the fluorinated aggregates formed by perfluorinated chains in ILs are less thermally stable and would be dissociated at temperatures above −25 °C.[49] High temperatures provide the positive excess enthalpy necessary for the mixing of fluorocarbons and hydrocarbons.[71] Fig. 5c shows that F8 exhibited a purely Newtonian flow behaviour above 80 °C. The segregated lamellar structure readily dissolved at this temperature through the mixing of fluorinated and alkylated segments as observed in macroscopic systems.[72] The temperature of transition to Newtonian behaviour for fluorinated ILs depended on the chain length; it occurred at 60 °C for F2, 70 °C for F4, and 80 °C for F6.

The flow behaviour index n at 25 °C decreased with increasing fluorine content, from 0.77 for F2 to 0.58 for F4.

All rheological data are consistent with the structure formation discussed above. To the best of our knowledge, this is the first report on a lamellar mesophase in ILs that induces a strong effect on flow behaviour. Shear thinning was previously only reported for ILs with strong interactions, *e.g.* protic ILs with a hydrogen-bond as in ref. 73 and trioctylalkylammonium bis(salicylato)borate in ref. 74.

4. Conclusions

We synthesized two series of new phosphonium dicyanamide ionic liquids, *i.e.*, alkylated ILs and fluorinated ILs, and studied their structure–property relationships by following the effect of increasing fluorination. Small angle X-ray scattering indicated a monotonic increase of the size of the non-polar region with chain length while the polar regions did not change. The trends were in accordance with previous reports on alkylated IL structure. Fluorination strongly changed the ILs' structure. There was no regular polar structure visible in the scattering data of F6 to F10. An additional lamellar structure with surprisingly long-ranged order was found in all fluorinated ILs.

We believe that the "fluorophobic" and "fluorophilic" interactions caused the strong microphase segregation and resulted in a lamellar mesophase structure. The perfluorinated segments packed densely and caused the absence of the polarity peak in F6 to F10 because of the rearrangements of the electrons accompanied by the formation of new lamellar structures. The lamellar structure introduced non-Newtonian behaviour that was entirely absent without fluorination. The temperature dependence of shear thinning strongly suggests that the lamellar structure disintegrates at increased temperatures or shear rates. It provides a straightforward strategy to tune the viscosity of fluorinated ionic liquids for applications such as lubrication.[75] Corrosion due to the presence of fluoride that has recently been observed[76,77] needs to be addressed for such applications.

Conflicts of interest

There are no conflicts of interest to declare.

Acknowledgements

D. Rauber and R. Hempelmann thank the Deutsche Bundesstiftung Umwelt (DBU) (31925-41) for financial support. Prof. Eduard Arzt is acknowledged for his continuing support of this project.

References

1 T. Welton, *Chem. Rev.*, 1999, **99**, 2071–2084.
2 Z.-P. Zheng, W.-H. Fan, S. Roy, K. Mazur, A. Nazet, R. Buchner, M. Bonn and J. Hunger, *Angew. Chem., Int. Ed.*, 2014, **54**, 687–690.
3 R. Hayes, G. G. Warr and R. Atkin, *Chem. Rev.*, 2015, **115**, 6357–6426.
4 *The Structure of Ionic Liquids*, ed. R. Caminiti and L. Gontrani, Springer International Publishing, Cham, 2014.
5 T. L. Greaves and C. J. Drummond, *Chem. Soc. Rev.*, 2013, **42**, 1096–1120.
6 B. Kirchner, F. Malberg, D. S. Firaha and O. Hollóczki, *J. Phys.: Condens. Matter*, 2015, **27**, 463002.
7 R. Ludwig, *J. Phys. Chem. B*, 2009, **113**, 15419–15422.
8 A. Strate, T. Niemann, D. Michalik and R. Ludwig, *Angew. Chem., Int. Ed.*, 2017, **56**, 496–500.
9 P. A. Hunt, C. R. Ashworth and R. P. Matthews, *Chem. Soc. Rev.*, 2015, **44**, 1257–1288.
10 K. Shimizu, M. F. Costa Gomes, A. A. H. Pádua, L. P. N. Rebelo and J. N. Canongia Lopes, *THEOCHEM*, 2010, **946**, 70–76.
11 M. A. A. Rocha, C. M. S. S. Neves, M. G. Freire, O. Russina, A. Triolo, J. A. P. Coutinho and L. M. N. B. F. Santos, *J. Phys. Chem. B*, 2013, **117**, 10889–10897.
12 K. Binnemans, *Chem. Rev.*, 2005, **105**, 4148–4204.
13 J. P. Hallett and T. Welton, *Chem. Rev.*, 2011, **111**, 3508–3576.
14 M. Kofu, M. Nagao, T. Ueki, Y. Kitazawa, Y. Nakamura, S. Sawamura, M. Watanabe and O. Yamamuro, *J. Phys. Chem. B*, 2013, **117**, 2773–2781.
15 K. Ueno, H. Tokuda and M. Watanabe, *Phys. Chem. Chem. Phys.*, 2010, **12**, 1649–1658.
16 P. Hapiot and C. Lagrost, *Chem. Rev.*, 2008, **108**, 2238–2264.
17 R. E. Morris, *Chem. Commun.*, 2009, 2990.
18 I. Minami, *Molecules*, 2009, **14**, 2286–2305.
19 S. Zhang, Q. Zhang, Y. Zhang, Z. Chen, M. Watanabe and Y. Deng, *Prog. Mater. Sci.*, 2016, **77**, 80–124.
20 T. L. Greaves, D. F. Kennedy, Y. Shen, A. Weerawardena, A. Hawley, G. Song and C. J. Drummond, *J. Mol. Liq.*, 2015, **210**, 279–285.
21 C. Yue, D. Fang, L. Liu and T.-F. Yi, *J. Mol. Liq.*, 2011, **163**, 99–121.
22 T. L. Greaves, D. F. Kennedy, Y. Shen, A. Hawley, G. Song and C. J. Drummond, *Phys. Chem. Chem. Phys.*, 2013, **15**, 7592–7598.
23 J. J. Tindale, K. L. Mouland and P. J. Ragogna, *J. Mol. Liq.*, 2010, **152**, 14–18.
24 O. Kysilka, M. Rybáčková, M. Skalický, M. Kvíčalová, J. Cvačka and J. Kvíčala, *J. Fluorine Chem.*, 2009, **130**, 629–639.
25 *Handbook of Fluorous Chemistry*, ed. J. A. Gladysz, D. P. Curran and I. T. Horváth, Wiley-VCH Verlag GmbH & Co. KGaA, Weinheim, FRG, 2004.
26 A. B. Pereiro, J. M. M. Araújo, S. Martinho, F. Alves, S. Nunes, A. Matias, C. M. M. Duarte, L. P. N. Rebelo and I. M. Marrucho, *ACS Sustainable Chem. Eng.*, 2013, **1**, 427–439.
27 M. L. Ferreira, M. J. Pastoriza-Gallego, J. M. M. Araújo, J. N. Canongia Lopes, L. P. N. Rebelo, M. M. Piñeiro, K. Shimizu and A. B. Pereiro, *J. Phys. Chem. C*, 2017, **121**, 5415–5427.
28 T. L. Merrigan, E. D. Bates, S. C. Dorman and J. H. Davis Jr., *Chem. Commun.*, 2000, 2051–2052.
29 J. Qu, J. J. Truhan, S. Dai, H. Luo and P. J. Blau, *Tribol. Lett.*, 2006, **22**, 207–214.
30 I. Minami, M. Kita, T. Kubo, H. Nanao and S. Mori, *Tribol. Lett.*, 2008, **30**, 215–223.

31 F. Atefi, M. T. Garcia, R. D. Singer and P. J. Scammells, *Green Chem.*, 2009, **11**, 1595–1604.
32 K. Tsunashima and M. Sugiya, *Electrochem. Commun.*, 2007, **9**, 2353–2358.
33 K. Tsunashima and M. Sugiya, *Electrochemistry*, 2007, **75**, 734–736.
34 K. Tsunashima, S. Kodama, M. Sugiya and Y. Kunugi, *Electrochim. Acta*, 2010, **56**, 762–766.
35 O. Russina, F. Lo Celso, M. Di Michiel, S. Passerini, G. B. Appetecchi, F. Castiglione, A. Mele, R. Caminiti and A. Triolo, *Faraday Discuss.*, 2013, **167**, 499–513.
36 Y. Shen, D. F. Kennedy, T. L. Greaves, A. Weerawardena, R. J. Mulder, N. Kirby, G. Song and C. J. Drummond, *Phys. Chem. Chem. Phys.*, 2012, **14**, 7981.
37 R. P. Matthews, T. Welton and P. A. Hunt, *Phys. Chem. Chem. Phys.*, 2014, **16**, 3238–3253.
38 A. Luís, K. Shimizu, J. M. M. Araújo, P. J. Carvalho, J. A. Lopes-da-Silva, J. N. Canongia Lopes, L. P. N. Rebelo, J. A. P. Coutinho, M. G. Freire and A. B. Pereiro, *Langmuir*, 2016, **32**, 6130–6139.
39 C. Patrascu, F. Gauffre, F. Nallet, R. Bordes, J. Oberdisse, N. de Lauth-Viguerie and C. Mingotaud, *ChemPhysChem*, 2006, **7**, 99–101.
40 R. Hayes, S. Imberti, G. G. Warr and R. Atkin, *Angew. Chem., Int. Ed.*, 2013, **52**, 4623–4627.
41 K. Dong, S. Zhang and J. Wang, *Chem. Commun.*, 2016, **52**, 6744–6764.
42 P. Stepnowski, J. Nichthauser, W. Mrozik and B. Buszewski, *Anal. Bioanal. Chem.*, 2006, **385**, 1483–1491.
43 N. V. Plechkova and K. R. Seddon, *Chem. Soc. Rev.*, 2008, **37**, 123–150.
44 Y. Yoshida, O. Baba and G. Saito, *J. Phys. Chem. B*, 2007, **111**, 4742–4749.
45 T. J. Wooster, K. M. Johanson, K. J. Fraser, D. R. MacFarlane and J. L. Scott, *Green Chem.*, 2006, **8**, 691.
46 J. J. Tindale and P. J. Ragogna, *Chem. Commun.*, 2009, 1831–1833.
47 J. J. Tindale, C. Na, M. C. Jennings and P. J. Ragogna, *Can. J. Chem.*, 2007, **85**, 660–667.
48 J. Liu, S. D. Chambreau and G. L. Vaghjiani, *J. Phys. Chem. A*, 2014, **118**, 11133–11144.
49 O. Russina, F. Lo Celso, M. Di Michiel, S. Passerini, G. B. Appetecchi, F. Castiglione, A. Mele, R. Caminiti and A. Triolo, *Faraday Discuss.*, 2013, **167**, 499–513.
50 P. Zhang, H. Huang, Y. Chen, S. Yu, C. Krywka, S. K. Vayalil, S. V. Roth and T. He, *Chin. J. Polym. Sci.*, 2014, **32**, 1188–1198.
51 T. P. Russell, J. F. Rabolt, R. J. Twieg, R. L. Siemens and B. L. Farmer, *Macromolecules*, 1986, **19**, 1135–1143.
52 J. J. Hettige, J. C. Araque and C. J. Margulis, *J. Phys. Chem. B*, 2014, **118**, 12706–12716.
53 H. V. R. Annapureddy, H. K. Kashyap, P. M. De Biase and C. J. Margulis, *J. Phys. Chem. B*, 2010, **114**, 16838–16846.
54 J. C. Araque, J. J. Hettige and C. J. Margulis, *J. Phys. Chem. B*, 2015, **119**, 12727–12740.
55 J. Dupont, *Acc. Chem. Res.*, 2011, **44**, 1223–1231.
56 K. Goossens, K. Lava, C. W. Bielawski and K. Binnemans, *Chem. Rev.*, 2016, **116**, 4643–4807.
57 G. Saielli, A. Bagno and Y. Wang, *J. Phys. Chem. B*, 2015, **119**, 3829–3836.
58 The calculation of the scattering length density (SLD) is based on the calculator provided by the NIST centre for neutron research, https://www.ncnr.nist.gov/resources/activation/. For the SLD of the perfluorinated nanodomain, the material C_8F_{18} and density value 1.766 g cm^{-3} were used and the real part of the SLD was 14.470 $\times$ 10^{-6} Å^{-2}; for the alkylated nanodomain, the material $C_{10}H_{22}$ and density value 0.730 g cm^{-3} were used and the real part value of SLD was 7.156 $\times$ 10^{-6} Å^{-2}; for F8, the material $C_{24}H_{31}F_{17}N_3P$ and density value 1.531 g cm^{-3}, extracted from the single-crystal data, were used and the real part of the SLD was 13.296 $\times$ 10^{-6} Å^{-2}. As a comparison, the real part value of SLD of C_8F_{18} is 109% times that of F8 single-crystal and 202% times that of $C_{10}H_{22}$.
59 V. Percec, G. Johansson, G. Ungar and J. Zhou, *J. Am. Chem. Soc.*, 1996, **118**, 9855–9866.
60 G. Johansson, V. Percec, G. Ungar and J. P. Zhou, *Macromolecules*, 1996, **29**, 646–660.
61 M. P. Krafft and J. G. Riess, *Chem. Rev.*, 2009, **109**, 1714–1792.
62 M. Blesic, J. N. C. Lopes, M. F. C. Gomes and L. P. N. Rebelo, *Phys. Chem. Chem. Phys.*, 2010, **12**, 9685–9692.
63 G. Marchionni, G. Ajroldi, M. C. Righetti and G. Pezzin, *Macromolecules*, 1993, **26**, 1751–1757.
64 Y. Ji, R. Shi, Y. Wang and G. Saielli, *J. Phys. Chem. B*, 2013, **117**, 1104–1109.
65 H. Vogel, *Phys. Z.*, 1921, **22**, 645–646.
66 G. S. Fulcher, *J. Am. Ceram. Soc.*, 1992, **75**, 1043–1055.
67 G. Tammann and W. Hesse, *Z. Anorg. Allg. Chem.*, 1926, **156**, 245–257.
68 H. Tokuda, K. Hayamizu, K. Ishii, M. A. B. H. Susan and M. Watanabe, *J. Phys. Chem. B*, 2005, **109**, 6103–6110.
69 A. Rupp, N. Roznyatovskaya, H. Scherer, W. Beichel, P. Klose, C. Sturm, A. Hoffmann, J. Tübke, T. Koslowski and I. Krossing, *Chem. – Eur. J.*, 2014, **20**, 9794–9804.
70 G. L. Burrell, N. F. Dunlop and F. Separovic, *Soft Matter*, 2010, **6**, 2080.
71 P. Morgado, J. Ben Lewis, C. M. C. Laginhas, L. F. G. Martins, C. McCabe, F. J. Blas and E. J. M. Filipe, *J. Phys. Chem. B*, 2011, **115**, 15013–15023.
72 I. T. Horvath and J. Rabai, *Science*, 1994, **266**, 72–75.
73 G. L. Burrell, N. F. Dunlop and F. Separovic, *Soft Matter*, 2010, **6**, 2080–2086.
74 R. Gusain, P. S. Bakshi, S. Panda, O. P. Sharma, R. Gardas and O. P. Khatri, *Phys. Chem. Chem. Phys.*, 2017, **19**, 6433–6442.
75 Z. Zeng, B. S. Phillips, J.-C. Xiao and J. M. Shreeve, *Chem. Mater.*, 2008, **20**, 2719–2726.
76 M. Itoga, S. Aoki, A. Suzuki, Y. Yoshida, Y. Fujinami and M. Masuko, *Tribol. Int.*, 2016, **93**, 640–650.
77 A. Arcifa, A. Rossi and N. D. Spencer, *J. Phys. Chem. C*, 2017, **121**, 7259–7275.

2.4 Publication D

Catalyst retention utilizing a novel fluorinated phosphonium ionic liquid in Heck reactions under fluorous biphasic conditions

Daniel Rauber, Frederik Philippi, Rolf Hempelmann.

J. Fluor. Chem., **2017**, 299, 115-122.

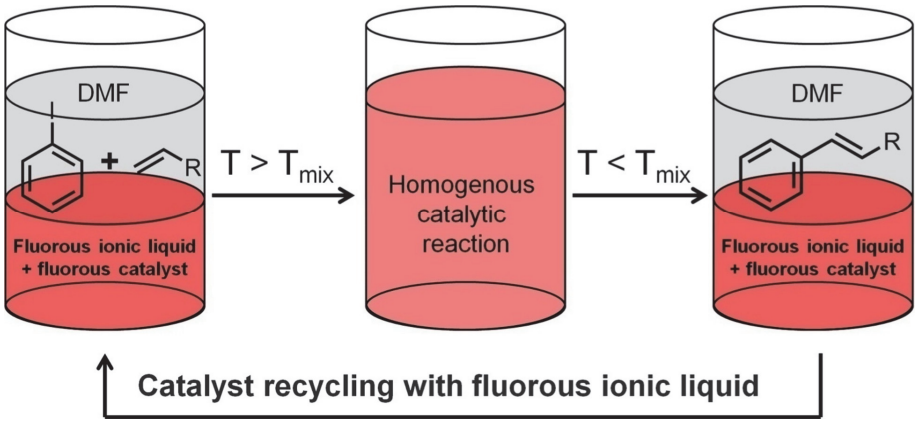

Journal of Fluorine Chemistry 200 (2017) 115–122

Contents lists available at ScienceDirect

Journal of Fluorine Chemistry

journal homepage: www.elsevier.com/locate/fluor

Catalyst retention utilizing a novel fluorinated phosphonium ionic liquid in Heck reactions under fluorous biphasic conditions

Daniel Rauber[a,*], Frederik Philippi[a], Rolf Hempelmann[a,b]

[a] Institute of Physical Chemistry, Saarland University, Campus B 2.2, 66123 Saarbrücken, Germany
[b] Korea Institute of Science and Technology Europe, Campus E 7.1, 66123 Saarbrücken, Germany

ARTICLE INFO

Keywords:
Ionic liquids
Fluorous biphasic catalysis
Heck reaction
Catalyst retention

ABSTRACT

A novel ionic liquid based on a highly fluorinated phosphonium cation was synthesized and its physicochemical properties were compared to its semi- and non-fluorinated analogue. The fluorinated ionic liquid was found to show a thermomorphic mixing behavior with organic solvents so that it could be applied as a substitute for volatile perfluorinated solvents in fluorous biphasic catalysis to achieve the recovery of perfluoro-tagged catalysts. Efficient immobilization of a perfluoro-tagged palladium catalyst in the fluorous ionic liquid phase was demonstrated for the Heck reaction as a model reaction of the widely applied Pd-catalysed C–C coupling reactions. The reaction of iodobenzene and methyl acrylate resulted in 83% yield after 20 runs proofing the efficient immobilization in the fluorophilic ionic liquid.

1. Introduction

Ionic liquids (ILs) and fluorous solvents are both regarded as "neoteric solvents" in the context of a greener, more sustainable chemistry since they share the potential to facilitate recycling procedures and reduce waste material as well as energy consumption [1–4]. However their physicochemical properties vary considerably. While ionic liquids have a negligible vapor pressure, polar structural motifs and are often hydrophilic, fluorous solvents show a significant vapor pressure and are highly apolar. Furthermore perfluoroalkyl groups show an even greater hydrophobicity than hydrocarbons through the reduced polarizability resulting from the high electronegativity of the fluorine atoms. The behavior of the perfluorocarbons of being hydro- and lipophobic at the same time is referred to as flurorophilicity [5]. Many fluorous and organic solvents are known to show a thermomorphic mixing behavior, forming a biphasic system at room temperature and a homogenous phase at elevated temperatures. This thermoregulated effect allows the specific separation and immobilization of components in liquid–liquid multiphasic systems and orthogonal chemistry in the separated phases [6]. A famous concept for thermoregulated chemistry is the fluorous biphasic catalysis (FBC) to achieve the recovery of perfluoro-tagged transition metal catalysts [7–10]. Important drawbacks of conventional fluorous solvents are their limited tuneability and relatively high vapor pressure, which restricts the useable temperature range. Furthermore bioaccumulation, persistence and the global warming potential of the volatile fluorous solvents can pose serious environmental problems [11,12]. The use of highly fluorinated ionic liquids [13] combines the advantages of fluorous solvents for efficient extraction and immobilization with non-volatility and a high degree of flexibility (through the task-specific and tailored designs) of ionic liquids. In this way it is possible to combine the benefits of these two neoteric solvents classes for effective and environmentally friendly reagent immobilization strategies. The use of fluorous groups in ionic liquids allows the implementation of fluorophilicity to the broad field of possible modifications beside the choices for anion and cation. This task-specific tuning allows new possible applications or the improvement of existing techniques [14]. It thus becomes feasible to modify the properties of liquid multiphasic systems in a wide range using non-volatile, modifiable fluorinated ILs as fluorous phase. The search for effective and reusable catalyst systems for multiphasic homogenous catalysis is an important issue in green chemistry since it saves energetic and chemical input [15,16]. ILs with perfluoroalkyl substituents have found numerous applications in many scientific fields like the use as surfactants [17], coating material [18] or liquid crystals [19,20], highly hydrophobic extraction agents [21], as well as for gas separation and gas dissolution [22,23] to name only a few. Furthermore fluorinated ILs are intensively investigated because of their unique microscopic heterogeneous structuring leading to a triphilic organization in ionic, hydrocarbon and fluorous domains driven by solvophobic interactions comparable to the macroscopic solvent behavior observed in limited miscibility and phase separation [24–27].

In this work we describe a new highly fluorinated phosphonium

* Corresponding author.
E-mail address: daniel.rauber@uni-saarland.de (D. Rauber).

http://dx.doi.org/10.1016/j.jfluchem.2017.06.014
Received 3 April 2017; Received in revised form 28 June 2017; Accepted 28 June 2017
Available online 29 June 2017

ionic liquid $[P(R_{f6})_3R_{f4}][NTf_2]$ (**1**) having four perfluoroalkyl chains ($R_{fx} = (CH_2)_2(CF_2)_xF$; x = 4, 6) in the cation combined with the bis (trifluoromethanesulfonyl)imide (NTf_2^-) anion. The application of this "building-block"-approach [28] for the synthesis of perfluoroalkyl substituted ILs allows the synthesis under laboratory conditions with easily adjustable structures. To investigate the effect of fluorination on important physicochemical properties and mixing behavior with organic solvents, IL **1** was compared to the non-fluorinated analogues hexyltrioctylphosphonium bis(trifluoromethanesulfonyl)imide $[P(oct)_3hex][NTf_2]$, the semifluorinated IL $[P(oct)_3R_{f4}][NTf_2]$ and the commonly used 1-butyl-3-methyl-imidazolium bis(trifluoromethanesulfonyl)imide $[BMIM][NTf_2]$. The highly fluorinated IL **1** shows a low solubility and thermomorphic phase-mixing behavior with many organic solvents as it is commonly found for perfluorinated molecular solvents. The combination of the perfluorinated IL **1** and DMF was found to be an effective liquid–liquid system for immobilization of a palladium catalyst with highly fluorinated ligands [29] in Heck reactions [30]. Van Koten and coworkers already reported the use of a highly fluorinated IL for the retention of a perfluoro-tagged rhodium catalyst in a hydrosilylation [13]. Since the palladium catalyzed C—C bond formation is of high interest for laboratory and industrial preparations we wanted to demonstrate the application of this concept to the cross coupling reactions utilizing a Pd-catalyst immobilized in a fluorous ionic liquid phase. As a model reaction for palladium catalysis we chose the widely used Heck reaction for the cross coupling reaction of iodobenzene with either methyl acrylate or styrene. The Heck reaction is one of the most important reactions for C-C-bond formation, but in most reports the catalyst is lost during work-up and cannot be recovered. Creating an efficient recycling protocol for the Heck cross coupling is found to be a tough challenge because of the instable catalytic cycle and the use of multiple reagents and products which are changing the system properties and may have a disturbing or inactivating effect on the catalyst [31].

2. Experimental

2.1. Synthesis of the ionic liquids

The investigated ILs were synthesized by modified quaternization reactions of the corresponding phosphines with 1-bromohexane or 1*H*,1*H*,2*H*,2*H*-perfluorohexyl iodide in acetonitrile or DMF under inert gas atmosphere at elevated temperatures [32]. Tris(1*H*,1*H*,2*H*,2*H*-perfluorooctyl)phosphine was synthesized following literature protocols [18,33]. The halide ILs were then converted to the corresponding NTf_2-ILs by anion metathesis reaction with $LiNTf_2$ in acetone. The exemplary synthesis of the fluorous IL **1** via quarternization of the fluorinated phosphine followed by anion metathesis is sketched in Scheme 1. Purity of the obtained ILs was checked by multinuclear NMR-spectroscopy and ESI–MS. The absence of halide ions was confirmed using methanolic $AgNO_3$ solution. Further details about the applied materials, synthesis conditions and multinuclear NMR-spectra are given in the Supporting information. $[BMIM][NTf_2]$ was prepared following literature reports [34].

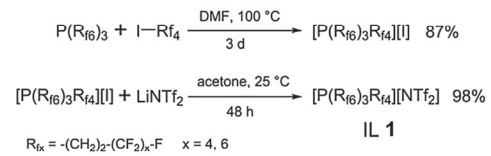

Scheme 1. Synthesis of the fluorinated ionic liquid **1** via quaternization of ternary phosphine and 1*H*,1*H*,2*H*,2*H*-perfluorohexyl iodide followed by anion metathesis reaction with $LiNTf_2$.

2.2. Thermal properties

Melting, glass transition and cold crystallization points were determined by differential scanning calorimetry (DSC) using a DSC 1 STARe System (Mettler Toledo, Gießen, Germany) equipped with liquid nitrogen cooling. For the measurements about 20 mg sample were weighted into aluminum crucibles and hermetically sealed. The temperature program started with a heating rate of +5 °C/min to 100 °C followed by 30 min isothermal step at 100 °C to remove thermal history. Afterwards a dynamic step with cooling rate of −1 °C/min to -120 °C was applied. The temperature was held constant at −120 °C for 10 min, followed by a heating step (+1 °C/min) to 120 °C and then returned to the initial conditions. Decomposition temperatures were determined by thermogravimetric analysis (TGA) using a TG 209 F1 Iris (Netzsch, Selb, Germany) and Al_2O_3 crucibles. The temperature program was set from 20 °C to 600 °C applying a heating rate of 10 °C/min and a nitrogen flow of 20 mL/min. Decomposition temperatures were determined as extrapolated onset temperatures.

2.3. Polarity determination using the solvatochromic dye Nile Red

To 0.5 g of the ILs was added a solution of 0.5 mL Nile Red (NR) in acetone ($c(NR) = 3.0 \times 10^{-3}$ mol L^{-1}) and stirred until the solution became homogenous. In case of IL 1 an additional milliliter acetone was added to ensure full dissolution. The solvent was then removed by drying in oil-pump vacuum for two days and the Nile Red solutions of the ILs were transferred to a quartz cuvette of 1 mm diameter to record a transmission UV/Vis spectrum. In case of 1 the UV/Vis-measurement was performed on a thin film of the sample in supercooled state as this IL showed a widely suppressed crystallization (see DCS results in Section 3.1). For each IL ten measurements were performed, the wavelength of the absorption maxima detected and the results averaged. The E_{NR} values were calculated after Eq. (1).

$$E_{NR} = hcN_A \lambda_{max}^{-1} \times 10^{-6} \quad (1)$$

with:
- h: Planck's constant
- c: speed of light
- N_A: Avogadro's constant
- λ_{max}: wavelength of the maximum absorbance (in nm)

2.4. Crystal structure determination of IL 1

Single crystal X-ray diffraction data were collected on a X8 Apex II diffractometer (Bruker AXS, Karlsruhe, Germany) at −121 °C using Mo-Kα radiation (λ = 0.71073 Å) in theta range from 0.607° to 27.811° collecting 88389 reflections in total. Crystal data: $C_{30}H_{16}F_{48}P^+$, $C_2F_6NO_4S_2^-$: M_r = 1599.55, triclinic, P-1, a = 9.1235(6) Å, b = 9.6920(6) Å, c = 33.677(2) Å, α = 86.357(3)°, β = 85.533(4)°, γ = 63.392(3)°, V = 2653.0(3) Å^3, Z = 2, ρ_r = 2.002 g cm^{-3}. The refinement using full-matrix least-squares on F^2 resulted in 12220 independent reflections, 381 restraints, 822 parameters, $R[F^2 > 2\sigma(F^2)] = 0.1245$, $wR(F^2) = 0.3897$.

2.5. Determination of ionic liquid solubility/miscibility in organic solvents

Solubilities or miscibilities of the phosphonium ILs with a range of organic solvents were determined by preparing saturated solutions of the ILs and 3.000 mL of purified and dried organic solvents under argon by stirring for at least 3 h in a thermostated bath keeping the temperature at 25 °C until a two phase system remained. Then the solution was allowed to settle for 16 h after which a completely homogenous upper phase was observed. A 2.000 mL sample of the organic phase was carefully taken and the solvent removed in oil pump vacuum by drying for at least one day until the mass remained constant. By weighting the remaining IL the solubility per liter could be calculated. If no second

phase was formed with varying the amount of organic solvent the IL was stated as miscible. Experiments were performed in triple and the results averaged. The phase diagram of IL 1 and DMF was constructed by inserting a molten sample of the IL into a graduated cylinder. Known volumes of DMF were added, the cylinder sealed and slowly heated with stirring until the phases became homogenous. The temperature at this point is the mixing temperature T_{mix} for the given volume fraction. After cooling to ambient temperature further volumes of DMF were added and the process repeated to construct the phase diagram.

2.6. Heck reactions under fluorous biphasic conditions using the fluorous IL

All reactions were carried out under inert atmosphere of argon. 1.00 g of IL 1 was degassed in vacuum and flushed with argon for 3 times. Then the IL-phase was saturated with DMF (about 0.2 mL) to obtain a slightly viscous, fluorous phase. In case of the cross coupling reactions performed at 85 °C, 8.0 mg of the catalyst [Pd(P(m-C_6H_4-$(CH_2)_2$-$(CF_2)_8$-F)$_3$)$_2$$Cl_2$] ($2.37 \times 10^{-3}$ mmol, 0.80 mol%) was added. For the coupling reaction carried out at 70 °C 10.0 mg of the catalyst (2.96×10^{-3} mmol, 1.00 mol%) was added. The catalyst was then dissolved under slight heating and 0.400 mL of a 0.740 mol L^{-1} iodobenzene stock solution in DMF (0.296 mmol 1.00 eq.), 0.400 mL of a 0.888 mol L^{-1} olefin stock solution in DMF (0.355 mmol, 1.20 eq.) and 0.200 mL of a 1.78 mol L^{-1} stock solution of triethylamine in DMF (0.355 mmol, 1.20 eq.) were added. The mixture was stirred and heated to 85 °C resp. 70 °C for 16 h (unless noted otherwise) and then cooled down to −18 °C. The upper organic phase was carefully removed and the fluorous phase extracted with 0.2 mL of DMF. The combined DMF-phases were filled up to 100 mL with acetonitrile and a sample was analyzed with high performance liquid chromatography (HPLC). The HPLC system consisted of ASI-100 automated sample injector, Degasys DG-1210 solvent degasser, P680 HPLC Pump, TCC100 Thermostated Column Compartment and UVD3404 UV/Vis detector (all from Dionex, Sunnyvale, USA). The used column was a Hibar 150 × 4 mm C18/5 µm (Merck, Darmstadt, Germany). The column temperature was controlled by a column oven at 25 °C. Gradient program with a total flow of 1.000 mL/min using water and acetonitrile started with 100% water at t = 0 min to 100% MeCN at t = 20 min. Wavelength for UV/Vis detection was set to 254 nm. Retention times of the fully resolved peaks were 13.8 min for methyl cinnamate, 17.8 min for stilbene, 15.8 min for iodobenzene and 15.0 min for styrene. The amount of product was calculated by integration of the product peak in comparison with calibration curves. For each sample at least three runs were performed and the results averaged. Facile product isolation for six times was proven in a separate experiment for the reaction of iodobenzene with methyl acrylate at reaction times of 16 h and a temperature of 70 °C. For this purpose six equivalents of water were added to the DMF-phase after the reaction and the resulting suspension was extracted with 3 mL hexane three times. The solvent of the combined organic phases was removed by rotary evaporation and the residue dried in vacuum yielding pure methyl cinnamate in high isolated yield as confirmed by ^{1}H- and ^{13}C{1H}-NMR spectroscopy (see Supporting information; ^{1}H NMR (400 MHz, $CDCl_3$): δ[ppm] = 7.70 (d, $^3J_{HH}$ = 16.0 Hz, 1H), 7.59–7.46 (m, 2H), 7.43–7.35 (m, 3H), 6.45 (d, $^3J_{HH}$ = 16.1 Hz, 1H), 3.81 (s, 3H); ^{13}C{^{1}H} NMR (101 MHz, $CDCl_3$): δ[ppm] = 167.47, 144.93, 134.42, 130.36, 128.95, 128.14, 117.84, 51.76.). Turnover number (TON) for the reaction was calculated using Eq. (2).

$$TON = n_{(product)}/n_{(catalyst)} \quad (2)$$

The cumulative TON is the summation of the individual TON per run after separation of the product phase and addition of new reagents. In further experiments leaching of the fluorous IL **1** was investigated by combining 1.00 g with 1.00 mL DMF without further reagents stirring at 70 °C for 30 min and cooling down to −18 °C. A sample of 0.500 mL was taken from the upper organic phase, the solvent removed in oil pump vacuum and the residue weighted. This process was repeated three times and the results averaged.

3. Results and discussion

3.1. Physical properties

The fluorous IL **1** is a thermal, air and water stable white solid if crystallized, forming a slightly yellow liquid above its melting point or in the presence of small amounts of organic solvents. In supercooled state the IL is observed as highly viscous, slightly yellow liquid. To investigate the effect of increasing fluorination in the cation on the physicochemical properties a comparison with the semi-fluorinated and non-fluorinated analogue was made. To investigate the influence of the anion choice the results were also compared to the widely used IL [BMIM][NTf_2] which incorporated the same anion. DSC measurements were performed to investigate the phase transition behavior. Low scan speeds of ± 1 °C/min were chosen to ensure the suppression of supercooling through thermal quenching which can result in solely glass formation and thereby incomplete determination of the phase transition points [35]. Thermal stability was examined by means of dynamic TGA. As method for the empirical determination of solvent polarity the solvatochromic dye Nile Red [36] was applied which was also used for polarity determination for a range of other ionic liquids [37]. The more commonly used Reichardt's Dye [38] was found to be insoluble in the fluorous IL **1**. The empirical polarity determination is used to gain insight into the interactions on molecular level instead of using macroscopic parameters like relative permittivity, dipole moment or refractive index [39]. The polarities of ILs are of special interest as they allow conclusions about miscibility and phase behavior along with comparison to molecular solvents. The results of the transition and decomposition temperatures along with the E_{NR} for empirical polarity are summarized in Table 1. The DSC traces of the phosphonium ILs with different degree of fluorination are shown in Fig. 1. Upon cooling, the fluorous IL **1** exhibits only a glass transition T_g at -18 °C and no crystallization peak which is a commonly observed phenomenon in ILs [40]. In the heating cycle a cold crystallization T_{cc} is observed at 14 °C followed by a melting T_m at 69 °C. These results show that although the fluorous IL **1** is not a room-temperature ionic liquid (RTIL), it can be observed in the liquid state at ambient temperature. This is due to supercooling and suppressed crystallization which is an intrinsic property of most ILs [41], resulting from anti-crystal engineering [42]. A similar behavior is observed for the non-fluorinated sample [$P(oct)_3$hex][NTf_2] and [BMIM][NTf_2] [43] as example of a widely applied imidazolium IL. For these salts also T_g, T_{cc} and T_m were observed in the heating curve and only T_g in the cooling step. In contrast for the semi-fluorinated ionic liquid [$P(oct)_3R_{f4}$][NTf_2] only T_g is observed for both heating and cooling.

Table 1
Glass transition T_g, cold crystallization T_{cc}, melting T_m and decomposition T_d temperatures along with the polarity values E_{NR} determined by the solvatochromic shift of Nile Red for the investigated ILs.

Property	IL **1** [P(R_{f6})$_3$$R_{f4}$][$NTf_2$]	[P(oct)$_3$$R_{f4}$][$NTf_2$]	[P(oct)$_3$hex][NTf_2]	[BMIM][NTf_2]
cation composition	highly fluorinated	semi-fluorinated	non-fluorinated	non-fluorinated, aromatic
T_g/°C	−18	−75	−89	−86 (−87)[a]
T_{cc}/°C	14	–	−40	−56
T_m/°C	69	–	−18	−2 (−3)[a]
T_d/°C	345	374	395	431 (427)[a]
λ_{max}/nm	546.6	548.2	548.6	548.8
E_{NR}/kJ mol^{-1}	218.8	218.2	218.1	218.0 (218.0)[b]

[a] Values taken from Ref. [44].
[b] Value taken from Ref. [37].

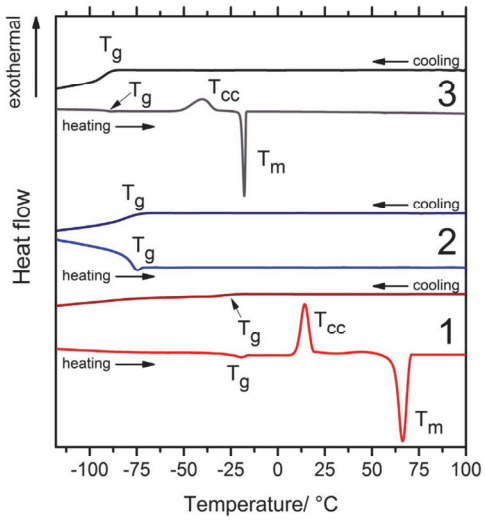

Fig. 1. DSC thermograms of the highly fluorinated IL **1** (1), the semi-fluorinated [P(oct)$_3$R$_{f4}$][NTf$_2$] (2) and the non-fluorinated [P(oct)$_3$hex][NTf$_2$] (3) with indicated transition temperatures. Exothermal transitions are plotted as positive peaks.

The absence of a melting point in the semi-fluorinated IL can be rationalized by symmetry-breaking effects [45] induced by the fluorinated chain leading to a destabilized crystalline structure due to packing effects. For IL **1** and the tetraalkylphosphonium IL a higher grade of symmetry is incorporated as these samples have four substituents of similar chemical composition. The thermal stability of the phosphonium ILs containing the NTf$_2^-$-anion was found to be lower than for the imidazolium-cation with the same anion. The obtained TGA curves are shown in Fig. 2. It is well known that the decomposition temperature of ILs is mainly related to the anion-cation choice and functional groups incorporated. Elongation of attached chains of similar chemical structure is reported to have only minor effects on the thermal stability [46]. By comparing the thermal stability of ILs with the same anion it is ensured that the determined decomposition is mainly related to the thermal stability of the cation. The decomposition temperatures of the phosphonium compounds decreases upon increasing number of attached perfluoroalkyl-chains. However the observed decomposition temperatures are still comparatively high with the lowest value being 345 °C for IL **1**. For the fluorous IL [P(R$_{f8}$)$_2$R$_{f6}$CH$_2$CH(CH$_3$)CH$_2$C(CH$_3$)$_3$][NTf$_2$] bearing three fluorinated chains, a T$_d$ of 407 °C was reported

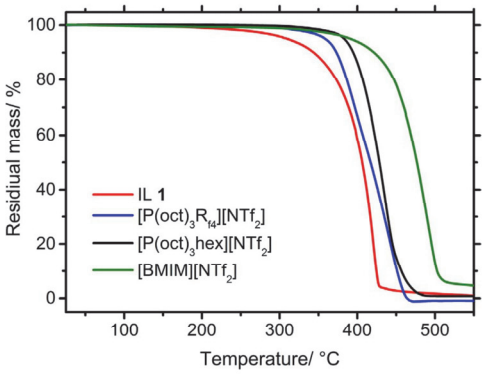

Fig. 2. TGA traces of the investigated ionic liquids at 10 °C/min heating rate.

[47]. Phosphonium ILs containing one fluorous tail and other anions like BF$_4^-$ or OTf$^-$ were furthermore found to have decomposition temperatures above 300 °C [48].

The polarity values E$_{NR}$ determined by the solvatochromic shift of Nile Red are increasing with the degree of fluorination but show only minor overall differences. Higher E$_{NR}$-values are related to lower solvent polarities. As the combination of other anions with the thoroughly investigated [BMIM] cation show similar ranges of deviations, the main contribution to the E$_{NR}$-values for the ILs investigated here seems to result from the NTf$_2^-$-anion. This is in accordance with literature reports that the dominating contribution to the solvatochromic shift of Nile Red is the hydrogen-bond ability of the cation towards the dye [49]. Protons of significant acidity are intrinsically absent in quarternary phosphonium cations due to their molecular structure in contrast to dialkylimidazolium or protic ILs. The application of Reichardt's Dye to other phosphonium-based ILs revealed much larger differences in the empirical polarity towards imidazolium based samples [38]. Molecular solvents of similar E$_{NR}$-values than these ILs are ethanol (E$_{NR}$ = 218.2 kJ/ mol^{-1}) or 1-butanol (E$_{NR}$ = 218.5 kJ/ mol^{-1}). The E$_{NR}$ value reported for a comparable IL [P(hex)$_3$C$_{14}$H$_{29}$][NTf$_2$] (E$_{NR}$ = 218.7 kJ mol^{-1}) is quite similar to the values obtained [50]. A slightly lower polarity was found for an IL based on [BMIM] and a highly fluorinated borate anion (E$_{NR}$ = 220.7 kJ mol^{-1}) [13].

3.2. Crystal structure of the fluorous ionic liquid

The crystalline structure of **1** was investigated by means of single crystal X-ray diffraction. Suitable single crystals could be obtained by slowly evaporating saturated solution IL **1** in benzotrifluoride. Crystal growth occurred in the form of colorless needles and plates. Although a lot of crystallization methods and solvents were investigated, benzotrifluoride was the only solvent applicable for crystal growth. Evaporation or slow cooling of a saturated solution of IL **1** in other solvents resulted in the formation of liquid biphasic systems. Owing to the nature of the substitution pattern, the shorter perfluoroalkyl-chain R$_{f4}$ and one of the slightly longer chains R$_{f6}$ occupied alternating positions leading to disordering. Furthermore the packing of the interactions between the perfluorinated molecular fragments driven by weak van der Waals forces lead to disordering in the periphery of the molecule. These effects overall lead to comparable high value for the final R-indices. Obtaining a suitable single crystal for XRD from ILs was found to be rather difficult even for symmetrical ions [51] as ILs are designed to contain destabilized crystalline structures. The highly fluorinated IL crystallizes in the triclinic, centrosymmetric P-1 space group showing two formula units per elemental cell. The unit cell and packing diagram are shown in Fig. 3. The NTf$_2^-$-anions adopted a *trans*-configuration in the solid state as it is reported for the majority of measured IL samples in literature [52]. The fluorinated IL **1** showed structuring in domains of ionic moieties consisting of the phosphonium core and the anion on the one hand and the perfluoroalkyl-segments on the other. This organization into blocks of molecular segments of the same polarity driven by solvophobic interactions was also reported for imidazolium ionic liquids with perfluorinated anions [19]. Similar structural motifs and self-assembled nanostructures resulting from solvophobic interactions were reported for ILs with perfluoro-groups in bulk state leading to tricontinuous nanostructures of ionic, alkyl and fluorinated domains [25,53].

3.3. Miscibility and phase behavior towards organic solvents

In order to find an appropriate solvent for the fluorous biphasic catalysis and to demonstrate the fluorophilic characteristics of IL **1** the miscibility of the phosphonium ILs with a range of commonly applied solvents was investigated. The solvents investigated ranged from solvents of high polarity such as water to the highly nonpolar, fluorophilic perfluoroheptane. Mixing behavior and miscibility of the three

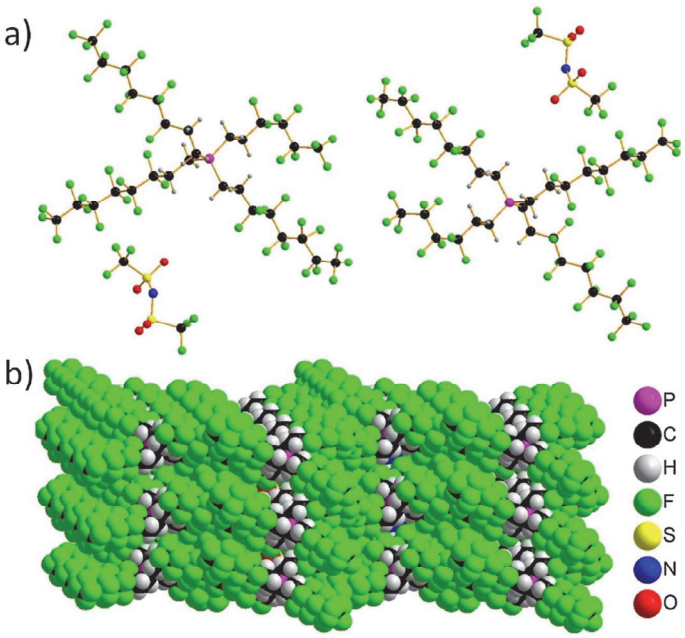

Fig. 3. Crystalline structure of the fluorous IL **1**. a) centrosymmetric elemental cell containing two formula units and b) packing diagram showing the composition of ionic and perfluorinated domains.

Table 2
Solubility of the investigated phosphonium ILs with common molecular solvents at 25 °C.

Solvent	IL **1**/g L^{-1}	$[P(oct)_3R_{f4}][NTf_2]$/g L^{-1}	$[P(oct)_3hex][NTf_2]$/g L^{-1}
perfluoroheptane	1.76	immiscible	immiscible
hexane	immiscible	13.76	12.30
toluene	1.6	miscible	miscible
Et_2O	8.3	miscible	miscible
THF	20.7	miscible	miscible
$CF_3C_5H_6$	4.7	miscible	miscible
CH_2Cl_2	0.65	miscible	miscible
acetone	274.5	miscible	miscible
DMF	15.6	miscible	miscible
methanol	76.6	miscible	miscible
H_2O	immiscible	immiscible	immiscible

phosphonium ILs with common solvents at 25 °C are listed in Table 2. The criteria to find an appropriate second solvent for fluorous biphasic catalysis are thermomorphic mixing behavior towards the fluorous solvent and minimal solubility at ambient temperature or the temperature at which the second solvent is extracted. The first criterion is crucial to ensure mixing of fluorous and organic phase and homogenous reaction kinetics. In general the FBC could also be performed if the catalyst with perfluorinated ligands shows a highly increased solubility in the organic phase at elevated temperatures so that a homogenous catalysis can be performed. The second criterion is demanded to avoid leaching of the fluorous phase accompanied with catalyst leaching. By this way an efficient catalyst retention and stable catalytic performance can be guaranteed. Furthermore it is in general preferable to apply high boiling solvents for both the fluorinated and organic phase as this minimizes losses through evaporation and allows higher critical mixing temperatures associated with lower miscibilities at moderate temperatures. All investigated ILs were found to be completely insoluble in water. This results from the combination of a hydrophobic anion with a hydrophobic cation. Although ILs with the NTf_2^--anion are well known to form a biphasic liquid system upon addition of water they display a slight water solubility when combined with a hydrophilic cation [54].

Upon combination with the highly hydrophobic cations which incorporate long hydrophobic alkyl or even fluorous chains, the solubility drops below the detection limit. The non-fluorinated and semi-fluorinated phosphonium ionic liquids show a similar phase behavior and were found to be completely miscible at ambient temperature with a wide range of organic solvents, ranging from polar methanol to nonpolar toluene. Only with the nonpolar aliphatic hydrocarbon hexane a limited solubility was found, being slightly higher for the semi-fluorinated $[P(oct)_3R_{f4}][NTf_2]$. Both ILs are immiscible with the fluorous solvent perfluoroheptane. The miscibility behavior towards organic solvents of a wide polarity range can be rationalized by the amphiphilic character of these ILs consisting of polar ionic and nonpolar alkyl motifs. These results show that a higher degree of fluorination is demanded to ensure a limited miscibility of ILs towards organic solvents at ambient temperature. For the highly fluorinated compound **1** the situation is indeed very different. The fluorous IL shows only limited solubility with the investigated organic solvents. The highest solubility was found for acetone reaching 274.5 g L^{-1}. Solubilities for the other molecular solvents were overall significantly lower but slightly higher for oxygen containing liquids like methanol, DMF, THF and Et_2O. Similar limited solubilities were obtained for the highly fluorinated IL described by van Koten and coworkers. where a solubility of 580 g/L of the fluorous IL in acetone was found [13]. For organic solvents without oxygen the solubility of IL **1** per liter was even lower. In the aliphatic hexane the fluorinated IL was found to be insoluble whereas it displayed a slight solubility in the fluorous solvent perfluoroheptane. In summary the IL **1** showed a miscibility behavior that is comparable to molecular fluorous solvents, showing limited solubilities with organic solvents at ambient temperature. However because of the additional ionic groups the solubility with the conventional fluorous liquids was also very limited. Following these results we investigated the thermomorphic mixing behavior of **1** with DMF in dependence on the volume fraction to determine the phase diagram. The thermoregulated mixing behavior and the obtained phase diagram are displayed in Fig. 4.

The aprotic DMF is a commonly applied solvent for the Heck cross

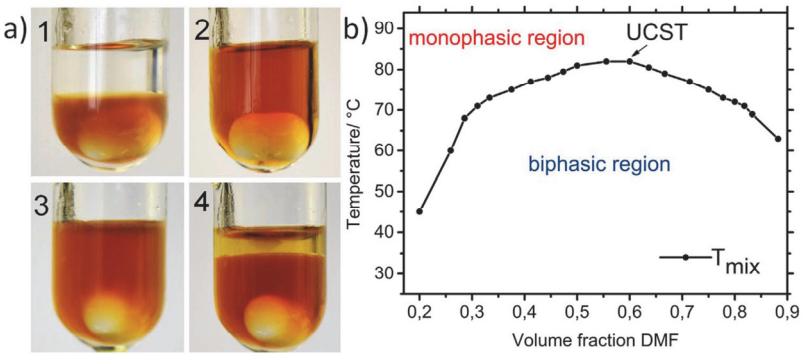

Fig. 4. a) Phase behavior of **1** (lower phase) with DMF (upper phase). Photographs: 1) formation of a biphasic mixture at room temperature; 2) heating above mixing temperature ($T > T_{mix}$); 3) cloud point upon cooling ($T < T_{mix}$); d) ongoing phase separation of fluorous and organic phase. b) Phase diagram: mixing temperatures T_{mix} in dependence of the volume fraction φ_{DMF}.

coupling reaction as it shows a comparatively high polarity capable to dissolve a wide range of educts and the base which is essential for the catalytic cycle in the reaction mechanism by base-induced reductive elimination [55]. It was found that IL **1** and DMF form a biphasic mixture at room temperature when the volume fraction of DMF (φ_{DMF}) exceeded 0.2 and had an upper critical solution temperature UCST of 82 °C at $\varphi_{DMF} = 0.57$. Above the respective mixing temperatures a homogenous monophasic system was found. The phase diagram showed the characteristic progression for liquid–liquid phase diagrams with upper critical solution temperature. As indicated in the phase diagram, slight amounts of DMF are miscible with **1** at room temperature resulting in a moderately viscous fluorine rich phase which remained liquid and homogeneous even at −18 °C.

3.4. Catalyst retention in Heck reactions

To investigate the performance of the fluorinated IL **1** as fluorous phase for the immobilization of a fluorous catalyst we investigated the Heck cross coupling as a model reaction for palladium catalysis. Homogenous palladium catalysis is a very important, widespread and versatile method utilized in chemical laboratories as well as on industrial scale [56]. One important drawback of conventional Pd-catalysis is the loss of the relative expensive catalyst that cannot or hardly be recovered [57]. Among other immobilization strategies the catalyst retention in a fluorous phase seems to be a promising way to overcome this drawback and to provide overall more sustainable processes [58]. Fluorophilic catalysts can be obtained by simply attaching perfluorinated alkyl-groups in the periphery of catalyst that are known to show high activity and stability [59]. By using highly fluorinated ionic liquids is should become possible to further eliminate the drawbacks of the volatile molecular perfluorinated solvents that were found to have a range of negative impacts on the environment. The Heck reaction allows the selective formation of C–C bonds between aryl halides and activated alkenes but an efficient catalyst recovery was found to be difficult [31]. This results from the usage of multiple reagents along with different obtained products or side products that disturb the catalytic cycle or lead to inactivation of the catalyst. The catalyst with highly fluorinated ligands $[Pd(P(m\text{-}C_6H_4\text{-}(CH_2)_2\text{-}(CF_2)_8F)_3)_2Cl_2]$ [29] used for the cross coupling reactions was found to be insoluble in pure DMF and many other common organic solvents at ambient temperatures. However concentrations of at least 1.2×10^{-2} mol L^{-1} could be obtained in IL **1** saturated with DMF. We first investigated a thermoregulated biphasic system consisting of 1.00 g of IL **1** and 1.00 mL DMF at 85 °C as this temperature is above the upper critical solution temperature UCST. Scheme 2 shows the reactions and conditions applied for the first experiments coupling iodobenzene with either methyl acrylate or styrene. The results for the yield, TON and cumulative TON are given in Table 3.

After each run the upper organic phase was carefully removed and

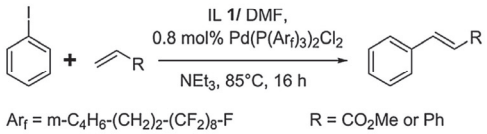

Scheme 2. Reaction scheme of iodobenzene and methyl acrylate or styrene applying IL **1** under fluorous biphasic catalysic conditions.

Table 3
Catalyst recycling using the thermomorphic biphasic system applying IL **1** as fluorous phase[a].

	R = CO_2Me[b]			R = Ph[c]		
run	yield[d]/%	TON	cumulative TON	yield[d]/%	TON	cumulative TON
blank[e]	99	124	–	94	118	–
1	99	124	124	93	116	116
2	99	124	248	94	118	234
3	98	123	371	93	116	350
4	99	124	495	92	115	465
5	97	121	616	94	118	583
6	96	120	736	93	116	699
7	96	120	855	90	113	812
8	88	110	965	86	108	920
9	76	95	1060	75	94	1014
10	67	84	1144	61	76	1090
11[f]	92	115	1259	85	106	1196

[a] Conditions: 1.0 g **1**, 0.296 mmol iodobenzene (1.0 eq.), 0.355 mmol olefine (1.2 eq.) and 0.355 mmol NEt_3 (1.2 eq.) in 1.00 mL DMF, 8.0 mg catalyst (0.8 mol%), 16 h (unless stated otherwise).
[b] *Trans* only.
[c] *Trans/cis*.
[d] Determined by HPLC.
[e] No fluorinated IL added; catalyst not recovered.
[f] t = 32 h.

the yield determined by means of HPLC. To proof the efficient catalyst retention fresh reagents were added and the catalytic process repeated. A blank run using only fluorous catalyst in DMF showed a similar thermoregulated mixing behavior and was able to efficiently catalyze the Heck reaction. However the recovery was not possible under these conditions. The catalyst recovery using the fluorous IL **1** was found to be efficient for seven runs without significant decrease in yield for both the coupling to methyl cinnamate and stilbene being 90% and more. The yields for methyl cinnamate were found to be slightly higher than those for stilbene which is also found for other multiphasic systems investigating the Heck reaction [60]. For the runs eight to ten a decrease in the catalytic activity was found. By doubling the reaction time for the eleventh run it was possible to increase the yield again whereby the obtained yields remained lower than for the initial runs.

These results already show the potential of the fluorous IL for the

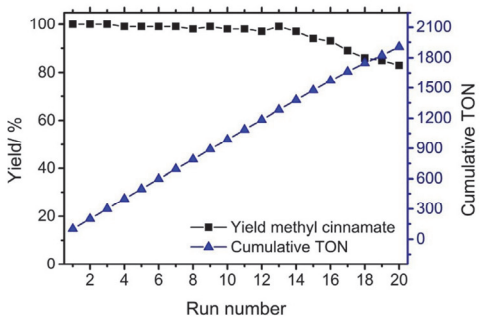

Fig. 5. Yield of methyl cinnamate per run and cumulative TON for the overall catalysis.

Table 4
Isolated mass of the pure methyl cinnamate and corresponding yield per run.

run	mass isolated methyl cinnamate/mg	yield/%
1	46.09	96
2	45.62	95
3	46.23	96
4	46.31	96
5	44.93	94
6	45.47	95

retention of the fluorous catalyst. We believe that the loss in catalytic activity results mainly from thermal degradation of the catalyst rather than leaching to the organic phase. This was indicated by a color change of the solutions of the blank run and the IL **1** in the thermomorphic catalysis to orange-red which was reported to result from the formation of nanoparticles in solution [61]. Inactivation of the same catalyst after prolonged exposure to higher temperatures was also reported before [62]. We therefore investigated the performance of the catalyst in the biphasic system at lower temperatures to reduce the extend of thermal catalyst degradation. Hence we performed the cross-coupling reactions at 70 °C, increased the catalyst concentration to 1 mol% and kept the same conditions for the coupling of iodobenzene and methyl acrylate to methyl cinnamate. The results for the TON and cumulative TON for this reaction conditions are plotted in Fig. 5.

By using these conditions the fluorous catalyst showed nearly quantitative yields for 14 runs and only a slight drop remaining 83% yield for run 20. Nearly quantitative yield of 96% could be restored for the 21. run by increasing the reaction time to 32 h. To demonstrate facile product isolation and removal of side product triethylammonium iodide from the reductive elimination an extraction process was performed for the first six runs in an additional experiment. For this purpose six equivalents of water were added to the carefully separated DMF phase after the reaction and the resulting suspension was extracted with 3 mL hexane three times. After solvent removal from the combined organic phases the residue was dried in oil-pump vacuum yielding pure methyl cinnamate in high isolated yield. Purity of the isolated methyl cinnamate was confirmed by ^{1}H- and ^{13}C{^{1}H}-NMR spectroscopy. The yields of the isolated methyl cinnamate are stated in Table 4 and were 95% in average. In further experiments the leaching of the fluorous IL **1** was found to be as low as 1.2% per run which is rather low and demonstrates the high fluorophilic character of the IL. Overall these results proofed the utilization of a highly fluorinated IL for catalyst retention in the Pd-catalyzed Heck reaction under fluorous biphasic conditions with high yields, high number of performable runs and low leaching of the fluorous phase.

4. Conclusion

We successfully synthesized a novel highly fluorinated ionic liquids and showed the effect of fluorination on the physicochemical properties in comparison to the non-fluorinated and semi-fluorinated analogue. The fluorous IL was found to have a higher melting point, high thermal stability and a slightly lower polarity investigated by means of the solvatochromic dye Nile Red. Single crystal X-ray analysis showed the formation of fluorinated and ionic domains driven by solvophobic interactions. The fluorinated IL was found to have only limited solubility in a wide range of investigated organic liquids comparable to molecular perfluorinated solvents. The non- and semi-fluorinated analogues showed completely different behavior being completely miscible in polar as well nonpolar organic solvents. The thermoregulated mixing behavior towards DMF was investigated in detail. The fluorinated IL could be successfully applied as a substitute for volatile fluorocarbon compounds that pose environmental threats but are still commonly applied solvents in the fluorous biphasic catalysis. Thus the incorporation of perfluoroalkyl-groups adds fluorophilicity as possible modification to the widely tuneable properties of ILs. By investigating the Heck reaction as exemplary reaction for palladium catalyzed C—C bond formation we were able to proof the applicability of the fluorous ionic liquid to the very widely used Pd-catalyzed reactions. The highly fluorinated IL was found to efficiently immobilize a perfluoro-tagged catalyst which allowed repetitive usage for up to 14 runs with only minor loss in catalytic activity and up to 21 runs with yields still being 83% and higher. By this multiphasic catalysis reaction conditions the activity of the expensive Pd-catalyst can be preserved for multiple reaction runs thus leading to more economic and environmental friendly processes. In further studies we will investigate the expansion of the fluorous IL to other catalytic systems and reactions as well as the application of catalytic systems that show increased thermal stability.

Acknowledgements

The authors gratefully acknowledge the Deutsche Bundesstiftung Umwelt (DBU) (31925-41) for financial support and thank Reiner Wintringer for performing the HPLC measurements and technical help.

References

[1] K. Francesca, M. Ray, Alternative Solvents for Green Chemistry, second ed., Royal Society of Chemistry, Cambridge, 2013, http://dx.doi.org/10.1039/9781849736824.
[2] T.L. Merrigan, E.D. Bates, S.C. Dorman, J.H. Davis Jr., New fluorous ionic liquids function as surfactants in conventional room-temperature ionic liquids, Chem. Commun. (2000) 2051–2052, http://dx.doi.org/10.1039/b005418f.
[3] H.R. Hobbs, N.R. Thomas, Biocatalysis in supercritical fluids, in fluorous solvents, and under solvent-free conditions, Chem. Rev. 107 (2007) 2786–2820, http://dx.doi.org/10.1021/cr0683820.
[4] E.G. Hope, A.P. Abbott, D.L. Davies, G.A. Solan, A.M. Stuart, Green organometallic chemistry, Compr. Organomet. Chem. III, Elsevier, 2007, pp. 837–864, http://dx.doi.org/10.1016/B0-08-045047-4/00182-5.
[5] F.T.T. Huque, K. Jones, R.A. Saunders, J.A. Platts, Statistical and theoretical studies of fluorophilicity, J. Fluor. Chem. 115 (2002) 119–128, http://dx.doi.org/10.1016/S0022-1139(02)00034-9.
[6] A.A. Zakhidov, J.-K. Lee, H.H. Fong, J.A. DeFranco, M. Chatzichristidi, P.G. Taylor, C.K. Ober, G.G. Malliaras, Hydrofluoroethers as orthogonal solvents for the chemical processing of organic electronic materials, Adv. Mater. 20 (2008) 3481–3484, http://dx.doi.org/10.1002/adma.200800557.
[7] I.T. Horvath, J. Rabai, Facile catalyst separation without water: fluorous biphase hydroformylation of olefins, Science 80 (266) (1994) 72–75, http://dx.doi.org/10.1126/science.266.5182.72.
[8] Handbook of Fluorous Chemistry, in: J.A. Gladysz, D.P. Curran, I.T. Horváth (Eds.), Wiley-VCH Verlag GmbH & Co. KGaA, Weinheim, FRG, 2004, , http://dx.doi.org/10.1002/3527603905.
[9] M. Wende, R. Meier, J.A. Gladysz, Fluorous catalysis without fluorous solvents: a friendlier catalyst recovery/recycling protocol based upon thermomorphic properties and liquid/solid phase separation, J. Am. Chem. Soc. 123 (2001) 11490–11491, http://dx.doi.org/10.1021/ja011444d.
[10] E.G. Hope, A.M. Stuart, Fluorous biphase catalysis, J. Fluor. Chem. 100 (1999) 75–83, http://dx.doi.org/10.1016/S0022-1139(99)00204-3.
[11] P. Kirsch, Modern Fluoroorganic Chemistry, Wiley-VCH Verlag GmbH & Co KGaA,

Weinheim, Germany, 2013, http://dx.doi.org/10.1002/9783527651351.
[12] L.P. Barthel-Rosa, J.A. Gladysz, Chemistry in fluorous media: a user's guide to practical considerations in the application of fluorous catalysts and reagents, Coord. Chem. Rev. 190–192 (1999) 587–605, http://dx.doi.org/10.1016/S0010-8545(99)00102-2.
[13] J. van den Broeke, F. Winter, B.-J. Deelman, G. van Koten, A highly fluorous room-temperature ionic liquid exhibiting fluorous biphasic behavior and its use in catalyst recycling, Org. Lett. 4 (2002) 3851–3854, http://dx.doi.org/10.1021/ol026700l.
[14] R. Giernoth, Task-specific ionic liquids, Angew. Chem. Int. Ed. 49 (2010) 2834–2839, http://dx.doi.org/10.1002/anie.200905981.
[15] C. Liu, X. Li, Z. Jin, Progress in thermoregulated liquid/liquid biphasic catalysis, Catal. Today 247 (2015) 82–89, http://dx.doi.org/10.1016/j.cattod.2014.07.060.
[16] R.T. Baker, HOMOGENEOUS CATALYSIS: enhanced: toward greener chemistry, Science 80 (284) (1999) 1477–1479, http://dx.doi.org/10.1126/science.284.5419.1477.
[17] J.M. Breen, S. Olejarz, K.R. Seddon, Microwave synthesis of short-chained fluorinated ionic liquids and their surface properties, ACS Sustain. Chem. Eng. 4 (2016) 387–391, http://dx.doi.org/10.1021/acssuschemeng.5b01265.
[18] J.J. Tindale, P.J. Ragogna, Highly fluorinated phosphonium ionic liquids: novel media for the generation of superhydrophobic coatings, Chem. Commun. (2009) 1831–1833, http://dx.doi.org/10.1039/b821174d.
[19] G. Cavallo, G. Terraneo, A. Monfredini, M. Saccone, A. Priimagi, T. Pilati, G. Resnati, P. Metrangolo, D.W. Bruce, Superfluorinated ionic liquid crystals based on supramolecular, halogen-bonded anions, Angew. Chem. Int. Ed. 55 (2016) 6300–6304, http://dx.doi.org/10.1002/anie.201601278.
[20] A. Abate, A. Petrozza, G. Cavallo, G. Lanzani, F. Matteucci, D.W. Bruce, N. Houbenov, P. Metrangolo, G. Resnati, Anisotropic ionic conductivity in fluorinated ionic liquid crystals suitable for optoelectronic applications, J. Mater. Chem. A 1 (2013) 6572–6578, http://dx.doi.org/10.1039/c3ta10990a.
[21] C. Yao, W.R. Pitner, J.L. Anderson, Ionic liquids containing the tris(pentafluoroethyl)trifluorophosphate anion: a new class of highly selective and ultra hydrophobic solvents for the extraction of polycyclic aromatic hydrocarbons using single drop microextraction, Anal. Chem. 81 (2009) 5054–5063, http://dx.doi.org/10.1021/ac900719m.
[22] J.E. Bara, C.J. Gabriel, T.K. Carlisle, D.E. Camper, A. Finotello, D.L. Gin, R.D. Noble, Gas separations in fluoroalkyl-functionalized room-temperature ionic liquids using supported liquid membranes, Chem. Eng. J. 147 (2009) 43–50, http://dx.doi.org/10.1016/j.cej.2008.11.021.
[23] A.B. Pereiro, L.C. Tomé, S. Martinho, L.P.N. Rebelo, I.M. Marrucho, Gas permeation properties of fluorinated ionic liquids, Ind. Eng. Chem. Res. 52 (2013) 4994–5001, http://dx.doi.org/10.1021/ie4002469.
[24] O. Russina, F. Lo Celso, M. Di Michiel, S. Passerini, G.B. Appetecchi, F. Castiglione, A. Mele, R. Caminiti, A. Triolo, Mesoscopic structural organization in triphilic room temperature ionic liquids, Faraday Discuss. 167 (2013) 499–513, http://dx.doi.org/10.1039/c3fd00056g.
[25] J.J. Hettige, J.C. Araque, C.J. Margulis, Bicontinuity and multiple length scale ordering in triphilic hydrogen-bonding ionic liquids, J. Phys. Chem. B 118 (2014) 12706–12716, http://dx.doi.org/10.1021/jp5068457.
[26] O. Hollóczki, M. Macchiagodena, H. Weber, M. Thomas, M. Brehm, A. Stark, O. Russina, A. Triolo, B. Kirchner, Triphilic ionic-liquid mixtures: fluorinated and non-fluorinated aprotic ionic-liquid mixtures, ChemPhysChem 16 (2015) 3325–3333, http://dx.doi.org/10.1002/cphc.201500473.
[27] R. Hayes, G.G. Warr, R. Atkin, Structure and nanostructure in ionic liquids, Chem. Rev. 115 (2015) 6357–6426, http://dx.doi.org/10.1021/cr500411q.
[28] J.C. Tatlow, Organofluorine Chemistry, in: R.E. Banks, B.E. Smart (Eds.), Springer US, Boston MA, 1994, , http://dx.doi.org/10.1007/978-1-4899-1202-2.
[29] S. Schneider, W. Bannwarth, Application of the fluorous biphase concept to palladium-catalyzedSuzuki couplings, Helv. Chim. Acta 84 (2001) 735–742, http://dx.doi.org/10.1002/1522-2675(20010321)84:3<735:AID-HLCA735>3.0.CO;2-L.
[30] R.F. Heck, J.P. Nolley, Palladium-catalyzed vinylic hydrogen substitution reactions with aryl, benzyl, and styryl halides, J. Org. Chem. 37 (1972) 2320–2322, http://dx.doi.org/10.1021/jo00979a024.
[31] I.P. Beletskaya, A.V. Cheprakov, The heck reaction as a sharpening stone of palladium catalysis, Chem. Rev. 100 (2000) 3009–3066, http://dx.doi.org/10.1021/cr9903048.
[32] C. Emnet, K.M. Weber, J.A. Vidal, C.S. Consorti, A.M. Stuart, J.A. Gladysz, Syntheses and properties of fluorous quaternary phosphonium salts that bear four ponytails; new candidates for phase transfer catalysts and ionic liquids, Adv. Synth. Catal. 348 (2006) 1625–1634, http://dx.doi.org/10.1002/adsc.200606138.
[33] P. Bhattacharyya, D. Gudmunsen, E.G. Hope, R.D.W. Kemmitt, D.R. Paige, A.M. Stuart, Phosphorus(III) ligands with fluorous ponytails, J. Chem. Soc. Perkin Trans. 1 (1997) 3609–3612, http://dx.doi.org/10.1039/a704872f.
[34] C.C. Weber, A.F. Masters, T. Maschmeyer, Pseudo-encapsulation-nanodomains for enhanced reactivity in ionic liquids, Angew. Chem. Int. Ed. 51 (2012) 11483–11486, http://dx.doi.org/10.1002/anie.201206113.
[35] P. Zürner, H. Schmidt, S. Bette, J. Wagler, G. Frisch, Ionic liquid, glass or crystalline solid? Structures and thermal behaviour of (C 4 mim) 2 CuCl 3, Dalt. Trans. 45 (2016) 3327–3333, http://dx.doi.org/10.1039/C5DT03772G.
[36] J.F. Deye, T. a Berger, A.G. Anderson, Nile Red as a solvatochromic dye for measuring solvent strength in normal liquids and mixtures of normal liquids with supercritical and near critical fluids, Anal. Chem. 62 (1990) 615–622, http://dx.doi.org/10.1021/ac00205a015.
[37] A.J. Carmichael, K.R. Seddon, Polarity study of some 1-alkyl-3-methylimidazolium ambient-temperature ionic liquids with the solvatochromic dye, Nile Red, J. Phys. Org. Chem. 13 (2000) 591–595, http://dx.doi.org/10.1002/1099-1395(200010)13:10<591:AID-POC305>3.0.CO;2-2.
[38] C. Reichardt, Polarity of ionic liquids determined empirically by means of solvatochromic pyridinium N-phenolate betaine dyes, Green Chem. 7 (2005) 339, http://dx.doi.org/10.1039/b500106b.
[39] L. Crowhurst, P.R. Mawdsley, J.M. Perez-Arlandis, P.A. Salter, T. Welton, Solvent–solute interactions in ionic liquids, Phys. Chem. Chem. Phys 5 (2003) 2790–2794, http://dx.doi.org/10.1039/B303095D.
[40] E. Gómez, N. Calvar, Á. Domínguez, Thermal behaviour of pure ionic liquids, Ion Liq. Curr. State Art, InTech, 2015, http://dx.doi.org/10.5772/59271.
[41] J. Kagimoto, K. Fukumoto, H. Ohno, Effect of tetrabutylphosphonium cation on the physico-chemical properties of amino-acid ionic liquids, Chem. Commun. (2006) 2254–2256, http://dx.doi.org/10.1039/b600771f.
[42] P.M. Dean, J. Turanjanin, M. Yoshizawa-Fujita, D.R. MacFarlane, J.L. Scott, Exploring an anti-crystal engineering approach to the preparation of pharmaceutically active ionic liquids, Cryst. Growth Des. 9 (2009) 1137–1145, http://dx.doi.org/10.1021/cg8009496.
[43] L. Xue, E. Gurung, G. Tamas, Y.P. Koh, M. Shadeck, S.L. Simon, M. Maroncelli, E.L. Quitevis, Effect of alkyl chain branching on physicochemical properties of imidazolium-based ionic liquids, J. Chem. Eng. Data 61 (2016) 1078–1091, http://dx.doi.org/10.1021/acs.jced.5b00658.
[44] H. Tokuda, K. Hayamizu, K. Ishii, M.A.B.H. Susan, M. Watanabe, Physicochemical properties and structures of room temperature ionic liquids. 2. Variation of alkyl chain length in imidazolium cation, J. Phys. Chem. B 109 (2005) 6103–6110, http://dx.doi.org/10.1021/jp044626d.
[45] N.V. Plechkova, K.R. Seddon, Applications of ionic liquids in the chemical industry, Chem. Soc. Rev. 37 (2008) 123–150, http://dx.doi.org/10.1039/B006677J.
[46] M. Villanueva, A. Coronas, J. García, J. Salgado, Thermal stability of ionic liquids for their application as new absorbents, Ind. Eng. Chem. Res. 52 (2013) 15718–15727, http://dx.doi.org/10.1021/ie401656e.
[47] J.J. Tindale, P.J. Ragogna, Highly fluorinated phosphonium ionic liquids: novel media for the generation of superhydrophobic coatings, Chem. Commun. (2009) 1831–1833, http://dx.doi.org/10.1039/b821174d.
[48] J.J. Tindale, C. Na, M.C. Jennings, P.J. Ragogna, Synthesis and characterization of fluorinated phosphonium ionic liquids, Can. J. Chem. 85 (2007) 660–667, http://dx.doi.org/10.1139/v07-035.
[49] J.P. Hallett, T. Welton, Room-Temperature ionic liquids: solvents for synthesis and catalysis. 2, Chem. Rev. 111 (2011) 3508–3576, http://dx.doi.org/10.1021/cr1003248.
[50] D.J. Heldebrant, H.N. Witt, S.M. Walsh, T. Ellis, J. Rauscher, P.G. Jessop, Liquid polymers as solvents for catalytic reductions, Green Chem. 8 (2006) 807, http://dx.doi.org/10.1039/b605405f.
[51] J. Alvarez-Vicente, S. Dandil, D. Banerjee, H.Q.N. Gunaratne, S. Gray, S. Felton, G. Srinivasan, A.M. Kaczmarek, R. Van Deun, P. Nockemann, Easily accessible rare-earth-containing phosphonium room-temperature ionic liquids: EXAFS, luminescence, and magnetic properties, J. Phys. Chem. B 120 (2016) 5301–5311, http://dx.doi.org/10.1021/acs.jpcb.6b03870.
[52] J.D. Holbrey, W.M. Reichert, R.D. Rogers, Crystal structures of imidazolium bis(trifluoromethanesulfonyl)imide ionic liquid salts: the first organic salt with a cis-TFSI anion conformation, Dalt. Trans. (2004) 2267–2271, http://dx.doi.org/10.1039/B405901H.
[53] R. Hayes, G.G. Warr, R. Atkin, Structure and nanostructure in ionic liquids, Chem. Rev. 115 (2015) 6357–6426, http://dx.doi.org/10.1021/cr500411q.
[54] M.G. Freire, P.J. Carvalho, R.L. Gardas, I.M. Marrucho, L.M.N.B.F. Santos, J.A.P. Coutinho, Mutual solubilities of water and the [C n mim][Tf 2 N] hydrophobic ionic liquids, J. Phys. Chem. B 112 (2008) 1604–1610, http://dx.doi.org/10.1021/jp7097203.
[55] G.T. Crisp, Variations on a theme—recent developments on the mechanism of the Heck reaction and their implications for synthesis, Chem. Soc. Rev. 27 (1998) 427–436, http://dx.doi.org/10.1039/a827427z.
[56] C. Torborg, M. Beller, Recent applications of palladium-catalyzed coupling reactions in the pharmaceutical, agrochemical, and fine chemical industries, Adv. Synth. Catal. 351 (2009) 3027–3043, http://dx.doi.org/10.1002/adsc.200900587.
[57] J.G. de Vries, The Heck reaction in the production of fine chemicals, Can. J. Chem. 79 (2001) 1086–1092, http://dx.doi.org/10.1139/v01-033.
[58] D. Duncan, E.G. Hope, K. Singh, A.M. Stuart, A recyclable perfluoroalkylated PCP pincer palladium complex, Dalt. Trans. 40 (2011) 1998–2005, http://dx.doi.org/10.1039/c0dt01004a.
[59] T. Bříza, J. Kvíčala, O. Paleta, J. Čermák, Preparation of bis(polyfluoroalkyl)cyclopentadienes, new highly fluorophilic ligands for fluorous biphase catalysis, Tetrahedron 58 (2002) 3841–3846, http://dx.doi.org/10.1016/S0040-4020(02)00212-0.
[60] C. Rocaboy, J.A. Gladysz, Highly active thermomorphic fluorous palladacycle catalyst precursors for the heck reaction; evidence for a palladium nanoparticle pathway, Org. Lett. 4 (2002) 1993–1996, http://dx.doi.org/10.1021/ol025790r.
[61] M.T. Reetz, E. Westermann, Phosphane-free palladium-catalyzed coupling reactions: the decisive role of Pd nanoparticles, Angew. Chem. Int. Ed. 39 (2000) 165–168, http://dx.doi.org/10.1002/(SICI)1521-3773(20000103)39:1<165:AID-ANIE165>3.0.CO;2-B.
[62] V. Misuk, A. Mai, K. Giannopoulos, D. Karl, J. Heinrich, D. Rauber, H. Löwe, Palladium-catalyzed carbon–carbon cross-coupling reactions in thermomorphous double emulsions, J. Flow Chem. 5 (2015) 43–47, http://dx.doi.org/10.1556/JFC-D-14-00040.

2.5 Publication E

Trioctylphosphonium room temperature ionic liquids with perfluorinated groups – Physical properties and surface behavior in comparison with the nonfluorinated analogues

Daniel Rauber, Florian Heib, Michael Schmitt, Rolf Hempelmann.

Colloids Surf. A, **2018**, 537, 116-125.

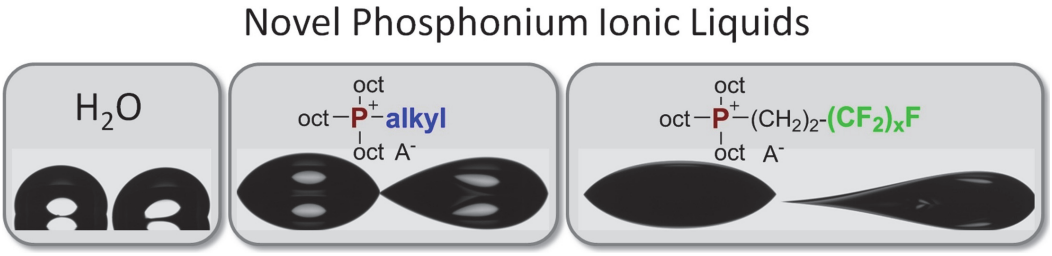

Colloids and Surfaces A 537 (2018) 116–125

Contents lists available at ScienceDirect

Colloids and Surfaces A

journal homepage: www.elsevier.com/locate/colsurfa

Trioctylphosphonium room temperature ionic liquids with perfluorinated groups – Physical properties and surface behavior in comparison with the nonfluorinated analogues

Daniel Rauber[a,b,*], Florian Heib[a], Michael Schmitt[a], Rolf Hempelmann[a,b,c]

[a] Institute of Physical Chemistry, Saarland University, Campus B 2 2, 66123 Saarbrücken, Germany
[b] Transfercenter Sustainable Electrochemistry, Saarland University, Am Markt, Zeile 3, 66125 Dudweiler, Germany
[c] Korea Institute of Science and Technology Europe, Campus E 7 1, 66123 Saarbrücken, Germany

GRAPHICAL ABSTRACT

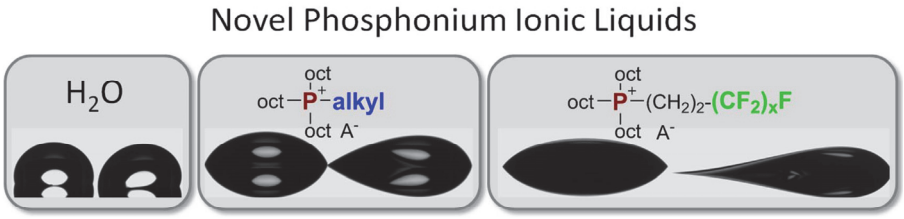

ARTICLE INFO

Keywords:
Ionic liquids
Phosphonium cation
High-precision drop shape analysis
Contact angle
Surface behavior

ABSTRACT

A series of novel ionic liquids (ILs) based on trioctylphosphonium-cations with attached perfluorinated chains and the anions bis(trifluoromethanesulfonyl)imide (NTf_2^-), dicyanamide ($N(CN)_2^-$) and tricyanomethanide ($C(CN)_3^-$) was synthesized. Their important physicochemical properties such as thermal behavior, solvatochromic polarities and viscosities were measured and compared to the alkyl analogues in order to investigate the influence of fluorination. The characteristic wetting behavior of these ILs on a hydrophobic modified surface was analyzed using the *high-precision drop shape analysis* (HPDSA) approach as this method is suitable to analyze highly non-symmetrical droplets. For the fluorinated ILs a more pronounced effect on the thermal transitions with increasing side chain length was found. The introduction of fluorinated alkyl groups leads to anion dependent decomposition temperatures, higher overall viscosities and a non-Newtonian flow shear thinning at higher shear rates. Furthermore, the fluorinated ILs showed a modified wetting behavior on the investigated surface, which was found to result in lower contact angle values and higher pinning compared to the non-fluorinated ILs.

1. Introduction

Ionic liquids (ILs) are a class of highly diverse functional solvents of organic salts with melting points below 100 °C and an unique property combination [1]. The subclass of room-temperature ionic liquids (RTILs) having melting points below ambient temperature is of special concern for most practical applications. ILs have a negligible vapor pressure along with inflammability, intrinsic conductivity, high electrochemical and thermal stability as well as wide liquid ranges and in general a good ability to solve both organic and inorganic compounds

* Corresponding author at: Institute of Physical Chemistry, Saarland University, Campus B 2 2, 66123 Saarbrücken, Germany.
E-mail address: daniel.rauber@uni-saarland.de (D. Rauber).

http://dx.doi.org/10.1016/j.colsurfa.2017.10.013
Received 13 July 2017; Received in revised form 8 September 2017; Accepted 6 October 2017
Available online 07 October 2017
0927-7757/

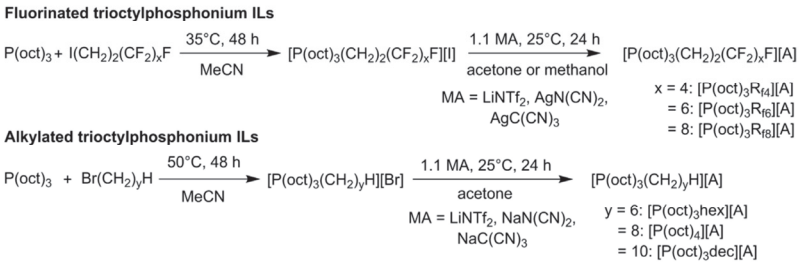

Scheme 1. Synthesis of the fluorinated and alkylated trioctylphosphonium-based ILs.

[2]. The properties of these "designer solvents" or "functional solvents" [3] are tailorable in a very wide range by their chemical composition and can be tuned depending on the demands of special processes, applications, solvent-systems etc. [4,5]. They have attracted a remarkable increase in interest throughout many scientific disciplines such as chemistry, physics, engineering and material science in the last decades as they offer completely novel opportunities for synthesis [6], analysis [7] or process technologies [8] along with the potential to optimize and improve existing technologies [9,10]. The properties of ILs can be fine-tuned by the nature of the anion and cation as well as through the introduction of additional functional groups. The incorporation of functionalities expands the possibilities of the "task-specific ILs" giving them additional desirable properties which are not achievable solely by cation-anion combinations. One functional segment of interest for ILs are perfluoroalkyl-segments as the resulting fluorous or fluorinated ILs (FILs) [11] show an altered behavior which is easily adjustable by common synthetic methods. The usage of FILs includes for example solvents for multiphasic systems [12], catalysis [13,14], as surfactants [15–17], media for CO_2-absorption [18,19], gas separation [20] or tribological applications [21,22]. As there is an immense number of possible ILs [23] it is highly important to know about the trends and properties of ILs for basic research and practical applications. Of special concern are the surface properties and adhesion of ILs as most of their applications include some kind of solid-liquid interfaces [24]. In addition the determination of the ionic liquid wetting behavior gives insight into structural organization of these solvents near solid surfaces [25] and their suitability as probe fluids [26]. As the IL surface behavior [27], such wetting and dewetting processes, is of high industrial relevance, it was subject to several studies [28–30] which are almost completely limited to imidazolium based ILs [31]. The investigation of ILs based on other cations such as the phosphonium is desirable since these solvents exhibit often superior properties such as higher degree of lipophilicity and improved electrochemical, thermal and chemical stability making them a better choice for selected applications [32]. In this study we prepared a series of novel FILs based on the trioctylphosphonium cation with perfluoroalkyl-groups of different chain lengths with either bis(trifluoromethanesulfonyl)imide (NTf_2^-), dicyanamide ($N(CN)_2^-$) or tricyanomethanide ($C(CN)_3^-$) anions to investigate the modification of the properties by the introduction of this functional groups. The substituted trioctylphosphonium cations were chosen as the long alkylchains are known to lead to comparably low viscosities despidte their large molecular size, high degree of lipophilicity as well as low glass transition and melting temperatures. This property combination is often desirable for technical applications since it allows fast thermal and mass transport, the absence of water for systems sensitive to hydrolysis and high operation temperature intervals as well as easy handling of RTILs. The physicochemical properties and wetting behavior of the novel FILs were compared to the corresponding non-fluorinated tetraalkyl IL analogues (AILs) to directly show the effect of fluorination on the properties of this substance class. Due to the comparably size of the attached fluorocarbon segment to the three octyl chains at the phosphonium core of the cation the influence of fluorination on the wetting behavior in the investigated ILs is demonstrated directly.

2. Experimental

2.1. Materials

Full details about the used reagents and their suppliers along with the synthesis protocols and characterization methods for the prepared ILs are given in the supporting information.

2.2. Syntheses of the perfluorinated and alkylated trioctylphosphonium ILs

The fluorinated and nonfluorinated phosphonium ILs were synthesized by nucleophilic substitution of the 1*H*,1*H*,2*H*,2*H*-perfluoralkyl iodides or 1-bromoalkanes with trioctylphosphine. The resulting quaternary phosphonium halide salts were then transferred to the $[NTf_2]$, $[N(CN)_2]$ or $[C(CN)_3]$ ILs by means of metathesis reactions with the lithium, sodium or silver salts (MA; M = metal-cation; A = anion) depending on the type of exchanged halide. The preparation of the investigated ILs is sketched in Scheme 1. Prior to all experiments the samples were dried in oil-pump vacuum at 50 °C for two days under intensive stirring. Karl-Fischer-titration showed water-contents for the dried ILs were below 200 ppm.

2.3. Thermal properties

Glass-, phase-transition- and melting points were measured by means of differential scanning calorimetry (DSC) on a DSC 1 STARe System (Mettler Toledo, Gießen, Germany) equipped with a liquid nitrogen cooling system. Vacuum dried samples of about 15 mg were sealed in aluminum crucibles and heated with a rate of 10 °C/min to 100 °C and kept at this temperature for 10 min to remove thermal history. In the next dynamical step the samples were cooled with a cooling rate of −1 °C/min to −120 °C followed by a 10 min isothermal treatment. The samples were subsequently heated with +1 °C/min to 100 °C. All experiments were repeated with three different samples of each ILs to ensure the correct determination of glass-, phase- and melting temperatures. Decomposition temperatures were determined by means of thermogravimetric analysis on a TG F1 Iris (Netzsch, Selb, Germany) using weighted samples of approximately 10 mg. The samples were heated applying a nitrogen flow of 25 mL/min and a heating rate of 10 °C/min from 30 °C to 550 °C. Decomposition temperatures are given as extrapolated onset temperatures.

2.4. Polarity measurements

Relative molecular polarities were measured using the two solvatochromic dyes Reichardt's betaine Dye and Nile Red dissolved in the bulk ionic liquids. The determination of the UV/Vis spectra was carried out on an UV Specord (Analytic Jena, Jena, Germany) in a thermostated measuring cell at 25 °C. For the sample preparation a solution of either

Reichardt's Dye or Nile red in dichloromethane was added to the pure ionic liquids. The organic solvent was rotated off and the solution dried in vacuum at 50 °C for two days. The obtained dye solutions were then filled in a dried quartz cuvette with a path length of 0.1 cm and an UV/Vis spectrum was measured in the range of 400–850 nm. Measurements were performed at least ten times and the results averaged. The $E_T(30)$ values (polarity values determined with Reichardt's dye) and E_{NR}-values (polarity values determined with Nile Red) were calculated from the absorbance maxima λ_{max} of the dissolved dyes by means of Eq. (1) with the Planck constant h, the speed of light c and Avogadro's Number N_A.

$$E = \frac{hcN_A}{\lambda_{max}} 10^{-6} \quad (1)$$

Since the $E_T(30)$ values in literature are frequently given in kcal mol^{-1} the polarity values detected with Reichardt's dye are additionally reported in this units to allow a better comparison with literature values.

2.5. Rheological properties

Shear- and temperature-dependent flow properties of the samples were measured on a MCR 301 Rheometer (Anton Paar, Graz, Austria), equipped with a PP25 measuring plate (diameter: 25 mm) and a DD41 dish (diameter: 41 mm). Rheological data was collected in the temperature range from 30 °C to 100 °C in 10 °C steps with an additional data acquisition at 25 °C. Before each measurement, the temperature of the sample was equilibrated for at least 25 min to ensure thermal stability (maximum derivation of ± 0.1 °C). For each measurement a constant shear rate of 100 s^{-1} was applied for 60 s to remove any shear-dependent effects. Afterwards the shear rates were varied from 100 s^{-1} to 20 000 s^{-1} in logarithmic steps collecting overall 40 data points. Zero-shear viscosity values of the fluorinated ILs for the fitting with Vogel-Fulcher-Tammann equation (Eq. (2) with η_∞, B and the Vogel temperature T_0 being material dependent parameters) were obtained by regression of shear region where linear Newtonian flow behavior was observed.

$$\eta = \eta_\infty \exp\left(\frac{B}{T - T_0}\right) \quad (2)$$

2.6. Wettability and contact angle analyses

For characterization of the wetting behavior, contact angle measurements were performed with the FILs and AILs and the results compared to water contact angle measurements. Therefore, a mono (1*H*,1*H*1,2*H*,2*H*-perfluorooctyl) siloxane hydrophobic modified silicon surface ($90° \leq \theta_w \leq 130°$) was used. The test surface was prepared by vapor deposition as described previously [33–35] using 1*H*,1*H*1,2*H*,2*H*-perfluorooctyltrichlorosilane (FOTCS) (Sigma Aldrich, used as received). The contact angle measurements were performed while continuously inclining the sample surfaces with an angular speed of $\dot{\varphi} = 0.57°/s$ (inclining-plate technique), using an OCA20 measuring system (Dataphysics, Filderstadt, Germany). During the experiment, 0.03 mL ultra-pure water (Milli-Q® Type 1 ultrapure water system, Merck KGaA, Darmstadt, Germany) or 0.03 mL ionic liquid droplets at temperature of 30.0 °C ± 0.2 °C and were video recorded with a frame rate of 25 frames/s (closed measuring chamber with definable measuring positions). Due to different force distributions between horizontal and inclined measuring setup (different positions of the centers of gravity) [36,37], the advancing angles are denoted as downhill angles $\theta_d(\varphi)$, which are measured at the front edge of the drop. The receding angles are denoted as uphill angles $\theta_u(\varphi)$, which are measured at the back edge of the drop. The static and dynamic contact angle analyses were performed using the *high-precision drop shape analysis* (HPDSA[1]) approach. This approach was developed to describe and analyze highly non-axisymmetric droplets, in particular during dynamic contact angle measurements with high local precision and resolution, which is not possible with commercial contact angle analysis software. Detailed description of the HPDSA-procedure can be found in literature [38,39]. Thereby, the static wetting analyses were performed by determine the contact angle hysteresis (CAH) $\Delta\theta = \theta_{d,e} - \theta_{u,e} \geq 0$, which is the difference between the static advancing/downhill (wetting new surface) and static receding/uphill (formerly wetted surface) contact angle. Therefore, the boundary points X_{B1o}, (corresponding to the triple points in the 2D projection) were calculated in subpixel resolution (in the range of 0.05 pixels) and the shift of the boundary points ΔX_{B1o} were estimated to identify the static downhill and uphill angles by taking the characteristic contact angle just before the contact line moved to formerly non-wetted area (static downhill angle $\theta_{d,e}(\varphi)$), retracted to formerly wetted area (static uphill angle $\theta_{u,e}(\varphi)$) respectively. An example of the procedure is illustrated within the supporting information Fig. S78. The dynamic wetting analyses were performed by using the recently introduced *overall curve shape analysis* [40,41] by fitting of a *Gompertzian function* [42] (Eq. (3)) onto the course of contact angles $\theta_{d,u}(\varphi)$ relative to the inclination angle φ, with θ_{shift}, A, k and φ_{shift} being adjustable fitting parameters.

$$f(\varphi) = \theta_{shift} + A \cdot \exp[-\exp(-k(\varphi - \varphi_{shift}))] \quad (3)$$

This procedure is able to visualize the overall contact angle behavior from a large amount of data (≈7500 images/contact angles per measurement//overall ≈97500 images/contact angles considered for the wetting analyses) with only four fitting parameters and to characterize the wettability of the surface by determine specific contact angles with lowest standard deviation. Additionally, a so-called "*residual analysis*" can be performed by subtracting the individual *Gompertzian* function from the measured course of contact angles. An example of a Gompertzian fitting is illustrated in the supporting information Fig. S78.

3. Results and discussion

3.1. Physicochemical properties

3.1.1. Thermal behavior

ILs are known to have a very diverse phase transition behavior even for a homologues series [43] that can include glass- (T_g), cold-crystallization (T_{cc}), solid-solid- ($T_{s\text{-}s}$) and melting (T_m) transitions depending on the thermal history of the sample. In order to ensure the complete detection of the thermal transition points low scan rates of ± 1 °C were applied as higher scan rates were found to may result in incomplete detection of the transition points [44]. The obtained thermal transition points and decomposition temperatures for the fluorinated and non-fluorinated ILs are given in Table 1. Both the fluorinated and the alkylated trioctylphosphonium salts showed very diverse thermal transitions behavior that included all above mentioned thermal transitions and is sensitive to the length of the attached side chain and the anion. Exemplary DSC-traces of typical thermal transitions of the fluorinated ILs are shown in Fig. 1 including only glass-transition ($[P(oct)_3R_{f4}][C(CN)_3]$), only melting and crystallization ($[P(oct)_3R_{f6}][N(CN)_2]$) and combination of T_g, T_{cc}, and T_m ($[P(oct)_3R_{f8}][NTf_2]$). The occurrence of these three types of thermal behaviors is a very common finding in the field of ionic liquids and a result of the highly destabilized crystal structures and competing molecular interactions [45]. While the fluorinated iodide and dicyanamide ILs exhibit melting points and in some cases additional solid-solid transitions the behavior of the bis

[1] M. Schmitt, HPDSA program package (beta version), DOI:10.13140/RG.2.1.1973.4805, 2015.

Table 1
Phase transition and decomposition temperatures of the fluorinated and alkylated trioctylphosphonium ILs.

Ionic Liquid		T_g [°C]	T_{cc} [°C]	$T_{s\text{-}s}$ [°C]	T_m [°C]	T_d [°C]
$[P(oct)_3R_{f4}]$	[I]	–	–	–	45	345
$[P(oct)_3R_{f6}]$	[I]	–	–	–	56	357
$[P(oct)_3R_{f8}]$	[I]	–	–	−30	52	352
$[P(oct)_3R_{f4}]$	$[NTf_2]$	−75	–	–	–	368
$[P(oct)_3R_{f6}]$	$[NTf_2]$	−72	−24	–	10	364
$[P(oct)_3R_{f8}]$	$[NTf_2]$	−67	−13	–	13	380
$[P(oct)_3R_{f4}]$	$[N(CN)_2]$	–	–	14	37	242
$[P(oct)_3R_{f6}]$	$[N(CN)_2]$	–	–	17	50	245
$[P(oct)_3R_{f8}]$	$[N(CN)_2]$	–	–	–	57	245
$[P(oct)_3R_{f4}]$	$[C(CN)_3]$	−74	–	–	–	316
$[P(oct)_3R_{f6}]$	$[C(CN)_3]$	−67	−32	–	19	309
$[P(oct)_3R_{f8}]$	$[C(CN)_3]$	−55	−39	–	25	314
$[P(oct)_3hex]$	[Br]	−69	−33	–	11	349
$[P(oct)_4]$	[Br]	–	–	11, 19, 31	42	340
$[P(oct)_3dec]$	[Br]	–	–	–	21	335
$[P(oct)_3hex]$	$[NTf_2]$	−89	−40	–	−18	392
$[P(oct)_4]$	$[NTf_2]$	−89	−57	–	15	385
$[P(oct)_3dec]$	$[NTf_2]$	−89	−53	−24	−13	380
$[P(oct)_3hex]$	$[N(CN)_2]$	−88	−47	–	−31	389
$[P(oct)_4]$	$[N(CN)_2]$	–	–	−44, −37, −18	−11	390
$[P(oct)_3dec]$	$[N(CN)_2]$	–	–	−28	−20	371
$[P(oct)_3hex]$	$[C(CN)_3]$	−86	−43	–	−31	409
$[P(oct)_4]$	$[C(CN)_3]$	−87	−56	−27	−21	408
$[P(oct)_3dec]$	$[C(CN)_3]$	−84	–	–	−38	407

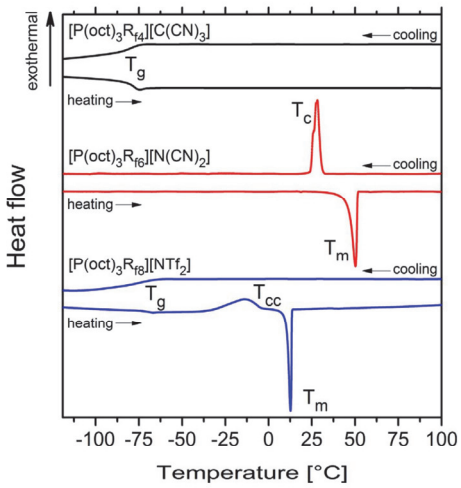

Fig. 1. Exemplary DSC traces for the fluorinated ILs showing three different types of thermal transition behavior.

(trifluoromethanesulfonyl)imide and tricyanomethanide salts is different. All the fluorinated iodides and dicyanamides are solids at ambient temperature whereas the fluorinated $[C(CN)_3]$ and $[NTf_2]$ are RTILs. The R_{f4} substituted $[NTf_2]$ and $[C(CN)_3]$ ILs showed only glass transitions whereas the elongation of the fluorinated chains leads to additional cold-crystallization and melting points although these transitions are absent in the cooling curves where only T_g is observed. These observations can be rationalized with the more pronounced symmetry breaking induced by the short fluorinated chains compared to the alkyl analogues bearing four alkyl sidechains. This effect is compensated by the stabilization of the crystalline structure for longer fluorinated side chains through favored homogenous interaction and packing of the fluorophilic perfluorocarbon segments leading to microsegregation. The stabilization of the ionic liquid crystalline structure through the formation of fluorinated domains was also reported for ILs with other anion-cation combinations [46,47]. Contrary to AILs the melting temperatures of the fluorinated ILs, beside the iodides, are increasing with the elongation of the fluorinated side chain. All alkylated trioctylphosphonium ILs possess melting transitions and most of them additional cold-crystallizations. The melting points for the alkyl ILs with the same anion were found to be always highest for $[P(oct)_4]$ as this cations shows the highest grade of symmetry whereby the bromide and dicyanamide ILs showed three additional solid-solid transitions. Beside the $[P(oct)_4][Br]$ all the alkylated ILs were found to be RTILs.

The decomposition temperatures T_d of the FILs exhibit a much stronger dependence on the incorporated anion than the alkylated analogues. The obtained TGA curves of the investigated ILs are shown in Fig. 2. All decomposition temperatures were observed to be nearly independent of the attached side chain length for both the fluorinated an alkylated compounds. For the tetralkyl phosphonium salts stability was found to decrease in the order $C(CN)_3^- > NTf_2^- > N(CN)_2^- > Br^-$ whereas there are only minor differences in T_g for the non-halide anions. For the fluorinated ILs the thermal stability was found to decrease in the order $NTf_2^- >> C(CN)_3^- > I^- >> N(CN)_2^-$. $[P(oct)_3R_{f4}][N(CN)_2]$ was found to have the lowest decomposition temperature being 242 °C whereas $[P(oct)_3R_{f4}][NTf_2]$ showed the highest decomposition at 368 °C. Overall the fluorinated ILs show a decreased thermal stability especially for the cyano-containing anions compared to the alkylated. These findings can be explained by the higher basicity of these anions that might lead to the abstraction of the more acidic protons in α-position to the fluorinated chains. Decomposition of the cyano-anions for imidazolium ILs was reported to occur via proton abstraction and cyclisation [48,49]. This is supported by the finding of the higher residual mass for the ILs incorporating these anions which were found to result in N-doped carbon materials by thermal decomposition in oxygen-free atmosphere [50].

3.1.2. Polarity determination

The two used solvatochromic dyes Reichardt's Dye and Nile Red were used to investigate the empirical polarity of the IL since they both display large solvatochromic shifts and good solubility in both molecular solvents and ionic liquids [51,52]. This approach using single-

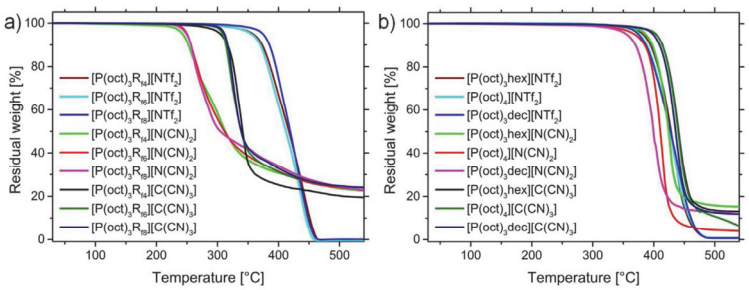

Fig. 2. TGA curves for a) the fluorinated and b) the alkylated ionic liquids.

molecule spectroscopic probes allows a comparison of these two different solvent classes and is therefore widely used for the empirical determination of the polarities in bulk solvent or solvent mixtures. Both dyes were also reported for the polarity determination in a broad range of ionic liquids [53–55]. The obtained absorbance maxima of the two dyes and calculated $E_T(30)$ (Reichardt's Dye) and E_{NR} (Nile Red) are listed in Table 2. As Reichardt's Dye is a negative solvatochromic probe lower $E_T(30)$ values correspond to lower polarities while for the positive solvatochromic dye Nile Red the situation is vice versa. All the obtained transition energies of the fluorinated ILs from measurements with Reichardt's Dye show higher values than for the alkylated analogues resulting in an overall higher obtained polarity. The $E_T(30)$ values of the FILs increase only slightly with elongation of the perfluorinated chain and decrease to minor extend for the alkylated samples. The anion influence of the FILs is less pronounced for the measurements with Reichardt's Dye showing comparable results for the NTf_2 and $C(CN)_3^-$ anions paired with the same cation. Polarities of the AILs slightly decreased in the anion order $C(CN)_3^- > NTf_2^- > N(CN)_2^-$ and with increasing side-chain length. Measurements of the relative polarity performed with Nile Red yielded an opposite trend for the FILs of decreasing polarity with increasing length of fluorinated chain and minimal lower polarities compared to the alkylated analogues. Furthermore the dependence on the anion of the E_{NR} values is more pronounced showing lower polarity values for samples incorporating the $C(CN)_3^-$ anion. For the AILs a decrease in polarity was found in the anion order $C(CN)_3^- > N(CN)_2^- > NTf_2^-$ and also with increase of the attached alkyl chain. It is reported that the measurements with Reichardt's Dye are more sensitive to the cation composition while Nile Red as single-molecule polarity probe is sensitive to the hydrogen bond ability of the investigated liquid [3].

Therefore it is desirable to combine different solvatochromic probes to obtain a more detailed picture of the solvent-solute interaction. $E_T(30)$ vales reported for other phosphonium ionic liquids at 20 °C with the same anions were found to be in the same range ($E_T(30)$ = 47.9 kcal mol^{-1} for [P(hex)$_3$((CH$_2$)$_{14}$H)][NTf$_2$]; $E_T(30)$ = 46.1 kcal mol^{-1} for [P(hex)$_3$((CH$_2$)$_{14}$H)][N(CN)$_2$] [56]). The comparably low polarity values obtained with Nile Red for all samples are in accordance with the absence of hydrogen bonding and long nonpolar molecular fragments from alkyl and perfluoroalkyl-groups. Literature values for the Nile Red as single-molecule polarity probe for other long alkyl chain based phosphonium ILs (E_{NR} = 218.3 kJ mol^{-1} for [P(hex)$_3$((CH$_2$)$_{14}$H)][NTf$_2$]; E_{NR} = 219.1 kJ mol^{-1} for [P(hex)$_3$((CH$_2$)$_{14}$H)][N(CN)$_2$]) are also very similar [57] showing only slight dependence on the side chain length in the quaternary phosphonium cations. Molecular liquids with similar $E_T(30)$ values are the nonprotic polar solvents DMSO ($E_T(30)$ = 45.1 kcal mol^{-1}) or DMF ($E_T(30)$ = 43.2 kcal mol^{-1}) [58] while for E_{NR} the values are similar to the values of Methanol (E_{NR} = 217.7 kJ mol^{-1}), DMSO (E_{NR} = 217.8 kJ mol^{-1}) and Ethanol (E_{NR} = 218.2 kJ mol^{-1}) [52]. Although having polarity values comparable to those of polar molecular liquids all investigated FILs and AILs are immiscible with water allowing novel applications were polar solvents are required that form liquid-liquid biphasic system with water.

3.1.3. Rheological behaviour

The knowledge about the rheological properties of IL is of high importance for a large variety of practical applications since it limits mass, charge and heat transfer if they are used for example as solvent, in mixing and separations processes or as working fluids. The rheological behavior of the FILs and AILs were investigated by shear rate and temperature dependent rheology to obtain a detailed picture of the ILs flow properties. All the investigated fluorinated ILs showed a region of Newtonian flow at low shear rates, a region of linear shear thinning at higher shear rates and a transition zone in between. For all investigated tetraalkylphosphonium ILs only Newtonian flow behavior is observed. Exemplary curves of the shear dependent viscosity of the fluorinated [P(oct)$_3$R$_{f8}$][NTf$_2$] and the alkylated analogue [P(oct)$_3$dec][NTf$_2$] with temperature are show in Fig. 3a) and b). All other plots of the stress controlled rheology can be found in the supporting information (Figs. S64–S77). Upon elongation of the fluorinated chain the onset of shear thinning is shifted to lower shear rates whereas the extend of viscosity decrease at higher shear strain becomes more pronounced. This non-Newtonian behavior was found to be similar for the $C(CN)_3^-$ and NTf_2^- anion. Upon increasing the temperature the shear thinning onset is shifted towards higher shear rates and the degree of shear thinning is reduced. At higher temperatures the shear thinning effects disappear and solely Newtonian flow is observed. The overall zero-shear viscosity at 25 °C of the FILs was furthermore found to be much higher than for the alkylated ILs and showed much higher increase upon elongation of the attached side chain. For example the zero-shear viscosity of [P(oct)$_3$R$_{f8}$][C(CN)$_3$] being 1367 mPa s is more than double the value of [P(oct)$_3$R$_{f4}$][C(CN)$_3$] being 532 mPa s. The plots of viscosities vs. temperature are displayed in Fig. 3c) and d). Both the fluorinated and alkylated ILs show an exponential decrease in viscosity with increasing temperature which could be fitted by the Vogel-Fulcher-Tammann (VFT) equation (Eq. (2)) which is well established for the description of ionic liquid transport properties [59–61]. The obtained VFT fitting parameters and zero-shear viscosities for the FILs and AILs are given in Table 3.

The FILs with the tricyanomethanide anion were less viscous than the ones incorporating the NTf_2^- anion, but the viscosity difference decreases upon elongation of the fluorinated side chain. For the AILs a

Table 2
Wavelength of the maximum absorption λ_{max} of the two solvatochromic dyes in the pure ionic liquids and corresponding transition energies.

Ionic liquid		Reichardt's Dye			Nile Red	
		λ_{max} [nm]	$E_T(30)$ [kJ mol^{-1}]	$E_T(30)$ [kcal mol^{-1}]	λ_{max} [nm]	E_{NR} [kJ mol^{-1}]
[P(oct)$_3$R$_{f4}$]	[NTf$_2$]	637.6	187.6	44.8	548.2	218.2
[P(oct)$_3$R$_{f6}$]	[NTf$_2$]	633.4	188.9	45.1	548.2	218.2
[P(oct)$_3$R$_{f8}$]	[NTf$_2$]	632.4	189.2	45.2	547.6	218.4
[P(oct)$_3$R$_{f4}$]	[C(CN)$_3$]	638.0	187.5	44.8	550.4	217.3
[P(oct)$_3$R$_{f6}$]	[C(CN)$_3$]	633.4	188.9	45.1	549.6	217.6
[P(oct)$_3$R$_{f8}$]	[C(CN)$_3$]	627.9	190.5	45.5	549.1	217.8
[P(oct)$_3$hex]	[NTf$_2$]	648.9	184.4	44.1	548.3	218.2
[P(oct)$_4$]	[NTf$_2$]	650.3	184.0	44.0	548.0	218.3
[P(oct)$_3$dec]	[NTf$_2$]	652.7	183.3	43.8	547.6	218.4
[P(oct)$_3$hex]	[N(CN)$_2$]	647.5	184.7	44.2	550.9	217.2
[P(oct)$_4$]	[N(CN)$_2$]	648.7	184.4	44.1	550.5	217.3
[P(oct)$_3$dec]	[N(CN)$_2$]	649.9	184.1	44.0	550.1	217.5
[P(oct)$_3$hex]	[C(CN)$_3$]	649.7	184.1	44.0	552.5	216.5
[P(oct)$_4$]	[C(CN)$_3$]	652.1	183.4	43.8	552.0	216.7
[P(oct)$_3$dec]	[C(CN)$_3$]	654.3	182.8	43.7	551.4	217.0

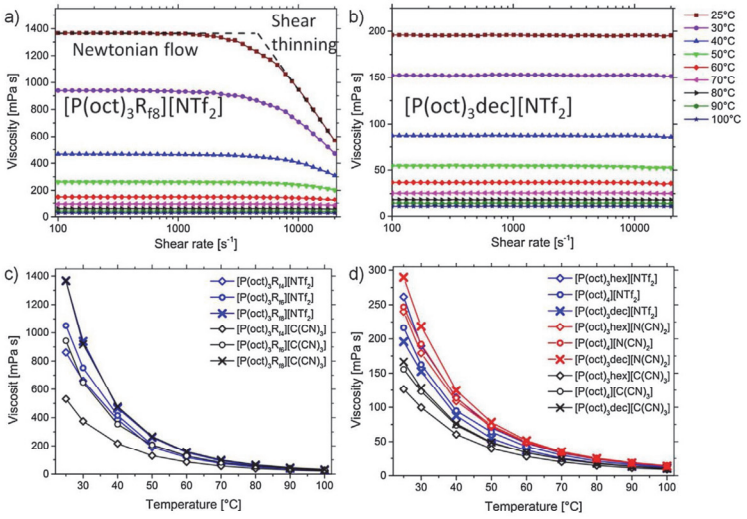

Fig. 3. Progression of shear dependent viscosity with temperature for a) $[P(oct)_3R_{f8}][NTf_2]$ showing non-Newtonian shear thinning and b) $[P(oct)_3dec][NTf_2]$ where solely Newtonian behavior is observed; c) and d) progression of the zero-shear viscosity with temperature for the fluorinated and alkylated ILs.

Table 3
Zero-shear viscosity η_o at 25 °C and VFT equation fit parameters of the zero-shear viscosity data of the investigated ILs.

Ionic Liquid		η_0 [mPa s]	$\eta_\infty \times 10^{-2}$ [mPa s]	B [K]	T_0 [K]
$[P(oct)_3R_{f4}]$	$[NTf_2]$	862	11.62	1175.90	166.54
$[P(oct)_3R_{f6}]$	$[NTf_2]$	1051	9.11	1178.77	172.24
$[P(oct)_3R_{f8}]$	$[NTf_2]$	1368	2.01	1579.07	156.28
$[P(oct)_3R_{f4}]$	$[C(CN)_3]$	532	16.01	962.34	179.38
$[P(oct)_3R_{f6}]$	$[C(CN)_3]$	944	14.19	1039.73	179.98
$[P(oct)_3R_{f8}]$	$[C(CN)_3]$	1367	1.202	1090.92	181.30
$[P(oct)_3hex]$	$[NTf_2]$	261	12.00	937.03	176.18
$[P(oct)_4]$	$[NTf_2]$	216	10.07	986.98	169.48
$[P(oct)_3dec]$	$[NTf_2]$	196	11.87	1635.59	129.88
$[P(oct)_3hex]$	$[N(CN)_2]$	240	8.78	1079.67	161.66
$[P(oct)_4]$	$[N(CN)_2]$	247	3.06	1448.58	137.24
$[P(oct)_3dec]$	$[N(CN)_2]$	290	2.71	1410.53	146.14
$[P(oct)_3hex]$	$[C(CN)_3]$	126	4.27	1190.55	149.33
$[P(oct)_4]$	$[C(CN)_3]$	156	5.25	1178.74	150.84
$[P(oct)_3dec]$	$[C(CN)_3]$	167	6.02	1091.36	160.50

decrease in viscosity from hexyl to decyl side chain was found for the $[NTf_2]$ ILs while for those incorporating the $N(CN)_2^-$ and $C(CN)_3^-$ anions an increase was observed. Literature reports about alkylated trioctylammonium ionic liquids explained a similar non-linear behavior with packing effects in the bulk liquid [62]. This might also be the case for these investigated phosphonium ILs as the NTf_2^- anion has a larger molecular volume than the cyano-anions. Viscosity values at 25 °C of all investigated alkyl ILs are comparably low especially as these compounds have comparable high molecular weights. The low viscosity along with highly hydrophobic character of the alkylated ILs makes these anion-cations combinations highly attractive for practical applications. The findings of the shear-thinning properties and higher overall viscosities of the fluorinated ILs can be rationalized with the formation of cohesive aggregates in the bulk state of the ILs. The formation of a third domain, beside polar ionic and non-polar alkyl domains that is a common finding in the field of ILs [63], consisting of the aggregated perfluorinated chains in the bulk, driven by fluorophilic/solvophobic interactions, was also reported for other ILs with perfluoroalkyl-groups [64–66].

These systems were found to show self-assembled nanostructures through the partial immiscibility and solvophobic interactions of the molecular fragments [63] that have a great influence on the macroscopic properties [67,68]. The cohesion of the microstructured aggregates composed of fluorinated chains is more pronounced the longer the perfluorocarbon segments because of increased homogenous interaction in the fluorinated domains and solvophobic heterogeneous interactions with ionic and alkyl groups. This leads to more cohesive fluorous domains that result in an increased zero-shear viscosity values in the investigated FILs. Similar results of shear thinning ILs were found to be the result of cohesion from pronounced bulk-structuring through hydrogen-bonding in hydrophilic ILs [69,70]. Upon temperature increase the shear thinning is much less pronounced which is believed to be the result of partial mixing between the perfluorinated and alkyl-groups leading to a lower amount of shear thinning. This is further supported by the finding that increasing the fluorinated side chain length leads to a higher degree of shear thinning and higher temperatures at which shear thinning vanishes. These microscopic mixing effects are similar to the macroscopic thermoregulated mixing behavior between perfluorocarbon and common hydrocarbon solvents forming biphasic liquid-liquids systems at lower temperatures and a homogenous mixture at elevated temperatures [71].

3.2. Wetting analyses: contact angle measurements and motion behaviors

Many practical applications of ionic liquids incorporate some types of surfaces, while the solid-liquids interface is probably one of the most important. It is therefore important to analyze the wetting and adhesion behavior and the factors that determine them for optimize the wetting of surfaces by this highly tunable solvents for specific tasks [72]. As illustrated in our previous studies [47,73] different parameters such as the interactions between the liquid and the surface, the polarity and the viscosity affect the wetting situation on a surface, whereby the greatest influence was found to result from incorporation and length of perfluorinated chains in the cation. The water contact angle measurements resulted in a contact angle range from ≈ 90° to ≈ 115°, which is the typical contact angle range of perfluorooctylsiloxane coatings [33,34,74]. All determined contact angles with ionic liquids as test liquids were found to be considerably smaller, which is the result of the lower liquid-vapor surface tension affecting the force balance as well as the observed contact angle. Furthermore, a strong pinning of the triple line at the uphill side was clearly recognizable. Examples for different drop shapes and contact angle measurements with the inclining-plate technique can be found within the supporting information Figs.

Table 4
Results for the determination of the static downhill $\theta_{d,e}(\varphi)$ and static uphill $\theta_{u,e}(\varphi)$ angles as well as the critical inclination for the downhill φ_d and uphill side φ_d with the HPDSA procedure on a hydrophobic modified silicon surface.

Test liquid		$\theta_{d,e}(\varphi)$ [°]	φ_d [°]	$\theta_{u,e}(\varphi)$ [°]	φ_u [°]	$\Delta\theta$ [°]
H_2O		106.9 ± 0.9	9.1 ± 1.3	96.4 ± 1.5	10.1 ± 2.3	10.5 ± 0.9
$[P(oct)_3R_{f4}]$	$[NTf_2]$	56.5 ± 1.0	2.9 ± 0.4	29.4 ± 1.5	12.7 ± 1.1	27.2 ± 0.6
$[P(oct)_3R_{f6}]$	$[NTf_2]$	48.8 ± 0.8	2.5 ± 0.5	24.8 ± 1.2	10.2 ± 0.7	24.1 ± 1.8
$[P(oct)_3R_{f8}]$	$[NTf_2]$	44.8 ± 0.9	2.8 ± 0.6	21.3 ± 3.9	16.6 ± 1.7	28.2 ± 4.1
$[P(oct)_3hex]$	$[NTf_2]$	64.2 ± 0.5	3.4 ± 0.2	42.4 ± 1.1	17.9 ± 0.4	21.8 ± 1.4
$[P(oct)_4]$	$[NTf_2]$	65.2 ± 0.5	3.4 ± 0.3	43.1 ± 1.4	18.1 ± 0.9	22.1 ± 1.9
$[P(oct)_3dec]$	$[NTf_2]$	67.0 ± 0.5	2.2 ± 0.5	44.9 ± 0.9	15.5 ± 0.7	22.2 ± 0.5
$[P(oct)_3R_{f4}]$	$[C(CN)_3]$	54.5 ± 1.3	1.7 ± 0.4	35.9 ± 0.9	10.6 ± 0.8	18.6 ± 1.3
$[P(oct)_3R_{f6}]$	$[C(CN)_3]$	52.8 ± 0.5	3.0 ± 0.3	16.7 ± 4.5	17.1 ± 1.3	36.2 ± 4.5
$[P(oct)_3R_{f8}]$	$[C(CN)_3]$	48.1 ± 0.7	2.5 ± 0.6	17.5 ± 3.8	16.8 ± 1.2	30.6 ± 3.7
$[P(oct)_3hex]$	$[C(CN)_3]$	68.0 ± 0.3	2.0 ± 0.4	45.5 ± 0.7	15.2 ± 0.6	22.4 ± 0.8
$[P(oct)_4]$	$[C(CN)_3]$	68.6 ± 0.9	2.9 ± 0.4	45.6 ± 1.2	16.2 ± 0.8	23.0 ± 1.9
$[P(oct)_3dec]$	$[C(CN)_3]$	71.3 ± 0.4	3.2 ± 0.5	47.5 ± 1.2	18.1 ± 0.7	23.8 ± 1.3

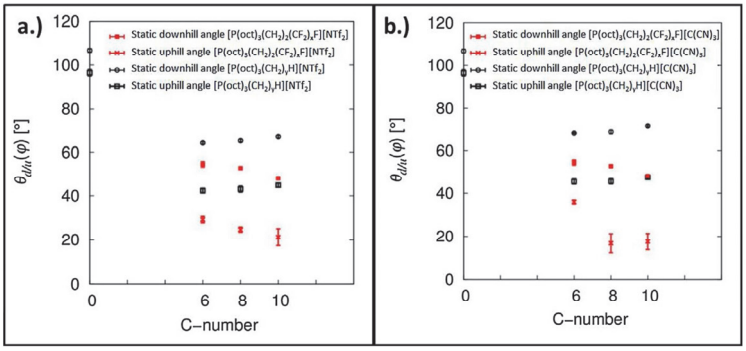

Fig. 4. Measured static downhill $\theta_{d,e}(\varphi)$ and uphill $\theta_{u,e}(\varphi)$ angles with standard deviations from contact angle measurements with water and ionic liquids in dependence on the degree of fluorination and on the number of C atoms in the side chain of the cation with a.) NTf_2^- as anion and b.) $C(CN)_3^-$ as anion. The C number "0" refers to the contact angle measurements with water as test liquid.

S80–S83. As highly non-axisymmetric drop shapes with uphill contact angles down to nearly 0° are observed, the *high-precision drop shape analysis*[1] approach was used, which guaranties a reproducible and comparable analysis of these highly non-axisymmetric systems. The results are summarized in Table 4 and illustrated in Fig. 4.

All investigated ionic liquids exhibited small critical inclination angles (inclination angles at which the first drop motion occurs) on the downhill side ($\varphi_d \leq 3.4°$) but relative large critical inclination angles on the uphill side ($\varphi_u \geq 10.2°$). In accordance to our previous studies [47,73], the attached alkyl side-chain lengths had considerably less influence on the contact angles than the length of the attached perfluorocarbon chain. This is represented by the static downhill- $\theta_{d,e}(\varphi)$ and uphill angles $\theta_{u,e}(\varphi)$ that are very similar for a series of AILs containing the same cation. The occurrence of this effect can mainly be attributed to the altered structure of the FILs at the interfaces were perfluorocarbon segments are reported to lead to lower surface energies [16,67] and layers at the solid-liquid interface [24].

The analysis and characterization of dynamic wetting properties is often of major importance for many applications where liquid interfaces are involved for example in microfluidics, electrochemical applications, lubrication or tribology as well as friction examinations. In contrast to the static wetting analyses, strong pinning effects such as at the uphill side with contact angle down to nearly 0° can only be investigated if the whole inclination angle range is taken into account. For example, the drain-off behavior of droplets cannot be characterized by the critical inclination angles $\varphi_{d,u}$ because these inclination angles

Table 5
Overview about the results of the overall curve shape analysis by *Gompertzian* fitting according to Eq. (3) to identify the contact angle/inclination angle pairs $\theta_{d,u}/\varphi_{d,u}$ with lowest standard deviation on a hydrophobic modified silicon surface. $\theta_{Ld,u}$ *and* $\varphi_{Ld,u}$ denote the limits of the fitting range for the contact angle and inclination angle on the uphill and downhill side.

Test liquid		$\theta_d \pm \sigma_d$ [°]	φ_d [°]	$\theta_{Ld} \pm \sigma_{Ld}$ [°]	φ_{Ld} [°]	$\theta_u \pm \sigma_u$ [°]	φ_u [°]	$\theta_{Lu} \pm \sigma_u$ [°]	φ_{Lu} [°]
H_2O		104.3 ± 0.3	3.7	109.3 ± 0.4	12.1	95.9 ± 1.5	9.2	93.2 ± 1.6	14.3
$[P(oct)_3R_{f4}]$	$[NTf_2]$	60.8 ± 0.7	9.7	62.9 ± 0.7	14.8	52.6 ± 1.4	0.0	8.8 ± 3.6	21.8
$[P(oct)_3R_{f6}]$	$[NTf_2]$	51.8 ± 0.3	6.2	52.3 ± 0.4	9.0	41.5 ± 0.5	3.1	0.8 ± 0.9	19.0
$[P(oct)_3R_{f8}]$	$[NTf_2]$	46.0 ± 0.1	0.0	59.9 ± 0.2	17.9	26.3 ± 0.1	11.0	3.3 ± 0.7	24.3
$[P(oct)_3hex]$	$[NTf_2]$	65.5 ± 0.3	19.9	65.5 ± 0.3	19.3	61.9 ± 0.3	0.0	32.5 ± 2.1	29.2
$[P(oct)_4]$	$[NTf_2]$	66.5 ± 0.2	28.1	66.5 ± 0.2	18.8	53.1 ± 0.6	10.2	34.6 ± 0.9	28.0
$[P(oct)_3dec]$	$[NTf_2]$	66.3 ± 0.2	6.4	68.7 ± 0.1	13.9	58.3 ± 0.2	8.5	36.6 ± 0.2	21.9
$[P(oct)_3R_{f4}]$	$[C(CN)_3]$	53.5 ± 1.1	0.0	59.6 ± 1.9	13.0	22.9 ± 0.6	18.9	23.0 ± 0.6	18.8
$[P(oct)_3R_{f6}]$	$[C(CN)_3]$	55.7 ± 0.6	6.8	62.7 ± 1.0	19.2	28.9 ± 1.0	10.3	2.9 ± 2.1	26.3
$[P(oct)_3R_{f8}]$	$[C(CN)_3]$	47.1 ± 0.6	1.2	60.8 ± 1.0	19.6	40.9 ± 0.5	3.9	0.6 ± 0.6	28.2
$[P(oct)_3hex]$	$[C(CN)_3]$	69.5 ± 0.2	6.0	70.1 ± 0.3	14.2	45.0 ± 0.2	16.0	39.6 ± 0.4	22.0
$[P(oct)_4]$	$[C(CN)_3]$	67.2 ± 0.9	0.3	70.3 ± 0.9	17.6	65.3 ± 0.7	1.8	37.8 ± 2.4	24.4
$[P(oct)_3dec]$	$[C(CN)_3]$	68.9 ± 0.4	6.6	69.7 ± 0.5	15.9	56.7 ± 0.1	7.9	39.3 ± 0.9	22.4

Table 6
Summary of the averaged data from the Gompertzian fitting following Eq. (3) for the downhill and uphill angle of the AILs, FILs and water as test liquids on the hydrophobic modified silicon surface.

		Downhill angle				Uphill angle			
Test liquid		θ_{shift} [°]	A [°]	k [$^{\circ -1}$]	φ_{shift} [°]	θ_{shift} [°]	A [°]	k [$^{\circ -1}$]	φ_{shift} [°]
H_2O		101.53	10.58	0.183	5.14	104.67	−13.12	0.121	−6.37
[P(oct)$_3$R$_{f4}$]	[NTf$_2$]	47.96	17.82	0.122	0.588	61.25	−106.08	0.058	−15.78
[P(oct)$_3$R$_{f6}$]	[NTf$_2$]	45.88	6.52	0.582	2.04	47.02	−69.38	0.115	−11.19
[P(oct)$_3$R$_{f8}$]	[NTf$_2$]	43.76	18.29	0.157	4.68	46.92	−58.84	0.094	−11.47
[P(oct)$_3$hex]	[NTf$_2$]	62.31	3.17	0.482	1.95	63.26	−38.10	0.095	12.82
[P(oct)$_4$]	[NTf$_2$]	63.46	2.98	0.458	−2.01	66.27	−41.08	0.083	11.77
[P(oct)$_3$dec]	[NTf$_2$]	63.54	5.31	0.307	1.85	63.26	−33.59	0.145	11.74
[P(oct)$_3$R$_{f4}$]	[C(CN)$_3$]	53.08	6.82	0.319	−3.21	56.26	−45.74	0.111	8.54
[P(oct)$_3$R$_{f6}$]	[C(CN)$_3$]	46.39	19.39	0.116	4.08	54.48	−71.97	0.083	11.78
[P(oct)$_3$R$_{f8}$]	[C(CN)$_3$]	44.25	20.82	0.117	7.05	48.21	−54.34	0.103	10.61
[P(oct)$_3$hex]	[C(CN)$_3$]	67.41	2.69	0.530	3.10	67.41	−32.11	0.139	8.66
[P(oct)$_4$]	[C(CN)$_3$]	66.26	4.07	0.337	1.31	68.82	−38.80	0.105	10.13
[P(oct)$_3$dec]	[C(CN)$_3$]	65.26	4.48	0.343	2.01	65.35	−30.21	0.148	9.44

only indicate the point when the drop motion starts, but do not contain information on the process and velocity of the drop motion and do not indicate a complete roll-off of the droplet. To analyze the dynamic wetting properties, the *overall curve shape analysis* by *Gompertzian* fittings was used to characterize the dynamic wetting behavior. The corresponding figures can be found within the supporting information Figs. S84–S87. The results of the overall curve shape analysis are summarized in Tables 5 and 6.

The reader should not be confused by the contact angle/inclination angle pairs in Table 5. They do not necessarily describe a "good wettable" or "bad wettable" surface but only indicate the value of the highest statistical certainty and the range, where the standard deviations of measurements was the lowest and can significantly vary from the static downhill and uphill angles. For example, the downhill angle with lowest standard deviation θ_d for [P(oct)$_4$][NTf$_2$] with 66.5° is located at an inclination angle of 28.1° whereas the static downhill angle $\theta_{d,e}$ with 65.2° is located at an inclination angle of 3.4°. Another benefit of the curve shape analysis is the correlation of the fitting parameters A (Amplitude of the contact angles ≡ difference between the theoretical smallest and largest contact angle) and k (rate constant of the data points) with the pinning behavior on the surface. These parameters determine the course of the averaged *Gompertzian* functions. This means that weak pinning results in small amplitudes A and large rate constants k, whereas strong pinning results in large amplitudes A and small rate constants k of the data points (Table 6).

As illustrated in Table 6, the elongation of the side-chain length or varying the anion does not significantly affect the A-values and k-values of the investigated ILs. A much larger influence results from the introduction of perfluorinated side-chains that lead to stronger pinning as expressed by larger amplitudes A and smaller rate constants k of the FILs in comparison to the alkylated ILs. This finding is in accordance to our previous studies that especially the fluorination of the IL cation considerably affects the dynamic wetting behavior on the investigated surfaces leading to lower contact angles and higher degree of pinning [47,73]. Concerning the analysis of the trend in k and A values for the increasing side-chain length additional experimental results and the analysis of additional parameters like the shift parameters and the maximal gradient of *Gompertzian* function are proposed.

4. Conclusion

We synthesized a series of novel trioctylphosphonium ionic liquids with perfluoroalkyl side chains paired with NTf_2^-, $N(CN)_2^-$ and $C(CN)_3^-$ anions and compared their physicochemical properties to the non-fluorinated analogues with hydrocarbon segments of same chain length. The FILs were found to have a more diverse phase transition behavior and highly anion dependent thermal stability. Their polarity determined by solvatochromic probes varies only slightly with increasing perfluoroalkyl-part and in comparison to the AILs. Furthermore the FILs showed altered flow properties including shear thinning and much higher overall viscosities. The dynamic wetting behavior of the highly non-symmetrical droplets on a hydrophobic surface was analyzed by the *high-precision drop shape analysis* (HPDSA) approach. It was found that the FILs show an altered wetting behavior resulting in lower values for the static uphill and downhill angles and stronger pinning to the surface. The wetting behavior was found to be mainly correlated with the degree of fluorination of the cation rather than the incorporated anion, polarity or viscosity which is in accordance to our previous studies [47,73]. The introduction of perfluorinated side chains into IL is therefore an easy accessible way for the tuning of surface properties and wetting behavior of these neoteric solvents when solid-liquid interfaces are included which is the case and critical for a broad range of scientific and industrial applications [75].

Acknowledgement

The authors gratefully acknowledge the Deutsche Bundesstiftung Umwelt (DBU) (31925-41) for financial support.

Appendix A. Supplementary data

Supplementary data associated with this article can be found, in the online version, at http://dx.doi.org/10.1016/j.colsurfa.2017.10.013.

References

[1] T.L. Greaves, C.J. Drummond, Protic ionic liquids: evolving structure–property relationships and expanding applications, Chem. Rev. 115 (2015) 11379–11448, http://dx.doi.org/10.1021/acs.chemrev.5b00158.
[2] T. Welton, Room-temperature ionic liquids. Solvents for synthesis and catalysis, Chem. Rev. 99 (1999) 2071–2084, http://dx.doi.org/10.1021/cr980032t.
[3] J.P. Hallett, T. Welton, Room-temperature ionic liquids: solvents for synthesis and catalysis. 2, Chem. Rev. 111 (2011) 3508–3576, http://dx.doi.org/10.1021/cr1003248.
[4] M. Smiglak, J.M. Pringle, X. Lu, L. Han, S. Zhang, H. Gao, D.R. MacFarlane, R.D. Rogers, Ionic liquids for energy, materials, and medicine, Chem. Commun. 50 (2014) 9228–9250, http://dx.doi.org/10.1039/c4cc02021a.
[5] Q. Zhang, J.M. Shreeve, Energetic ionic liquids as explosives and propellant fuels: a new journey of ionic liquid chemistry, Chem. Rev. 114 (2014) 10527–10574, http://dx.doi.org/10.1021/cr500364t.
[6] R.E. Morris, Ionothermal synthesis—ionic liquids as functional solvents in the preparation of crystalline materials, Chem. Commun. (2009) 2990, http://dx.doi.org/10.1039/b902611h.
[7] T.D. Ho, C. Zhang, L.W. Hantao, J.L. Anderson, Ionic liquids in analytical chemistry: fundamentals, advances, and perspectives, Anal. Chem. 86 (2014) 262–285, http://dx.doi.org/10.1021/ac4035554.
[8] E. García-Verdugo, B. Altava, M.I. Burguete, P. Lozano, S.V. Luis, Ionic liquids and

continuous flow processes: a good marriage to design sustainable processes, Green Chem. 17 (2015) 2693–2713, http://dx.doi.org/10.1039/C4GC02388A.
[9] M. Armand, F. Endres, D.R. MacFarlane, H. Ohno, B. Scrosati, Ionic-liquid materials for the electrochemical challenges of the future, Nat. Mater. 8 (2009) 621–629, http://dx.doi.org/10.1038/nmat2448.
[10] D.R. MacFarlane, N. Tachikawa, M. Forsyth, J.M. Pringle, P.C. Howlett, G.D. Elliott, J.H. Davis, M. Watanabe, P. Simon, C.A. Angell, Energy applications of ionic liquids, Energy Environ. Sci. 7 (2014) 232–250, http://dx.doi.org/10.1039/c3ee42099j.
[11] A.B. Pereiro, J.M.M. Araújo, S. Martinho, F. Alves, S. Nunes, A. Matias, C.M.M. Duarte, L.P.N. Rebelo, I.M. Marrucho, Fluorinated ionic liquids: properites and applications, ACS Sustain. Chem. Eng. 1 (2013) 427–439.
[12] A.M. Ferreira, P.D.O. Esteves, I. Boal-Palheiros, A.B. Pereiro, L.P.N. Rebelo, M.G. Freire, Enhanced tunability afforded by aqueous biphasic systems formed by fluorinated ionic liquids and carbohydrates, Green Chem. 18 (2016) 1070–1079, http://dx.doi.org/10.1039/C5GC01610J.
[13] J. van den Broeke, F. Winter, B.-J. Deelman, G. van Koten, A highly fluorous room-temperature ionic liquid exhibiting fluorous biphasic behavior and its use in catalyst recycling, Org. Lett. 4 (2002) 3851–3854, http://dx.doi.org/10.1021/ol026700l.
[14] C. Emnet, K.M. Weber, J.A. Vidal, C.S. Consorti, A.M. Stuart, J.A. Gladysz, Syntheses and properties of fluorous quaternary phosphonium salts that bear four ponytails; new candidates for phase transfer catalysts and ionic liquids, Adv. Synth. Catal. 348 (2006) 1625–1634, http://dx.doi.org/10.1002/adsc.200606138.
[15] T.L. Merrigan, E.D. Bates, S.C. Dorman, J.H. Davis Jr., New fluorous ionic liquids function as surfactants in conventional room-temperature ionic liquids, Chem. Commun. (2000) 2051–2052, http://dx.doi.org/10.1039/b005418f.
[16] J.M. Breen, S. Olejarz, K.R. Seddon, Microwave synthesis of short-chained fluorinated ionic liquids and their surface properties, ACS Sustain. Chem. Eng. 4 (2016) 387–391, http://dx.doi.org/10.1021/acssuschemeng.5b01265.
[17] A.B. Pereiro, J.M.M. Araújo, F.S. Teixeira, I.M. Marrucho, M.M. Piñeiro, L.P.N. Rebelo, Aggregation behavior and total miscibility of fluorinated ionic liquids in water, Langmuir 31 (2015) 1283–1295, http://dx.doi.org/10.1021/la503961h.
[18] M.J. Muldoon, S.N.V.K. Aki, J.L. Anderson, J.K. Dixon, J.F. Brennecke, Improving carbon dioxide solubility in ionic liquids, J. Phys. Chem. B 111 (2007) 9001–9009, http://dx.doi.org/10.1021/jp071897q.
[19] D. Almantariotis, T. Gefflaut, A.A.H. Pádua, J.-Y. Coxam, M.F. Costa Gomes, Effect of fluorination and size of the alkyl side-chain on the solubility of carbon dioxide in 1-Alkyl-3-methylimidazolium bis(trifluoromethylsulfonyl)amide ionic liquids, J. Phys. Chem. B 114 (2010) 3608–3617, http://dx.doi.org/10.1021/jp912176n.
[20] J.E. Bara, C.J. Gabriel, T.K. Carlisle, D.E. Camper, A. Finotello, D.L. Gin, R.D. Noble, Gas separations in fluoroalkyl-functionalized room-temperature ionic liquids using supported liquid membranes, Chem. Eng. J. 147 (2009) 43–50, http://dx.doi.org/10.1016/j.cej.2008.11.021.
[21] M. Fan, C. Zhang, Y. Guo, R. Zhang, L. Lin, D. Yang, F. Zhou, W. Liu, An investigation on the friction and wear properties of perfluorooctane sulfonate ionic liquids, Tribol. Lett. 63 (2016) 11, http://dx.doi.org/10.1007/s11249-016-0698-3.
[22] I. Minami, M. Kita, T. Kubo, H. Nanao, S. Mori, The tribological properties of ionic liquids composed of trifluorotris(pentafluoroethyl) phosphate as a hydrophobic anion, Tribol. Lett. 30 (2008) 215–223, http://dx.doi.org/10.1007/s11249-008-9329-y.
[23] N.V. Plechkova, K.R. Seddon, Applications of ionic liquids in the chemical industry, Chem. Soc. Rev. 37 (2008) 123–150, http://dx.doi.org/10.1039/B006677J.
[24] M. Mezger, H. Schroder, H. Reichert, S. Schramm, J.S. Okasinski, S. Schoder, V. Honkimaki, M. Deutsch, B.M. Ocko, J. Ralston, M. Rohwerder, M. Stratmann, H. Dosch, Molecular layering of fluorinated ionic liquids at a charged sapphire (0001) surface, Science 322 (2008) 424–428, http://dx.doi.org/10.1126/science.1164502.
[25] J. Restolho, J.L. Mata, B. Saramago, On the interfacial behavior of ionic liquids: surface tensions and contact angles, J. Colloid Interface Sci. 340 (2009) 82–86, http://dx.doi.org/10.1016/j.jcis.2009.08.013.
[26] L. Gao, T.J. McCarthy, Ionic liquids are useful contact angle probe fluids, J. Am. Chem. Soc. 129 (2007) 3804–3805, http://dx.doi.org/10.1021/ja070169d.
[27] D. Blanco, M. Bartolomé, B. Ramajo, J.L. Viesca, R. González, A. Hernández Battez, Wetting properties of seven phosphonium cation-based ionic liquids, Ind. Eng. Chem. Res. 55 (2016) 9594–9602, http://dx.doi.org/10.1021/acs.iecr.6b00821.
[28] H. Liu, L. Jiang, Wettability by ionic liquids, Small 12 (2016) 9–15, http://dx.doi.org/10.1002/smll.201501526.
[29] R. Sedev, Surface tension, interfacial tension and contact angles of ionic liquids, Curr. Opin. Colloid Interface Sci. 16 (2011) 310–316, http://dx.doi.org/10.1016/j.cocis.2011.01.011.
[30] G. Tiago, J. Restolho, A. Forte, R. Colaço, L.C. Branco, B. Saramago, Novel ionic liquids for interfacial and tribological applications, Colloids Surf. A: Physicochem. Eng. Aspects 472 (2015) 1–8, http://dx.doi.org/10.1016/j.colsurfa.2015.02.030.
[31] T. Batchelor, J. Cunder, A.Y. Fadeev, Wetting study of imidazolium ionic liquids, J. Colloid Interface Sci. 330 (2009) 415–420, http://dx.doi.org/10.1016/j.jcis.2008.10.019.
[32] K.J. Fraser, D.R. MacFarlane, Phosphonium-based ionic liquids: an overview, Aust. J. Chem. 62 (2009) 309, http://dx.doi.org/10.1071/CH08558.
[33] F. Heib, R. Hempelmann, W.M. Munief, S. Ingebrandt, F. Fug, W. Possart, K. Groß, M. Schmitt, High-precision drop shape analysis (HPDSA) of quasistatic contact angles on silanized silicon wafers with different surface topographies during inclining-plate measurements: influence of the surface roughness on the contact line dynamics, Appl. Surf. Sci. 342 (2015) 11–25, http://dx.doi.org/10.1016/j.apsusc.2015.03.032.
[34] M. Schmitt, R. Hempelmann, S. Ingebrandt, W. Munief, D. Durneata, K. Groß, F. Heib, Statistical approach for contact angle determination on inclining surfaces: “slow moving” analyses of non-axisymmetric drops on a flat silanized silicon wafer, Int. J. Adhes. Adhes. 55 (2014) 123–131, http://dx.doi.org/10.1016/j.ijadhadh.2014.08.007.
[35] M. Schmitt, K. Groß, J. Grub, F. Heib, Detailed statistical contact angle analyses; “slow moving” drops on inclining silicon-oxide surfaces, J. Colloid Interface Sci. 447 (2014) 229–239, http://dx.doi.org/10.1016/j.jcis.2014.10.047.
[36] M. Schmitt, R. Hempelmann, F. Heib, Experimental investigation of dynamic contact angles on horizontal and inclined surfaces part I: flat silicon oxide surfaces, Z. Phys. Chem. 228 (2014) 629–648, http://dx.doi.org/10.1515/zpch-2014-0443.
[37] M. Schmitt, R. Hempelmann, F. Heib, Experimental investigation of dynamic contact angles on horizontal and inclined surfaces part II: rough homogenous surfaces, Z. Phys. Chem. 228 (2014) 629–648, http://dx.doi.org/10.1515/zpch-2014-0484.
[38] M. Schmitt, F. Heib, High-precision drop shape analysis on inclining flat surfaces: introduction and comparison of this special method with commercial contact angle analysis, J. Chem. Phys. 139 (2013) 134201, http://dx.doi.org/10.1063/1.4822261.
[39] F. Heib, M. Schmitt, Statistical contact angle analyses with the high-precision drop shape analysis (HPDSA) approach: basic principles and applications, Coatings 6 (2016) 57, http://dx.doi.org/10.3390/coatings6040057.
[40] M. Schmitt, K. Groß, J. Grub, F. Heib, Detailed statistical contact angle analyses; “slow moving” drops on inclining silicon-oxide surfaces, J. Colloid Interface Sci. 447 (2014) 229–239, http://dx.doi.org/10.1016/j.jcis.2014.10.047.
[41] M. Schmitt, J. Grub, F. Heib, Statistical contact angle analyses; “slow moving” drops on a horizontal silicon-oxide surface, J. Colloid Interface Sci. 447 (2015) 248–253, http://dx.doi.org/10.1016/j.jcis.2014.11.054.
[42] M. Schmitt, R. Schulze-Pillot, R. Hempelmann, Kinetics of bulk polymerisation and Gompertz’s law, Phys. Chem. Chem. Phys. 13 (2011) 690–695, http://dx.doi.org/10.1039/C0CP00447B.
[43] C.P. Fredlake, J.M. Crosthwaite, D.G. Hert, S.N.V.K. Aki, J.F. Brennecke, Thermophysical properties of imidazolium-based ionic liquids, J. Chem. Eng. Data 49 (2004) 954–964, http://dx.doi.org/10.1021/je034261a.
[44] E. Gómez, N. Calvar, Á. Domínguez, Thermal behaviour of pure ionic liquids, Ion. Liq. – Curr. State Art, InTech, 2015, http://dx.doi.org/10.5772/59271.
[45] J.M. Crosthwaite, M.J. Muldoon, J.K. Dixon, J.L. Anderson, J.F. Brennecke, Phase transition and decomposition temperatures, heat capacities and viscosities of pyridinium ionic liquids, J. Chem. Thermodyn. 37 (2005) 559–568, http://dx.doi.org/10.1016/j.jct.2005.03.013.
[46] J.J. Tindale, C. Na, M.C. Jennings, P.J. Ragogna, Synthesis and characterization of fluorinated phosphonium ionic liquids, Can. J. Chem. 85 (2007) 660–667, http://dx.doi.org/10.1139/v07-035.
[47] D. Rauber, F. Heib, M. Schmitt, R. Hempelmann, Influence of perfluoroalkyl-chains on the surface properties of 1-methylimidazolium bis(trifluoromethanesulfonyl) imide ionic liquids, J. Mol. Liq. 216 (2016) 246–258, http://dx.doi.org/10.1016/j.molliq.2016.01.011.
[48] T.J. Wooster, K.M. Johanson, K.J. Fraser, D.R. MacFarlane, J.L. Scott, Thermal degradation of cyano containing ionic liquids, Green Chem. 8 (2006) 691, http://dx.doi.org/10.1039/b606395k.
[49] J. Liu, S.D. Chambreau, G.L. Vaghjiani, Dynamics simulations and statistical modeling of thermal decomposition of 1-Ethyl-3-methylimidazolium dicyanamide and 1-Ethyl-2,3-dimethylimidazolium dicyanamide, J. Phys. Chem. A 118 (2014) 11133–11144, http://dx.doi.org/10.1021/jp5095849.
[50] T.-P. Fellinger, A. Thomas, J. Yuan, M. Antonietti, 25th Anniversary Article: “Cooking Carbon with Salt”: carbon materials and carbonaceous frameworks from ionic liquids and poly(ionic liquid)s, Adv. Mater. 25 (2013) 5838–5855, http://dx.doi.org/10.1002/adma.201301975.
[51] C. Reichardt, Solvatochromic dyes as solvent polarity indicators, Chem. Rev. 94 (1994) 2319–2358, http://dx.doi.org/10.1021/cr00032a005.
[52] J.F. Deye, T.A. Berger, A.G. Anderson, Nile Red as a solvatochromic dye for measuring solvent strength in normal liquids and mixtures of normal liquids with supercritical and near critical fluids, Anal. Chem. 62 (1990) 615–622, http://dx.doi.org/10.1021/ac00205a015.
[53] C. Reichardt, Polarity of ionic liquids determined empirically by means of solvatochromic pyridinium N-phenolate betaine dyes, Green Chem. 7 (2005) 339, http://dx.doi.org/10.1039/b500106b.
[54] A.J. Carmichael, K.R. Seddon, Polarity study of some 1-alkyl-3-methylimidazolium ambient-temperature ionic liquids with the solvatochromic dye, Nile Red, J. Phys. Org. Chem. 13 (2000) 591–595, http://dx.doi.org/10.1002/1099-1395(200010)13:10<591:AID-POC305>3.0.CO;2-2.
[55] K.A. Fletcher, I.A. Storey, A.E. Hendricks, S.S. Pandey, S.S. Pandey, Behavior of the solvatochromic probes Reichardt{’}s dye{,} pyrene{,} dansylamide{,} Nile Red and 1-pyrenecarbaldehyde within the room-temperature ionic liquid bmimPF, Green Chem. 3 (2001) 210–215, http://dx.doi.org/10.1039/B103592B.
[56] R. Byrne, S. Coleman, S. Gallagher, D. Diamond, Designer molecular probes for phosphonium ionic liquids, Phys. Chem. Chem. Phys. 12 (2010) 1895, http://dx.doi.org/10.1039/b920580b.
[57] D.J. Heldebrant, H.N. Witt, S.M. Walsh, T. Ellis, J. Rauscher, P.G. Jessop, Liquid polymers as solvents for catalytic reductions, Green Chem. 8 (2006) 807, http://dx.doi.org/10.1039/b605405f.
[58] C. Reichardt, T. Welton, Solvents and Solvent Effects in Organic Chemistry, WILEY-VCH, Weinheim, 2003, http://dx.doi.org/10.1002/3527601791.
[59] H. Tokuda, K. Hayamizu, K. Ishii, M.A.B.H. Susan, M. Watanabe, Physicochemical properties and structures of room temperature ionic liquids. 2. Variation of alkyl chain length in imidazolium cation, J. Phys. Chem. B 109 (2005) 6103–6110, http://dx.doi.org/10.1021/jp044626d.

[60] A. Noda, K. Hayamizu, M. Watanabe, Pulsed-gradient spin–echo 1 H and 19 F NMR ionic diffusion coefficient, viscosity, and ionic conductivity of non-chloroaluminate room-temperature ionic liquids, J. Phys. Chem. B 105 (2001) 4603–4610, http://dx.doi.org/10.1021/jp004132q.
[61] A. Rupp, N. Roznyatovskaya, H. Scherer, W. Beichel, P. Klose, C. Sturm, A. Hoffmann, J. Tübke, T. Koslowski, I. Krossing, Size matters! On the way to ionic liquid systems without ion pairing, Chem. Eur. J. 20 (2014) 9794–9804, http://dx.doi.org/10.1002/chem.201400168.
[62] R. Gusain, P.S. Bakshi, S. Panda, O.P. Sharma, R. Gardas, O.P. Khatri, Physicochemical and tribophysical properties of trioctylalkylammonium bis(salicylato)borate (N888n-BScB) ionic liquids: effect of alkyl chain length, Phys. Chem. Chem. Phys. 19 (2017) 6433–6442, http://dx.doi.org/10.1039/C6CP05990B.
[63] R. Hayes, G.G. Warr, R. Atkin, Structure and nanostructure in ionic liquids, Chem. Rev. 115 (2015) 6357–6426, http://dx.doi.org/10.1021/cr500411q.
[64] Y. Shen, D.F. Kennedy, T.L. Greaves, A. Weerawardena, R.J. Mulder, N. Kirby, G. Song, C.J. Drummond, Protic ionic liquids with fluorous anions: physicochemical properties and self-assembly nanostructure, Phys. Chem. Chem. Phys. 14 (2012) 7981, http://dx.doi.org/10.1039/c2cp40463j.
[65] O. Russina, F. Lo Celso, M. Di Michiel, S. Passerini, G.B. Appetecchi, F. Castiglione, A. Mele, R. Caminiti, A. Triolo, Mesoscopic structural organization in triphilic room temperature ionic liquids, Faraday Discuss. 167 (2013) 499–513, http://dx.doi.org/10.1039/c3fd00056g.
[66] O. Hollóczki, M. Macchiagodena, H. Weber, M. Thomas, M. Brehm, A. Stark, O. Russina, A. Triolo, B. Kirchner, Triphilic ionic-liquid mixtures: fluorinated and non-fluorinated aprotic ionic-liquid mixtures, ChemPhysChem 16 (2015) 3325–3333, http://dx.doi.org/10.1002/cphc.201500473.
[67] A. Luís, K. Shimizu, J.M.M. Araújo, P.J. Carvalho, J.A. Lopes-da-Silva, J.N. Canongia Lopes, L.P.N. Rebelo, J.A.P. Coutinho, M.G. Freire, A.B. Pereiro, Influence of nanosegregation on the surface tension of fluorinated ionic liquids, Langmuir 32 (2016) 6130–6139, http://dx.doi.org/10.1021/acs.langmuir.6b00209.
[68] M.L. Ferreira, M.J. Pastoriza-Gallego, J.M.M. Araújo, J.N. Canongia Lopes, L.P.N. Rebelo, M.M. Piñeiro, K. Shimizu, A.B. Pereiro, Influence of nanosegregation on the phase behavior of fluorinated ionic liquids, J. Phys. Chem. C 121 (2017) 5415–5427, http://dx.doi.org/10.1021/acs.jpcc.7b00516.
[69] G.L. Burrell, N.F. Dunlop, F. Separovic, Non-Newtonian viscous shear thinning in ionic liquids, Soft Matter 6 (2010) 2080, http://dx.doi.org/10.1039/b916049n.
[70] G. Zarca, M. Fernández, A. Santamaría, I. Ortiz, A. Urtiaga, Non-Newtonian shear-thinning viscosity of carbon monoxide-selective ionic liquid 1-hexyl-3-methylimidazolium chloride doped with CuCl, Sep. Purif. Technol. 155 (2015) 96–100, http://dx.doi.org/10.1016/j.seppur.2015.07.032.
[71] I.T. Horvath, J. Rabai, Facile catalyst separation without water: fluorous biphase hydroformylation of olefins, Science 266 (1994) 72–75, http://dx.doi.org/10.1126/science.266.5182.72.
[72] M.M. Pereira, K.A. Kurnia, F.L. Sousa, N.J.O. Silva, J.A. Lopes-da-Silva, J.A.P. Coutinho, M.G. Freire, Contact angles and wettability of ionic liquids on polar and non-polar surfaces, Phys. Chem. Chem. Phys. 17 (2015) 31653–31661, http://dx.doi.org/10.1039/C5CP05873B.
[73] D. Rauber, F. Heib, T. Dier, D.A. Volmer, R. Hempelmann, M. Schmitt, On the physicochemical and surface properties of 1-alkyl 3-methylimidazolium bis(nonafluorobutylsulfonyl)imide ionic liquids, Colloids Surf. A: Physicochem. Eng. Aspects 529 (2017) 169–177, http://dx.doi.org/10.1016/j.colsurfa.2017.05.092.
[74] F. Heib, W.M. Munief, S. Ingebrandt, R. Hempelmann, M. Schmitt, Influence of different chemical surface patterns on the dynamic wetting behaviour on flat and silanized silicon wafers during inclining-plate measurements: an experimental investigation with the high-precision drop shape analysis approach, Colloids Surf. A: Physicochem. Eng. Aspects 508 (2016) 274–285, http://dx.doi.org/10.1016/j.colsurfa.2016.08.061.
[75] I. Delcheva, J. Ralston, D.A. Beattie, M. Krasowska, Static and dynamic wetting behaviour of ionic liquids, Adv. Colloid Interface Sci. 222 (2014) 162–171, http://dx.doi.org/10.1016/j.cis.2014.07.003.

2.6 Publication F

On the physicochemical and surface properties of 1-alkyl 3-methylimidazolium bis(nonafluorobutylsulfonyl)imide ionic liquids

Daniel Rauber, Florian Heib, Tobias Dier, Dietrich A. Volmer, Michael Schmitt, Rolf Hempelmann.

Colloids Surf. A, **2017**, 529, 169-177.

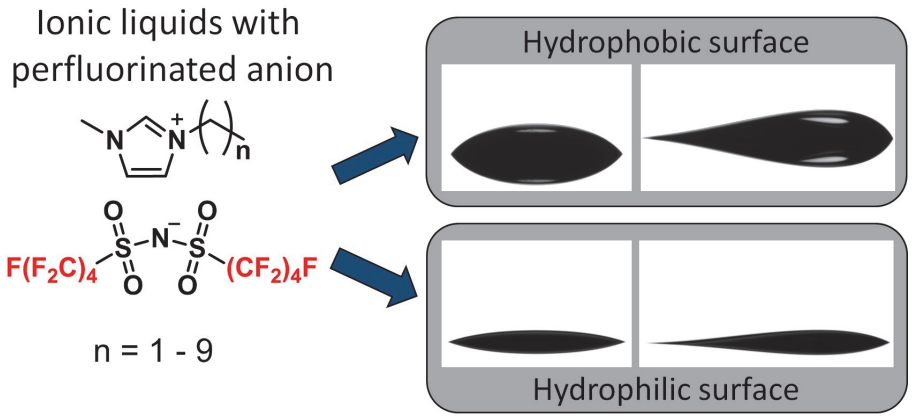

Colloids and Surfaces A 529 (2017) 169–177

Contents lists available at ScienceDirect

Colloids and Surfaces A

journal homepage: www.elsevier.com/locate/colsurfa

On the physicochemical and surface properties of 1-alkyl 3-methylimidazolium bis(nonafluorobutylsulfonyl)imide ionic liquids

Daniel Rauber[a,1], Florian Heib[a,1,*], Tobias Dier[c], Dietrich A. Volmer[c], Rolf Hempelmann[a,b], Michael Schmitt[a]

[a] Institute of Physical Chemistry, Saarland University, Campus B2.2, 66123 Saarbrücken, Germany
[b] Korean Institute of Science and Technology, Campus E 7.1, 66123 Saarbrücken, Germany
[c] Institute of Bioanalytical Chemistry, Saarland University, Campus B2.2, 66123, Saarbrücken, Germany

GRAPHICAL ABSTRACT

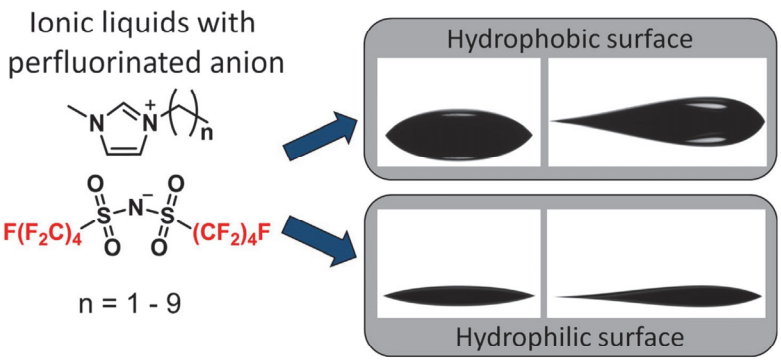

ARTICLE INFO

Keywords:
Ionic liquids contact angle
Wetting
Perfluoroalkyl-substituents
Advancing angle
Receding angle
High-precision drop shape analysis

ABSTRACT

In this study, a series of 1-alkyl-3-methylimidazolium ionic liquids with bis(nonafluorobutylsulfonyl)imide anion ([NNf_2]-anion) was synthesized. Their physicochemical properties and surface behaviours were analysed and compared to the widely used 1-alkyl-3-methylimidazolium bis(trifluoromethanesulfonyl)imides ([NTf_2]-anion) ionic liquids. For the [NNf_2]-ionic liquids, a dominating influence of the anion on physical properties such as thermal transitions, viscosity and polarity than the [NTf_2]-IL was observed. With the high-precision drop shape analysis (HPDSA) approach static and dynamic wetting behaviours on both hydrophilic and hydrophobic substrates were characterised and compared to water and imidazolium ionic liquids with perfluoroalkyl-bearing cations. The [NNf_2]-ionic liquids exhibited only minor differences of their static wetting properties, but showed noticeable differences of their dynamic wetting properties. It is shown that the wetting properties strongly depend on the degree and position of the fluorous side chain (for both in the cation and anion), but only slightly depend on the elongation of the alkyl side chain.

* Corresponding author.
E-mail address: f.heib@mx.uni-saarland.de (F. Heib).
[1] These authors contributed equally to this work.

http://dx.doi.org/10.1016/j.colsurfa.2017.05.092
Received 7 February 2017; Received in revised form 31 May 2017; Accepted 31 May 2017
Available online 03 June 2017
0927-7757/

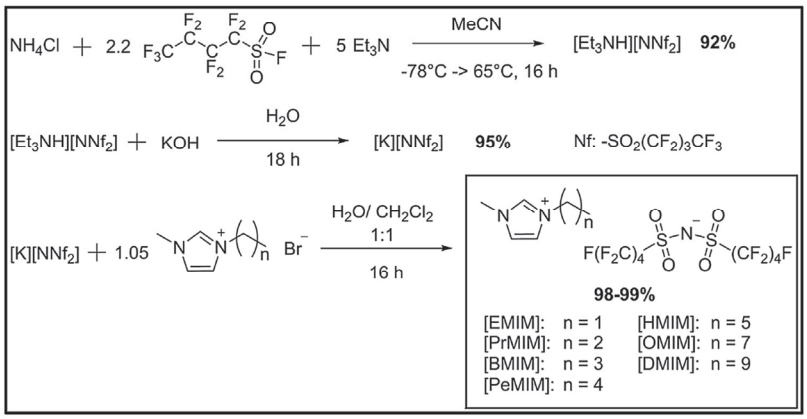

Scheme 1. Synthesis of the 1-alkyl-3-methylimidazolium bis(nonafluorobutylsulfonyl)imide [MIM][NNf_2] ionic liquids according to [19] via anion exchange reaction of the bromide IL and potassium bis(nonafluorobutylsulfonyl)imide.

1. Introduction

Ionic liquids (IL) are organic salts with melting points below 100 °C. They have attracted a significant increase of interest over the past two decades in many scientific disciplines such as chemistry, physics, electrical engineering and materials science [1–5]. This is mainly due to their unique and custom properties such as nonvolatility, non-inflammability, intrinsic conductivity along with their wide thermal and electrochemical stability. Furthermore, they offer the possibility to design entirely new and more environmental friendly processes in the context of sustainable chemistry [6]. Many applications of ionic liquids utilize unique surface characteristics of these chemicals [7,8]. Thus, analysing and modifying interfacial properties of ionic liquids is essential for their successful application [9]. The introduction of perfluorinated alkyl chains (fluorous ionic liquids, FIL) into the cation (cationic FIL) or the anion (anionic FIL) is one promising possibility to manipulate the physical and chemical properties of these liquids [10,11]. Example of FIL applications include gas separation [12], use as surfactants [13], solvents for multi-phase catalysis [14], phase-transfer-catalysts [15], liquid crystals [16,17] or artificial blood substituents [18].

In this study, we synthesized rarely studied anionic FIL, which are based on the fluorous bis(nonafluorobutylsulfonyl)imide ([NNf_2]) anion in combination with methyl-imidazolium ([MIM]) cations [19,20]. IL with perfluoroalkyl-anions exhibit some unique properties such as strongly enhanced hydrophobicity [21], gas solubility [22], reduced friction coefficients [23] and high surface activity [24]. Similar to our previous work [25], important physical properties were investigated and compared to the corresponding cationic FIL and non-fluorinated IL. [NNf_2]-IL exhibited high thermal stability and wide liquid range; they were also less polar than the corresponding widely applied bis(trifluoromethanesulfonyl)imide anion ([NTf_2]) based IL and had moderate viscosities. To characterize the wetting behaviour, contact angle measurements using the inclining plate technique were performed and analysed using the *high-precision drop shape analysis* (HPDSA) approach and statistical contact angle analysis [46,47]. Ionic liquids are rarely used as contact angle test liquids [26,27] although there is a strong potential due to their simple fabrication, low vapour pressure, high purity, poor solubility in water and possibility for simple chemical modifications to control and adjust e.g. surface tension [28–30]. The results illustrate that the properties of the test liquids (e.g. viscosity and polarity) as a function of the chain lengths and degree of fluorination strongly influence the wetting behaviour on a surface. Our results emphasize the possibility to readily modify the surface behaviour of ionic liquids via introduction of perfluorinated chains. Using this approach, it is possible to fine- tune the abilities of IL for different uses involving solid- liquid- interfaces to ensure optimal wetting behaviour and achieve higher performance. Furthermore, IL with perfluoroalkyl anions show higher degree of hydrophobicity and may therefore be used in a broad range of potential applications; for example for blending with other IL [31], for selective extraction [32] or solution as well as separation of gases [18].

2. Experimental

2.1. Materials

Details on the reagents, synthesis protocols and characterization of the used anionic FIL are described in the supporting information [72]. The two solvatochromic dyes Reichardt's Dye (90%) and Nile Red (technical grade), were purchased from Sigma Aldrich (Steinheim, Germany) and used without further purification.

2.2. Synthesis of the 1-alkyl-3-methylimidazolium bis(nonafluorobutylsulfonyl)imide ionic liquids

The seven investigated 1-alkyl-3-methylimidazolium bis(nonafluorobutylsulfonyl)imide IL were synthesized according to [19] from the corresponding bromide IL via anion exchange reaction using the slightly modified protocol illustrated in Scheme 1. The purity of the [NNf_2]-IL was confirmed by multinuclear NMR-spectroscopy, Karl-Fischer titration and electrospray ionization-mass spectrometry (ESI–MS).

2.3. Physical properties

2.3.1. Phase transition-, melting- and decomposition-temperatures

Phase transition and melting points were measured on a DSC 1 STARe System (Mettler Toledo, Gießen, Germany) equipped with a liquid nitrogen cooling system using precisely weighted samples of about 10 mg in hermetically sealed Al-crucibles. The temperature program started with a cooling rate of −1 °C/min from 25 °C to −120 °C followed by a 10 min isothermal step and a dynamic segment from −120 °C to 80 °C with heating rate of 1 °C/min. All experiments were performed at least 3-fold to ensure the correct determination of the phase transition and melting points independent from thermal history. Thermogravimetric analyses were performed on a TGA/DSC 1 STARe System (Mettler Toledo, Gießen, Germany) using approximately 10 mg sample in Al_2O_3 crucibles. The temperature program increased from 30 °C to 550 °C with heating rate of 10 °C/min under nitrogen gas flow of 25 mL/min. The melting- and decomposition- temperatures were determined as extrapolated onset temperatures.

2.3.2. Polarity

Measurements of the relative polarity were performed with the commonly used two solvatochromic dyes Reichardt's betaine Dye [33] and Nile Red [34], which are widely applied for empirical determination of polarities in liquid systems because they display large solvatochromic shifts [35,36]. The adaption of theses dyes to IL was based on their successful application to a broad range of different anions and cations [37–39]. The UV/Vis spectra were recorded on an UV SPECORD 210 Plus (Analytic Jena, Jena, Germany) spectrometer using a quartz cuvette with path length of 0.1 cm in a thermostated cell at 25 °C. The samples [EMIM][NNf_2] and [DMIM][NNf_2] were measured in supercooled state, which was possible because of strongly suppressed crystallization, as is common for most ionic liquids. The samples were prepared by adding a solution of the dye in dichloromethane to the pure ionic liquids, stirring until a homogenous phase was observed, evaporating of the solvent and drying in vacuum at ambient temperature under stirring conditions for 2d. All polarity measurements were performed at least ten times and results averaged. The corresponding $E_T(30)$ (for Reichardt's Dye) and E_{NR}-values (for Nile Red) were calculated from the maximum of the absorbance band λ_{max} of the dyes dissolved in the IL by means of equation 1 (with h the Planck constant, c the speed of light and N_A Avogadro's number)

$$E = \frac{h \cdot c \cdot N_A}{\lambda_{max} \cdot 10^6} \quad \text{eq 1}$$

For better comparison with literature results, the $E_T(30)$-values are also reported in more commonly used kcal mol^{-1} units.

2.3.3. Viscosity

Shear controlled viscosities were measured on an MCR 301 (Anton Paar, Graz, Austria) Rheometer using a cone-plate geometry with cone diameter of 50 mm and cone angle of 1.008°. The applied shear rates were increased linearly from 5 s^{-1} to 150 s^{-1}. Viscosities were reported starting from 25 °C and then varied from 30 °C to 100 °C in 10 °C intervals. The temperature was allowed to equilibrate for at least 25 min before each measurement with a maximum derivation of ± 0.1 °C.

2.3.4. Crystal structure

The crystal structure of [DMIM][NNf_2] was obtained using a suitable single crystal, which was generated by drying a solution in dichloromethane under a stream of water-free nitrogen. The data set was recorded on an AXS X8 Apex 2 (Bruker, Billerica, USA) at −143 °C using the Mo-K_α radiation from 1.052° to 26.511° Theta range collecting 64277 reflexes in total. Data refinement was done with full-matrix least-squares on F^2-method. Final R-index using anisotropic refinements of hydrogen atoms with SHELX [40] resulted in R1 = 0.0847.

2.4. Wettability and contact angle analyses

For characterization of the wetting behaviour, contact angle measurements were performed with the synthesized ionic liquids and compared to results of water contact angle measurements. Therefore, two types of surfaces (hydrophobic 90° ≤ θ_w ≤ 130° and hydrophilic 30° ≤ θ_w ≤ 90°) were used as substrates to cover a wide range of contact angles. The hydrophobic surface was prepared by vapour deposition as described previously [41,42] using 1*H*,1*H*1,2*H*,2*H*-perfluorooctyltrichlorosilane (FOTCS) (Sigma Aldrich, used as received). For the hydrophilic surface, an aged silicon wafer *p*-type 100 (MicroChemicals, Ulm, Germany) covered with its native oxide was used without further purification. The contact angle measurements were performed while continuously inclining the sample surfaces with an angular speed of $\dot{\varphi}$ = 0.57°/s (inclining-plate technique), using an OCA20 measuring system (Dataphysics, Filderstadt, Germany). During the experiment, 0.03 mL ultra-pure water (Milli-Q® Type 1 ultrapure water system, Merck KGaA, Darmstadt, Germany) and 0.03 mL ionic liquid droplets at temperature of 30.0 °C ± 0.2 °C and under saturated vapour atmosphere of the test liquid (closed measuring chamber with definable measuring positions) were video recorded with a frame rate of 25 frames/s. Due to different force distributions between horizontal and inclined measuring setup (different positions of the centres of gravity) [43,44], the advancing angles are denoted as downhill angles $\theta_d(\varphi)$, which are measured at the front edge of the drop. The receding angles are denoted as uphill angles $\theta_u(\varphi,)$ which are measured at the back edge of the drop. The static and dynamic contact angle analyses were performed using the *high-precision drop shape analysis* (HPDSA[3]) approach. This approach was developed to be able to describe and analyse highly non-axisymmetric droplets, in particular during dynamic contact angle measurements with high local precision and resolution, which is not possible with commercial contact angle analysis software. Detailed description of the HPDSA-procedure can be found in literature [45–47]. Thereby, the static wetting analyses were performed by determine the contact angle hysteresis CAH $\Delta\theta = \theta_{d,e} - \theta_{u,e} \geq 0$, which is the difference between the static advancing/downhill (wetting new surface) and static receding/uphill (formerly wetted surface) contact angle. Therefore, the boundary points X_{B1o}, (correspond to the triple points in the 2D projection) were calculated in subpixel resolution (in the range of 0.05 pixels) and the shift of the boundary points ΔX_{B1o} were estimated to identify the static downhill and uphill angles by taking the characteristic contact angle just before the contact line moved to formerly non-wetted area (static downhill angle $\theta_{d,e}(\varphi)$), respectively retracted to formerly wetted area (static uphill angle $\theta_{u,e}(\varphi)$). An example of the procedure is illustrated within supporting information [72] Figure I in Supplementary material. The dynamic wetting analyses were performed by using the recently introduced *overall curve shape analysis* [46,47,71] by fitting of a *Gompertzian function* [48,49] onto the course of contact angles $\theta_{d,u}(\varphi)$ relative to the inclination angle φ. This procedure is able to visualize the overall contact angle behaviour from a large amount of data (≈ 6000 images/contact angles per measurement//overall ≈ 45000 images/contact angles considered for the wetting analyses) with only four fitting parameters and to characterize the wettability of the surface by determine specific contact angles with lowest standard deviation. Additionally, a so-called "*residual analysis*" can be performed by subtracting the individual *Gompertzian* function from the measured course of contact angles. An example of a Gompertzian fitting is illustrated within the supporting information [72] Figure II in Supplementary material.

3. Results and discussion

3.1. Thermal properties

Phase transition, melting and decomposition temperatures of the investigated IL are summarized in Table 1. Only [EMIM][NNf_2] and [DMIM][NNf_2] had melting points slightly above room temperature, which could remain in supercooled state for several days until crystallization occurred. The length of the alkyl side chain for the [MIM][NNf_2] had only a minor influence on the melting points. The progression of the melting points with increasing alkyl side chain length showed a decrease from [EMIM][NNf_2] to [BMIM][NNf_2], which had the lowest melting point of the investigated [NNf_2]-IL followed again by increasing melting points. The DSC traces of the bis(nonafluorobutylsulfonyl)-imide IL are shown in Fig. 1.

All of the investigated IL exhibited sharp crystallization, phase transition and melting peaks in the DSC trace and no glass transition points. This behaviour is significantly different from that observed for the commonly used [NTf_2]-anion based 1-alkyl-3-methyl imidazolium

[3] M. Schmitt, HPDSA program package (beta version), DOI:10.13140/RG.2.1.1973.4805

Table 1
Phase transition (T_{trans}), melting (T_m) and decomposition temperatures (T_d), corresponding enthalpies (ΔH_{trans} and $\Delta H_{m,fus}$) and liquid range of the investigated [NNf_2]-IL.

Ionic liquid	T_{trans} [°C]	ΔH_{trans} [kJ mol^{-1}]	T_m [°C]	$\Delta H_{m,fus}$ [kJ mol^{-1}]	T_d [°C]	liquid range [°C]
[EMIM][NNf_2]	1	3.32	27	10.26	395	368
[PrMIM][NNf_2]	13	6.51	16	11.84	396	380
[BMIM][NNf_2]	–	–	11	9.79	395	384
[PeMIM][NNf_2]	−32	9.27	17	11.64	394	377
[HMIM][NNf_2]	−49	8.37	16	11.98	395	379
[OMIM][NNf_2]	−58	9.20	21	13.73	391	370
[DMIM][NNf_2]	−40	7.67	28	16.22	397	369

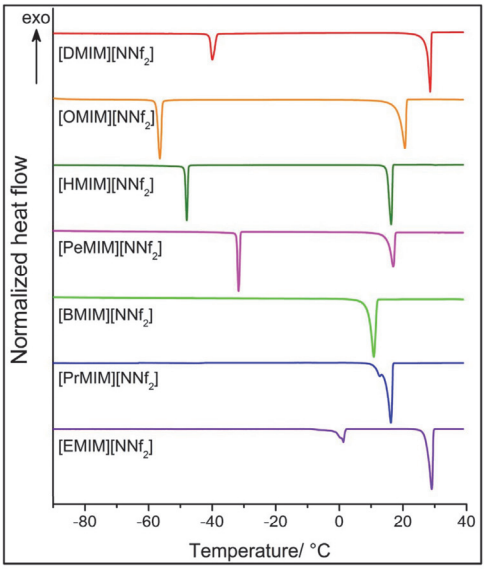

Fig. 1. DSC heating traces of the [NNf_2]-ionic liquids observed at a heating rate of 1 °C/min showing only melting points and additional phase transitions in the solid state.

IL, which showed no phase transition temperatures in solid state while some of them exhibited only glass transition points. For example, [EMIM][NTf_2] has a melting point of −18 °C [50], which is lower than [BMIM][NTf_2] at −4 °C. [OMIM][NTf_2] is reported to have only a glass transition point at −80 °C with the lowest solidification temperature [50], while [DMIM][NTf_2] again shows a melting point of 6 °C [25]. In the [NNf_2]-IL the anion had a greater influence on the melting points than seen for the more common [NTf_2]-IL, where the effect of the alkyl side chain length was more strongly pronounced. The molar enthalpies of melting $\Delta H_{m,fus}$ for the ionic liquids with [NNf_2]-anion were all in the same range, with [BMIM][NNf_2] having the lowest and [DMIM][NNf_2] the highest values. This situation is different for the corresponding [NTf_2]-based IL ($\Delta H_{m,fus}$ [EMIM][NTf_2] = 24.8 kJ mol^{-1} [50]; $\Delta H_{m,fus}$ [BMIM][NTf_2] = 22.43 kJ mol^{-1} [51]; $\Delta H_{m,fus}$ [HMIM][NTf_2] = 4.6 kJ mol^{-1} [50]). All of the investigated samples, except [BMIM][NNf_2], showed a phase transition in the crystalline state. The observed endothermic phase transitions in the solid state of one [NNf_2] ionic liquid with ammonium cation was also reported in the literature [52], where these peaks were defined as solid–solid transitions. The smallest temperature difference between phase transition and melting was observed for [PrMIM][NNf_2] with only 3 °C; the highest for [OMIM][NNf_2] at 79 °C. All investigated IL had high and nearly identical decomposition temperatures reaching almost 400 °C. The TGA curves of the [NNf_2]-IL are illustrated in Fig. 2. The observed behaviour, i.e. decomposition is mainly dependent on the

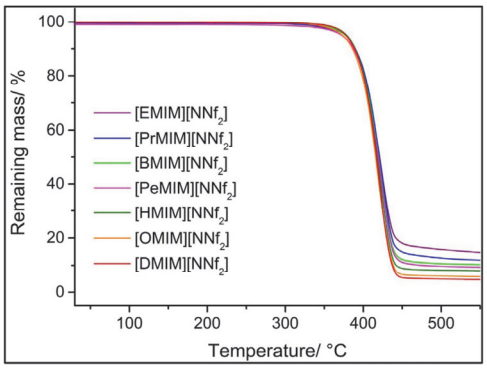

Fig. 2. TGA curves of the [NNf_2]-based ionic liquids observed at a heating rate of 10 °C/min showing similar decomposition temperatures that are independent of the attached alkyl side chain.

chemical structure of the anion and independent of the alkyl side chain length, a finding also observed for other imidazolium based IL [53]. All decomposition temperatures of IL with [NNf_2]-anion were slightly lower than those of the dialkyl imidazolium IL incorporating the [NTf_2]-anion, where T_d −values above 400 °C are reported [25,53]. The overall liquid range of the investigated IL with perfluoroalkyl anions was quite high, although smaller than for [MIM][NTf_2]-IL with [BMIM][NNf_2] having the value at 384 °C and [EMIM][NNf_2] the lowest at 368 °C.

3.2. Polarity measurements

The polarity of a liquid system is one of the important properties because it gives preliminary information about the miscibility and interactions with other compounds, which is crucial in many applications such as the use of multiphasic systems or extraction processes. Empirical determination of polarity values with solvatochromic dyes gives insight into the molecular level of solvation, rather than using macroscopic parameters such as relative permittivity, dipole moment or refractive index [38]. Polarity values of ionic liquids are of particular interest, because they allow comparison of these neoteric solvents with classical molecular liquids [54]. The measured wavelength of the absorption maxima of the two dyes in the bulk IL and the corresponding energies for the transition to the excited state are summarized in Table 2. The measured transition energies with the negative solvatochromic Reichardt's betaine dye showed a clear trend in polarity with increasing alkyl side chain length. [EMIM][NNf_2] exhibited the highest polarity with an absorption maximum of 542.6 nm, while the decyl substituted IL had the lowest polarity corresponding to a maximum at 553.4 nm, showing an overall difference of 4.3 kJ mol^{-1}. All detected values were only slightly higher than those of the widely

Table 2
Wavelengths of the maximum absorption λ_{max} of the two solvatochromic dyes and corresponding transition energies in the pure ionic liquids with [NNf_2]-anion.

Ionic liquid	Reichardt's Dye			Nile Red	
	λ_{max} [nm]	$E_T(30)$ [kJ mol^{-1}]	$E_T(30)$ [kcal mol^{-1}]	λ_{max} [nm]	E_{NR} [kJ mol^{-1}]
[EMIM][NNf_2]	542.6	220.5	52.7	539.4	221.6
[PrMIM][NNf_2]	545.7	219.2	52.4	541.6	220.9
[BMIM][NNf_2]	547.7	218.4	52.2	541.9	220.7
[PeMIM][NNf_2]	549.4	217.7	52.0	542.8	220.4
[HMIM][NNf_2]	551.9	216.8	51.8	543.1	220.3
[OMIM][NNf_2]	552.6	216.5	51.7	543.6	220.1
[DMIM][NNf_2]	553.4	216.2	51.6	544.0	219.9

used family of 1-alkyl-3-methyl imidazolium [NTf_2]-IL, ranging from $E_T(30)$ = 52.6 kcal mol^{-1} for [EMIM][NTf_2] [55] to $E_T(30)$ = 51.0 kcal mol^{-1} for [DMIM][NTf_2] [56]. The measured E_{NR}-values showed minor differences of only 1.7 kJ mol^{-1}, because of the lower solvatochromic shift, which is an intrinsic characteristic of this dye. The polarities measured with Nile Red displayed a similar trend to Reichardt's Dye, where the elongation of the alkyl chain leaded to a decrease of polarity. Interestingly, the situation is different when comparing this to the [NTf_2]-liquid salts for the polarity measurements with Nile Red. The measured wavelength of the absorption maxima ranged from 548.7 nm for [BMIM][NTf_2] to 547.5 nm [37] for [DMIM][NTf_2] [56], exhibiting significant differences to the [NNf_2]-IL and a consequently greater influence of the anion. These results indicate that polarity measurements for a comparison of the solvent behaviour of ionic liquids should be carried out using multiple probe molecules, to observe a more complete picture of the interactions on a molecular level.

3.3. Rheological behaviour

The rheological properties of a liquid system are very important in practical applications. In case of ionic liquids, viscosity is also related to the conductivity and may give some insight into the numerous competing interactions on a molecular level. For ionic liquids, these are mainly the electrostatic Coulomb and van-der-Waals interactions, hydrogen bonds and other interionic interactions [57]. For the [NNf_2]-IL with perfluoroalkyl chains in the anion, a preferred interaction between the fluorinated groups could also be considered, as it is observed in the crystal structure (section 3.4). The formation of fluorous domains, which can even lead to a tricontinous nanostructure, is a behaviour previously reported for a series of ionic liquids with either perfluoro groups in the cation or the anion [58,59]. These aggregation phenomena in bulk IL are driven by the preferred interaction of the highly lipophilic and hardly polarizable perfluorinated groups rather than the interaction with alkyl chains or polar ionic parts of the molecules. The viscosity dependence of the different IL with the [NNf_2]-anion on temperature is shown in Fig. 3. The plots of shear force and viscosity as a function of the applied shear rate can be found in the supporting information [72]. For the investigated bis(nonafluorobutylsulfonyl) imide IL, the viscosities at 25 °C ranged from 365 mPa s for [PrMIM][NNf_2] to 448 mPa s for [OMIM][NNf_2] exhibiting an increase in viscosity with elongation of the alkyl side group in the imidazolium cation. All compounds showed an exponential decrease of viscosity with temperature and only Newtonian behaviour with no time or shear rate dependent flow in the investigated temperature and shear-rate ranges. The investigated perfluorinated IL showed increased viscosities when compared to the [NTf_2]-IL, with values slightly larger than 300 mPa s. This indicates the high influence of the anion on viscosity, whereas the increased viscosity for the [NNf_2]-IL may result from the formation of different domain structures on a nanoscale, such as alkyl, fluorous and ionic domains with unbiased interactions between them. Also, the relative stiffness and conformational inflexibility of perfluorinated alkyl groups [60] surely will contribute to the viscosity increase.

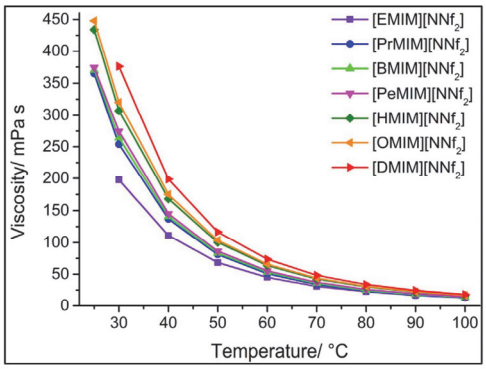

Fig. 3. Viscosities of the [NNf_2]-ionic liquids in dependence on the temperature showing exponential decrease with temperature and increase upon elongation of the alkyl side chain length.

Table 3
Lattice parameters of [DMIM][NNf_2].

Unit cell vector length [Å]	Unit cell angles [°]
a = 20.250	α = 90°
b = 10.3928	β = 107.040°
c = 32.213	γ = 90°

3.4. Crystal structure of [DMIM][NNf_2]

[DMIM][NNf_2] crystallizes in a monoclinic crystal system with the space group $P2_1$ with the lattice parameters given in Table 3.

All four independent anions are coordinated with the nitrogen atom of one of the charge bearing imidazolium cores of the cations. In all anions, the nonafluorobutylsulfonyl groups had a trans configuration, which is also the by far most common geometry for [NTf_2]-anions in the crystal state [61]. Three of the decyl chains exhibited a cis configuration of C_2 towards the C_3 atom, while all fluorous chains showed a trans configuration at each position of the chain. The favoured homogenous interactions between the three molecular structures of different polarity (ionic, perfluoroalkyl and alkyl) leads to a formation of differently packed domains, which are visualized in Fig. 4.

The occurrence of layered structures in the crystal state was also reported for other types of imidazolium IL [62]. The limited miscibility of perfluorocarbon with hydrocarbon fragments is also known for some IL in the liquid state, which leads to tricontinous nanostructures in the bulk liquid [58,63,64] and is also observed in the crystalline state of the triphilic [DMIM][NNf_2] here.

3.5. Wetting analyses: contact angle measurements and motion behaviours

For the sake of clarity, the results of the contact angle analyses for hydrophobic modified silicon surface are presented within the main manuscript, whereas results of the contact angle analyses for the hydrophilic silicon surface are presented within the supporting information [72]. In contrast to standard molecular test liquids, ionic liquids are derived from organic cations and non-coordinating, highly delocalized anions, which together form liquid salts with non-directed interionic interactions. That means the interionic interactions between the liquid and the surface considerably affect the wetting situation on the surface. As illustrated in [25], this effect was particularly pronounced during the drop application of the cationic FIL. In the case of the anionic FIL this effect was not noticeable. However, the motion behaviours of the droplets were significantly influenced by the ionic character of these liquids (Figures IV and V within the supporting information [72]). The contact angle measurements with water as test liquid (Figures IVa and Va in Supplementary material [72]) resulted in a contact angle range between 90° to 115°, which proves the formation of a perfluorooctylsiloxane coating on the surface as demonstrated in previous studies [25,41,42]. In comparison, the contact angle range for the anionic FIL was between 0° to 70° due to the smaller liquid-vapour surface tension $\gamma_{l,v}$ and illustrated a very pronounced pinning at the uphill side similar to the cationic FIL [25]. At this point, it should be noted that the reproducible and comparable analysis of these highly non-axisymmetric droplets with contact angles down to nearly 0° is only possible with the *Fast-Circle-Fitting* implemented in the HPDSA

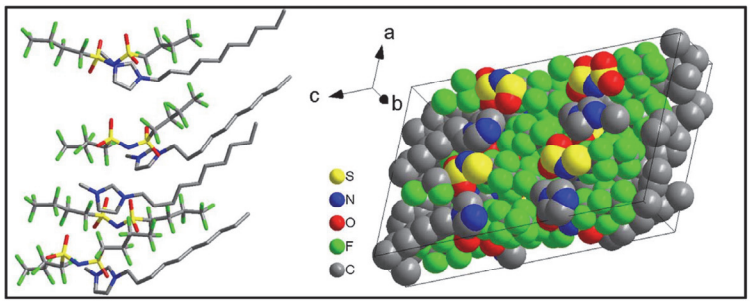

Fig. 4. Orientation of the anion towards the imidazolium core (left side) of the cation and the formation of three different domains through favoured homogenous interactions in the unit cell (right side) in the crystal of [DMIM][NNf_2]. Hydrogen atoms are omitted for clarity.

Table 4
Results for the determination of the static downhill $\theta_{d,e}(\varphi)$ and static uphill $\theta_{u,e}(\varphi)$ angles with the HPDSA procedure on the hydrophobic modified silicon surface.

Test liquid	$\theta_{d,e}(\varphi)$ [°]	φ_d [°]	$\theta_{u,e}(\varphi)$ [°]	φ_u [°]	$\Delta\theta$ [°]
H_2O	108.4 ± 1.2	8.6 ± 1.1	99.1 ± 1.3	7.5 ± 1.3	9.3 ± 0.7
[EMIM] [NNf_2]	52.6 ± 0.8	1.0 ± 0.2	44.3 ± 1.7	4.5 ± 1.0	8.4 ± 2.4
[PrMIM] [NNf_2]	50.5 ± 0.6	2.2 ± 0.1	41.0 ± 0.9	5.1 ± 0.4	9.5 ± 1.1
[BMIM] [NNf_2]	49.5 ± 0.4	1.8 ± 0.4	42.5 ± 0.4	3.6 ± 0.3	7.0 ± 0.7
[PeMIM] [NNf_2]	47.6 ± 0.9	1.3 ± 0.4	40.0 ± 1.1	4.4 ± 0.2,	7.6 ± 0.4
[HMIM] [NNf_2]	47.7 ± 1.4	1.5 ± 0.4	37.8 ± 1.4	5.5 ± 0.4	9.9 ± 1.1
[OMIM] [NNf_2]	46.7 ± 0.2	2.0 ± 0.3	38.8 ± 0.4	4.3 ± 0.4	7.9 ± 0.5

program. If the measurements with the ionic liquids were compared regarding the influence of the chain lengths, it was observed that the initial contact angles $\theta_{d,u}(0^\circ)$ only slightly decreased from 52° ([EMIM][NNf_2]) to 44° ([OMIM][NNf_2]). Furthermore, the range of the downhill angle ($\Delta\theta_d = \theta_d(\varphi)_{max} - \theta_d(\varphi)_{min}$) increased with increasing chain lengths in the cation from 2 to 8, which illustrated the influence of the molecular structure, polarity and viscosity on the pinning behaviour. To characterize pinning effects on the surface the contact angle hysteresis CAH $\Delta\theta = \theta_{d,e} - \theta_{r,e} \geq 0$ were determined taking the characteristic contact angle just before the contact line moved to formerly non-wetted area (static downhill angle $\theta_{d,e}(\varphi)$), respectively retracted to formerly wetted area (static uphill angle $\theta_{u,e}(\varphi)$). The results are summarized in Table 4.

All investigated anionic FIL exhibited small critical inclination angles on the downhill ($\varphi_d \leq 2.2^\circ$) and uphill ($\varphi_u \leq 5.5^\circ$) side and small standard deviations. The static downhill $\theta_{d,e}(\varphi)$ and uphill angles $\theta_{u,e}(\varphi)$ only slightly increased, respectively decreased, if the chain lengths increased from 2 to 8. This resulted in approximately the same CAH for all investigated FIL. As a consequence, the variation of the alky chain lengths of the anionic FIL had significantly less influence on the static wetting properties in contrast to the variation of the degree of fluorination, compared to the measurements with the cationic FIL [25], as illustrated in Fig. 5.

Beside the static wetting characteristics, the characterisation of the dynamic wetting properties is of major importance for many applications such as microfluidics, electrochemical applications, lubrication or tribology and friction [65–70]. The strong pinning at the uphill side down to contact angle of about 0° (Figures IV and V [72]) cannot be investigated by only analysing the static wetting situation. For example, the drain-off behaviour of droplets cannot be characterised by the critical inclination angles $\varphi_{d,u}$ because this inclination angles only indicate the point when the drop motion starts, but do not contain any information on the process and velocity of the drop motion and do not

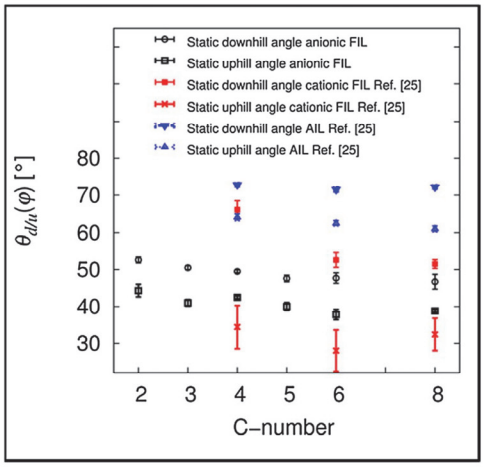

Fig. 5. Measured static downhill $\theta_{d,e}(\varphi)$ and uphill $\theta_{u,e}(\varphi)$ angles with standard deviations from contact angle measurements with ionic liquids in dependence on the number of C atoms in the side chain for the anionic FIL (black, this study), the cationic FIL (red, Ref. [25]) and the non-fluorinated AIL (blue, Ref. [25]). (For interpretation of the references to colour in this figure legend, the reader is referred to the web version of this article.)

indicate a complete roll-off of the droplet. But the characterisation and understanding of these quantities can be crucial if dynamic wetting processes are involved. Therefore, the *overall curve shape analysis* by *Gompertzian* fittings was used to characterize the dynamic wetting behaviour. Contrary to the static wetting analyses, this approach also considered the quasi-static and dynamic movement of the droplets during the measurements so that e.g. strong pinning effects on the uphill side (Figures IVb–IVd, Figures Vb–Vd in Supplementary material [72]) could be analysed, which resulted in an overall characterization of the wettability of the surface. By averaging the data from the individual fittings (see supporting information [72], Tables I to XIV in Supplementary material) the trend of the measurements can be represented by an averaged *Gompertzian* function, which is able to characterize the wetting behaviour from very large amount of contact angle data (≈6000 images contact angles per measurements) by only four fitting parameters. An additional benefit of this procedure is the possibility to identify contact angles with smallest standard deviations θ_d, θ_u. The averaged *Gompertzian* function are illustrated within the supporting information [72] in Figures VI and VII and represents the average dynamic wetting situation on the hydrophobic modified silicon surface with 0.03 mL droplets of the anionic FIL, respectively water as test liquid. Due to the fact that *Gompertzian* functions start at minus infinity [48,49], physically meaningful values are only obtainable within the fitting range ($0^\circ \leq \varphi_{d,u} \leq \varphi_{Ld,Lu}$). If an inclining plate experiment on ideal solid surface (chemically and physically

Table 5
Overview about the results of the overall curve shape analysis by Gompertzian fitting to identify the contact angle/inclination angle pairs $\theta_{d,u}/\varphi_{d,u}$ with lowest standard deviation on a hydrophobic modified silicon surface.

Test liquid	$\theta_d \pm \sigma_d$ [°]	φ_d [°]	$\theta_{Ld} \pm \sigma_{Ld}$ [°]	φ_{Ld} [°]	$\theta_u \pm \sigma_u$ [°]	φ_u [°]	$\theta_{Lu} \pm \sigma_u$ [°]	φ_{Lu} [°]
H_2O	105.6 ± 0.4	2.6	110.1 ± 0.5	10.7	98.6 ± 1.2	8.6	96.1 ± 1.3	13.8
[EMIM][NNf_2]	52.7 ± 0.6	0.1	56.0 ± 1.2	5.0	52.7 ± 0.3	0.1	26.4 ± 3.6	14.4
[PrMIM][NNf_2]	50.3 ± 0.3	0.9	53.5 ± 0.4	9.0	49.8 ± 0.7	7.1	21.1 ± 2.5	14.4
[BMIM][NNf_2]	52.6 ± 0.7	3.9	55.0 ± 1.0	9.2	47.5 ± 0.6	0.1	18.4 ± 1.2	14.3
[PeMIM][NNf_2]	47.9 ± 0.5	1.7	50.4 ± 1.4	8.8	41.7 ± 0.5	3.7	14.3 ± 2.5	15.2
[HMIM][NNf_2]	48.4 ± 1.0	1.3	56.5 ± 1.1	12.6	13.3 ± 0.5	16.9	5.1 ± 1.5	20.0
[OMIM][NNf_2]	50.4 ± 0.4	5.2	55.4 ± 0.7	12.2	39.9 ± 0.2	4.1	6.6 ± 0.4	20.2

homogeneous) is now considered, an intersection point (depending on the initial situation) of all *Gompertzian* functions for every measuring position should exist, which corresponds to a characteristic contact angle/inclination angle pair ($\theta_{d,u}/\varphi_{d,u}$). However, the experimental situation on a real solid surface is much more complex. This will result in a variance of the contact angle behaviour depending on the degree of local physical and chemical non-homogeneities. In addition to the physical and chemical properties of the surface, different properties of the test liquids, e.g. surface tension, viscosity and polarity, also affect the motion behaviour on a solid surface. Thus, the identification of a contact angle/inclination angle pair/range with lowest standard deviation is appropriate to characterize the overall wettability of the surface. The characteristic contact angle/inclination angle pairs with smallest standard deviation and the contact angle/inclination angle pairs for the fitting limits for the downhill φ_{Ld} and uphill motion φ_{Lu} are summarized in Table 5.

The contact angles with lowest standard deviation $\theta_{d,u}$ were located within the fitting range and therefore called "real". At this point it is noted that the contact angle/inclination angle pairs in Table 5 do not necessarily describe a "good wettable" or "bad wettable" surface. They only indicate the value of the highest statistical certainty and the range, where the standard deviations of measurements was the lowest. The difference in standard deviation can be used to investigate the homogeneity of the surface [71]. As illustrated in Table 5, the downhill angles with lowest standard deviations θ_d were located at an inclination angle $\varphi_d \leq 5.2°$. This example illustrates, that e.g. the characterization of the wettability of a surface by taking the initial contact angle is neither reliable nor reproducible. Beside the identification of contact angle/inclination angle pairs with lowest standard deviation, the overall curve shape analysis by *Gompertzian* fitting can be used to analyse the pinning and drain-off behaviour of liquids on solid surfaces. In particular the fitting parameters *A* (Amplitude of the contact angles ≡difference between the theoretical smallest and largest contact angle) and *k* (slope of the data points) determine the course of the averaged *Gompertzian* function. That means that weak pinning results in small amplitudes *A* and large slopes *k*, whereas strong pinning results in large amplitudes and small slopes of the data points. The averaged data from the fittings are summarized in Table 6 for the downhill and Table 7 for the uphill angles.

Regarding the downhill (wetting new surface) and uphill (formerly wetted surface) motion, the amplitude *A* increased whereas the slope *k* decreased if the carbon number in the side chain of the anionic FIL varied from 2 to 8. As previously described, the variation of chain lengths had no significant influence of the static wetting properties. But the dynamic wetting processes were strongly influenced by the variation of chain lengths. In comparison to the previously investigated cationic FIL [25], the *k*-values for the downhill and uphill sides were generally smaller (Fig. 6). This example illustrates that the overall wettability of a surface strongly depends on the molecular structure of the test liquid. Furthermore, to analyse the wetting properties of surfaces by only performing static contact angle analyses is insufficient to characterize the overall wettability, in particular if dynamic wetting processes are involved.

4. Conclusions

The physical properties and surface behaviour of rarely investigated [MIM] ionic liquids with the perfluorinated [NNf_2]-anion were investigated in this study. The single crystal structure of [DMIM][NNf_2] revealed three domains of different polarity, which is also known for other types of FIL and expected to occur in the liquid state as well. In the investigated samples, the anion had a larger influence on the physical properties than the elongation of the alkyl side chain in the cation. The [NNf_2]-IL exhibited high thermal stabilities, moderate viscosities and lower polarities in comparison to the broadly distributed [NTf_2]-IL. In this regard, the wetting analyses using the *HPDSA* approach illustrated that the static wetting properties mainly depended on the degree of fluorination of the ionic liquid and only slightly differed as a function of the elongation of the alkyl side chain. In comparison to the cationic [NTf_2]-FIL and AIL, it was clearly shown that the dynamic wetting properties strongly depended on the degree of fluorination and the introduction of perfluorinated chains either into the cation or the anion. Strong pinning only occurred if FIL were used as test liquids, which resulted in large contact angle amplitudes *A* and small slopes of the data points *k*. In this study, we illustrated the potential of the *Gompertzian fitting* procedure to analyse dynamic wetting properties in detail and to classify a liquid-solid combination in terms of their *A*- and *k*-values, which are important parameters when liquids and liquid-solid

Table 6
Summary of the averaged data from the Gompertzian fitting for the downhill angles of the FIL and water as test liquids on the hydrophobic modified silicon surface.

Test liquid	θ_{shift} [°]	*A* [°]	*k* [°$^{-1}$]	φ_{shift} [°]	θ_{di}^{30} [°]	φ_{Ld} [°]	$f_{Ld}(\varphi_{Ld}) = \theta_{Ld}^{30}(\varphi_{Ld})$[°]
H_2O	102.88	10.47	0.162	4.52	104.2	10.7	110.1
[EMIM][NNf_2]	52.14	4.23	0.626	1.19	52.7	5.0	56.0
[PrMIM][NNf_2]	48.83	4.63	0.546	1.20	49.5	9.0	53.4
[BMIM][NNf_2]	45.29	10.84	0.239	0.00	49.3	9.2	55.0
[PeMIM][NNf_2]	44.16	6.62	0.312	0.00	46.6	8.8	50.4
[HMIM][NNf_2]	39.48	20.63	0.132	0.00	47.1	12.6	56.5
[OMIM][NNf_2]	37.16	23.10	0.123	0.41	45.2	12.2	55.4

Table 7
Summary of the averaged data from the *Gompertzian* fitting for the uphill angles of the FIL and water as test liquids on the hydrophobic modified silicon surface.

Test liquid	θ_{shift} [°]	A [°]	k [°$^{-1}$]	φ_{shift} [°]	$f(0°) = \theta_{u_1}^{30}$ [°]	φ_{Lu} [°]	$f_{Ld}(\varphi_{Lu}) = \theta_{Lu}^{30}(\varphi_{Lu})$[°]
H_2O	105.33	−12.90	0.134	−5.26	103.6	13.8	96.1
[EMIM][NNf_2]	53.22	−44.05	0.131	9.04	51.5	14.4	26.4
[PrMIM][NNf_2]	53.22	−76.66	0.087	12.69	49.5	14.4	20.7
[BMIM][NNf_2]	50.32	−110.92	0.076	17.19	47.6	14.3	18.4
[PeMIM][NNf_2]	48.58	−109.86	0.075	17.21	45.7	15.2	14.2
[HMIM][NNf_2]	49.36	−108.21	0.066	18.32	45.6	20.0	5.2
[OMIM][NNf_2]	48.15	−133.37	0.054	23.05	44.0	20.2	6.6

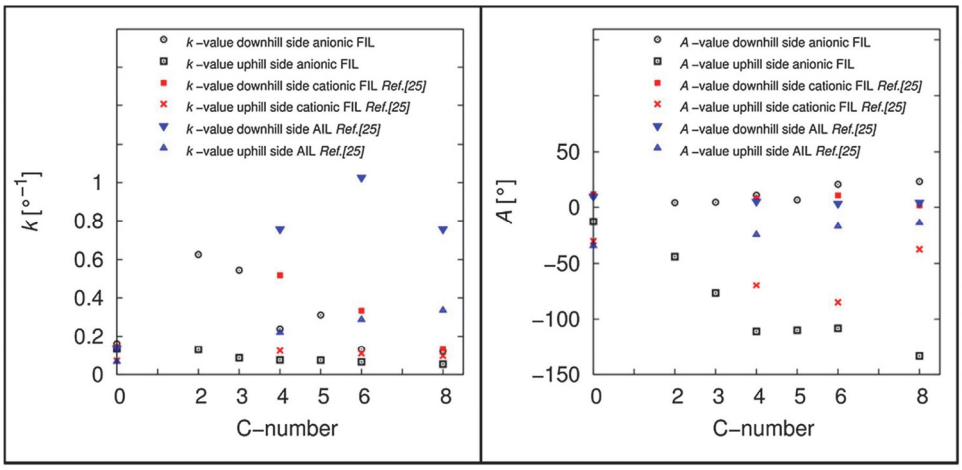

Fig. 6. Plot of the *k*-values (left) and plot of the *A*-values (right) from the averaged *Gompertzian* function against the number of carbon atoms in the side chain of the anionic FIL (black, this study) the cationic FIL (red, Ref. [25]) and the non-fluorinated AIL (blue, Ref. [25]). The C number = 0 refers to the contact angle measurements with water as test liquid. (For interpretation of the references to colour in this figure legend, the reader is referred to the web version of this article.)

interfaces are involved in processes. In this regard, it was illustrated that by introducing fluorous side chains and varying the degree of fluorination the investigated AIL, cationic and anionic FIL exhibited great potential for fine-tuning their abilities for different applications, where solid-liquid-interfaces are involved to ensure an optimal wetting behaviour and an achievement of higher performances, which make them promising for future research.

Acknowledgements

The authors gratefully acknowledge the Deutsche Bundesstiftung Umwelt (DBU) (31925-41) for financial support, Dr. Volker Huch for the crystal structure analyses and Prof. Wulff Possart for his support.

Appendix A. Supplementary data

Supplementary data associated with this article can be found, in the online version, at http://dx.doi.org/10.1016/j.colsurfa.2017.05.092.

References

[1] T. Welton, Room-temperature ionic liquids. Solvents for synthesis and catalysis, Chem. Rev. 99 (1999) 2071–2083.
[2] P. Anatas, Stark, Handbook of Green Chemistry, Volume 6, Green Solvents, Ionic Liquids, WILEY-VCH, Weinheim, 2013.
[3] D.R. MacFarlane, et al., Energy applications of ionic liquids, Energy Environ. Sci. 7 (2014) 232–250.
[4] R.D. Rogers, K.R. Seddon, Ionic liquids–solvents of the future? Science 302 (2003) 792–793.
[5] G.G. Eshetu, M. Armand, H. Ohno, B. Scrosati, S. Passerini, Ionic liquids as tailored media for the synthesis and processing of energy conversion materials, Energy Environ. Sci. 9 (2016) 49–61.
[6] F. Kerton, R. Marriott, Alternative Solvents for Green Chemistry, 2nd edition, RSC Green Chemistry Book Series, Cambridge, 2013.
[7] M. Mezger, et al., Molecular layering of fluorinated ionic liquids at a charged sapphire (0001) surface, Science 322 (2008) 424–428.
[8] H. Liu, Y. Liu, J. Li, Ionic liquids in surface electrochemistry, Phys. Chem. Chem. Phys. 12 (2010) 1685–1697.
[9] I. Delcheva, J. Ralston, D.A. Beattie, M. Krasowska, Static and dynamic wetting behaviour of ionic liquids, Adv. Colloid Interface Sci. 222 (2015) 162–171.
[10] Z.-B. Zhou, H. Matsumoto, K. Tatsumi, Cyclic quaternary ammonium ionic liquids with perfluoroalkyltrifluoroborates: synthesis, characterization, and propertie, Chem. Eur. J. 12 (2006) 2196–2212.
[11] H. Xue, J.M. Shreeve, Ionic liquids with fluorine-containing cations, Eur. J. Inorg. Chem. 13 (2005) 2573–2580.
[12] J.E. Bara, C.J. Gabriel, T.K. Carlisle, D.E. Camper, A. Finotello, D.L. Gin, R.D. Noble, Gas separations in fluoroalkyl-functionalized room-temperature ionic liquids using supported liquid membranes, Chem. Eng. J. 147 (2009) 43–50.
[13] T.L. Merrigan, E.D. Bates, S.C. Dorman Jr., J.H. Davis, New fluorous ionic liquids function as surfactants in conventional room-temperature ionic liquid, Chem. Commun. (2000) 2051–2052.
[14] F. Broeke, B.-J. Deelman, G.v. Koten, A highly fluorous room-Temperature ionic liquid exhibiting fluorous biphasic behavior and its use in catalyst recycling, Org. Lett. 4 (2002) 3851–3854.
[15] C. Emnet, K.M. Weber, J.A. Vidal, C.S. Consorti, A.M. Stuart, J.A. Gladysz, Syntheses and properties of fluorous quaternary phosphonium salts that bear four ponytails; new candidates for phase transfer catalysts and ionic liquids, Adv. Synth. Catal. 348 (2006) 1625–1634.
[16] A. Abate, et al., Anisotropic ionic conductivity in fluorinated ionic liquid crystals suitable for optoelectronic applications, J. Mater. Chem. A 1 (2013) 6572–6578.
[17] C. Rocaboy, F. Hampel, J.A. Gladysz, Syntheses and reactivities of disubstituted and trisubstituted fluorous pyridines with high fluorous phase affinities: solid state, liquid crystal, and ionic liquid-Phase properties, J. Org. Chem. 67 (2002) 6863–6870.
[18] A.B. Pereiro, et al., Fluorinated ionic liquids: properties and applications, ACS Sustain Chem Eng. 1 (2013) 427–439.
[19] S.K. Quek, I.M. Lyapkalo, H.V. Huynh, Synthesis and properties of N,N′-dialkylimidazolium bis(nonafluorobutane-1-sulfonyl)imides: a new subfamily of ionic liquids, Tetrahedron 62 (2006) 3137–3245.
[20] J. Zhang, G.R. Martin, D.D. DesMarteau, Direct methylation and trifluoroethylation

of imidazole and pyridine derivatives, Chem. Commun. (2003) 2334–2335.
[21] N.V. Ignat'ev, U. Welz-Biermann, A. Kucheryna, G. Bissky, H. Willner, New ionic liquids with tris(perfluoroalkyl)trifluorophosphate (FAP) anions, J. Fluorine Chem. 126 (2005) 1150–1159.
[22] M.J. Muldoon, S.N.V.K. Aki, J.L. Anderson, J.K. Dixon, J.F. Brennecke, Improving carbon dioxide solubility in ionic liquids, J. Phys. Chem. B 111 (2007) 9001–9009.
[23] I. Minami, M. Kita, T. Kubo, H. Nanao, S. Mori, The tribological properties of ionic liquids composed of trifluorotris(pentafluoroethyl) phosphate as a hydrophobic anion, Tribol. Lett. 30 (2008) 215–233.
[24] J.M. Breen, S. Olejarz, K.R. Seddon, Microwave synthesis of short-Chained fluorinated ionic liquids and their surface properties, ACS Sustain Chem Eng. 4 (2016) 387–391.
[25] D. Rauber, F. Heib, M. Schmitt, R. Hempelmann, Influence of perfluoroalkyl-chains on the surface properties of 1-methylimidazolium bis(trifluoromethanesulfonyl) imide ionic liquid, J. Mol. Liq. 216 (2016) 246–258.
[26] J. Restolho, José L. Mata, Benilde Saramago, On the interfacial behavior of ionic liquids: surface tensions and contact angles, J. Colloid Interface Sci. 340 (2009) 82–86.
[27] T. Batchelor, J. Cunder, A.Y. Fadeev, Wetting study of imidazolium ionic liquids, J. Colloid Interface Sci. 330 (2009) 415–420.
[28] R. Sedev, Surface tension, interfacial tension and contact angles of ionic liquids, Curr. Opin. Colloid Interface Sci. 16 (2011) 310–316.
[29] L. Gao, T.J. McCarthy, Ionic liquids are useful contact angle probe fluids, J. Am. Chem. Soc. 129 (2007) 3804–3805.
[30] J.W. Krumpfer, P. Bian, P. Zheng, L. Gao, T.J. McCarthy, Contact angle hysteresis on superhydrophobic surfaces: an ionic liquid probe fluid offers mechanistic insight, Langmuir 27 (2011) 2166–2169.
[31] F. Castiglione, et al., Blending ionic liquids: how physico-chemical properties change, Phys. Chem. Chem. Phys. 12 (2010) 1784–1792.
[32] C. Yao, W.R. Pitner, J.L. Anderson, Ionic liquids containing the tris(pentafluoroethyl)trifluorophosphate anion: a new class of highly selective and ultra hydrophobic solvents for the extraction of polycyclic aromatic hydrocarbons using single drop microextraction, Anal. Chem. 81 (2009) 5054–5063.
[33] K. Dimroth, C. Reichardt, T. Siepmann, F. Bohlmann, Über pyridinium-N-phenolbetaine und ihre verwendung zur charakterisierung der polarität von Lösungsmitteln, Liebigs Ann. 661 (1963) 1–37.
[34] J.F. Deye, T.A. Berger, A.G. Anderson, Nile Red as a solvatochromic dye for measuring solvent strength in normal liquids and mixtures of normal liquids with supercritical and near critical fluids, Anal. Chem. 62 (1990) 615–622.
[35] C. Reichardt, Solvatochromic dyes as solvent polarity indicators, Chem. Rev. 94 (1994) 2319–2358.
[36] J.P. Cerón-Carrasco, D. Jacquemin, C. Laurence, A. Planchat, C. Reichardt, K. Sraïdi, Solvent polarity scales: determination of new $E_T(30)$ values for 84 organic solvents, J. Phys. Org. Chem. 27 (2014) 512–518.
[37] A.J. Carmichael, K.R. Seddon, Polarity study of some 1-alkyl-3-methylimidazolium ambient-temperature ionic liquids with the solvatochromic dye, Nile Red, J. Phys. Org. Chem. 13 (2000) 591–595.
[38] C. Reichardt, Polarity of ionic liquids determined empirically by means of solvatochromic pyridinium N-phenolate betaine dyes, Green Chem. 7 (2005) 339–351.
[39] S. Saha, P.K. Mandal, A. Samanta, Solvation dynamics of Nile Red in a room temperature ionic liquid using streak camera, Phys. Chem. Chem. Phys. (2004) 3106–3110.
[40] G.M. Sheldrick, A short history of *SHELX*, Acta Cryst. A 64 (2008) 112–122.
[41] M. Schmitt, R. Hempelmann, S. Ingebrandt, W. Munief, D. Durneata, K. Groß, F. Heib, Statistical approach for contact angle determination on inclining surfaces: *slow-moving* analyses of *non-axisymmetric* drops on a flat silanized silicon wafer, Int. J. Adhes. Adhes. 55 (2014) 123–131.
[42] F. Heib, R. Hempelmann, W.M. Munief, S. Ingebrandt, F. Fug, W. Possart, K. Groß, M. Schmitt, High-precision drop shape analysis (HPDSA) of quasistatic contact angles on silanized silicon wafers with different surface topographies during inclining-plate measurements: influence of the surface roughness on the contact line dynamic, Appl. Surf. Sci. 342 (2015) 11–25.
[43] M. Schmitt, R. Hempelmann, F. Heib, Experimental investigation of contact angles on horizontal and inclined surfaces part I: flat silicon oxide surfaces, Z. Phys. Chem. 228 (2014) 11–25.
[44] M. Schmitt, R. Hempelmann, F. Heib, Experimental investigation of dynamic contact angles on horizontal and inclined surfaces part II: rough homogeneous surfaces, Z. Phys. Chem. 228 (2014) 629–648.
[45] M. Schmitt, R. Hempelmann, F. Heib, High-precision drop shape analysis on inclining flat surfaces: introduction and comparison of this special method with commercial contact angle analysis, J. Chem. Phys 139 (2013) 134201.
[46] M. Schmitt, K. Groß, J. Grub, F. Heib, Detailed statistical contact angle analyses; slow moving drops on inclining silicon-oxide surfaces, J. Colloid Interface Sci. 447 (2015) 229–239.
[47] M. Schmitt, J. Grub, F. Heib, Statistical contact angle analyses; slow moving drops on a horizontal silicon-oxide surface, J. Colloid Interface Sci. 447 (2015) 248–253.
[48] B. Gompertz, On the nature of the function expressive of the law of human mortality, and on a new mode of determining the value of life contingencies, Philos. Trans. R. Soc. London I (1825) 513–518.
[49] M. Schmitt, R. Schulze-Pilot, R. Hempelmann, Kinetics of bulk polymerisation and Gompertz's law, Phys. Chem. Chem. Phys. 13 (2011) 690–695.
[50] H. Tokuda, K. Hayamizu, K. Ishii, M.A.B.H. Susan, M. Watanabe, Physicochemical properties and structures of room temperature ionic liquids. 2. variation of alkyl chain length in imidazolium cation, J. Phys. Chem. B 109 (2005) 6103–6110.
[51] J. Troncoso, C.A. Cerdeirin, Y.A. Sanmamed, L. Romani, L.P.N. Rebelo, Thermodynamic properties of imidazolium-based ionic liquids: densities, heat capacities, and enthalpies of fusion of [bmim][PF_6] and [bmim][NTf_2], J. Chem. Eng. Data 51 (2006) 1856–1859.
[52] Y. Yoshida, G. Saito, Ionic liquids based on diethylmethyl(2-methoxyethyl)ammonium cations and bis(perfluoroalkanesulfonyl)amide anions: influence of anion structure on liquid properties, Phys. Chem. Chem. Phys. 13 (2011) 20302–20310.
[53] M. Villanueva, A. Coronas, J. Garcia, J. Salgado, Thermal stability of ionic liquids for their application as new absorbents, Ind. Eng. Chem. Res. 53 (2013) 15718–15727.
[54] P.G. Jessop, D.A. Jessop, D. Fu, L. Phan, Solvatochromic parameters for solvents of interest in green chemistry, Green Chem. 14 (2012) 1245–1259.
[55] K.A. Fletcher, S.N. Baker, G.A. Baker, S. Pandey, Probing solute and solvent interactions within binary ionic liquid mixtures, New J. Chem. 27 (2003) 1706–1712.
[56] S.V. Dzyuba, R.A. Bartsch, Expanding the polarity range of ionic liquids, Tetrahedron Lett. 43 (2002) 4657–4659.
[57] Robert Hayes, Gregory G. Warr, Rob Atkin, Structure and nanostructure in ionic liquids, Chem. Rev. 115 (2015) 6357–6426.
[58] Y. Shen, et al., Protic ionic liquids with fluorous anions: physicochemical properties and self-Assembly nanostructure, Phys. Chem. Chem. Phys. 14 (2012) 7981–7992.
[59] M. Brehm, H. Weber, M. Thomas, O. Holloczki, B. Kirchner, Domain analysis in nanostructured liquids: a post-Molecular dynamics study at the example of ionic liquids, ChemPhysChem 16 (2015) 3271–3277.
[60] J.A. Gladysz, D.P. Curran, I.T. Horvath, Handbook of Fluorous Chemistry, WILEY-VCH, Weinheim, 2004.
[61] J.D. Holbrey, W.M. Reichert, R.D. Rogers, Crystal structures of imidazolium bis (trifluoromethanesulfonyl)imide 'ionic liquid' salts: the first organic salt with a *cis*-TFSI anion conformation, Dalton Trans. (2004) 2267–2271.
[62] A. Downard, M.J. Earle, C. Hardacre, S.E.J. McMath, M. Nieuwenhuyzen, S.J. Teat, Structural studies of crystalline 1-Alkyl-3-Methylimidazolium chloride salts, Chem. Mater. 16 (2004) 43–48.
[63] A.B. Pereiro, M.J. Pastoriza-Gallego, K. Shimizu, I.M. Marrucho, J.N. Canongia Lopes, M.M. Pineiro, L.P.N. Rebelo, On the formation of a third, nanostructured domain in ionic liquids, J. Phys. Chem. B 117 (2013) 10826–10833.
[64] J.J. Hettige, J.C. Araque, C.J. Margulis, Bicontinuity and multiple length scale ordering in triphilic hydrogen-bonding ionic liquids, J. Phys. Chem. B 118 (2014) 12706–12716.
[65] Z. Barikbin, et al., Ionic liquid-based compound droplet microfluidics for 'on-drop'separations and sensing, Lab Chip 10 (2010) 2458–2463.
[66] I. Otero, E.R. López, M. Reichelt, M. Villanueva, J. Salgado, J. Fernández, Ionic liquids based on phosphonium cations As neat lubricants or lubricant additives for a Steel/Steel contact, ACS Appl. Mater. Interfaces 6 (2014) 13115–13128.
[67] F. Zhou, Y. Liang, W. Liu, Ionic liquid lubricants: designed chemistry for engineering applications, Chem. Soc. Rev. 38 (2009) 2590–2599.
[68] H.J. Castejón, T.J. Wynn, Z.M. Marcin, Wetting and tribological properties of ionic liquids, J. Phys. Chem. B 118 (2014) 3661–3668.
[69] I. Minami, Ionic liquids in tribology, Molecules 14 (2009) 2286–2305.
[70] Y. Wu, Q. Wei, M. Cai, F. Zhou, Interfacial friction control, Adv. Mater. Interfaces 2 (2014) 1400392.
[71] M. Schmitt, R. Hempelmann, S. Ingebrandt, W.-M. Munief, K. Groß, J. Grub, F. Heib, Statistical contact angle analyses: slow moving drops on inclining flat mono-aminopropylsiloxane surfaces, J. Adhes. Technol. Sci. 29 (2015) 1796–1806.
[72] Electronic Supplementary Information.

2.7 Publication G

Influence of perfluoroalkyl-chains on the surface properties of 1-methylimidazolium bis(trifluoromethanesulfonyl)imide ionic liquid

Daniel Rauber, Florian Heib, Michael Schmitt, Rolf Hempelmann.

J. Mol. Liqu., **2016**, 216, 246-258.

Journal of Molecular Liquids 216 (2016) 246–258

Contents lists available at ScienceDirect

Journal of Molecular Liquids

journal homepage: www.elsevier.com/locate/molliq

Influence of perfluoroalkyl-chains on the surface properties of 1-methylimidazolium bis(trifluoromethanesulfonyl)imide ionic liquids

Daniel Rauber [a,*], Florian Heib [a], Michael Schmitt [a], Rolf Hempelmann [a,b]

[a] Physical Chemistry, Saarland University, Campus B 2.2, 66123 Saarbrücken, Germany
[b] Korean Institute of Science and Technology, Campus E 7.1, 66123 Saarbrücken, Germany

ARTICLE INFO

Article history:
Received 22 October 2015
Received in revised form 23 December 2015
Accepted 3 January 2016
Available online xxxx

Keywords:
Ionic liquids
Perfluoroalkyl-substituents
Surface properties
Contact angle
High-precision drop shape analysis

ABSTRACT

A series of 1-(1*H*,1*H*,2*H*,2*H*-perfluoroalkyl-)-3-methyl-imidazolium bis(trifluoromethanesulfonyl)imide ionic liquids with varying lengths of the perfluorinated side chain was synthesized and some of their important physical properties were compared to their non-fluorinated analogs. They were found to have a high thermal stability, wide liquid range and higher or comparable polarities. Furthermore evidences for the formation of fluorous domains in the bulk ionic liquids were found. Their contact angles on various substrates were determined using the *high-precision drop shape analysis* (HPDSA) approach and were found to show a greatly modified behavior on all investigated surfaces.

1. Introduction

Ionic liquids (ILs) which are salts melting below 100 °C have received great attention in recent years in a broad range of different fields like chemistry, physics, electronics, engineering and material science because of their unique and tailorable properties [1–3]. Especially in the context of a more environmentally friendly and sustainable chemistry responsibility. Processing these neoteric solvents are a field of intensive research because of their recyclability, nonvolatility, noninflammability, high thermal resistivity, conductivity and wide electrochemical window [4–6]. A vast majority of their applications involve some kind of surfaces, mainly solid–liquid interfaces [7]. This makes the tuning of the interface properties of ionic liquids highly important for their successful application. One very promising way to manipulate the behavior of ILs and fine tune their characteristics is the introduction of perfluorinated alkyl chains into either the cation or the anion resulting in fluorinated ionic liquids (FILs) [8–10]. Ionic liquids with perfluorinated groups have been studied for a range of possible applications. Examples include gas separation [11], as surfactants [8], solvents for multiphase catalysis [12,13], phase-transfer-catalysts [14], liquid crystals [15], liquid–liquid extraction or artificial blood substituents [16]. In this work we investigate some important physical properties for applications of the methyl-imidazolium-cations ([MIM]-cation) with perfluoro groups and the bis(trifluoromethanesulfonyl)imide-anion ([NTf_2]-anion) and compare these results with the nonfluorinated alkyl derivated ionic liquids (AILs). We found strong evidence for an aggregation behavior in the pure liquids with increasing side chain length in the FILs similar to the AILs. A strong aggregation behavior for ILs with perfluorinated chains in the anion was recently demonstrated in aqueous solutions [17]. Furthermore we found a significant change of the wetting behavior of the FILs compared with the AILs determined via their contact angle. Contact angle measurements are a standard and widely used analytical technique in science and industry to characterize solid surface and wetting behavior. Water and a wide range of different organic liquids [18] are the most commonly used test liquids. Due to the simple fabrication, negligible vapor pressure, high purity, often poor solubility in water and simple chemical modification to control and adjust, e.g., the surface tension, there is a great potential for the use of ionic liquids as contact angle test liquids [19–22]. Therefore, the static and dynamic wetting behavior of the synthesized FILs and AILs on different wettable sample surfaces is studied and compared to the results of water contact angle measurements. The contact angle analyses were performed with the *high-precision drop shape analysis* (HPDSA) [23] which was developed for analyzing highly non-axisymmetric droplets especially during dynamic contact angle measurements with high local precision and resolution. The results illustrate that the properties of the test liquid like viscosity and polarity also strongly influence the wetting behavior on a surface. Especially the strong oppositely polarized character of the FILs results in a distinct pinning on the uphill side which is most likely caused by the charged interface of the ionic liquid which interacts with the surface charge. These results underline the ability of altering the behavior of ionic liquids by the introduction of fluorinated alkyl chains and make them suitable candidates for a broad range of

* Corresponding author.
E-mail address: daniel.rauber@uni-saarland.de (D. Rauber).

http://dx.doi.org/10.1016/j.molliq.2016.01.011
0167-7322/

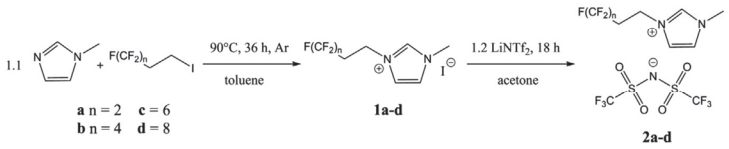

Scheme 1. Synthesis of the perfluoroalkyl-substituted imidazolium ionic liquids.

possible practical applications. Of special interest in this context may be the immobilization of fluorinated compounds in fluorous domains, blending of ionic liquids [24] or the modification of surface properties for higher performance when solid–liquid-interfaces are involved in the process.

2. Experimental and methods

2.1. Materials

Details of the reagents, synthesis and characterization of the FILs and AILs are described in the supplementary information. Reichardt's Dye (90%) and Nile Red (technical grade), were purchased from Sigma Aldrich and used without further purification. [1-Alkyl-3-methylimidazolium][NTf_2] ionic liquids were synthesized from the corresponding iodide ILs after modified literature protocols (nomenclature of the alkyl-groups: C_4: butyl; C_6: hexyl; C_8: octyl; C_{10}: decyl) [25].

2.2. Synthesis of the perfluoroalkyl-substituted imidazolium ionic liquids

The perfluoroalkyl-substituted imidazolium ionic liquids with the formula [$F(CF_2)_n(CH_2)_2$-MIM][NTf_2] (n = 2, 4, 6) were synthesized via nucleophilic substitution of 1-methylimidazole with the corresponding iodides [8,26,27] and subsequent anion-metathesis reaction with $LiNTf_2$ according to scheme 1 following modified literature synthesis protocols [11,28,29].

2.3. Physical properties

2.3.1. Melting and decomposition temperatures

Melting points were measured on a DSC 1 STARe System (Mettler Toledo, Gießen, Germany) equipped with a liquid nitrogen cooling system using Al-crucibles. In the case of liquid samples ([alkyl-MIM][I], [alkyl-MIM][NTf_2], **2a–c**) the ILs were cooled with a rate of -1 °C min^{-1} to -120 °C were they remained at this temperature for 20 min and then heated with a rate of $+1$ °C min^{-1} to 25 °C. If the sample was in solid state (**1a–d** and **2d**) the program was set to heat with a rate of $+1$ °C min^{-1} to 120 °C, held at this temperature for 20 min and then cooled with -1 °C min^{-1} to 25 °C. All cycles were repeated three times to ensure that stable values for the melting points are observed. Thermogravimetric analyses were performed on a TGA/DSC 1 STARe System (Mettler Toledo, Gießen, Germany) using Al_2O_3 crucibles in the temperature range from 20 to 550 °C with a heating rate of 10 °C/min and a nitrogen flow of 25 mL/min. The melting and decomposition temperatures were determined as extrapolated onset temperatures.

2.3.2. Polarity

Polarity measurements were performed with two different solvatochromic dyes (Reichardt's Dye [30] and Nile Red [31]) which are common for the empirical determination of liquid system polarities because of their large solvatochromic shifts [32,33] and were also successfully applied to ILs [34–36]. The molecular structures of the dyes are given in Fig. 1. The UV/vis spectra were recorded on an UV SPECORD

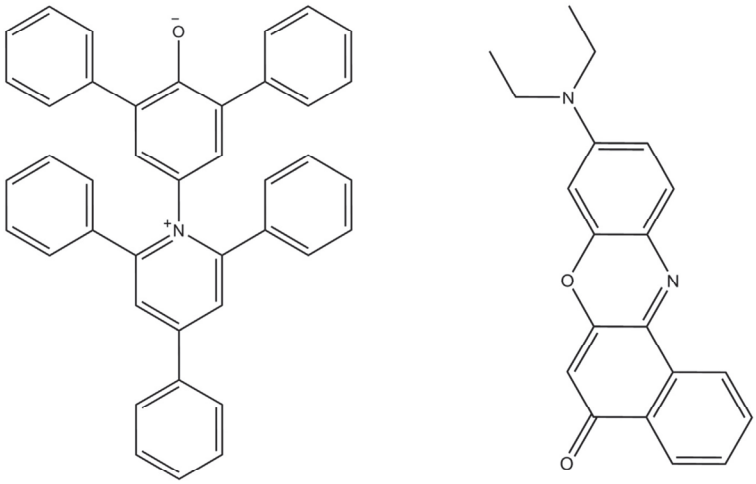

Fig. 1. Molecular structures of Reichardt's Dye (left) and Nile Red (right).

Table 1
Melting (T_m) and decomposition (T_d) temperatures of the fluoroalkyl substituted iodides and bis(trifluoromethanesulfonyl)imides in comparison with the nonfluorinated AILs with the same number of C-atoms in the side chain.

Compound	T_m/°C	T_d/°C	Liquid range/°C	Compound	T_m/°C	T_d/°C	Liquid range/°C
1a	69	274	205	$[C_4MIM][I]$	−64	293	357
1b	54	274	220	$[C_6MIM][I]$	−61	288	349
1c	80	277	197	$[C_8MIM][I]$	−60	284	344
1d	119	258	139	$[C_{10}MIM][I]$	−23	284	307
2a	−65	422	487	$[C_4MIM][NTf_2]$	−2 (−3)[a]	438 (427)[a]	440
2b	−57	423	480	$[C_6MIM][NTf_2]$	−6 (−6)[a]	447 (428)[a]	453
2c	−53 (−50)[b]	423	476	$[C_8MIM][NTf_2]$	−84	434 (425)[a]	518
2d	31	416	385	$[C_{10}MIM][NTf_2]$	6	411	405

[a] Values from ref. [54].
[b] Value from ref. [28].

210 Plus (Analytic Jena, Jena, Germany) using a quartz cuvette with a path length of 0.1 cm in a thermostated cell at 25 °C. Samples were prepared by adding a diluted solution of one of the dyes in dichloromethane to the pure ionic liquids, stirring until homogenous, evaporating the solvent and drying in high vacuum for two days. All measurements were performed 5 times and the results averaged. $E_T(30)$- (Reichardt's Dye) and E_{NR}-values (Nile Red) were calculated from the maximum of the absorbance band λ_{max} (in nm) of the dyes after Eq. 1, with *h* being Planck's constant, *c* the speed of light and N_A being Avogadro's number.

$$E = hcN_A\,\lambda_{max}^{-1} \times 10^6 \quad (1)$$

For a better comparison with literature results the $E_T(30)$-values are also given in the more widely used units kcal mol^{-1}.

2.3.3. Viscosity

Viscosities were studied using a Haake Mars Rheometer (Thermo Fisher Scientific, Braunschweig, Germany) with plate–plate geometry with a 0.1 mm slit at 23 °C by applying a constant shear stress of 0.5 Pa to a 20 mm diameter steel plate. The setup and parameters were chosen because they can handle smaller sample volumes that didn't show evidence for non-Newtonian behavior.

2.3.4. Crystal structure

The crystal structure of compound **2d** could be obtained on a suitable single crystal generated by drying a dichloromethane solution of **2d** in a stream of nitrogen. Data was collected on an AXS X8 Apex 2 (Bruker, Billerica, USA) at −101 °C using Mo-Kα radiation at a Theta range from 1.452 to 27.177°. In total 77,254 reflexes were collected and refined using full-matrix least-squares on F^2. Final R-index using anisotropic refinements of hydrogen atoms with SHELX [37] results in R1 = 0.0772. The final data and further details are given in the supporting information.

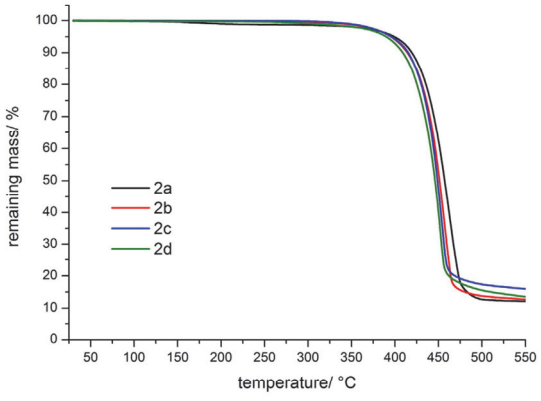

Fig. 2. TGA measurements of the perfluoroalkyl substituted imidazolium NTf_2 ionic liquids.

2.4. Wettability and contact angle analyses

For the characterization of the wetting behavior contact angle measurements were performed with the synthesized ionic liquids and were compared with the results of water contact angle measurements. Therefore, three different types of surfaces (hydrophobic $90° \le \theta_w \le 130°$; hydrophilic $30° \le \theta_w \le 90°$; superhydrophilic $0° \le \theta_w \le 30°$) were used as substrates to cover a wide range of contact angles. The hydrophobic surface was prepared by a vapor deposition method as described earlier [38–40] using 1*H*,1*H*,2*H*,2*H*-perfluorooctly-trichlorosiloxane (FOTCS) purchased from Sigma Aldrich and used as received. For the hydrophilic surface, an aged silicon wafer p-type 100 (MicroChemicals, Ulm, Germany) covered with its native oxide was used without further purification. For the superhydrophilic surface, an aged silicon wafer p-type 100 was cleaned and activated by immersing the wafer into a freshly prepared RCA solution consisting of 1 part aqueous H_2O_2 (30 wt.%), 1 part aqueous NH_4OH (25 wt.%) and 5 parts of deionized water for 30 min at 80 °C followed by sufficient rinsing with ultrapure water and drying under dry nitrogen flow. After that, the cleaned surface was activated by immersing into a freshly prepared piranha solution consisting of 1 part concentrated H_2SO_4 and 2 parts aqueous H_2O_2 (30 wt%) for 30 min followed by sufficient rinsing with ultrapure water and drying under dry nitrogen flow. The contact angle measurements were performed while continuously inclining the sample surfaces with an angular speed of $\dot{\varphi} = 0.57°/s$ (inclining-plate technique), using an OCA20 measuring system (Dataphysics, Filderstadt, Germany). Thereby, 0.03 mL ultra-pure water (Milli-Q® Type 1 ultrapure water system, Merck KGaA, Darmstadt, Germany) and 0.03 mL ionic liquid droplets at a temperature of 30.0 °C ± 0.2 °C and under saturated vapor atmosphere of the test liquid (closed measuring chamber with definable measuring positions) were video recorded with a frame rate of 25 frames per second. To enhance the reproducibility, the measurements were repeated on ten defined measuring positions for each

Table 2
Wavelength maxima λ_{max} of the two solvatochromic dyes in the pure ionic liquids.

Compound	Reichardt's Dye			Nile Red	
	λ_{max}/nm	$E_T(30)$/kJ mol^{-1}	$E_T(30)$/kcal mol^{-1}	λ_{max}/nm	E_{NR}/kJ mol^{-1}
2a	506.3	236.3	56.5	576.2	207.6
2b	531.5	225.1	53.8	547.2	218.6
2c	534.2	224.0	53.5	545.6	219.3
$[C_4MIM][NTf_2]$	555.1	215.5	51.5	546.8	218.7
$[C_6MIM][NTf_2]$	556.3	215.0	51.4	545.5	219.3
$[C_8MIM][NTf_2]$	558.2	214.3	51.2	544.1	219.9
$[C_{10}MIM][NTf_2]$	560.4	213.5	51.0	543.2	220.2

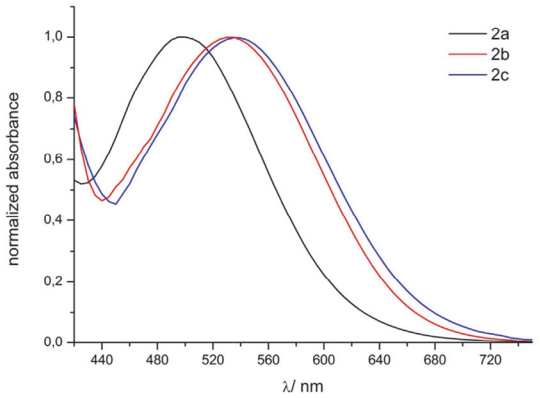

Fig. 3. Normalized absorption spectra of Reichardt's Dye in the ionic liquids **2a**–**2c**.

surface. The main advantage of the inclining-plate technique is the simultaneous measurement of the advancing/downhill and receding/uphill motion. Due to different force distributions between horizontal and inclined measuring setups (different positions of the centers of gravity) [41,42] the advancing angles are denoted as downhill angles $\theta_d(\varphi)$ which are measured at the front edge of the drop and the receding angles are denoted as uphill angles $\theta_u(\varphi)$ which are measured at the back edge of the drop.

2.5. Data processing and contact angle calculation with HPDSA

In this study, about 400,000 drop images from the video recording are considered for the wetting analyses which were performed with the *high precision drop shape analysis* (HPDSA) procedure. The intention of the HPDSA procedure is not only to be able to calculate contact angles from axisymmetric droplets. On the contrary, the HPDSA procedure was developed to be able to describe the drop shape and to calculate contact angles from highly non-axisymmetric droplets as they appear e.g. during inclining-plate measurements in a reproducible and controllable way which is not possible with commercial contact angle software. A short summary of the procedure is presented in the following and detailed descriptions can be found in Ref. [23,43,44]. Firstly, the drop shape is extracted from gray-scale bmp images. Therefore, the color values of every pixel in the *x*- and *y*-directions are read out and

Table 3
Viscosities measured at 23 °C and constant shear stress of 0.5 Pa.

Compound	Viscosity/mPa s^{-1}	Compound	Viscosity/mPa s^{-1}
2a	399	$[C_4MIM][NTf_2]$	87.52
2b	732	$[C_6MIM][NTf_2]$	119.54
2c	1869	$[C_8MIM][NTf_2]$	143.95
		$[C_{10}MIM][NTf_2]$	209.84

transferred from the *hexadecimal* color code (e.g. black ≡ 000000; white ≡ FFFFFF) into the *RGB* color code (e.g. black ≡ 0 0 0; white ≡ 255 255 255). Then, the sum of color values *col* for every pixel point (e.g. black ≡ col = 0; white ≡ col = 765) is determined and a dynamic linear regression of three and five neighboring pixel points *P* is performed using Eq. (2)

$$\left(\frac{d\,col}{dP}\right)_{x/y} = \frac{\sum(col_i \cdot P_i)\cdot n - \sum P_i}{n\cdot\sum P_i^2 - \left(\sum P_i\right)^2} = p_{x/y} \tag{2}$$

to determine the rates of color $p_{x/y}$. To detect the gray scale transition a limit value *lv* for the rates of color can be set by the operator which is 10/pixel in this study. This means that only pixel points with $p_{x/y} \equiv lv > 10$/pixel are considered for the drop shape extraction. This procedure results in at least two points for one step in color. To determine the "*real*" drop shape, a weighting procedure of the former determined points for the gray-scale transitions is performed by using Eq. 3.

$$E(x) = \frac{\sum\left(x_i \cdot p_{x_i}\right)}{\sum p_{x_i}};\quad E(y) = \frac{\sum\left(y_i \cdot p_{y_i}\right)}{\sum p_{y_i}} \tag{3}$$

Simultaneously, the pixel coordinates are transferred into µm-coordinates whereby one pixel corresponds to a length of 18.3×10^{-6} m. If the resolution of the images is well enough, this procedure results in a transfer of the drop shape with sub-pixel resolution. To detect the baseline, two linear functions per side of the droplet, one for the real drop shape and one for the drop reflection, are applied to determine the intersection points on both sides of the 2D projection which correspond to the triple line. This procedure offers the possibility for dynamically controlling the baseline so that also non-horizontal baselines are uncomplicated. To be able to calculate the contact angles on the right-hand and left-hand side independent of each other, the extracted drop shape is split at the highest point (X_{max}:Y_{max}) in two parts and a semi-

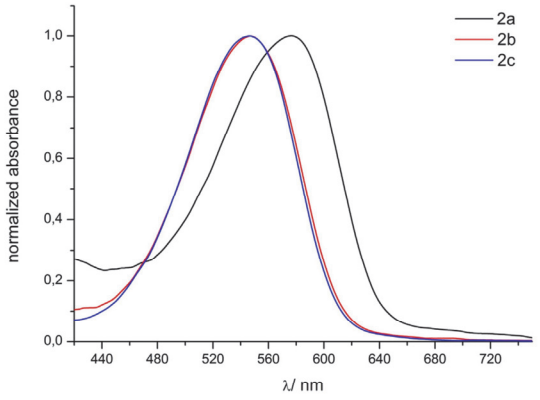

Fig. 4. Normalized absorption spectra of Nile Red in the ionic liquids **2a**–**2c**.

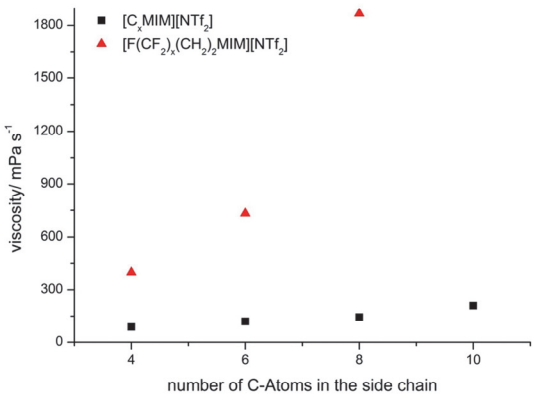

Fig. 5. Viscosity of the investigated ILs as a dependence of the side chain length.

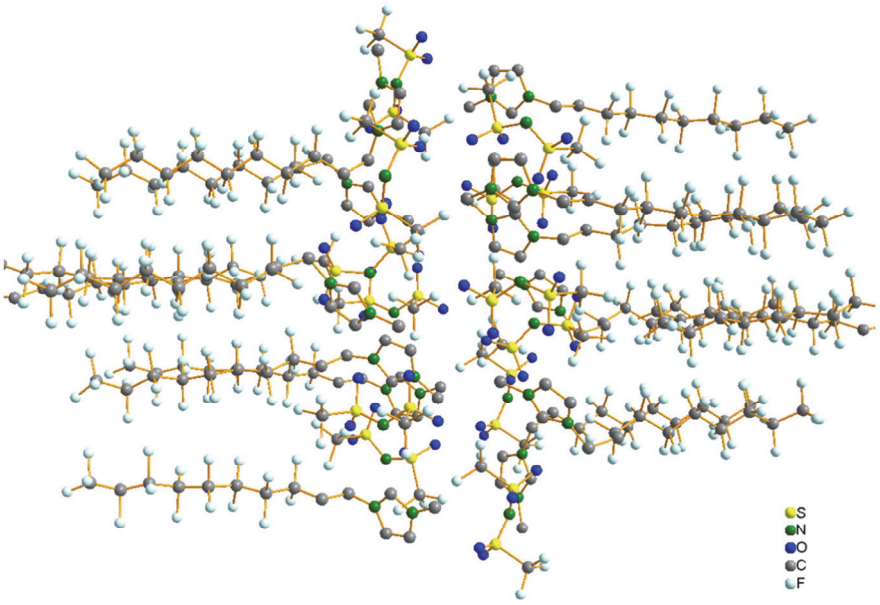

Fig. 6. The arrangement of fluorous and ionic domains in the crystal of compound **2d** (hydrogen atoms are omitted for clarity).

circle function is applied to fit the left-hand and right-hand side independently of each other by using Eq. 4

$$y_{1/2}(x) = y_{cc} \pm \sqrt{R^2 - (x - x_{cc})^2} \tag{4}$$

whereby x_{cc} and y_{cc} define the center of a fitting circle and R is the radius of curvature. This approach is very suitable for strongly curved droplets (hygrophobic and superhygrophobic but also for hygrophilic) and leads to a tangent free computation of the apparent contact angle θ_m using Eq. 5,

$$\theta_m = 90^\circ + \arcsin\left(\frac{\Delta y}{R}\right) \pm \alpha_{BL} \tag{5}$$

from the mean radius R, the inclination angle α_{BL} of the baseline and the distance Δy in height coordinates of the center of the fitting-circle (X_{MP}:Y_{MP}) relative to the intersection point. Because the contact angle is a microscopic property of the three phase interface (triple line) not the entire drop shape is fitted as performed by commercial contact angle analysis software but only the meniscus near the triple line is considered for the fitting procedure. The minimal length of a calculation arc (≈length of the considered meniscus; in this study 1.5 mm) can be varied in dependence of the radius R to ensure convergence of the fitting routine. An additional benefit is the calculation of the triple points which corresponds to the intersection points of the fitting circle with the baseline. These points can also be used to detect the static advancing/downhill $\theta_{d,e}$ and static receding/uphill $\theta_{u,e}$ angles with a high local resolution in a reproducible manner. To be able to calculate contact angles below 20°, two additional fitting procedures are implemented in the HPDSA. The first one is a linear fit of approximately 10 pixel points of the extracted drop shape near the triple line. The second one is a circle fit whereby the three parameters of the fitting circle were determined using three computed points. These points are the results of multipoint polynomial (2th order) regression. Thereby, the start, middle and end of the fitting range were calculated. Further details of the procedure will be published in an additional publication. Both procedures are especially suitable for very small contact angles ($0^\circ \le \theta \le 20^\circ$) where the drop shape is almost linear. Also droplets where the drop curvatures change from a positive to a negative drop curvature can be evaluated.

Table 4
Lattice parameters of ionic liquid **2d**.

Unit cell vector length/Å	Unit cell angles/°
a = 9.9413 (6)	α = 107.9765 (14)
b = 22.1626 (9)	β = 91.8248 (15)
c = 25.9861 (16)	γ = 91.1214 (15)

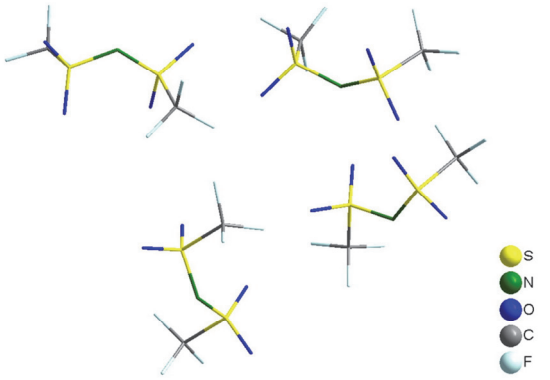

Fig. 7. The four different conformations of the [NTf_2]-anions in the crystal showing two *trans* (upper and lower left), one *cis* (upper right) and one intermediate configurations.

Table 5
Bond angles and dihedral angles for the different anion conformations in the crystal of **2d**.

Conformation	S–N–S/°	C–S···S–C	S–N–S/° [66]	C–S···S–C/° [66]
trans	125.462 (8)	166.286 (6)	124.97 (13)	175.67 (16)
trans	124.704	178.813 (6)	124.97 (13)	175.67 (16)
cis	126.938 (8)	19.388 (8)	126.33 (18)	32 (1)
Intermediate	122.229 (7)	81.845 (8)		

2.6. Overall curve shape of the contact angle data: Gompertzian analysis

The *Gompertzian* analysis starts with the individual fitting of a *Gompertzian* function [45] onto the course of contact angles relative to an independent parameter for every measuring position by using Eq. 6,

$$f(\varphi) = \theta_{shift} + A \cdot \exp\left[-\exp\left(-k\left(\varphi - \varphi_{shift}\right)\right)\right] \quad (6)$$

whereby θ_{shift}, A, k and φ_{shift} are adjustable fitting parameters. Due to the fact that the inclining-plate technique was used for the contact angle analysis the Gompertzian function is fitted relative to the inclination angle φ of the sample desk. Thereby, the fitting limits for the downhill side φ_{Ld} (right edge of the droplet; motion onto formerly non-wetted area ≡ advancing motion) and the uphill side φ_{Lu} (left edge of the droplet; motion to formerly wetted area ≡ receding motion) are manually defined at the point when the motion transition from the static range (non-moving/slow-moving) to the dynamic range (high velocity) occurs. This procedure is able to visualize the overall contact angle behavior from a huge amount of data (≈10,000 images/contact angles per measurement) with only four fitting parameters by simulating and fitting of the average data. These specific/average *Gompertzian* functions from the average contact angle data of a surface with the corresponding test liquid are representative and reproducible wetting characteristics of the surface. Furthermore, the calculation of standard deviations leads to specific contact angles $\theta_{d,u}$ with the smallest standard deviations which can be used to describe the wettability of the surface.

3. Results and discussion

3.1. Thermal behavior

The determined melting and decomposition temperatures of the FILs and AILs are summarized in Table 1. As expected and widely known the anion has a great influence on the melting and decomposition points [46]. All iodide ionic salts with a fluorinated side chain show contrary to the non-fluorinated analogs melting points above room temperature. While the length of the alkyl side chain had only a small effect on the melting points in the non-fluorinated ionic liquids, there is a stronger dependence seen in the fluorous analogs. The decomposition temperatures for the alkyl-imidazolium iodides are slightly higher than those for the fluoroalkyl-iodides leading to a higher overall liquid range for the nonfluorous iodides. For the NTf_2 molten salts where the anion shows a high degree of charge delocalization there is a different tendency. While **2a** and **2b** have significantly lower melting points than the corresponding alkyl-derivatives, **2c** and **2d** have slightly higher ones. This trend is in accordance with experimental results from the literature, that small fluorinated side chains can depress the melting points in ionic liquids [47–49] but larger perfluorosidechains can lead to higher ones [50]. Experimental results indicate that the higher melting points observed in imidazolium ionic liquids with longer perfluoroalkyl chains result from the higher grade of aggregation in the bulk IL [51], because of the higher degree of fluorophilicity and from the greater rigidity [52] with the perfluorocarbon fragment elongation. While the exchange of iodide with NTf_2 reduces the melting points of the FILs remarkably the situation is dependent on the number of C-atoms in the side chain for the AILs. The decomposition temperatures of all NTf_2 ionic liquids are much higher than those of the iodides and nearly independent of the side chain length which is also observed in literature results [53]. The TGA curves for compounds **2a**–**d** are shown in Fig. 2. All FILs showed decomposition temperatures above 400 °C and are slightly lower than the corresponding AILs except for **2d**. The fluorinated ionic liquids investigated showed very wide ranges were they are in liquid state which is important for practical applications.

3.2. Polarity studies

Polarity is one of the most important properties of a liquid system because it allows conclusions about the mixing behavior and ability to extract selected compounds. The measured wavelength of the absorption maximum and the corresponding transition energies of the two solvatochromic dyes in the pure ionic liquids are summarized in Table 2 and the UV/vis spectra are reported in Figs. 3 and 4. It should be noted that a red shift of the absorbance of Reichardt's Dye indicates a lower polarity while in Nile Red a higher polarity results from a shifting to higher wavelengths of the absorbance maxima. While in the alkylated ionic liquids there is only little influence of the chain length on polarity of about 2 kJ mol^{-1} by varying the side chain from

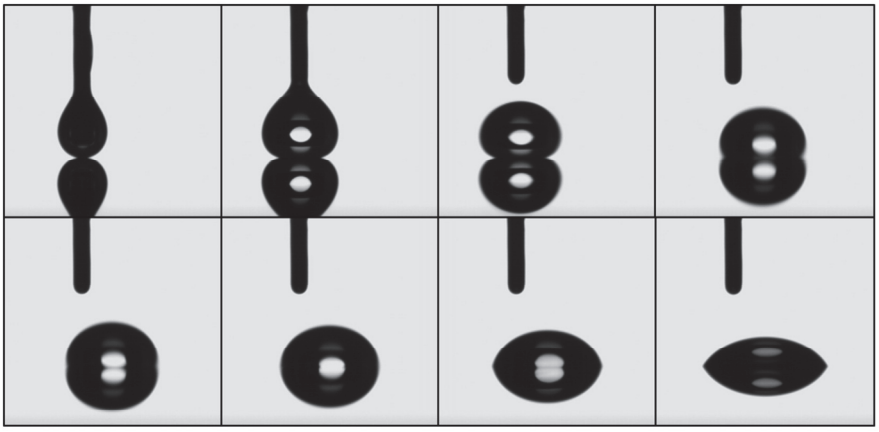

Fig. 8. Visualization of the drop application of a FIL on the sample surfaces.

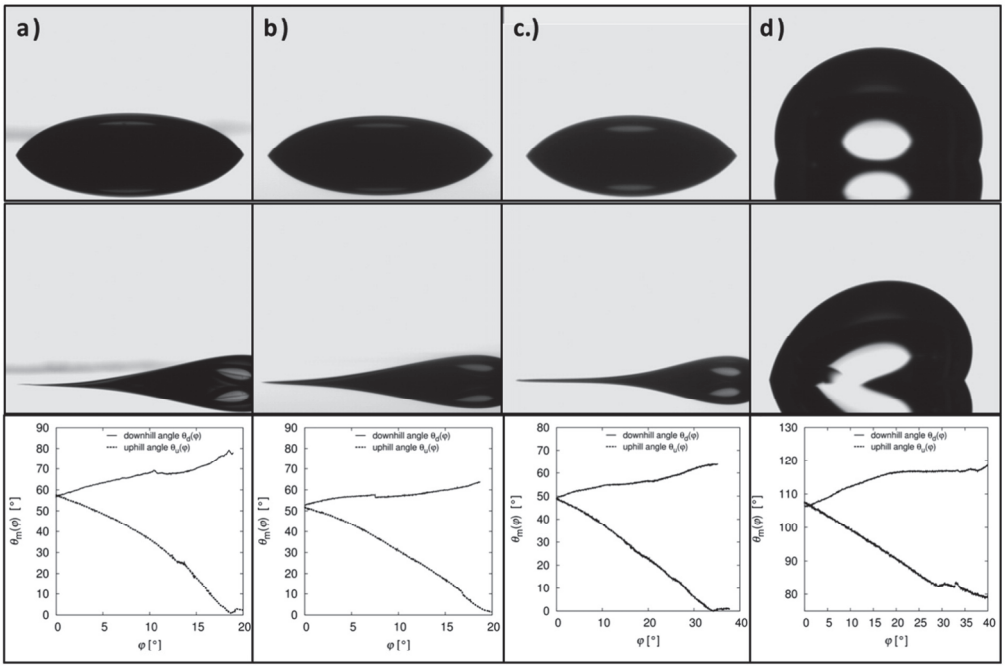

Fig. 9. Example for sessile drops on a hydrophobic modified silicon surface with a) **2a** as test liquid at inclination angles of $\varphi = 0°$ (top) and $\varphi = 17°$ (middle) and an example for a contact angle measurement (bottom), b) **2b** as test liquid at inclination angles of $\varphi = 0°$ (top) and $\varphi = 17°$ (middle) and an example for a contact angle measurement (bottom), c) **2c** as test liquid at inclination angles of $\varphi = 0°$ (top) and $\varphi = 35°$ (middle) and an example for a contact angle measurement (bottom) and d) water as test liquid at inclination angles of $\varphi = 0°$ (top) and $\varphi = 30°$ (middle) and an example for a contact angle measurement (bottom).

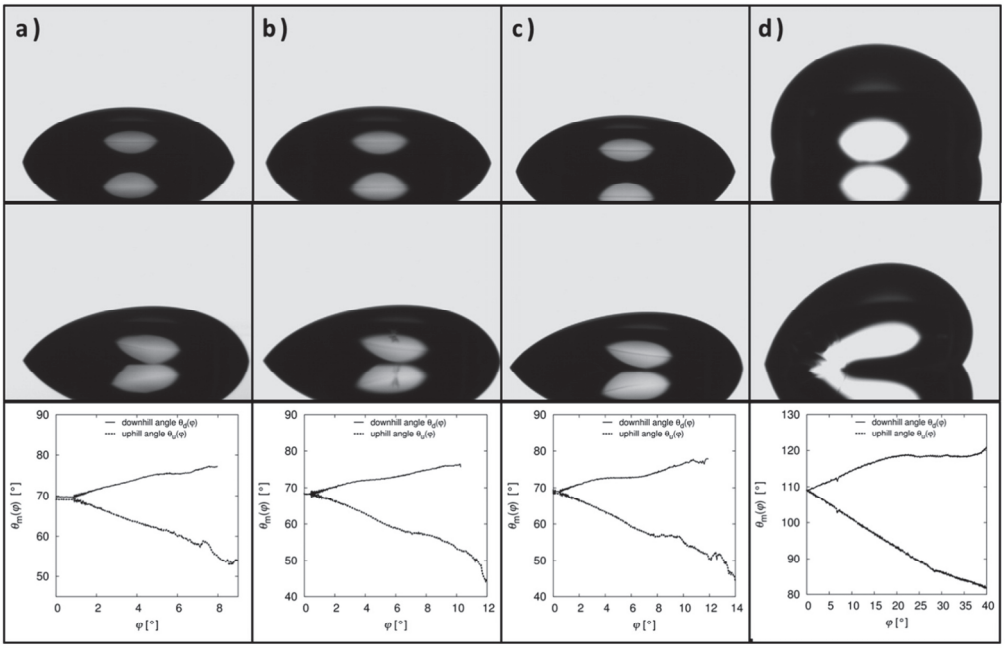

Fig. 10. Example for sessile drops on a hydrophobic modified silicon surface with a) [C_4MIM][NTf_2] as test liquid at inclination angles of $\varphi = 0°$ (top) and $\varphi = 17°$ (middle) and an example for the contact angle analysis (bottom), b) [C_6MIM][NTf_2] as test liquid at inclination angles of $\varphi = 0°$ (top) and $\varphi = 17°$ (middle) and an example for the contact angle analysis (bottom), c) [C_8MIM][NTf_2] as test liquid at inclination angles of $\varphi = 0°$ (top) and $\varphi = 35°$ (middle) and an example for the contact angle analysis (bottom), and d) water as test liquid at inclination angles of $\varphi = 0°$ (top) and $\varphi = 30°$ (middle) and an example for the contact angle analysis (bottom).

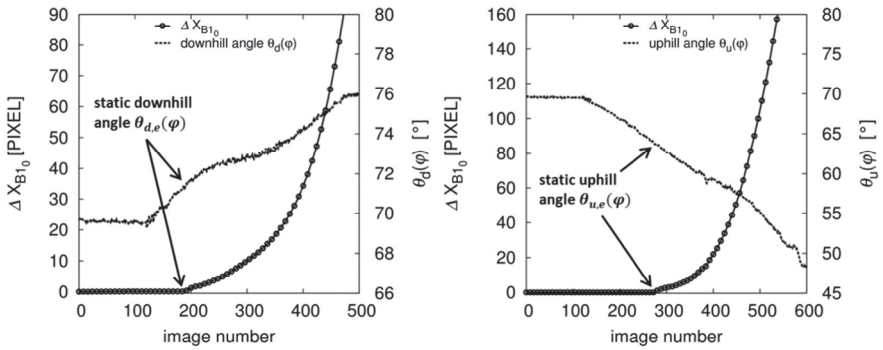

Fig. 11. Example for the determination of the static downhill $\theta_{d,e}(\varphi)$ (left) and static uphill $\theta_{u,e}(\varphi)$ (right) angles dependent on the shift of the triple points ΔX_{B1o} with the high precision drop shape analysis.

Table 6
Results for the determination of the static downhill $\theta_{d,e}(\varphi)$ and static uphill $\theta_{u,e}(\varphi)$ angles on the hydrophobic modified silicon surface.

Test liquid	$\theta_{d,e}(\varphi)$ [°]	φ_d [°]	$\theta_{u,e}(\varphi)$ [°]	φ_u [°]	$\Delta\theta$ [°]
H_2O	112.4 ± 4.1	11.8 ± 4.3	92.5 ± 3.5	20.0 ± 5.2	17.6 ± 4.7
2a	66.1 ± 2.4	3.8 ± 2.4	34.4 ± 5.9	9.8 ± 1.7	31.7 ± 5.4
2b	52.6 ± 2.0	1.4 ± 0.4	28.0 ± 5.6	9.5 ± 2.5	24.7 ± 5.1
2c	51.5 ± 1.2	3.1 ± 0.6	32.4 ± 4.4	15.5 ± 2.1	19.1 ± 3.5
$[C_4MIM][NTf_2]$	72.8 ± 0.5	2.3 ± 0.4	64.1 ± 0.9	3.8 ± 0.3	8.8 ± 0.9
$[C_6MIM][NTf_2]$	71.5 ± 0.6	2.3 ± 0.2	62.5 ± 0.7	4.3 ± 0.3	9.0 ± 0.7
$[C_8MIM][NTf_2]$	72.2 ± 0.5	2.7 ± 0.3	61.0 ± 0.8	5.4 ± 0.4	11.2 ± 1.0

a butyl- to decyl-group, the situation in the fluoroalkylated ionic liquids is different. The dyes dissolved in **2b** and **2c** show only a small change in molar transition energies whereas the values for **2a** differ markedly more with values higher than 11 kJ mol^{-1} for both Reichardt's Dye and Nile Red. This indicates that **2a** is notably more polar than **2b** and **2c**. The polarity measurements with Reichardt's Dye show a higher polarity for all fluorinated ionic liquids while the measurements with Nile Red reveal polarities for **2b** and **2c** being in the same range as those for the ionic liquids with alkyl chains. The higher polarities for the fluoroalkyl substituted compounds may result from a higher charge localization resulting from the strong electron withdrawing effect of the highly electronegative fluorine atoms. These results are supported by the comparison of the ^{1}H-NMR shifts which are higher for the perfluoroalkyl group containing ionic liquids and theoretical calculations [51]. A formation of nanodomains and structuring in ILs [55] with the separation of the apolar and charged polar part is well known for 1-alkyl-3-methyl-imidazolium ionic liquids with side chains equal or larger than the butyl-group [56,57]. This manner is expected to occur also for perfluorinated side groups as the heterogeneous interactions between the hard to polarize fluorous groups and the ionic parts are even less favored [16]. Evidence for this is also given in the results of [58] were nanodomains in ionic liquids with the perfluoralkyl group containing anions were found. For longer perfluorinated chains the effect of charge localization leading to higher polarities may be overcompensated by the higher apolarity in fluorocarbons compared to hydrocarbons [59].

3.3. Rheological behavior

The viscosity of a liquid is of vital interest when it comes to practical applications and processing because it does not only control heat and mass transfer but also conductivity in the case of ionic liquids. It also gives insight to the intermolecular interactions like the strength of coulomb, Van-der-Waals-forces or hydrogen bonding [60] where it was found that these forces are competing in ionic liquids and that long alkyl chains lead to aggregation behavior because of favored Van-der-Waals-attraction between these [61]. This aggregation behavior is

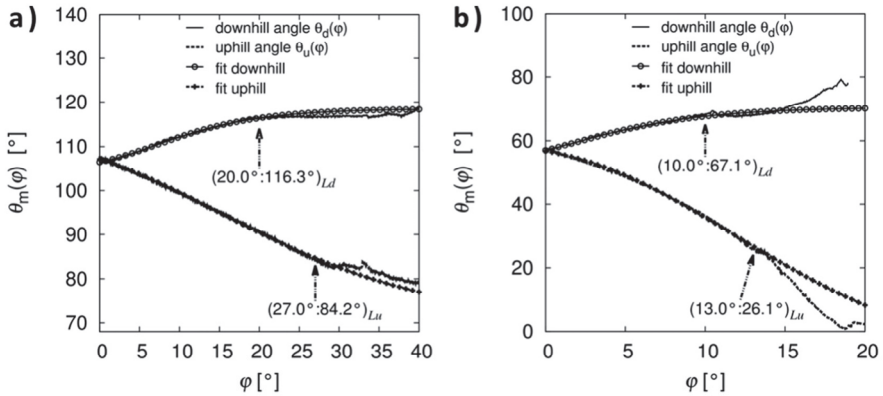

Fig. 12. Example for the fitting of a modified *Gompertzian* function onto the course of contact angles relative to the inclination angle on a) a hydrophobic modified silicon surface with water as test liquid (Fig. 9d) and b) a hydrophobic modified silicon surface with **2a** as test liquid (Fig. 9a). The limits of the fitting range at the downhill side φ_{Ld} and on the uphill side φ_{Lu} are marked with arrows.

Table 7
Summary of the averaged data from the *Gompertzian* fitting for the FILs and water as test liquids on the hydrophobic modified silicon surface.

Test liquid	θ_{shift} [°]	A [°]	k [°$^{-1}$]	φ_{shift} [°]	$f(0°)=\theta_{d_i}$ [°]	φ_{Ld} [°]	$f_{Ld}(\varphi_{Ld})=(\varphi_{Ld})$ [°]
H_2O	108.87	11.80	0.146	5.670	110.1	17.3	118.7
2a	58.20	8.11	0.520	−0.004	61.2	6.6	66.1
2b	46.71	10.78	0.334	1.830	48.4	9.6	56.7
2c	46.27	11.77	0.135	−0.001	50.6	16.3	56.8

	θ_{shift} [°]	A [°]	k [°$^{-1}$]	φ_{shift} [°]	$f(0°)=\theta_{\mu_i}$ [°]	φ_{Lu} [°]	$f_{Lu}(\varphi_{Lu})=(\varphi_{Lu})$ [°]
H_2O	112.33	−30.48	0.072	−11.96	109.5	22.7	93.1
2a	64.16	−69.48	0.125	−8.47	60.3	12.3	26.8
2b	52.11	−85.03	0.110	−11.28	49.4	12.8	15.6
2c	50.76	−37.63	0.097	−12.46	49.4	24.3	23.4

believed to be responsible for the higher viscosities in ionic liquids with long side chains [62]. The measured viscosity values of the fluoroalkylated ionic liquids and the nonfluorinated analogs are summarized in Table 3 and plotted as a function of the side chain length in Fig. 5.

All fluorinated ionic liquids show distinct higher viscosity values at 23 °C than the nonfluorinated ones with the same number of C-atoms in the side chain. While the 1-alkyl-3-imidazolium NTf_2 show only a moderate change in viscosity with elongation of the side chain, the situation is more drastic in the case of the ionic liquids containing a perfluorinated group with the viscosity of **2c** being more than fourfold higher than **2a**. This is a strong hint for the growing formation of fluorous domains with increasing length of the fluorinated side groups. The strong repulsion of the polar charged domains of the imidazolium ring together with the anion forming one kind of domain and the highly lipophilic, hard to polarize perfluoroalkyl-groups forming another. This effect is more distinct when using fluorinated side chains, because perfluoro-groups are known to show stronger lipophilicity than hydrocarbons which makes the heterogeneous interactions with the ionic parts even less preferred. This overall results in a higher repulsion of the domains corresponding with increasing viscosity. The formation of these nanodomains and the higher viscosity is certainly supported by the helical structures and rigidity which are common in fluorinated alkyl compounds and resist the breakup of the different domains [63,64].

3.4. Packing in the solid state

The favored fluorophilic interactions between the perfluoroalkyl side chains in the investigated FILs dominates for long chains and leads to a separation of the polar, ionic imidazolium ring and the highly nonpolar fluorous domain. Further evidence for the preferred homogenous interactions can be seen in the packing of the crystal structure of compound **2d** which is visualized in Fig. 6. It crystallizes in a triclinic crystal system with the space group P1 and the lattice parameters given in Table 4.

The X-ray data clearly showed a packing of the fluorous side chains to highly lipophilic/fluorophilic domains and ionic domains of the imidazolium ring and the bis(trifluoromethanesulfonyl)imide anions. The fluorous domains are arranged as a bilayer, which is also found for alkyl-methyl-imidazolium ILs with long side-chains [65]. All fluorous groups show a helical structure in the crystal as it is expected from the rigidity and the steric effects of the fluorine atoms having a larger Van-der-Waals radius than hydrogen [59]. Some of the anions have a disordered arrangement.

The four anions show different conformation in the packing which is illustrated in Fig. 7. The crystal structure contains four different conformations having two *trans*, and one *cis*, which is very unusual [66] and one intermediate. The values for the bond angles and dihedral angles and a comparison with literature values are given in Table 5. The full data for the crystal structure analysis are given in the supporting information.

3.5. Contact angle measurements and motion behaviors

For the sake of clarity, the results of the contact angle analyses on the hydrophobic modified silicon surface are presented within the main manuscript whereas the results of the contact angle analyses on the hydrophilic silicon surface and the superhydrophilic silicon surface are presented within the supplementary materials. Ionic liquids are derived from organic cations and non-coordinating anions that together form salts with weak interionic interactions. The ionic character of these liquids is especially noticeable in the case of the FILs during the application of the droplets onto the surface (Fig. 8).

When the liquid is disposed the droplet firstly does not wet the surface and forms a large contact angle of approximately 160°. If the dispensing needle is removed the droplet stays stable for a few seconds and then collapses to a contact angle of approximately 60°. This behavior is most likely caused due to the charged interface of the ionic liquid which interacts with the surface charge. Of particular interest is that this behavior only occurs for the FILs whereas AILs do not show this manner. These differences of the interionic interactions between the liquids and the surface also influences the wetting behavior and contact angle determination. To illustrate the different motion behaviors of the droplets different images of sessile drops at different inclination angles of the investigated FILs and water are illustrated in Fig. 9 and of the AILs and water in Fig. 10.

As illustrated in Figs. 9d and 10d the water contact angle measurements result in a dynamic contact angle range dependent on the inclination angle between 80° to 120° which proves the formation of a perfluorooctylsiloxane coating on the silicon surface as illustrated in our former studies [38,39]. Both fluorinated surfaces which were used for the measurements (Figs. 9d and 10d) show a similar contact angle range and contact angle behavior so that it can be assumed that there hardly exists any significant difference of the physical and chemical surface properties between both surfaces. In comparison to the

Table 8
Summary of the averaged data from the *Gompertzian* fitting for the AILs and water as test liquids on the hydrophobic modified silicon surface.

Test liquid	θ_{shift} [°]	A [°]	k [°$^{-1}$]	φ_{shift} [°]	$f(0°)=\theta_{d_i}$ [°]	φ_{Ld} [°]	$f_{Ld}(\varphi_{Ld})=(\varphi_{Ld})$ [°]
H_2O	105.39	9.84	0.139	4.49	106.9	19.1	114.0
$[C_4MIM][NTf_2]$	70.63	5.28	0.756	2.11	70.7	5.2	75.4
$[C_6MIM][NTf_2]$	69.29	3.39	1.026	1.42	69.3	4.8	72.6
$[C_8MIM][NTf_2]$	69.30	4.36	0.756	−1.63	69.4	5.5	73.4

	θ_{shift} [°]	A [°]	k [°$^{-1}$]	φ_{shift} [°]	$f(0°)=\theta_{\mu_i}$ [°]	φ_{Lu} [°]	$f_{Lu}(\varphi_{Lu})=(\varphi_{Lu})$ [°]
H_2O	110.93	−34.56	0.067	−10.96	106.6	24.2	88.0
$[C_4MIM][NTf_2]$	71.91	−24.65	0.221	−4.56	70.3	6.3	59.4
$[C_6MIM][NTf_2]$	70.14	−17.22	0.288	−3.70	69.2	8.0	57.3
$[C_8MIM][NTf_2]$	68.95	−14.20	0.336	−3.80	68.6	8.2	57.7

measurements with water as test liquid, the resulting contact angle range for the AILs (Fig. 10) is between 40° to 80° and the contact angle range of the FILs is between 0° to 80° (Fig. 9). Note that the reproducible and comparable analysis of these highly non-axisymmetric droplets is only possible with the HPDSA procedure. The smaller contact angles in comparison to the water contact angles can be explained by the smaller surface tension $\gamma_{l,v}$ of the ionic liquids. If the initial contact angles $\theta_{d,u}(0°)$ are compared, then it can be noticed that almost no difference between the contact angles of the AILs can be recognized, whereas there exists a small difference of about 10° of the FILs if the length of the fluorinated side changes from 2 to 4. Especially interesting is the different dynamic drain-off behavior of the FILs and AILs due to a different strong pinning especially on the uphill side. Whereas the AILs (Fig. 10) behave like "normal" organic test liquids with small surface tension, which means small critical inclination angles for the first drop motion and a relatively small increase of the downhill angle $\theta_d(\varphi)$, respectively, with a small decrease of the uphill angle $\theta_u(\varphi)$ ($\Delta\theta_{max} = \theta_d(\varphi)_{max} - \theta_u(\varphi)_{max} = 30°$), the FILs illustrate a strong pinning, especially on the uphill side (Fig. 9).

Pinning effects on a solid surface during wetting experiments are mainly caused by surface roughness and chemical surface heterogeneities. Due to the fact that both surfaces have similar wetting characteristics, the different pinning behavior of the ionic liquids is most likely caused by the different polarities which influence the interionic interactions between the surface and the liquid and also the different viscosities of the liquids. As illustrated in Fig. 8, the ionic interaction between the FILs and the surfaces are especially pronounced which explains the strong pinning at the uphill side down to contact angles near 0°. A quantitative measure of pinning effects on a surface represents the *contact angle hysteresis CAH* $\Delta\theta = \theta_{d,e} - \theta_{r,e} \geq 0$ which is the difference between the static advancing/downhill (wetting new surface) and static receding/uphill (formerly wetted surface) contact angles. In this study the static downhill $\theta_{d,e}$ and uphill $\theta_{u,e}$ contact angles were determined to calculate the contact angle hysteresis. Both angles were determined using the HPDSA approach by taking the characteristic contact angle just before the contact line moves to the formerly non-wetted area (static downhill angle), and respectively retracts to the formerly wetted area (static uphill angle). This procedure is normally performed by observing the triple line motion with the human eye and has the main disadvantage that it depends on many subjective criteria of the operator and different conditions during the measurements like frame rate of the video recording, resolution of the CCD camera etc. As a result especially the determination of receding/uphill contact angles is neither reliable nor reproducible whereas the advancing/downhill angles can normally be determined in a reproducible manner. The HPDSA procedure has the main advantage that due to the transfer of the drop shape into μm-coordinates, the boundary points X_{B1o} which corresponds to the triple points can be calculated with high reproducibility and therefore the change of the boundary points ΔX_{B1o} can be estimated with high local resolution and can be used to identify the static downhill

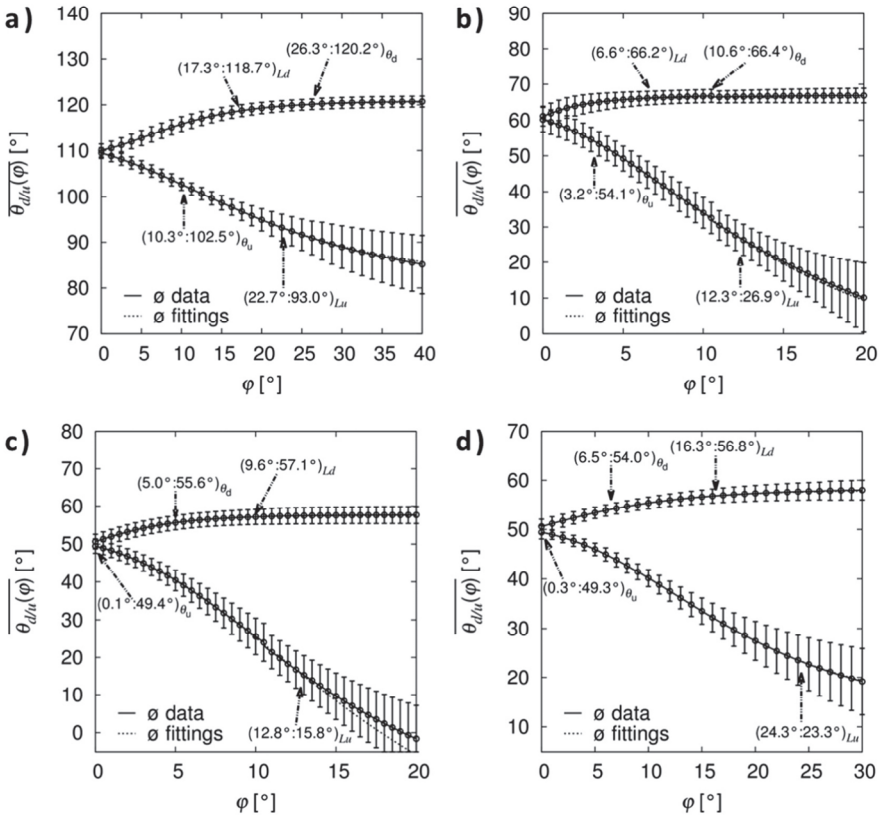

Fig. 13. Overall *Gompertzian* analysis on a hydrophobic modified silicon surface with a) water as test liquid, b) **2a** as test liquid, c) **2b** as test liquid and d) **2c** as test liquid. The limits of the fitting range for the downhill side φ_{Ld} and the uphill side φ_{Lu} as well as the contact angles with the lowest standard deviations $\theta_{d,u}$ are marked with arrows.

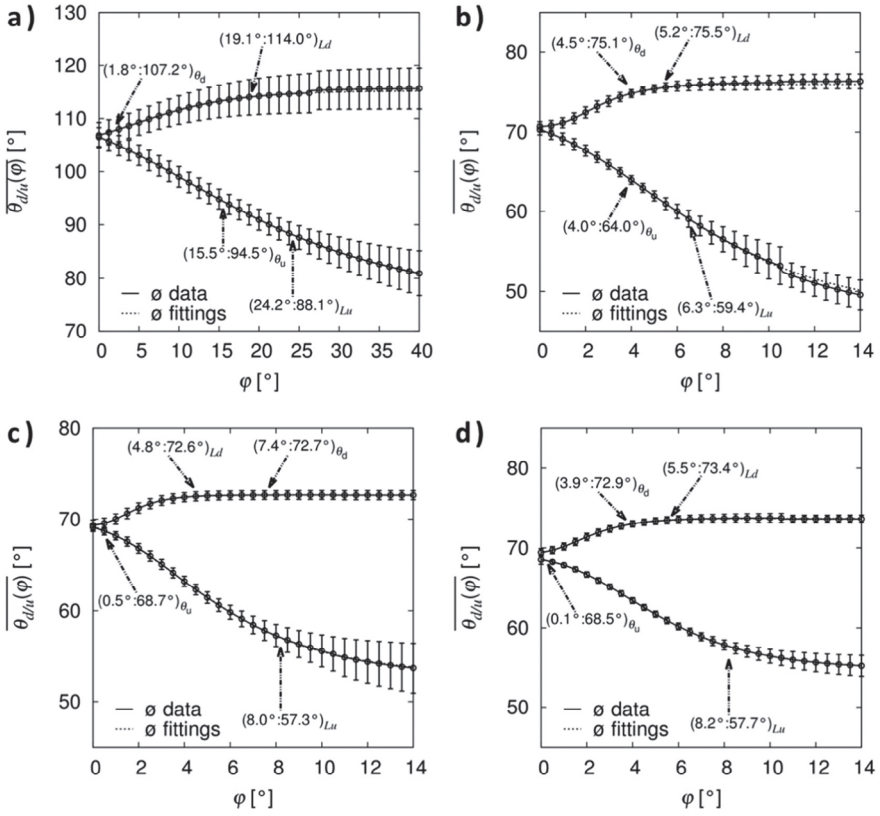

Fig. 14. Overall *Gompertzian* analysis on a hydrophobic modified silicon surface with a) water as test liquid, b) [C_4MIM][NTf_2] as test liquid, c) [C_6MIM][NTf_2] as test liquid, and d) [C_8MIM][NTf_2] as test liquid. The limits of the fitting range for the downhill side φ_{Ld} and the uphill side φ_{Lu} as well as the contact angles with lowest standard deviations $\theta_{d,u}$ are marked with arrows.

and static uphill angles from a huge amount of contact angle data. The procedure is illustrated in Fig. 11 and the results are summarized in Table 6.

A difference of the static downhill angles and contact angle hysteresis of about 10° is visible between the FILs **2a** and **2b** whereas there is no significant difference between **2b** and **2c**. This step between **2a** and **2b**, **2c** is caused by the influence of length of the side chain and the degree of fluorination which results in a change of the polarization (subsection 3.2) and an increase of the viscosity (subsection 3.3). Both quantities also influence the wetting behavior on the surface. In contrast no significant change of polarization and viscosity was estimated for the AILs and therefore the resulting contact angle values do not illustrate any significant differences.

3.6. Overall curve shape of the contact angle data: Gompertzian analyses

Besides the static wetting characteristics the dynamic wetting properties of a liquid on solid surfaces is important for many application, e.g. microfluidics, lubrication or tribology and friction [67–72]. Therefore, the overall curve shape analysis by a *Gompertzian* fitting procedure is an approach to characterize a solid surface in terms of dynamic wetting. The fitting of the data for the downhill and uphill angles $\theta_{d,u}(\varphi)$ relative to the inclination angle φ for every measuring position by a modified *Gompertzian* function which is given by Eq. 6 is the first step of the analysis procedure. All fitting parameters for every investigated test liquid are summarized within the supplementary materials, Table I to Table XXXXII. Thereby, the limits of the fitting range for the downhill

Table 9
Overview about the results of the overall curve shape analysis by *Gompertzian* fitting to identify the contact angles $\theta_{d,u}$ with the lowest standard deviation on a hydrophobic modified silicon surface.

Test liquid	$\theta_d \pm \sigma_d$ [°]	φ_d [°]	$\theta_{Ld} \pm \sigma_{Ld}$ [°]	φ_{Ld} [°]	$\theta_u \pm \sigma_u$ [°]	φ_u [°]	$\theta_{Lu} \pm \sigma_u$ [°]	φ_{Lu} [°]
H_2O	107.2 ± 2.3	1.8	114.0 ± 3.3	19.1	94.5 ± 1.9	15.5	88.1 ± 2.2	24.2
2a	66.4 ± 1.6	10.6	66.2 ± 1.9	6.6	54.1 ± 3.4	3.2	26.9 ± 4.4	12.3
2b	55.6 ± 1.9	5.0	57.1 ± 2.0	9.6	49.4 ± 1.7	0.1	15.8 ± 5.2	12.8
2c	54.0 ± 1.1	6.5	56.8 ± 1.5	16.3	49.3 ± 0.9	0.3	23.3 ± 5.2	24.3
[C_4MIM][NTf_2]	75.1 ± 0.5	4.5	75.5 ± 0.5	5.2	64.0 ± 0.5	4.0,	59.4 ± 1.0	6.3
[C_6MIM][NTf_2]	72.7 ± 0.5	7.4	72.6 ± 0.5	4.8	68.7 ± 0.4	0.5	57.3 ± 1.2	8.0
[C_8MIM][NTf_2]	72.9 ± 0.4	3.9	73.4 ± 0.4	5.5	68.5 ± 0.2	0.1	57.7 ± 0.6	8.2

side φ_{Ld} and for the uphill side φ_{Lu} are manually defined at the point when a drop motion from the static (non-moving/slow-moving) to the dynamic range (high velocity) is observed. The procedure is illustrated in Fig. 12.

Thereby, the *Gompertzian* function simulates an idealized course of contact angles relative to the inclination angle without any pinning effect. By averaging these data, the procedure is able to describe the trend of the measurements from a huge amount of contact angle data (≈10,000 images/contact angles per measurement) by only four fitting parameters. Furthermore, it is possible to identify contact angles with the smallest standard deviations θ_d, θ_u. Contrary to the static wetting analyses (subsection 3.5), this approach also considers the quasi-static (slow-moving) and dynamic (high velocity) range of the measurements so that e.g. strong pinning effects on the uphill side (Fig. 9, S1–3) can also be analyzed and an overall characterization of the wettability of the surface is possible. The motion behavior of sessile drops on inclining plates is strongly influenced by the initial conditions of the drop displacement (e.g. dispense rate, different initial drop diameters, different local surface properties) and may result in possible outliners. These outliners can be identified by performing the first step of the analysis (Fig. 12) but are not removed to keep external non-automatic interventions by the experimenter as low as possible. Averaging of the Gompertzian fittings for every measuring position leads to average data slopes and standard deviations. These data can also be represented by a Gompertzian function leading to the averaged data for the FILs (Table 7) and for the AILs (Table 8) which describe the average dynamic wetting behavior of 0.03 mL droplets of the test liquids on a hydrophobic silicon surface.

The fitting parameters *A* (*Amplitude* of the contact angles ≡ difference between the smallest and largest contact angle) and *k* (slope of the data points) of the averaged *Gompertzian* functions are especially important because they can be used to characterize the pinning of the droplets on the surface during the dynamic wetting experiments. This means that a strong pinning results in a large *A*-value and a small *k*-value whereas a weak pinning results in a small *A*-value and a large *k*-value. The average data of the Gompertzian fittings for the FILs as test liquid are illustrated in Fig. 13 and for the AILs in Fig. 14.

The Gompertzian function starts at minus infinity [45] so that physically meaningful values are only obtainable within the fitting range ($0 \le \varphi_{d,u} \le \varphi_{Ld,Lu}$). On an ideal solid surface, this means atomically flat, rigid, and chemically homogeneous; it can be assumed that a characteristic contact angle/inclination angle pair for the downhill motion θ_d/φ_d and for the uphill motion θ_u/φ_u should exist which corresponds to an intersection point of all Gompertzian functions for every position. On real solid surfaces, local inhomogeneities concerning the surface roughness and/or chemical properties of the surface will result in a variance of the contact angle behavior. Furthermore, different properties of the used test liquids, e.g. viscosity and polarization, also influence the motion behavior as already illustrated in subsection 3.5. To find a meaningful contact angle which characterizes the dynamic wetting properties of the surface it is therefore reasonable to identify the contact angle/inclination angle pair/range with the lowest standard deviations for all measuring positions. For all sample surfaces the contact angle/inclination angle pairs with the smallest standard deviation which are characteristic for the overall wetting properties of the surfaces and the contact angles/inclination angle pairs for the fitting limits for the downhill φ_{Ld} and uphill motion φ_{Lu} are summarized in Table 9.

The contact angles with the lowest standard deviation $\theta_{d,u}$ are located with the exception of the downhill angle for **2a** and [C_6MIM][NTf_2] within the fitting range and are therefore called "real". The downhill angle for **2a** and [C_6MIM][NTf_2] are located beyond the fitting range and are therefore called "imaginary". In this case it is physically more reasonable to present the angles at the limit of the fitting range. These are also the last contact angles which are less influenced by the motion dynamics of the drop which generally results in larger standard deviations.

4. Conclusion

The introduction of fluorous side chains into methyl-imidazolium ILs is a useful tool for the tailoring of the properties of the common and widely used family of imidazolium-based ionic liquids. The investigated fluorous FILs showed a high thermal stability and wide liquid range which is in the case of **2a** and **2b** even bigger than in the alkyl-imidazolium ILs with the same number of C-atoms in the side chain. These properties make the investigated fluorous ionic liquids promising candidates for practical uses like being used as solvents, for immobilization/extraction techniques or applications that demand higher temperatures. The FILs show a higher polarity when the measurements were performed with Reichardt's Dye and a polarity in the same range of the AILs, when measured with Nile Red. Only **2a** showed a markedly higher polarity with both dyes. Viscosity and the crystal structure of **2d** gave strong evidence for the formation of structured nanodomains like they were observed in the alkyl-derivatives with long hydrocarbon-chains. The contact angle analyses with the HPDSA approach illustrate a significant difference of the static and dynamic wetting between the FILs and AILs. Whereas the AILs show similar wetting characteristics like "normal" organic test liquids with a small surface tension, the FILs illustrate a strong pinning, especially on the uphill side. These differences demonstrate the strong ionic character of the liquids which most likely leads to structuring on nanoscale and a charged solid–liquid interface. This effect depends strongly on the polarization of the liquid and results in a step of the static contact angles of about 10° if the length of fluorinated side changes from 2 to 4. Furthermore, the dynamic wetting properties of the ionic liquids were analyzed using a *Gompertzian* fitting procedure. In this work, it is illustrated that this approach is able to analyze even strongly non-axisymmetric systems down to a contact angle range near 0°. Using this procedure, the overall contact angle behavior can be visualized from a huge amount of contact angle data (≈10,000 images/contact angles per measurement) with only four fitting parameters. By calculating standard deviations, the procedure results in the possibility to identify contact angle/inclination angle pairs with the lowest standard deviation which can be called "characteristic" for the dynamic overall wetting situation on the surface which is an important parameter in science and industry when liquids are involved in a process.

Acknowledgement

We want to thank the Deutsche Bundesstiftung Umwelt (DBU) (31925-41) for financial support, Dr. Volker Huch for the crystal structure analysis and Heike Höltzen for the TGA-measurements.

Appendix A. Supplementary data

Supplementary data to this article can be found online at http://dx.doi.org/10.1016/j.molliq.2016.01.011.

References

[1] T. Welton, Chem. Rev. 99 (1999) 2071–2083.
[2] R.D. Rogers, K.R. Seddon, Science 302 (2003) 792–793.
[3] P. Wasserscheid, T. Welton, Ionic Liquids in Synthesis, second ed. Weinheim, WILEY-VCH, 2007.
[4] J.F. Wishart, Energy Environ. Sci. 2 (2009) 956–961.
[5] M. Armand, F. Endres, D.R. MacFarlane, B. Scrosati, H. Ohno, Nat. Mater. 8 (2009) 621–629.
[6] D.R. MacFarlane, et al., Energy Environ. Sci. 7 (2014) 232–250.
[7] M. Mezger, et al., Science 322 (2008) 424–428.
[8] T.L. Merrigan, E.D. Bates, S.C. Dorman, J.J.H. Davis, Chem. Commun. (2000) 2051–2052.
[9] J.J. Tindale, C. Na, M.C. Jennings, P.J. Ragogna, Can. J. Chem. 85 (2007) 660–667.
[10] H. Xue, J.M. Shreeve, Eur. J. Inorg. Chem. (2005) 2573–2580.
[11] J.E. Bara, C.J. Gabriel, T.K. Carlisle, D.E. Camper, A. Finotello, D.L. Gin, R.D. Noble, Chem. Eng. J. 147 (2009) 43–50.
[12] M.J. Muldoon, S.N.V.K. Aki, J.L. Anderson, J.K. Dixon, J.F. Brennecke, J. Phys. Chem. B 111 (2007) 9001–9009.

[13] J.v.d. Broeke, F. Winter, B.-J. Deelman, G.v. Koten, Org. Lett. 4 (2002) 3851–3854.
[14] C. Emnet, K.M. Weber, J.A. Vidal, C.S. Consorti, A.M. Stuart, J.A. Gladysz, Adv. Synth. Catal. 348 (2006) 1625–1634.
[15] A. Abate, et al., J. Mater. Chem. A 1 (2013) 6572–6578.
[16] A.B. Pereiro, et al., ACS Sustainable Chem. Eng. 1 (2013) 427–439.
[17] A.B. Pereiro, J.M.M. Araújo, F.S. Teixeira, I.M. Marrucho, M.M. Pineiro, L.P.N. Rebelo, Langmuir 31 (2015) 1283–1295.
[18] A.Y. Fadeev, T.J. McCarthy, Langmuir 15 (1999) 7238–7243.
[19] R. Sedev, Curr. Opin. Colloid Interface Sci. 16 (2011) 310–316.
[20] L. Gao, T.J. McCarthy, J. Am. Chem. Soc. 129 (2007) 3804–3805.
[21] J.W. Krumpfer, P. Bian, P. Zheng, L. Gao, T.J. McCarthy, Langmuir 27 (2011) 2166–2169.
[22] I. Delcheva, J. Ralston, D.A. Beattie, M. Krasowska, Adv. Colloid Interf. Sci. 222 (2015) 162–171.
[23] M. Schmitt, F. Heib, J. Chem. Phys. 139 (2013) 134201.
[24] F. Castiglione, et al., Phys. Chem. Chem. Phys. 12 (2010) 1784–1792.
[25] C.C. Weber, A.F. Masters, T. Maschmeyer, Angew. Chem. Int. Ed. 51 (2012) 11483–11486.
[26] R. Taniki, N. Kenmochi, K. Matsumoto, R. Hagiwara, J. Fluor. Chem. 149 (2013) 112–118.
[27] L. Xu, W. Chen, J.F. Bickley, A. Steiner, J. Xiao, J. Organomet. Chem. 598 (2000) 409–416.
[28] R.P. Sigh, R.W. Winter, G.L. Gard, Y. Gao, J.M. Shreeve, Inorg. Chem. 42 (2003) 6142–6146.
[29] H. Heitzman, B.A. Young, D.J. Ruasch, P. Rickert, D.C. Stepinski, M.L. Dietz, Talanta 69 (2006) 527–531.
[30] K. Dimroth, C. Reichardt, Liebigs Ann. 661 (1963) 1–37.
[31] J.F. Deye, T.A. Berger, A.G. Anderson, Anal. Chem. 62 (1990) 615–622.
[32] C. Reichardt, Chem. Rev. 94 (1994) 2319–2358.
[33] J.P. Cerón-Carrasco, D. Jacquemin, C. Laurence, A. Planchat, C. Reichardt, K. Sraïdi, J. Phys. Org. Chem. 27 (2014) 512–518.
[34] A.J. Carmichael, K.R. Seddon, J. Phys. Org. Chem. 13 (2000) 591–595.
[35] C. Reichardt, Green Chem. 7 (2005).
[36] H. Tokuda, S. Tsuzuki, M.A.B.H. Susan, K. Hayamizu, M. Watanabe, J. Phys. Chem. B 110 (2006) 19593–19600.
[37] G.M. Sheldrick, Acta Crystallogr. A64 (2008) 112–122.
[38] M. Schmitt, R. Hempelmann, S. Ingebrandt, W. Munief, D. Durneata, K. Groß, F. Heib, Int. J. Adhes. Adhes. 55 (2014) 123–131.
[39] F. Heib, R. Hempelmann, W.M. Munief, S. Ingebrandt, F. Fug, W. Possart, K. Groß, M. Schmitt, Appl. Surf. Sci. 342 (2015) 11–25.
[40] M. Schmitt, R. Hempelmann, S. Ingebrandt, W.M. Munief, K. Groß, J. Grub, F. Heib, J. Adhes. Sci. Technol. 29 (2015) 1796–1806.
[41] M. Schmitt, R. Hempelmann, F. Heib, Z. Phys. Chem. 228 (2014) 11–25.
[42] M. Schmitt, R. Hempelmann, F. Heib, Z. Phys. Chem. 228 (2014) 629–648.
[43] M. Schmitt, K. Groß, J. Grub, F. Heib, J. Colloid Interface Sci. 447 (2015) 229–239.
[44] M. Schmitt, J. Grub, F. Heib, J. Colloid Interface Sci. 447 (2015) 248–253.
[45] B. Gompertz, Philos. Trans. R. Soc. Lond. 1 (1825) 513–518.
[46] C. Maton, N.D. Vos, C.V. Stevens, Chem. Soc. Rev. 42 (2013) 5963–5977.
[47] R.P. Sigh, S. Manandhar, J.M. Shreeve, Tetrahedron Lett. 43 (2002) 9497–9499.
[48] A.N. Tran, T.-N.V. Do, L.-P.M. Le, T.N. Le, J. Fluor. Chem. 164 (2014) 38–43.
[49] R.P. Sigh, S. Manandhar, J.M. Shreeve, Synthesis 10 (2003) 1579–1585.
[50] O.D. Gupta, P.D. Armstrong, J.M. Shreeve, Tetrahedron Lett. 44 (2003) 9367–9370.
[51] G.D. Smith, et al., Phys. Chem. Chem. Phys. 12 (2010) 7064–7076.
[52] P. Kirsch, Modern Fluoroorganic Chemistry: Synthesis, Reactivity, Applications, Weinheim, WILEY-VCH, 2004.
[53] M. Villanueva, A. Coronas, J. Garcia, J. Salgado, Ind. Eng. Chem. Res. 53 (2013) 15718–15727.
[54] H. Tokuda, K. Hayamizu, K. Ishii, M.A.B.H. Susan, M. Watanabe, J. Phys. Chem. B 109 (2005) 6103–6110.
[55] R. Hayes, G.G. Warr, R. Atkin, Chem. Rev. 115 (2015) 6357–6426.
[56] J.N.A. Canongia Lopes, A.A.H. Pádua, J. Phys. Chem. B 110 (2006) 3330–3335.
[57] O. Russina, A. Triolo, H.-J. Bleif, E.D. Cola, J. Phys. Chem. B 111 (2007) 4641–4644.
[58] Y. Shen, et al., Phys. Chem. Chem. Phys. 14 (2012) 7981–7992.
[59] J.A. Gladysz, D.P. Curran, I.T. Horvath, Handbook of Fluorous Chemistry, Weinheim, WILEY-VCH, 2004.
[60] J. Jacquemin, P. Husson, A.A.H. Padua, V. Majer, Green Chem. 8 (2006) 172–180.
[61] K. Ueno, H. Tokuda, M. Watanabe, Phys. Chem. Chem. Phys. 12 (2010) 1649–1658.
[62] Y. Wang, G.A. Voth, J. Phys. Chem. B 110 (2006) 18601–18608.
[63] F. Kerton, R. Marriott, Alternative Solvents for Green Chemistry, second ed. Royal Society of Chemistry, Cambridge, 2013.
[64] C. Reichardt, T. Welton, Solvents and Solvent Effects in Organic Chemistry, forth ed. Weinheim, WILEY-VCH, 2011.
[65] A. Downard, M.J. Earle, C. Hardacre, S.E.J. McMath, M. Nieuwenhuyzen, S.J. Teat, Chem. Mater. 16 (2004) 43–48.
[66] J.D. Holbrey, W.M. Reichert, R.D. Rogers, Dalton Trans. (2004).
[67] Z. Barikbin, et al., Lab Chip 10 (2010) 1458–2463.
[68] I. Otero, E.R. López, M. Reichelt, M. Villanueva, J. Salgado, J. Fernández, ACS Appl. Mater. Interfaces 6 (2014) 13115–13128.
[69] F. Zhou, Y. Liang, W. Liu, Chem. Soc. Rev. 38 (2009) 2590–2599.
[70] H.J. Castejón, T.J. Wynn, Z.M. Marcin, J. Phys. Chem. B 118 (2014) 3661–3668.
[71] I. Minami, Molecules 14 (2009) 2286–2305.
[72] Y. Wu, Q. Wei, M. Cai, F. Zhou, Adv. Mater. Interfaces 2 2 (2015).

3. References

[1] H. Weingärtner, NMR studies of ionic liquids: Structure and dynamics, *Curr. Opin. Colloid Interface Sci.*, **2013**, 18, 183–189. DOI: 10.1016/j.cocis.2013.04.001.

[2] G. Zarubin, M. Bier, Static dielectric properties of dense ionic fluids, *J. Chem. Phys.*, **2015**, 142, 184502. DOI: 10.1063/1.4920976.

[3] N. V Plechkova, K. R. Seddon, Applications of ionic liquids in the chemical industry, *Chem. Soc. Rev.*, **2008**, 37, 123–150. DOI: 10.1039/B006677J.

[4] P. Wasserscheid, W. Keim, Ionic Liquids—New "Solutions" for Transition Metal Catalysis, *Angew. Chemie.*, **2000**, 39, 3772–3789. DOI: 10.1002/1521-3773(20001103)39:21<3772::AID-ANIE3772>3.0.CO;2-5.

[5] M. Freemantle, Designer Solvents, *Chem. Eng. News.*, **1998**, 76, 32–37. DOI: 10.1021/cen-v076n013.p032.

[6] R. Giernoth, Task-Specific Ionic Liquids, *Angew. Chemie Int. Ed.*, **2010**, 49, 2834–2839. DOI: 10.1002/anie.200905981.

[7] S. Zahn, F. Uhlig, J. Thar, C. Spickermann, B. Kirchner, Intermolecular Forces in an Ionic Liquid ([Mmim][Cl]) versus Those in a Typical Salt (NaCl), *Angew. Chemie Int. Ed.*, **2008**, 47, 3639–3641. DOI: 10.1002/anie.200705526.

[8] K. Fumino, V. Fossog, K. Wittler, R. Hempelmann, R. Ludwig, Dissecting Anion-Cation Interaction Energies in Protic Ionic Liquids, *Angew. Chemie Int. Ed.*, **2013**, 52, 2368–2372. DOI: 10.1002/anie.201207065.

[9] T. Köddermann, D. Paschek, R. Ludwig, Ionic Liquids: Dissecting the Enthalpies of Vaporization, *ChemPhysChem.*, **2008**, 9, 549–555. DOI: 10.1002/cphc.200700814.

[10] S. Che, R. Dao, W. Zhang, X. Lv, H. Li, C. Wang, Designing an anion-functionalized fluorescent ionic liquid as an efficient and reversible turn-off sensor for detecting SO 2, *Chem. Commun.*, **2017**, 53, 3862–3865. DOI: 10.1039/C7CC00676D.

[11] J. M. Delgado, A. Raymundo, M. Vilarigues, L. C. Branco, C. A. T. Laia, Characterization of a novel intrinsic luminescent room-temperature ionic liquid based on [P6,6,6,14][ANS], *Chem. - A Eur. J.*, **2015**, 21, 726–732. DOI: 10.1002/chem.201402534.

[12] S. Tang, A. Babai, A.-V. Mudring, Europium-Based Ionic Liquids as Luminescent Soft Materials, *Angew. Chemie Int. Ed.*, **2008**, 47, 7631–7634. DOI: 10.1002/anie.200801159.

[13] B. Mallick, B. Balke, C. Felser, A. V. Mudring, Dysprosium room-temperature ionic liquids with strong luminescence and response to magnetic fields, *Angew. Chemie - Int. Ed.*, **2008**, 47, 7635–7638. DOI: 10.1002/anie.200802390.

[14] T. Peppel, M. Köckerling, M. Geppert-Rybczyńska, R. V. Ralys, J. K. Lehmann, S. P. Verevkin, A. Heintz, Low-Viscosity Paramagnetic Ionic Liquids with Doubly Charged $[Co(NCS)_4]_2^-$ Ions, *Angew. Chemie Int. Ed.*, **2010**, 49, 7116–7119. DOI: 10.1002/anie.201000709.

[15] V. Misuk, A. Mai, K. Giannopoulos, F. Alobaid, B. Epple, H. Loewe, Micro magnetofluidics: droplet manipulation of double emulsions based on paramagnetic ionic liquids, *Lab Chip.*, **2013**, 13, 4542. DOI: 10.1039/c3lc50897h.

[16] A. Joseph, G. Żyła, V. I. Thomas, P. R. Nair, A. S. Padmanabhan, S. Mathew, Paramagnetic ionic liquids for advanced applications: A review, *J. Mol. Liq.*, **2016**, 218, 319–331. DOI: 10.1016/j.molliq.2016.02.086.

[17] D. K. Bwambok, M. M. Thuo, M. B. J. Atkinson, K. A. Mirica, N. D. Shapiro, G. M. Whitesides, Paramagnetic Ionic Liquids for Measurements of Density Using Magnetic Levitation, *Anal. Chem.*, **2013**, 85, 8442–8447. DOI: 10.1021/ac401899u.

[18] E. Santos, J. Albo, A. Rosatella, C. A. M. Afonso, Á. Irabien, Synthesis and characterization of Magnetic Ionic Liquids (MILs) for CO 2 separation, *J. Chem. Technol. Biotechnol.*, **2014**, 89, 866–871. DOI: 10.1002/jctb.4323.

[19] E. Santos, J. Albo, A. Irabien, Magnetic ionic liquids: synthesis, properties and applications, *RSC Adv.*, **2014**, 4, 40008–40018. DOI: 10.1039/C4RA05156D.

[20] J. Ding, D. W. Armstrong, Chiral ionic liquids: Synthesis and applications, *Chirality.*, **2005**, 17, 281–292. DOI: 10.1002/chir.20153.

[21] C. Baudequin, D. Brégeon, J. Levillain, F. Guillen, J.-C. Plaquevent, A.-C. Gaumont, Chiral ionic liquids, a renewal for the chemistry of chiral solvents? Design, synthesis and applications for chiral recognition and asymmetric synthesis, *Tetrahedron: Asymmetry.*, **2005**, 16, 3921–3945. DOI: 10.1016/j.tetasy.2005.10.026.

[22] S. Rizzo, S. Arnaboldi, V. Mihali, R. Cirilli, A. Forni, A. Gennaro, A. A. Isse, M. Pierini, P. R. Mussini, F. Sannicolò, "Inherently Chiral" Ionic-Liquid Media: Effective Chiral Electroanalysis on Achiral Electrodes, *Angew. Chemie Int. Ed.*, **2017**, 56, 2079–2082. DOI: 10.1002/anie.201607344.

[23] P. Oulevey, S. Luber, B. Varnholt, T. Bürgi, Symmetry Breaking in Chiral Ionic Liquids Evidenced by Vibrational Optical Activity, *Angew. Chemie Int. Ed.*, **2016**, 55, 11787–11790. DOI: 10.1002/anie.201605792.

[24] R. Caminiti, L. Gontrani, Eds., *The Structure of Ionic Liquids*, Springer International Publishing, Cham, **2014**.

[25] R. Hayes, G. G. Warr, R. Atkin, Structure and Nanostructure in Ionic Liquids, *Chem. Rev.*, **2015**, 115, 6357–6426. DOI: 10.1021/cr500411q.

[26] H.-O. Hamaguchi, R. Ozawa, in *Advances in Chemical Physics*, **2005**, vol. 131, p. 85–104. DOI: 10.1002/0471739464.ch3.

[27] P. Hapiot, C. Lagrost, Electrochemical Reactivity in Room-Temperature Ionic Liquids, *Chem. Rev.*, **2008**, 108, 2238–2264. DOI: 10.1021/cr0680686.

[28] C. Reichardt, Polarity of ionic liquids determined empirically by means of solvatochromic pyridinium N-phenolate betaine dyes, *Green Chem.*, **2005**, 7, 339. DOI: 10.1039/b500106b.

[29] C. F. Poole, Chromatographic and spectroscopic methods for the determination of solvent properties of room temperature ionic liquids, *J. Chromatogr. A.*, **2004**, 1037, 49–82. DOI: 10.1016/j.chroma.2003.10.127.

[30] Y. Zhou, J. Qu, Ionic Liquids as Lubricant Additives: A Review, *ACS Appl. Mater. Interfaces.*, **2017**, 9, 3209–3222. DOI: 10.1021/acsami.6b12489.

[31] J. Qu, D. G. Bansal, B. Yu, J. Y. Howe, H. Luo, S. Dai, H. Li, P. J. Blau, B. G. Bunting, G. Mordukhovich, D. J. Smolenski, Antiwear Performance and Mechanism of an Oil-Miscible Ionic Liquid as a Lubricant Additive, *ACS Appl. Mater. Interfaces.*, **2012**, 4, 997–1002. DOI: 10.1021/am201646k.

[32] B. Yu, D. G. Bansal, J. Qu, X. Sun, H. Luo, S. Dai, P. J. Blau, B. G. Bunting, G. Mordukhovich, D. J. Smolenski, Oil-miscible and non-corrosive phosphonium-based ionic liquids as candidate lubricant additives, *Wear.*, **2012**, 289, 58–64. DOI: 10.1016/j.wear.2012.04.015.

[33] I. Krossing, J. M. Slattery, C. Daguenet, P. J. Dyson, A. Oleinikova, H. Weingärtner, Why Are Ionic Liquids Liquid? A Simple Explanation Based on Lattice and Solvation Energies, *J. Am. Chem. Soc.*, **2006**, 128, 13427–13434. DOI: 10.1021/ja0619612.

[34] A. A. H. Pádua, M. F. Costa Gomes, J. N. A. Canongia Lopes, Molecular Solutes in Ionic Liquids: A [1] A. A. H. Pádua, M. F. Costa Gomes, J. N. A. Canongia Lopes, Molecular Solutes in Ionic Liquids: A Structural Perspective, Acc. Chem. Res., 2007, 40, 1087–1096. DOI: 10.1021/ar700050q.Structural Perspective, *Acc. Chem. Res.*, **2007**, 40, 1087–1096. DOI: 10.1021/ar700050q.

[35] T. Welton, Ionic liquids in catalysis, *Coord. Chem. Rev.*, **2004**, 248, 2459–2477. DOI: 10.1016/j.ccr.2004.04.015.

[36] P. M. Dean, J. Turanjanin, M. Yoshizawa-Fujita, D. R. MacFarlane, J. L. Scott, Exploring an Anti-Crystal Engineering Approach to the Preparation of Pharmaceutically Active Ionic Liquids, *Cryst. Growth Des.*, **2009**, 9, 1137–1145. DOI: 10.1021/cg8009496.

[37] I. López-Martin, E. Burello, P. N. Davey, K. R. Seddon, G. Rothenberg, Anion and Cation Effects on Imidazolium Salt Melting Points: A Descriptor Modelling Study, *ChemPhysChem.*, **2007**, 8, 690–695. DOI: 10.1002/cphc.200600637.

[38] S. M. Murray, R. A. O'Brien, K. M. Mattson, C. Ceccarelli, R. E. Sykora, K. N. West, J. H. Davis, The Fluid-Mosaic Model, Homeoviscous Adaptation, and Ionic Liquids: Dramatic Lowering of the Melting Point by Side-Chain Unsaturation, *Angew. Chemie Int. Ed.*, **2010**, 49, 2755–2758. DOI: 10.1002/anie.200906169.

[39] A. M. Fernandes, M. A. A. Rocha, M. G. Freire, I. M. Marrucho, J. A. P. Coutinho, L. M. N. B. F. Santos, Evaluation of Cation−Anion Interaction Strength in Ionic Liquids, *J. Phys. Chem. B.*, **2011**, 115, 4033–4041. DOI: 10.1021/jp201084x.

[40] D. R. MacFarlane, S. A. Forsyth, J. Golding, G. B. Deacon, Ionic liquids based on imidazolium, ammonium and pyrrolidinium salts of the dicyanamide anion, *Green Chem.*, **2002**, 4, 444–448. DOI: 10.1039/b205641k.

[41] E. I. Izgorodina, M. Forsyth, D. R. MacFarlane, Towards a Better Understanding of 'Delocalized Charge' in Ionic Liquid Anions, *Aust. J. Chem.*, **2007**, 60, 15. DOI: 10.1071/CH06304.

[42] P. M. Dean, J. M. Pringle, D. R. MacFarlane, Structural analysis of low melting organic salts: perspectives on ionic liquids, *Phys. Chem. Chem. Phys.*, **2010**, 12, 9144. DOI: 10.1039/c003519j.

[43] J. D. Holbrey, R. D. Rogers, R. A. Mantz, P. C. Trulove, V. A. Cocalia, A. E. Visser, J. L. Anderson, J. L. Anthony, J. F. Brennecke, E. J. Maginn, T. Welton, R. A. Mantz, in *Ionic Liquids in Synthesis*, eds. P. Wasserscheid and T. Welton, Wiley-VCH Verlag GmbH & Co. KGaA, Weinheim, Germany, **2007**, p. 57–174. DOI: 10.1002/9783527621194.ch3.

[44] S. Tang, G. A. Baker, H. Zhao, Ether- and alcohol-functionalized task-specific ionic liquids: attractive properties and applications, *Chem. Soc. Rev.*, **2012**, 41, 4030. DOI: 10.1039/c2cs15362a.

[45] Z.-B. Zhou, H. Matsumoto, K. Tatsumi, Low-Melting, Low-Viscous, Hydrophobic Ionic Liquids: Aliphatic Quaternary Ammonium Salts with Perfluoroalkyltrifluoroborates, *Chem. - A Eur. J.*, **2005**, 11, 752–766. DOI: 10.1002/chem.200400817.

[46] K. Tsunashima, M. Sugiya, Physical and electrochemical properties of low-viscosity phosphonium ionic liquids as potential electrolytes, *Electrochem. commun.*, **2007**, 9, 2353–2358. DOI: 10.1016/j.elecom.2007.07.003.

[47] Z.-B. Zhou, H. Matsumoto, K. Tatsumi, Cyclic Quaternary Ammonium Ionic Liquids with Perfluoroalkyltrifluoroborates: Synthesis, Characterization, and Properties, *Chem. - A Eur. J.*, **2006**, 12, 2196–2212. DOI: 10.1002/chem.200500930.

[48] J. M. Crosthwaite, M. J. Muldoon, J. K. Dixon, J. L. Anderson, J. F. Brennecke, Phase transition and decomposition temperatures, heat capacities and viscosities of pyridinium ionic liquids, *J. Chem. Thermodyn.*, **2005**, 37, 559–568. DOI: 10.1016/j.jct.2005.03.013.

[49] Z. Chen, Y. Huo, J. Cao, L. Xu, S. Zhang, Physicochemical Properties of Ether-Functionalized Ionic Liquids: Understanding Their Irregular Variations with the Ether Chain Length, *Ind. Eng. Chem. Res.*, **2016**, 55, 11589–11596. DOI: 10.1021/acs.iecr.6b02875.

[50] E. Gómez, N. Calvar, Á. Domínguez, in *Ionic Liquids - Current State of the Art*, ed. K. Pesek, InTech, **2015**, p. 199–208. DOI: 10.5772/59271.

[51] J. S. Moreno, S. Jeremias, A. Moretti, S. Panero, S. Passerini, B. Scrosati, G. B. Appetecchi, Ionic liquid mixtures with tunable physicochemical properties, *Electrochim. Acta.*, **2015**, 151, 599–608. DOI: 10.1016/j.electacta.2014.11.056.

[52] G. M. A. Girard, M. Hilder, H. Zhu, D. Nucciarone, K. Whitbread, S. Zavorine, M. Moser, M. Forsyth, D. R. MacFarlane, P. C. Howlett, Electrochemical and physicochemical properties of small phosphonium cation ionic liquid electrolytes with high lithium salt content, *Phys. Chem. Chem. Phys.*, **2015**, 17, 8706–8713. DOI: 10.1039/C5CP00205B.

[53] C. P. Fredlake, J. M. Crosthwaite, D. G. Hert, S. N. V. K. Aki, J. F. Brennecke, Thermophysical Properties of Imidazolium-Based Ionic Liquids, *J. Chem. Eng. Data.*, **2004**, 49, 954–964. DOI: 10.1021/je034261a.

[54] P. Zürner, H. Schmidt, S. Bette, J. Wagler, G. Frisch, Ionic liquid, glass or crystalline solid? Structures and thermal behaviour of (C 4 mim) 2 CuCl 3, *Dalt. Trans.*, **2016**, 45, 3327–3333. DOI: 10.1039/C5DT03772G.

[55] M. Galiński, A. Lewandowski, I. Stępniak, Ionic liquids as electrolytes, *Electrochim. Acta.*, **2006**, 51, 5567–5580. DOI: 10.1016/j.electacta.2006.03.016.

[56] V. Armel, D. Velayutham, J. Sun, P. C. Howlett, M. Forsyth, D. R. MacFarlane, J. M. Pringle, Ionic liquids and organic ionic plastic crystals utilizing small phosphonium cations, *J. Mater. Chem.*, **2011**, 21, 7640. DOI: 10.1039/c1jm10417a.

[57] S. V Dzyuba, R. A. Bartsch, Influence of Structural Variations in 1-Alkyl(aralkyl)-3-Methylimidazolium Hexafluorophosphates and Bis(trifluoromethyl-sulfonyl)imides on Physical Properties of the Ionic Liquids, *Chem. Phys. Chem.*, **2002**, 3, 161–166.

[58] C. M. Gordon, J. D. Holbrey, A. R. Kennedy, K. R. Seddon, Ionic liquid crystals: hexafluorophosphate salts, *J. Mater. Chem.*, **1998**, 8, 2627–2636. DOI: 10.1039/a806169f.

[59] P. Bonhôte, A.-P. Dias, N. Papageorgiou, K. Kalyanasundaram, M. Grätzel, Hydrophobic, Highly Conductive Ambient-Temperature Molten Salts †, *Inorg. Chem.*, **1996**, 35, 1168–1178. DOI: 10.1021/ic951325x.

[60] A. E. Bradley, C. Hardacre, J. D. Holbrey, S. Johnston, S. E. J. McMath, M. Nieuwenhuyzen, Small-Angle X-ray Scattering Studies of Liquid Crystalline 1-Alkyl-3-methylimidazolium Salts, *Chem. Mater.*, **2002**, 14, 629–635. DOI: 10.1021/cm010542v.

[61] S. Zhang, X. Lu, Q. Zhou, X. Li, X. Zhang, S. Li, *Ionic Liquids - Physicochemical Properties*, Elsevier, Amsterdam, **2009**.

[62] T. L. Greaves, C. J. Drummond, Solvent nanostructure, the solvophobic effect and amphiphile self-assembly in ionic liquids, *Chem. Soc. Rev.*, **2013**, 42, 1096–1120. DOI: 10.1039/C2CS35339C.

[63] E. Gómez, N. Calvar, Á. Domínguez, E. A. Macedo, Thermal Analysis and Heat Capacities of 1-Alkyl-3-methylimidazolium Ionic Liquids with NTf 2 – , TFO – , and DCA – Anions, *Ind. Eng. Chem. Res.*, **2013**, 52, 2103–2110. DOI: 10.1021/ie3012193.

[64] M. C. Castro, A. Arce, A. Soto, H. Rodríguez, Liquid-liquid equilibria of mutually immiscible ionic liquids with a common anion of basic character, *J. Chem. Thermodyn.*, **2016**, 102, 12–21. DOI: 10.1016/j.jct.2016.05.023.

[65] J. G. Huddleston, A. E. Visser, W. M. Reichert, H. D. Willauer, G. A. Broker, R. D. Rogers, Characterization and comparison of hydrophilic and hydrophobic room temperature ionic liquids incorporating the imidazolium cation, *Green Chem.*, **2001**, 3, 156–164. DOI: 10.1039/b103275p.

[66] C. Deferm, A. Van den Bossche, J. Luyten, H. Oosterhof, J. Fransaer, K. Binnemans, Thermal stability of trihexyl(tetradecyl)phosphonium chloride, *Phys. Chem. Chem. Phys.*, **2018**, 20, 2444–2456. DOI: 10.1039/C7CP08556G.

[67] H. F. D. Almeida, J. N. Canongia Lopes, L. P. N. Rebelo, J. A. P. Coutinho, M. G. Freire, I. M. Marrucho, Densities and Viscosities of Mixtures of Two Ionic Liquids Containing a Common Cation, *J. Chem. Eng. Data.*, **2016**, 61, 2828–2843. DOI: 10.1021/acs.jced.6b00178.

[68] Z. P. McAtee, M. P. Heitz, Density, viscosity and excess properties in the trihexyltetradecylphosphonium chloride ionic liquid/methanol cosolvent system, *J. Chem. Thermodyn.*, **2016**, 93, 34–44. DOI: 10.1016/j.jct.2015.09.030.

[69] R. Salinas, J. Pla-Franco, E. Lladosa, J. B. Montón, Density, Speed of Sound, Viscosity, and Excess Properties of Binary Mixtures Formed by Ethanol and Bis(trifluorosulfonyl)imide-Based Ionic Liquids, *J. Chem. Eng. Data.*, **2015**, 60, 525–540. DOI: 10.1021/je500594z.

[70] T. Ito, N. Kojima, A. Nagashima, Redetermination of the viscosity of molten NaCl at elevated temperatures, *Int. J. Thermophys.*, **1989**, 10, 819–831. DOI: 10.1007/BF00514478.

[71] M. A. A. Rocha, C. F. R. A. C. Lima, L. R. Gomes, B. Schröder, J. A. P. Coutinho, I. M. Marrucho, J. M. S. S. Esperança, L. P. N. Rebelo, K. Shimizu, J. N. C. Lopes, L. M. N. B. F. Santos, High-Accuracy Vapor Pressure Data of the Extended [C n C 1 im][Ntf 2] Ionic Liquid Series: Trend Changes and Structural Shifts, *J. Phys. Chem. B.*, **2011**, 115, 10919–10926. DOI: 10.1021/jp2049316.

[72] C. T. Ewing, K. H. Stern, Vaporization kinetics of solid and liquid silver, sodium chloride, potassium bromide, cesium iodide, and lithium fluoride, *J. Phys. Chem.*, **1975**, 79, 2007–2017. DOI: 10.1021/j100586a006.

[73] C. T. Ewing, K. H. Stern, Equilibrium vaporization rates and vapor pressures of solid and liquid sodium chloride, potassium chloride, potassium bromide, cesium iodide, and lithium fluoride, *J. Phys. Chem.*, **1974**, 78, 1998–2005. DOI: 10.1021/j100613a005.

[74] A. Cháfer, J. de la Torre, A. Font, E. Lladosa, Liquid–Liquid Equilibria of Water + Ethanol + 1-Butyl-3-

methylimidazolium Bis(trifluoromethanesulfonyl)imide Ternary System: Measurements and Correlation at Different Temperatures, *J. Chem. Eng. Data*., **2015**, 60, 2426–2433. DOI: 10.1021/acs.jced.5b00301.

[75] H. F. D. Almeida, J. A. Lopes-da-Silva, M. G. Freire, J. A. P. Coutinho, Surface tension and refractive index of pure and water-saturated tetradecyltrihexylphosphonium-based ionic liquids, *J. Chem. Thermodyn*., **2013**, 57, 372–379. DOI: 10.1016/j.jct.2012.09.004.

[76] J. Marcoux, Measurement of the Index of Refraction of Some Molten Ionic Salts, *Rev. Sci. Instrum*., **1971**, 42, 600–602. DOI: 10.1063/1.1685180.

[77] Q.-S. Liu, M. Yang, P. Yan, X. Liu, Z. Tan, U. Welz-Biermann, Density and Surface Tension of Ionic Liquids [C n py][NTf 2] (n = 2, 4, 5), *J. Chem. Eng. Data*., **2010**, 55, 4928–4930. DOI: 10.1021/je100507n.

[78] D. Blanco, M. Bartolomé, B. Ramajo, J. L. Viesca, R. González, A. Hernández Battez, Wetting Properties of Seven Phosphonium Cation-Based Ionic Liquids, *Ind. Eng. Chem. Res.*, **2016**, 55, 9594–9602. DOI: 10.1021/acs.iecr.6b00821.

[79] G. Liu, J. M. Toguri, N. M. Stubina, Surface tension and density of the molten LaCl 3 –NaCl binary system, *Can. J. Chem*., **1987**, 65, 2779–2782. DOI: 10.1139/v87-462.

[80] R. Ge, C. Hardacre, J. Jacquemin, P. Nancarrow, D. W. Rooney, Heat Capacities of Ionic Liquids as a Function of Temperature at 0.1 MPa. Measurement and Prediction, *J. Chem. Eng. Data*., **2008**, 53, 2148–2153. DOI: 10.1021/je800335v.

[81] A. F. Ferreira, P. N. Simões, A. G. M. Ferreira, Quaternary phosphonium-based ionic liquids: Thermal stability and heat capacity of the liquid phase, *J. Chem. Thermodyn*., **2012**, 45, 16–27. DOI: 10.1016/j.jct.2011.08.019.

[82] G. J. Janz, *Molten Salts Handbook*, Academic Press, New York, **1967**.

[83] H. Chen, Y. He, J. Zhu, H. Alias, Y. Ding, P. Nancarrow, C. Hardacre, D. Rooney, C. Tan, Rheological and heat transfer behaviour of the ionic liquid, [C4mim][NTf2], *Int. J. Heat Fluid Flow*., **2008**, 29, 149–155. DOI: 10.1016/j.ijheatfluidflow.2007.05.002.

[84] R. Ge, C. Hardacre, P. Nancarrow, D. W. Rooney, Thermal Conductivities of Ionic Liquids over the Temperature Range from 293 K to 353 K, *J. Chem. Eng. Data*., **2007**, 52, 1819–1823. DOI: 10.1021/je700176d.

[85] Y. Nagasaka, N. Nakazawa, A. Nagashima, Experimental determination of the thermal diffusivity of molten alkali halides by the forced Rayleigh scattering method. I. Molten LiCl, NaCl, KCl, RbCl, and CsCl, *Int. J. Thermophys*., **1992**, 13, 555–574. DOI: 10.1007/BF00501941.

[86] C. Reichardt, T. Welton, *Solvents and Solvent Effects in Organic Chemistry*, Wiley-VCH Verlag GmbH & Co. KGaA, Weinheim, Germany, **2010**.

[87] M. J. Muldoon, C. M. Gordon, I. R. Dunkin, Investigations of solvent–solute interactions in room temperature ionic liquids using solvatochromic dyes, *J. Chem. Soc. Perkin Trans. 2*., **2001**, 433–435. DOI: 10.1039/b101449h.

[88] J. M. Padró, M. Reta, Solvatochromic parameters of imidazolium-, hydroxyammonium-, pyridinium- and phosphonium-based room temperature ionic liquids, *J. Mol. Liq.*, **2016**, 213, 107–114. DOI: 10.1016/j.molliq.2015.10.055.

[89] W. M. Haynes, Ed., *CRC Handbook of Chemistry and Physics*, Taylor & Francis Group, Boca Raton, 95th edn., **2014**.

[90] T. Itoh, Ionic Liquids as Tool to Improve Enzymatic Organic Synthesis, *Chem. Rev*., **2017**, 117, 10567–10607. DOI: 10.1021/acs.chemrev.7b00158.

[91] R. Hayes, G. G. Warr, R. Atkin, At the interface: solvation and designing ionic liquids, *Phys. Chem. Chem. Phys*., **2010**, 12, 1709. DOI: 10.1039/b920393a.

[92] K. Dong, X. Liu, H. Dong, X. Zhang, S. Zhang, Multiscale Studies on Ionic Liquids, *Chem. Rev*., **2017**, 117, 6636–6695. DOI: 10.1021/acs.chemrev.6b00776.

[93] P. G. Jessop, Fundamental properties and practical applications of ionic liquids: concluding remarks, *Faraday Discuss*., **2018**, 206, 587–601. DOI: 10.1039/C7FD90090B.

[94] G. Durga, A. Mishra, in *Encyclopedia of Inorganic and Bioinorganic Chemistry*, John Wiley & Sons, Ltd, Chichester, UK, **2016**, p. 1–13. DOI: 10.1002/9781119951438.eibc2434.

[95] K. R. Seddon, Ionic liquids: A taste of the future, *Nat. Mater*., **2003**, 2, 363–365. DOI: 10.1038/nmat907.

[96] P. Saling, M. Maase, U. Vagt, in *Handbook of Green Chemistry*, Wiley-VCH Verlag GmbH & Co. KGaA, Weinheim, Germany, **2010**. DOI: 10.1002/9783527628698.hgc070.

[97] W. Xu, E. I. Cooper, C. A. Angell, Ionic Liquids: Ion Mobilities, Glass Temperatures, and Fragilities, *J. Phys. Chem. B*., **2003**, 107, 6170–6178. DOI: 10.1021/jp0275894.

[98] J. Dupont, From Molten Salts to Ionic Liquids: A "Nano" Journey, *Acc. Chem. Res*., **2011**, 44, 1223–1231. DOI: 10.1021/ar2000937.

[99] K. Grzybowska, A. Grzybowski, Z. Wojnarowska, J. Knapik, M. Paluch, Ionic liquids and their bases: Striking differences in the dynamic heterogeneity near the glass transition, *Sci. Rep*., **2015**, 5, 16876. DOI: 10.1038/srep16876.

[100] S. Zein El Abedin, F. Endres, Ionic Liquids: The Link to High-Temperature Molten Salts?, *Acc. Chem. Res*., **2007**, 40, 1106–1113. DOI: 10.1021/ar700049w.

[101] J.-P. Belieres, C. A. Angell, Protic Ionic Liquids: Preparation, Characterization, and Proton Free Energy Level Representation, *J. Phys. Chem. B*., **2007**, 111, 4926–4937. DOI: 10.1021/jp067589u.

[102] A. R. Hajipour, F. Rafiee, Recent Progress in Ionic Liquids and their Applications in Organic Synthesis, *Org. Prep.*

Proced. Int., **2015**, 47, 249–308. DOI: 10.1080/00304948.2015.1052317.

[103] D. R. MacFarlane, J. M. Pringle, K. M. Johansson, S. A. Forsyth, M. Forsyth, Lewis base ionic liquids, *Chem. Commun.*, **2006**, 1905. DOI: 10.1039/b516961p.

[104] T. L. Greaves, C. J. Drummond, Protic ionic liquids: Properties and applications, *Chem. Rev.*, **2008**, 108, 206–237. DOI: 10.1021/cr068040u.

[105] C. A. Angell, N. Byrne, J.-P. Belieres, Parallel Developments in Aprotic and Protic Ionic Liquids: Physical Chemistry and Applications, *Acc. Chem. Res.*, **2007**, 40, 1228–1236. DOI: 10.1021/ar7001842.

[106] V. N. Emel'yanenko, G. Boeck, S. P. Verevkin, R. Ludwig, Volatile Times for the Very First Ionic Liquid: Understanding the Vapor Pressures and Enthalpies of Vaporization of Ethylammonium Nitrate, *Chem. - A Eur. J.*, **2014**, 20, 11640–11645. DOI: 10.1002/chem.201403508.

[107] T. L. Greaves, A. Weerawardena, C. Fong, I. Krodkiewska, C. J. Drummond, Protic Ionic Liquids: Solvents with Tunable Phase Behavior and Physicochemical Properties, *J. Phys. Chem. B.*, **2006**, 110, 22479–22487. DOI: 10.1021/jp0634048.

[108] P. Walden, Molecular weights and electrical conductivity of several fused salts, *Bull. Acad. Imper. Sci.*, **1914**, 405–422.

[109] S. Gabriel, Ueber einige Abkömmlinge des Aethylamins, *Berichte der Dtsch. Chem. Gesellschaft.*, **1891**, 24, 1110–1121. DOI: 10.1002/cber.189102401200.

[110] K. Fumino, A. Wulf, R. Ludwig, Hydrogen Bonding in Protic Ionic Liquids: Reminiscent of Water, *Angew. Chemie Int. Ed.*, **2009**, 48, 3184–3186. DOI: 10.1002/anie.200806224.

[111] R. Hayes, S. Imberti, G. G. Warr, R. Atkin, The Nature of Hydrogen Bonding in Protic Ionic Liquids, *Angew. Chemie Int. Ed.*, **2013**, 52, 4623–4627. DOI: 10.1002/anie.201209273.

[112] T. Murphy, L. M. Varela, G. B. Webber, G. G. Warr, R. Atkin, Nanostructure–Thermal Conductivity Relationships in Protic Ionic Liquids, *J. Phys. Chem. B.*, **2014**, 118, 12017–12024. DOI: 10.1021/jp507408r.

[113] M. Hoque, M. L. Thomas, M. S. Miran, M. Akiyama, M. Marium, K. Ueno, K. Dokko, M. Watanabe, Protic ionic liquids with primary alkylamine-derived cations: the dominance of hydrogen bonding on observed physicochemical properties, *RSC Adv.*, **2018**, 8, 9790–9794. DOI: 10.1039/C8RA00402A.

[114] T. L. Greaves, A. Weerawardena, C. Fong, C. J. Drummond, Formation of Amphiphile Self-Assembly Phases in Protic Ionic Liquids, *J. Phys. Chem. B.*, **2007**, 111, 4082–4088. DOI: 10.1021/jp066511a.

[115] T. Méndez-Morales, J. Carrete, Ó. Cabeza, O. Russina, A. Triolo, L. J. Gallego, L. M. Varela, Solvation of Lithium Salts in Protic Ionic Liquids: A Molecular Dynamics Study, *J. Phys. Chem. B.*, **2014**, 118, 761–770. DOI: 10.1021/jp410090f.

[116] T. L. Greaves, A. Weerawardena, I. Krodkiewska, C. J. Drummond, Protic Ionic Liquids: Physicochemical Properties and Behavior as Amphiphile Self-Assembly Solvents, *J. Phys. Chem. B.*, **2008**, 112, 896–905. DOI: 10.1021/jp0767819.

[117] T. L. Greaves, C. J. Drummond, Protic Ionic Liquids: Evolving Structure–Property Relationships and Expanding Applications, *Chem. Rev.*, **2015**, 115, 11379–11448. DOI: 10.1021/acs.chemrev.5b00158.

[118] J. Stoimenovski, E. I. Izgorodina, D. R. MacFarlane, Ionicity and proton transfer in protic ionic liquids, *Phys. Chem. Chem. Phys.*, **2010**, 12, 10341. DOI: 10.1039/c0cp00239a.

[119] M. S. Miran, H. Kinoshita, T. Yasuda, M. A. B. H. Susan, M. Watanabe, Physicochemical properties determined by ΔpKa for protic ionic liquids based on an organic super-strong base with various Brønsted acids, *Phys. Chem. Chem. Phys.*, **2012**, 14, 5178. DOI: 10.1039/c2cp00007e.

[120] M. Yoshizawa, W. Xu, C. A. Angell, Ionic Liquids by Proton Transfer: Vapor Pressure, Conductivity, and the Relevance of ΔpK a from Aqueous Solutions, *J. Am. Chem. Soc.*, **2003**, 125, 15411–15419. DOI: 10.1021/ja035783d.

[121] T. L. Greaves, K. Ha, B. W. Muir, S. C. Howard, A. Weerawardena, N. Kirby, C. J. Drummond, Protic ionic liquids (PILs) nanostructure and physicochemical properties: development of high-throughput methodology for PIL creation and property screens, *Phys. Chem. Chem. Phys.*, **2015**, 17, 2357–2365. DOI: 10.1039/C4CP04241G.

[122] J. P. Hallett, T. Welton, Room-Temperature Ionic Liquids: Solvents for Synthesis and Catalysis. 2, *Chem. Rev.*, **2011**, 111, 3508–3576. DOI: 10.1021/cr1003248.

[123] J. S. Wilkes, M. J. Zaworotko, Air and water stable 1-ethyl-3-methylimidazolium based ionic liquids, *J. Chem. Soc. Chem. Commun.*, **1992**, 965. DOI: 10.1039/c39920000965.

[124] J. S. Wilkes, A short history of ionic liquids—from molten salts to neoteric solvents, *Green Chem.*, **2002**, 4, 73–80. DOI: 10.1039/b110838g.

[125] J. S. Wilkes, J. A. Levisky, R. A. Wilson, C. L. Hussey, Dialkylimidazolium chloroaluminate melts: a new class of room-temperature ionic liquids for electrochemistry, spectroscopy and synthesis, *Inorg. Chem.*, **1982**, 21, 1263–1264. DOI: 10.1021/ic00133a078.

[126] F. H. Hurley, T. P. Wier, The Electrodeposition of Aluminum from Nonaqueous Solutions at Room Temperature, *J. Electrochem. Soc.*, **1951**, 98, 207. DOI: 10.1149/1.2778133.

[127] T. Welton, Room-Temperature Ionic Liquids. Solvents for Synthesis and Catalysis, *Chem. Rev.*, **1999**, 99, 2071–2084. DOI: 10.1021/cr980032t.

[128] Y. Chauvin, L. Mussmann, H. Olivier, A Novel Class of Versatile Solvents for Two-Phase Catalysis: Hydrogenation, Isomerization, and Hydroformylation of Alkenes Catalyzed by Rhodium Complexes in Liquid

1,3-Dialkylimidazolium Salts, *Angew. Chemie Int. Ed. English.*, **1996**, 34, 2698–2700. DOI: 10.1002/anie.199526981.

[129] H. Weingärtner, Understanding Ionic Liquids at the Molecular Level: Facts, Problems, and Controversies, *Angew. Chemie Int. Ed.*, **2008**, 47, 654–670. DOI: 10.1002/anie.200604951.

[130] C. Mao, Z. Wang, Z. Wang, P. Ji, J.-P. Cheng, Weakly Polar Aprotic Ionic Liquids Acting as Strong Dissociating Solvent: A Typical "Ionic Liquid Effect" Revealed by Accurate Measurement of Absolute p K a of Ylide Precursor Salts, *J. Am. Chem. Soc.*, **2016**, 138, 5523–5526. DOI: 10.1021/jacs.6b02607.

[131] M. G. Freire, C. M. S. S. Neves, P. J. Carvalho, R. L. Gardas, A. M. Fernandes, I. M. Marrucho, L. M. N. B. F. Santos, J. A. P. Coutinho, Mutual Solubilities of Water and Hydrophobic Ionic Liquids, *J. Phys. Chem. B.*, **2007**, 111, 13082–13089. DOI: 10.1021/jp076271e.

[132] W. Yao, H. Wang, G. Cui, Z. Li, A. Zhu, S. Zhang, J. Wang, Tuning the Hydrophilicity and Hydrophobicity of the Respective Cation and Anion: Reversible Phase Transfer of Ionic Liquids, *Angew. Chemie Int. Ed.*, **2016**, 55, 7934–7938. DOI: 10.1002/anie.201600419.

[133] S. P. M. Ventura, F. A. e Silva, M. V. Quental, D. Mondal, M. G. Freire, J. A. P. Coutinho, Ionic-Liquid-Mediated Extraction and Separation Processes for Bioactive Compounds: Past, Present, and Future Trends, *Chem. Rev.*, **2017**, 117, 6984–7052. DOI: 10.1021/acs.chemrev.6b00550.

[134] N. L. Mai, K. Ahn, Y.-M. Koo, Methods for recovery of ionic liquids—A review, *Process Biochem.*, **2014**, 49, 872–881. DOI: 10.1016/j.procbio.2014.01.016.

[135] K. E. Gutowski, G. A. Broker, H. D. Willauer, J. G. Huddleston, R. P. Swatloski, J. D. Holbrey, R. D. Rogers, Controlling the Aqueous Miscibility of Ionic Liquids: Aqueous Biphasic Systems of Water-Miscible Ionic Liquids and Water-Structuring Salts for Recycle, Metathesis, and Separations, *J. Am. Chem. Soc.*, **2003**, 125, 6632–6633. DOI: 10.1021/ja0351802.

[136] Y. Fukaya, H. Ohno, Hydrophobic and polar ionic liquids, *Phys. Chem. Chem. Phys.*, **2013**, 15, 4066. DOI: 10.1039/c3cp44214d.

[137] H. Passos, T. B. V. Dinis, E. V. Capela, M. V Quental, J. Gomes, J. Resende, P. P. Madeira, M. G. Freire, J. A. P. Coutinho, Mechanisms ruling the partition of solutes in ionic-liquid-based aqueous biphasic systems – the multiple effects of ionic liquids, *Phys. Chem. Chem. Phys.* DOI: 10.1039/C8CP00383A.

[138] T. Kuboki, T. Okuyama, T. Ohsaki, N. Takami, Lithium-air batteries using hydrophobic room temperature ionic liquid electrolyte, *J. Power Sources.*, **2005**, 146, 766–769. DOI: 10.1016/j.jpowsour.2005.03.082.

[139] J. L. Anderson, J. Ding, T. Welton, D. W. Armstrong, Characterizing Ionic Liquids On the Basis of Multiple Solvation Interactions, *J. Am. Chem. Soc.*, **2002**, 124, 14247–14254. DOI: 10.1021/ja028156h.

[140] M. A. Ab Rani, A. Brant, L. Crowhurst, A. Dolan, M. Lui, N. H. Hassan, J. P. Hallett, P. A. Hunt, H. Niedermeyer, J. M. Perez-Arlandis, M. Schrems, T. Welton, R. Wilding, Understanding the polarity of ionic liquids, *Phys. Chem. Chem. Phys.*, **2011**, 13, 16831. DOI: 10.1039/c1cp21262a.

[141] Z. Liu, P. Hu, X. Meng, R. Zhang, H. Yue, C. Xu, Y. Hu, Synthesis and properties of switchable polarity ionic liquids based on organic superbases and fluoroalcohols, *Chem. Eng. Sci.*, **2014**, 108, 176–182. DOI: 10.1016/j.ces.2013.12.040.

[142] H. Zhao, S. Xia, P. Ma, Use of ionic liquids as 'green' solvents for extractions, *J. Chem. Technol. Biotechnol.*, **2005**, 80, 1089–1096. DOI: 10.1002/jctb.1333.

[143] J. Dupont, G. S. Fonseca, A. P. Umpierre, P. F. P. Fichtner, S. R. Teixeira, Transition-Metal Nanoparticles in Imidazolium Ionic Liquids: Recycable Catalysts for Biphasic Hydrogenation Reactions, *J. Am. Chem. Soc.*, **2002**, 124, 4228–4229. DOI: 10.1021/ja025818u.

[144] A. J. Carmichael, M. J. Earle, J. D. Holbrey, P. B. McCormac, K. R. Seddon, The Heck Reaction in Ionic Liquids: A Multiphasic Catalyst System, *Org. Lett.*, **1999**, 1, 997–1000. DOI: 10.1021/ol9907771.

[145] Y. Qiao, W. Ma, N. Theyssen, C. Chen, Z. Hou, Temperature-Responsive Ionic Liquids: Fundamental Behaviors and Catalytic Applications, *Chem. Rev.*, **2017**, 117, 6881–6928. DOI: 10.1021/acs.chemrev.6b00652.

[146] S. Zhang, J. Zhang, Y. Zhang, Y. Deng, Nanoconfined Ionic Liquids, *Chem. Rev.*, **2017**, 117, 6755–6833. DOI: 10.1021/acs.chemrev.6b00509.

[147] S. Perkin, Ionic liquids in confined geometries, *Phys. Chem. Chem. Phys.*, **2012**, 14, 5052. DOI: 10.1039/c2cp23814d.

[148] J. Le Bideau, L. Viau, A. Vioux, Ionogels, ionic liquid based hybrid materials, *Chem. Soc. Rev.*, **2011**, 40, 907–925. DOI: 10.1039/C0CS00059K.

[149] A. Riisager, Continuous fixed-bed gas-phase hydroformylation using supported ionic liquid-phase (SILP) Rh catalysts, *J. Catal.*, **2003**, 219, 452–455. DOI: 10.1016/S0021-9517(03)00223-9.

[150] A. Riisager, R. Fehrmann, S. Flicker, R. van Hal, M. Haumann, P. Wasserscheid, Very Stable and Highly Regioselective Supported Ionic-Liquid-Phase (SILP) Catalysis: Continuous-Flow Fixed-Bed Hydroformylation of Propene, *Angew. Chemie Int. Ed.*, **2005**, 44, 815–819. DOI: 10.1002/anie.200461534.

[151] S. Herrmann, L. De Matteis, J. M. de la Fuente, S. G. Mitchell, C. Streb, Removal of Multiple Contaminants from Water by Polyoxometalate Supported Ionic Liquid Phases (POM-SILPs), *Angew. Chemie Int. Ed.*, **2017**, 56, 1667–1670. DOI: 10.1002/anie.201611072.

[152] A. Riisager, R. Fehrmann, M. Haumann, P. Wasserscheid, Supported Ionic Liquid Phase (SILP) catalysis: An innovative concept for homogeneous catalysis in continuous fixed-bed reactors, *Eur. J. Inorg. Chem.*, **2006**, 695–706. DOI: 10.1002/ejic.200500872.

[153] A. C. Forse, J. M. Griffin, C. Merlet, P. M. Bayley, H. Wang, P. Simon, C. P. Grey, NMR Study of Ion Dynamics

and Charge Storage in Ionic Liquid Supercapacitors, *J. Am. Chem. Soc.*, **2015**, 137, 7231–7242. DOI: 10.1021/jacs.5b03958.

[154] M. Armand, F. Endres, D. R. MacFarlane, H. Ohno, B. Scrosati, Ionic-liquid materials for the electrochemical challenges of the future, *Nat. Mater.*, **2009**, 8, 621–629. DOI: 10.1038/nmat2448.

[155] I. Osada, H. de Vries, B. Scrosati, S. Passerini, Ionic-Liquid-Based Polymer Electrolytes for Battery Applications, *Angew. Chemie Int. Ed.*, **2016**, 55, 500–513. DOI: 10.1002/anie.201504971.

[156] P. A. Hunt, C. R. Ashworth, R. P. Matthews, Hydrogen bonding in ionic liquids, *Chem. Soc. Rev.*, **2015**, 44, 1257–1288. DOI: 10.1039/C4CS00278D.

[157] R. Hayes, S. Imberti, G. G. Warr, R. Atkin, Amphiphilicity determines nanostructure in protic ionic liquids, *Phys. Chem. Chem. Phys.*, **2011**, 13, 3237–3247. DOI: 10.1039/C0CP01137A.

[158] K. Dong, S. Zhang, J. Wang, Understanding the hydrogen bonds in ionic liquids and their roles in properties and reactions, *Chem. Commun.*, **2016**, 52, 6744–6764. DOI: 10.1039/C5CC10120D.

[159] T. L. Greaves, D. F. Kennedy, S. T. Mudie, C. J. Drummond, Diversity Observed in the Nanostructure of Protic Ionic Liquids, *J. Phys. Chem. B.*, **2010**, 114, 10022–10031. DOI: 10.1021/jp103863z.

[160] A. Triolo, O. Russina, H.-J. Bleif, E. Di Cola, Nanoscale segregation in room temperature ionic liquids, *J. Phys. Chem. B.*, **2007**, 111, 4641–4644. DOI: 10.1021/jp067705t.

[161] C. P. Frizzo, C. R. Bender, A. Z. Tier, I. M. Gindri, P. R. S. Salbego, A. R. Meyer, M. A. P. Martins, Energetic and topological insights into the supramolecular structure of dicationic ionic liquids, *CrystEngComm.*, **2015**, 17, 2996–3004. DOI: 10.1039/C5CE00073D.

[162] K. Goossens, K. Lava, C. W. Bielawski, K. Binnemans, Ionic Liquid Crystals: Versatile Materials, *Chem. Rev.*, **2016**, 116, 4643–4807. DOI: 10.1021/cr400334b.

[163] K. Binnemans, Ionic Liquid Crystals, *Chem. Rev.*, **2005**, 105, 4148–4204. DOI: 10.1021/cr0400919.

[164] S. Zhang, Q. Zhang, Y. Zhang, Z. Chen, M. Watanabe, Y. Deng, Beyond solvents and electrolytes: Ionic liquids-based advanced functional materials, *Prog. Mater. Sci.*, **2016**, 77, 80–124. DOI: 10.1016/j.pmatsci.2015.10.001.

[165] S. Luo, X. Mi, L. Zhang, S. Liu, H. Xu, J.-P. Cheng, Functionalized Chiral Ionic Liquids as Highly Efficient Asymmetric Organocatalysts for Michael Addition to Nitroolefins, *Angew. Chemie Int. Ed.*, **2006**, 45, 3093–3097. DOI: 10.1002/anie.200600048.

[166] S. Hisamitsu, N. Yanai, N. Kimizuka, Photon-Upconverting Ionic Liquids: Effective Triplet Energy Migration in Contiguous Ionic Chromophore Arrays, *Angew. Chemie Int. Ed.*, **2015**, 54, 11550–11554. DOI: 10.1002/anie.201505168.

[167] B. Gélinas, D. Rochefort, Synthesis and characterization of an electroactive ionic liquid based on the ferrocenylsulfonyl(trifluoromethylsulfonyl)imide anion, *Electrochim. Acta.*, **2015**, 162, 36–44. DOI: 10.1016/j.electacta.2014.11.154.

[168] Q. Zhang, J. M. Shreeve, Energetic Ionic Liquids as Explosives and Propellant Fuels: A New Journey of Ionic Liquid Chemistry, *Chem. Rev.*, **2014**, 114, 10527–10574. DOI: 10.1021/cr500364t.

[169] E. Sebastiao, C. Cook, A. Hu, M. Murugesu, Recent developments in the field of energetic ionic liquids, *J. Mater. Chem. A.*, **2014**, 2, 8153–8173. DOI: 10.1039/C4TA00204K.

[170] A. Branco, L. C. Branco, F. Pina, Electrochromic and magnetic ionic liquids, *Chem. Commun.*, **2011**, 47, 2300–2302. DOI: 10.1039/C0CC03892J.

[171] T. Ogawa, M. Yoshida, H. Ohara, A. Kobayashi, M. Kato, A dual-emissive ionic liquid based on an anionic platinum(<scp>ii</scp>) complex, *Chem. Commun.*, **2015**, 51, 13377–13380. DOI: 10.1039/C5CC04407C.

[172] Y. Yoshida, G. Saito, Design of functional ionic liquids using magneto- and luminescent-active anions, *Phys. Chem. Chem. Phys.*, **2010**, 12, 1675–1684. DOI: 10.1039/B920046K.

[173] S. Zeng, X. Zhang, L. Bai, X. Zhang, H. Wang, J. Wang, D. Bao, M. Li, X. Liu, S. Zhang, Ionic-Liquid-Based CO 2 Capture Systems: Structure, Interaction and Process, *Chem. Rev.*, **2017**, 117, 9625–9673. DOI: 10.1021/acs.chemrev.7b00072.

[174] K. S. Egorova, E. G. Gordeev, V. P. Ananikov, Biological Activity of Ionic Liquids and Their Application in Pharmaceutics and Medicine, *Chem. Rev.*, **2017**, 117, 7132–7189. DOI: 10.1021/acs.chemrev.6b00562.

[175] M. Talebi, R. A. Patil, D. W. Armstrong, Physicochemical properties of branched-chain dicationic ionic liquids, *J. Mol. Liq.*, **2018**, 256, 247–255. DOI: 10.1016/j.molliq.2018.02.016.

[176] T. Payagala, J. Huang, Z. S. Breitbach, P. S. Sharma, D. W. Armstrong, Unsymmetrical Dicationic Ionic Liquids: Manipulation of Physicochemical Properties Using Specific Structural Architectures, *Chem. Mater.*, **2007**, 19, 5848–5850. DOI: 10.1021/cm702325a.

[177] J. L. Anderson, R. Ding, A. Ellern, D. W. Armstrong, Structure and Properties of High Stability Geminal Dicationic Ionic Liquids, *J. Am. Chem. Soc.*, **2005**, 127, 593–604. DOI: 10.1021/ja046521u.

[178] R. A. Patil, M. Talebi, C. Xu, S. S. Bhawal, D. W. Armstrong, Synthesis of Thermally Stable Geminal Dicationic Ionic Liquids and Related Ionic Compounds: An Examination of Physicochemical Properties by Structural Modification, *Chem. Mater.*, **2016**, 28, 4315–4323. DOI: 10.1021/acs.chemmater.6b01247.

[179] N. Zhou, G. Zhao, K. Dong, J. Sun, H. Shao, Investigations on a series of novel ionic liquids containing the [closo-B12Cl12]2− dianion, *RSC Adv.*, **2012**, 2, 9830. DOI: 10.1039/c2ra21700g.

[180] N. Byrne, P. C. Howlett, D. R. MacFarlane, M. Forsyth, The Zwitterion Effect in Ionic Liquids: Towards Practical

Rechargeable Lithium-Metal Batteries, *Adv. Mater.*, **2005**, 17, 2497–2501. DOI: 10.1002/adma.200500595.

[181] X. Gao, F. Lu, B. Dong, T. Zhou, Y. Liu, L. Zheng, Temperature-responsive proton-conductive liquid crystals formed by the self-assembly of zwitterionic ionic liquids, *RSC Adv.*, **2015**, 5, 63732–63737. DOI: 10.1039/C5RA10830F.

[182] P. Sun, L. Shi, F. Lu, L. Zheng, Aggregation behavior of zwitterionic surface active ionic liquids with different counterions, cations, and alkyl chains, *RSC Adv.*, **2016**, 6, 27370–27377. DOI: 10.1039/C6RA02986H.

[183] A. Eftekhari, Ed., *Polymerized Ionic Liquids*, Royal Society of Chemistry, Cambridge, **2017**.

[184] W. Qian, J. Texter, F. Yan, Frontiers in poly(ionic liquid)s: syntheses and applications, *Chem. Soc. Rev.*, **2017**, 46, 1124–1159. DOI: 10.1039/C6CS00620E.

[185] A. Eftekhari, T. Saito, Synthesis and properties of polymerized ionic liquids, *Eur. Polym. J.*, **2017**, 90, 245–272. DOI: 10.1016/j.eurpolymj.2017.03.033.

[186] D. Mecerreyes, Polymeric ionic liquids: Broadening the properties and applications of polyelectrolytes, *Prog. Polym. Sci.*, **2011**, 36, 1629–1648. DOI: 10.1016/j.progpolymsci.2011.05.007.

[187] J. Yuan, D. Mecerreyes, M. Antonietti, Poly(ionic liquid)s: An update, *Prog. Polym. Sci.*, **2013**, 38, 1009–1036. DOI: 10.1016/j.progpolymsci.2013.04.002.

[188] Z. Dai, R. D. Noble, D. L. Gin, X. Zhang, L. Deng, Combination of ionic liquids with membrane technology: A new approach for CO 2 separation, *J. Memb. Sci.*, **2016**, 497, 1–20. DOI: 10.1016/j.memsci.2015.08.060.

[189] H. Niedermeyer, J. P. Hallett, I. J. Villar-Garcia, P. A. Hunt, T. Welton, Mixtures of ionic liquids, *Chem. Soc. Rev.*, **2012**, 41, 7780. DOI: 10.1039/c2cs35177c.

[190] F. Castiglione, G. Raos, G. Battista Appetecchi, M. Montanino, S. Passerini, M. Moreno, A. Famulari, A. Mele, Blending ionic liquids: how physico-chemical properties change, *Phys. Chem. Chem. Phys.*, **2010**, 12, 1784. DOI: 10.1039/b921816e.

[191] O. Russina, F. Lo Celso, N. V. Plechkova, A. Triolo, Emerging Evidences of Mesoscopic-Scale Complexity in Neat Ionic Liquids and Their Mixtures, *J. Phys. Chem. Lett.*, **2017**, 8, 1197–1204. DOI: 10.1021/acs.jpclett.6b02811.

[192] A. K. Burrell, R. E. Del Sesto, S. N. Baker, T. M. McCleskey, G. A. Baker, The large scale synthesis of pure imidazolium and pyrrolidinium ionic liquids, *Green Chem.*, **2007**, 9, 449. DOI: 10.1039/b615950h.

[193] C. J. Clarke, W.-C. Tu, O. Levers, A. Bröhl, J. P. Hallett, Green and Sustainable Solvents in Chemical Processes, *Chem. Rev.*, **2018**, 118, 747–800. DOI: 10.1021/acs.chemrev.7b00571.

[194] C. M. Gordon, M. J. Muldoon, M. Wagner, C. Hilgers, J. H. Davis, P. Wasserscheid, in *Ionic Liquids in Synthesis*, eds. P. Wasserscheid and T. Welton, Wiley-VCH Verlag GmbH & Co. KGaA, Weinheim, Germany, **2007**, p. 7–55. DOI: 10.1002/9783527621194.ch2.

[195] P. Nockemann, K. Binnemans, K. Driesen, Purification of imidazolium ionic liquids for spectroscopic applications, *Chem. Phys. Lett.*, **2005**, 415, 131–136. DOI: 10.1016/j.cplett.2005.08.128.

[196] E. C. Achinivu, R. M. Howard, G. Li, H. Gracz, W. A. Henderson, Lignin extraction from biomass with protic ionic liquids, *Green Chem.*, **2014**, 16, 1114–1119. DOI: 10.1039/C3GC42306A.

[197] P. A. J. Warner, *Green Chemistry: Theory and Practice*, Oxford University Press, **2000**.

[198] N. V. Ignat'ev, P. Barthen, A. Kucheryna, H. Willner, P. Sartori, A Convenient Synthesis of Triflate Anion Ionic Liquids and Their Properties, *Molecules.*, **2012**, 17, 5319–5338. DOI: 10.3390/molecules17055319.

[199] J. Jacquemin, P. Goodrich, W. Jiang, D. W. Rooney, C. Hardacre, Are Alkyl Sulfate-Based Protic and Aprotic Ionic Liquids Stable with Water and Alcohols? A Thermodynamic Approach, *J. Phys. Chem. B.*, **2013**, 117, 1938–1949. DOI: 10.1021/jp312241h.

[200] C. C. Cassol, G. Ebeling, B. Ferrera, J. Dupont, A Simple and Practical Method for the Preparation and Purity Determination of Halide-Free Imidazolium Ionic Liquids, *Adv. Synth. Catal.*, **2006**, 348, 243–248. DOI: 10.1002/adsc.200505295.

[201] C. J. Bradaric, A. Downard, C. Kennedy, A. J. Robertson, Y. Zhou, Industrial preparation of phosphonium ionic liquids, *Green Chem.*, **2003**, 5, 143–152. DOI: 10.1039/b209734f.

[202] L. Leclercq, I. Suisse, G. Nowogrocki, F. Agbossou-Niedercorn, Halide-free highly-pure imidazolium triflate ionic liquids: Preparation and use in palladium-catalysed allylic alkylation, *Green Chem.*, **2007**, 9, 1097. DOI: 10.1039/b703096g.

[203] X. Jiang, Y. Nie, C. Li, Z. Wang, Imidazolium-based alkylphosphate ionic liquids – A potential solvent for extractive desulfurization of fuel, *Fuel.*, **2008**, 87, 79–84. DOI: 10.1016/j.fuel.2007.03.045.

[204] E. Kuhlmann, S. Himmler, H. Giebelhaus, P. Wasserscheid, Imidazolium dialkylphosphates—a class of versatile, halogen-free and hydrolytically stable ionic liquids, *Green Chem.*, **2007**, 9, 233–242. DOI: 10.1039/B611974C.

[205] Y. Fukaya, K. Hayashi, M. Wada, H. Ohno, Cellulose dissolution with polar ionic liquids under mild conditions: required factors for anions, *Green Chem.*, **2008**, 10, 44–46. DOI: 10.1039/B713289A.

[206] J. Zhang, G. R. Martin, D. D. DesMarteau, Direct methylation and trifluoroethylation of imidazole and pyridine derivatives, *Chem. Commun.*, **2003**, 0, 2334. DOI: 10.1039/b307230d.

[207] P. D. Vu, A. J. Boydston, C. W. Bielawski, Ionic liquids via efficient, solvent-free anion metathesis, *Green Chem.*, **2007**, 9, 1158. DOI: 10.1039/b705745h.

[208] N. W. Smith, S. P. Gourisankar, J.-L. Montchamp, S. V. Dzyuba, Silver-free synthesis of nitrate-containing room-temperature ionic liquids, *New J. Chem.*, **2011**, 35, 909. DOI: 10.1039/c0nj00881h.

[209] R. P. Swatloski, J. D. Holbrey, R. D. Rogers, Ionic liquids are not always green: hydrolysis of 1-butyl-3-methylimidazolium hexafluorophosphate, *Green Chem.*, **2003**, 5, 361. DOI: 10.1039/b304400a.

[210] E. García-Verdugo, B. Altava, M. I. Burguete, P. Lozano, S. V. Luis, Ionic liquids and continuous flow processes: a good marriage to design sustainable processes, *Green Chem.*, **2015**, 17, 2693–2713. DOI: 10.1039/C4GC02388A.

[211] H. Srour, H. Rouault, C. C. Santini, Y. Chauvin, A silver and water free metathesis reaction: a route to ionic liquids, *Green Chem.*, **2013**, 15, 1341. DOI: 10.1039/c3gc37034h.

[212] L. Cammarata, S. G. Kazarian, P. A. Salter, T. Welton, Molecular states of water in room temperature ionic liquids, *Phys. Chem. Chem. Phys.*, **2001**, 3, 5192–5200. DOI: 10.1039/b106900d.

[213] D. Fang, J. Cheng, K. Gong, Q.-R. Shi, X.-L. Zhou, Z.-L. Liu, A green and novel procedure for the preparation of ionic liquid, *J. Fluor. Chem.*, **2008**, 129, 108–111. DOI: 10.1016/j.jfluchem.2007.09.004.

[214] J. Fuller, R. T. Carlin, H. C. De Long, D. Haworth, Structure of 1-ethyl-3-methylimidazolium hexafluorophosphate: model for room temperature molten salts, *J. Chem. Soc. Chem. Commun.*, **1994**, 299. DOI: 10.1039/c39940000299.

[215] A. J. S. McIntosh, J. Griffith, J. Gräsvik, in *Application, Purification, and Recovery of Ionic Liquids*, Elsevier, **2016**, p. 59–99. DOI: 10.1016/B978-0-444-63713-0.00002-X.

[216] D.-N. Cai, K. Huang, Y.-L. Chen, X.-B. Hu, Y.-T. Wu, Systematic Study on the General Preparation of Ionic Liquids with High Purity via Hydroxide Intermediates, *Ind. Eng. Chem. Res.*, **2014**, 53, 6871–6880. DOI: 10.1021/ie500086r.

[217] T. Vander Hoogerstraete, S. Jamar, S. Wellens, K. Binnemans, Determination of Halide Impurities in Ionic Liquids by Total Reflection X-ray Fluorescence Spectrometry, *Anal. Chem.*, **2014**, 86, 3931–3938. DOI: 10.1021/ac5000812.

[218] D. S. Silvester, R. G. Compton, Electrochemistry in Room Temperature Ionic Liquids: A Review and Some Possible Applications, *Z. Phys. Chem.*, **2006**, 220, 1247–1274. DOI: 10.1524/zpch.2006.220.10.1247.

[219] I. Dinarès, C. Garcia de Miguel, A. Ibáñez, N. Mesquida, E. Alcalde, Imidazolium ionic liquids: A simple anion exchange protocol, *Green Chem.*, **2009**, 11, 1507. DOI: 10.1039/b915743n.

[220] M. S. Miran, H. Kinoshita, T. Yasuda, M. A. B. H. Susan, M. Watanabe, Hydrogen bonds in protic ionic liquids and their correlation with physicochemical properties, *Chem. Commun.*, **2011**, 47, 12676. DOI: 10.1039/c1cc14817f.

[221] C. Zhao, G. Burrell, A. A. J. Torriero, F. Separovic, N. F. Dunlop, D. R. MacFarlane, A. M. Bond, Electrochemistry of Room Temperature Protic Ionic Liquids, *J. Phys. Chem. B.*, **2008**, 112, 6923–6936. DOI: 10.1021/jp711804j.

[222] S. Tsuzuki, H. Tokuda, K. Hayamizu, M. Watanabe, Magnitude and Directionality of Interaction in Ion Pairs of Ionic Liquids: Relationship with Ionic Conductivity, *J. Phys. Chem. B.*, **2005**, 109, 16474–16481. DOI: 10.1021/jp0533628.

[223] Q. Wang, Y. Geng, X. Lu, S. Zhang, First-Row Transition Metal-Containing Ionic Liquids as Highly Active Catalysts for the Glycolysis of Poly(ethylene terephthalate) (PET), *ACS Sustain. Chem. Eng.*, **2015**, 3, 340–348. DOI: 10.1021/sc5007522.

[224] R. E. Del Sesto, T. M. McCleskey, A. K. Burrell, G. A. Baker, J. D. Thompson, B. L. Scott, J. S. Wilkes, P. Williams, Structure and magnetic behavior of transition metal based ionic liquids, *Chem. Commun.*, **2008**, 447–449. DOI: 10.1039/B711189D.

[225] É. McCourt, Z. Wojnarowska, J. Jacquemin, P. Nockemann, H. G. Manyar, L. Hawelek, M. Paluch, Temperature- and Pressure-Induced Structural Changes of Cobalt(II) in a Phosphonium-Based Ionic Liquid, *J. Phys. Chem. C.*, **2016**, 120, 10156–10161. DOI: 10.1021/acs.jpcc.6b01325.

[226] P. Nockemann, B. Thijs, N. Postelmans, K. Van Hecke, L. Van Meervelt, K. Binnemans, Anionic Rare-Earth Thiocyanate Complexes as Building Blocks for Low-Melting Metal-Containing Ionic Liquids, *J. Am. Chem. Soc.*, **2006**, 128, 13658–13659. DOI: 10.1021/ja0640391.

[227] C. Hardacre, R. W. Murphy, K. R. Seddon, G. Srinivasan, M. Swadźba-Kwa(ś)ny, Speciation of Chlorometallate Ionic Liquids Based on Gallium(III) and Indium(III), *Aust. J. Chem.*, **2010**, 63, 845. DOI: 10.1071/CH10014.

[228] H. A. Øye, M. Jagtoyen, T. Oksefjell, J. S. Wilkes, Vapour Pressure and Thermodynamics of the System 1-Methyl-3-Ethyl-Imidazolium Chloride - Aluminium Chloride, *Mater. Sci. Forum.*, **1991**, 73–75, 183–190. DOI: 10.4028/www.scientific.net/MSF.73-75.183.

[229] J. Estager, J. D. Holbrey, M. Swadźba-Kwaśny, Halometallate ionic liquids – revisited, *Chem. Soc. Rev.*, **2014**, 43, 847–886. DOI: 10.1039/C3CS60310E.

[230] Y. Yoshida, G. Saito, Influence of structural variations in 1-alkyl-3-methylimidazolium cation and tetrahalogenoferrate(III) anion on the physical properties of the paramagnetic ionic liquids, *J. Mater. Chem.*, **2006**, 16, 1254. DOI: 10.1039/b515391c.

[231] T. C. Monson, T. E. Stevens, J. L. Leger, J. L. Manson, K. S. Lovejoy, A. L. Newsham, R. E. Del Sesto, Unprecedented magnetic behaviour in lanthanide-based ionic liquids, *Chem. Commun.*, **2017**, 53, 11682–11685. DOI: 10.1039/C7CC07060H.

[232] J. Alvarez-Vicente, S. Dandil, D. Banerjee, H. Q. N. Gunaratne, S. Gray, S. Felton, G. Srinivasan, A. M. Kaczmarek, R. Van Deun, P. Nockemann, Easily Accessible Rare-Earth-Containing Phosphonium Room-Temperature Ionic Liquids: EXAFS, Luminescence, and Magnetic Properties, *J. Phys. Chem. B.*, **2016**, 120, 5301–5311. DOI: 10.1021/acs.jpcb.6b03870.

[233] M. Deetlefs, K. R. Seddon, Improved preparations of ionic liquids using microwave irradiation, *Green Chem.*,

2003, 5, 181–186. DOI: 10.1039/b300071k.

[234] V. V. Namboodiri, R. S. Varma, Solvent-Free Sonochemical Preparation of Ionic Liquids, *Org. Lett.*, **2002**, 4, 3161–3163. DOI: 10.1021/ol026608p.

[235] J. Hulsbosch, D. E. De Vos, K. Binnemans, R. Ameloot, Biobased Ionic Liquids: Solvents for a Green Processing Industry?, *ACS Sustain. Chem. Eng.*, **2016**, 4, 2917–2931. DOI: 10.1021/acssuschemeng.6b00553.

[236] M. Petkovic, K. R. Seddon, L. P. N. Rebelo, C. Silva Pereira, Ionic liquids: a pathway to environmental acceptability, *Chem. Soc. Rev.*, **2011**, 40, 1383–1403. DOI: 10.1039/C004968A.

[237] A. Jordan, N. Gathergood, Biodegradation of ionic liquids – a critical review, *Chem. Soc. Rev.*, **2015**, 44, 8200–8237. DOI: 10.1039/C5CS00444F.

[238] M. Amde, J.-F. Liu, L. Pang, Environmental Application, Fate, Effects, and Concerns of Ionic Liquids: A Review, *Environ. Sci. Technol.*, **2015**, 49, 12611–12627. DOI: 10.1021/acs.est.5b03123.

[239] M. McCoy, Chevron embraces ionic liquids, *Chem. Eng. News.*, **2016**, 94, 16.

[240] D. R. MacFarlane, M. Forsyth, P. C. Howlett, J. M. Pringle, J. Sun, G. Annat, W. Neil, E. I. Izgorodina, Ionic Liquids in Electrochemical Devices and Processes: Managing Interfacial Electrochemistry, *Acc. Chem. Res.*, **2007**, 40, 1165–1173. DOI: 10.1021/ar7000952.

[241] M. Salanne, Ionic Liquids for Supercapacitor Applications, *Top. Curr. Chem.*, **2017**, 375, 63. DOI: 10.1007/s41061-017-0150-7.

[242] M. V. Fedorov, A. A. Kornyshev, Ionic Liquids at Electrified Interfaces, *Chem. Rev.*, **2014**, 114, 2978–3036. DOI: 10.1021/cr400374x.

[243] M. Watanabe, M. L. Thomas, S. Zhang, K. Ueno, T. Yasuda, K. Dokko, Application of Ionic Liquids to Energy Storage and Conversion Materials and Devices, *Chem. Rev.*, **2017**, 117, 7190–7239. DOI: 10.1021/acs.chemrev.6b00504.

[244] Q. Yang, Z. Zhang, X.-G. Sun, Y.-S. Hu, H. Xing, S. Dai, Ionic liquids and derived materials for lithium and sodium batteries, *Chem. Soc. Rev.*, **2018**, 47, 2020–2064. DOI: 10.1039/C7CS00464H.

[245] A. Eftekhari, Y. Liu, P. Chen, Different roles of ionic liquids in lithium batteries, *J. Power Sources.*, **2016**, 334, 221–239. DOI: 10.1016/j.jpowsour.2016.10.025.

[246] A. S. Shaplov, R. Marcilla, D. Mecerreyes, Recent Advances in Innovative Polymer Electrolytes based on Poly(ionic liquid)s, *Electrochim. Acta.*, **2015**, 175, 18–34. DOI: 10.1016/j.electacta.2015.03.038.

[247] A. Basile, A. I. Bhatt, A. P. O'Mullane, Stabilizing lithium metal using ionic liquids for long-lived batteries, *Nat. Commun.*, **2016**, 7, ncomms11794. DOI: 10.1038/ncomms11794.

[248] Y. Lu, K. Korf, Y. Kambe, Z. Tu, L. A. Archer, Ionic-Liquid-Nanoparticle Hybrid Electrolytes: Applications in Lithium Metal Batteries, *Angew. Chemie Int. Ed.*, **2014**, 53, 488–492. DOI: 10.1002/anie.201307137.

[249] S. Wilken, S. Xiong, J. Scheers, P. Jacobsson, P. Johansson, Ionic liquids in lithium battery electrolytes: Composition versus safety and physical properties, *J. Power Sources.*, **2015**, 275, 935–942. DOI: 10.1016/j.jpowsour.2014.11.071.

[250] A. Balducci, Ionic Liquids in Lithium-Ion Batteries, *Top. Curr. Chem.*, **2017**, 375, 20. DOI: 10.1007/s41061-017-0109-8.

[251] G. A. Elia, J. Hassoun, W.-J. Kwak, Y.-K. Sun, B. Scrosati, F. Mueller, D. Bresser, S. Passerini, P. Oberhumer, N. Tsiouvaras, J. Reiter, An Advanced Lithium–Air Battery Exploiting an Ionic Liquid-Based Electrolyte, *Nano Lett.*, **2014**, 14, 6572–6577. DOI: 10.1021/nl5031985.

[252] J. Scheers, S. Fantini, P. Johansson, A review of electrolytes for lithium–sulphur batteries, *J. Power Sources.*, **2014**, 255, 204–218. DOI: 10.1016/j.jpowsour.2014.01.023.

[253] S. A. Mohd Noor, P. C. Howlett, D. R. MacFarlane, M. Forsyth, Properties of sodium-based ionic liquid electrolytes for sodium secondary battery applications, *Electrochim. Acta.*, **2013**, 114, 766–771. DOI: 10.1016/j.electacta.2013.09.115.

[254] F. Wu, N. Zhu, Y. Bai, L. Liu, H. Zhou, C. Wu, Highly Safe Ionic Liquid Electrolytes for Sodium-Ion Battery: Wide Electrochemical Window and Good Thermal Stability, *ACS Appl. Mater. Interfaces.*, **2016**, 8, 21381–21386. DOI: 10.1021/acsami.6b07054.

[255] B. Pan, K.-C. Lau, J. T. Vaughey, L. Zhang, Z. Zhang, C. Liao, Ionic Liquid as an Effective Additive for Rechargeable Magnesium Batteries, *J. Electrochem. Soc.*, **2017**, 164, A902–A906. DOI: 10.1149/2.1551704jes.

[256] G. A. Giffin, Ionic liquid-based electrolytes for "beyond lithium" battery technologies, *J. Mater. Chem. A.*, **2016**, 4, 13378–13389. DOI: 10.1039/C6TA05260F.

[257] R. Chen, R. Hempelmann, Ionic liquid-mediated aqueous redox flow batteries for high voltage applications, *Electrochem. commun.*, **2016**, 70, 56–59. DOI: 10.1016/j.elecom.2016.07.003.

[258] K. Periyapperuma, Y. Zhang, D. R. MacFarlane, M. Forsyth, C. Pozo-Gonzalo, P. C. Howlett, Towards Higher Energy Density Redox-Flow Batteries: Imidazolium Ionic Liquid for Zn Electrochemistry in Flow Environment, *ChemElectroChem.*, **2017**, 4, 1051–1058. DOI: 10.1002/celc.201600875.

[259] C. Iojoiu, M. Hana, Y. Molmeret, M. Martinez, L. Cointeaux, N. El Kissi, J. Teles, J.-C. Leprêtre, P. Judeinstein, J.-Y. Sanchez, Ionic Liquids and Their Hosting by Polymers for HT-PEMFC Membranes, *Fuel Cells.*, **2010**, 10, 778–789. DOI: 10.1002/fuce.201000026.

[260] S.-Y. Lee, A. Ogawa, M. Kanno, H. Nakamoto, T. Yasuda, M. Watanabe, Nonhumidified intermediate

temperature fuel cells using protic ionic liquids, *J. Am. Chem. Soc.*, **2010**, 132, 9764–9773. DOI: 10.1021/ja102367x.

[261] T. Yasuda, M. Watanabe, Protic ionic liquids: Fuel cell applications, *MRS Bull.*, **2013**, 38, 560–566. DOI: 10.1557/mrs.2013.153.

[262] G.-R. Zhang, M. Munoz, B. J. M. Etzold, Accelerating Oxygen-Reduction Catalysts through Preventing Poisoning with Non-Reactive Species by Using Hydrophobic Ionic Liquids, *Angew. Chemie Int. Ed.*, **2016**, 55, 2257–2261. DOI: 10.1002/anie.201508338.

[263] G.-R. Zhang, M. Munoz, B. J. M. Etzold, Boosting Performance of Low Temperature Fuel Cell Catalysts by Subtle Ionic Liquid Modification, *ACS Appl. Mater. Interfaces.*, **2015**, 7, 3562–3570. DOI: 10.1021/am5074003.

[264] M. Gorlov, L. Kloo, Ionic liquid electrolytes for dye-sensitized solar cells, *Dalt. Trans.*, **2008**, 2655. DOI: 10.1039/b716419j.

[265] Y. J. Kim, S. Kim, Y. K. Joshi, A. G. Fedorov, P. A. Kohl, Thermodynamic analysis of an absorption refrigeration system with ionic-liquid/refrigerant mixture as a working fluid, *Energy.*, **2012**, 44, 1005–1016. DOI: 10.1016/j.energy.2012.04.048.

[266] S. Werner, M. Haumann, P. Wasserscheid, Ionic Liquids in Chemical Engineering, *Annu. Rev. Chem. Biomol. Eng.*, **2010**, 1, 203–230. DOI: 10.1146/annurev-chembioeng-073009-100915.

[267] N. J. Bridges, A. E. Visser, E. B. Fox, Potential of Nanoparticle-Enhanced Ionic Liquids (NEILs) as Advanced Heat-Transfer Fluids, *Energy & Fuels.*, **2011**, 25, 4862–4864. DOI: 10.1021/ef2012084.

[268] J. D. Holbrey, W. M. Reichert, R. G. Reddy, R. D. Rogers, in *Ionic Liquids as Green Solvents - Progress and Prospects*, **2003**, p. 121–133. DOI: 10.1021/bk-2003-0856.ch011.

[269] I. Minami, Ionic Liquids in Tribology, *Molecules.*, **2009**, 14, 2286–2305. DOI: 10.3390/molecules14062286.

[270] W. C. Barnhill, J. Qu, H. Luo, H. M. Meyer, C. Ma, M. Chi, B. L. Papke, Phosphonium-Organophosphate Ionic Liquids as Lubricant Additives: Effects of Cation Structure on Physicochemical and Tribological Characteristics, *ACS Appl. Mater. Interfaces.*, **2014**, 6, 22585–22593. DOI: 10.1021/am506702u.

[271] H. Xiao, D. Guo, S. Liu, G. Pan, X. Lu, Film Thickness of Ionic Liquids Under High Contact Pressures as a Function of Alkyl Chain Length, *Tribol. Lett.*, **2011**, 41, 471–477. DOI: 10.1007/s11249-010-9729-7.

[272] A. Somers, P. Howlett, D. MacFarlane, M. Forsyth, A Review of Ionic Liquid Lubricants, *Lubricants.*, **2013**, 1, 3–21. DOI: 10.3390/lubricants1010003.

[273] M.-D. Bermúdez, A.-E. Jiménez, J. Sanes, F.-J. Carrión, Ionic Liquids as Advanced Lubricant Fluids, *Molecules.*, **2009**, 14, 2888–2908. DOI: 10.3390/molecules14082888.

[274] H. J. Castejón, T. J. Wynn, Z. M. Marcin, Wetting and Tribological Properties of Ionic Liquids, *J. Phys. Chem. B.*, **2014**, 118, 3661–3668. DOI: 10.1021/jp411765f.

[275] M. M. Pereira, K. A. Kurnia, F. L. Sousa, N. J. O. Silva, J. A. Lopes-da-Silva, J. A. P. Coutinho, M. G. Freire, Contact angles and wettability of ionic liquids on polar and non-polar surfaces, *Phys. Chem. Chem. Phys.*, **2015**, 17, 31653–31661. DOI: 10.1039/C5CP05873B.

[276] W. Wu, B. Han, H. Gao, Z. Liu, T. Jiang, J. Huang, Desulfurization of Flue Gas: SO2 Absorption by an Ionic Liquid, *Angew. Chemie Int. Ed.*, **2004**, 43, 2415–2417. DOI: 10.1002/anie.200353437.

[277] A. Yokozeki, M. B. Shiflett, C. P. Junk, L. M. Grieco, T. Foo, Physical and Chemical Absorptions of Carbon Dioxide in Room-Temperature Ionic Liquids, *J. Phys. Chem. B.*, **2008**, 112, 16654–16663. DOI: 10.1021/jp805784u.

[278] C. Wang, H. Luo, D. Jiang, H. Li, S. Dai, Carbon Dioxide Capture by Superbase-Derived Protic Ionic Liquids, *Angew. Chemie.*, **2010**, 122, 6114–6117. DOI: 10.1002/ange.201002641.

[279] L. C. Tomé, I. M. Marrucho, Ionic liquid-based materials: a platform to design engineered CO 2 separation membranes, *Chem. Soc. Rev.*, **2016**, 45, 2785–2824. DOI: 10.1039/C5CS00510H.

[280] X. Zhang, X. Zhang, H. Dong, Z. Zhao, S. Zhang, Y. Huang, Carbon capture with ionic liquids: overview and progress, *Energy Environ. Sci.*, **2012**, 5, 6668. DOI: 10.1039/c2ee21152a.

[281] Q. R. Sheridan, W. F. Schneider, E. J. Maginn, Role of Molecular Modeling in the Development of CO2 –Reactive Ionic Liquids, *Chem. Rev.*, **2018**, 118, 5242–5260. DOI: 10.1021/acs.chemrev.8b00017.

[282] D. R. MacFarlane, N. Tachikawa, M. Forsyth, J. M. Pringle, P. C. Howlett, G. D. Elliott, J. H. Davis, M. Watanabe, P. Simon, C. A. Angell, Energy applications of ionic liquids, *Energy Environ. Sci.*, **2014**, 7, 232–250. DOI: 10.1039/c3ee42099j.

[283] S. Imaizumi, Y. Ohtsuki, T. Yasuda, H. Kokubo, M. Watanabe, Printable Polymer Actuators from Ionic Liquid, Soluble Polyimide, and Ubiquitous Carbon Materials, *ACS Appl. Mater. Interfaces.*, **2013**, 5, 6307–6315. DOI: 10.1021/am401351q.

[284] Y. Kitazawa, K. Ueno, M. Watanabe, Advanced Materials Based on Polymers and Ionic Liquids, *Chem. Rec.*, **2018**, 18, 391–409. DOI: 10.1002/tcr.201700041.

[285] M. A. B. H. Susan, T. Kaneko, A. Noda, M. Watanabe, Ion Gels Prepared by in Situ Radical Polymerization of Vinyl Monomers in an Ionic Liquid and Their Characterization as Polymer Electrolytes, *J. Am. Chem. Soc.*, **2005**, 127, 4976–4983. DOI: 10.1021/ja045155b.

[286] S. Imaizumi, Y. Kato, H. Kokubo, M. Watanabe, Driving Mechanisms of Ionic Polymer Actuators Having Electric Double Layer Capacitor Structures, *J. Phys. Chem. B.*, **2012**, 116, 5080–5089. DOI: 10.1021/jp301501c.

[287] X. Sun, H. Luo, S. Dai, Ionic Liquids-Based Extraction: A Promising Strategy for the Advanced Nuclear Fuel Cycle, *Chem. Rev.*, **2012**, 112, 2100–2128. DOI: 10.1021/cr200193x.

[288] Z. Radai, N. Z. Kiss, G. Keglevich, An Overview of the Applications of Ionic Liquids as Catalysts and Additives in Organic Chemical Reactions, *Curr. Org. Chem.*, **2018**, 22, 533–556. DOI: 10.2174/1385272822666171227152013.

[289] R. E. Morris, Ionothermal synthesis—ionic liquids as functional solvents in the preparation of crystalline materials, *Chem. Commun.*, **2009**, 2990. DOI: 10.1039/b902611h.

[290] P. Wasserscheid, C. Hilgers, C. M. Gordon, M. J. Muldoon, I. R. Dunkin, Ionic liquids: polar, but weakly coordinating solvents for the first biphasic oligomerisation of ethene to higher α-olefins with cationic Ni complexes, *Chem. Commun.*, **2001**, 1, 1186–1187. DOI: 10.1039/b101400p.

[291] M. A. Klingshirn, G. A. Broker, J. D. Holbrey, K. H. Shaughnessy, R. D. Rogers, Polar, non-coordinating ionic liquids as solvents for the alternating copolymerization of styrene and CO catalyzed by cationic palladium catalysts, *Chem. Commun.*, **2002**, 2, 1394–1395. DOI: 10.1039/b203367d.

[292] M. J. Earle, S. P. Katdare, K. R. Seddon, Paradigm Confirmed: The First Use of Ionic Liquids to Dramatically Influence the Outcome of Chemical Reactions, *Org. Lett.*, **2004**, 6, 707–710. DOI: 10.1021/ol036310e.

[293] Z. Ma, J. Yu, S. Dai, Preparation of Inorganic Materials Using Ionic Liquids, *Adv. Mater.*, **2010**, 22, 261–285. DOI: 10.1002/adma.200900603.

[294] P. Wasserscheid, C. Hilgers, W. Keim, Ionic liquids - Weakly-coordinating solvents for the biphasic ethylene oligomerization to α-olefins using cationic Ni-complexes, *J. Mol. Catal. A Chem.*, **2004**, 214, 83–90. DOI: 10.1016/j.molcata.2003.11.032.

[295] J. G. Huddleston, H. D. Willauer, R. P. Swatloski, A. E. Visser, R. D. Rogers, Room temperature ionic liquids as novel media for 'clean' liquid–liquid extraction, *Chem. Commun.*, **1998**, 1765–1766. DOI: 10.1039/A803999B.

[296] M. Haumann, A. Riisager, Hydroformylation in Room Temperature Ionic Liquids (RTILs): Catalyst and Process Developments, *Chem. Rev.*, **2008**, 108, 1474–1497. DOI: 10.1021/cr078374z.

[297] W. Kunz, K. Häckl, The hype with ionic liquids as solvents, *Chem. Phys. Lett.*, **2016**, 661, 6–12. DOI: 10.1016/j.cplett.2016.07.044.

[298] A. C. Cole, J. L. Jensen, I. Ntai, K. L. T. Tran, K. J. Weaver, D. C. Forbes, J. H. Davis, Novel Brønsted Acidic Ionic Liquids and Their Use as Dual Solvent−Catalysts, *J. Am. Chem. Soc.*, **2002**, 124, 5962–5963. DOI: 10.1021/ja026290w.

[299] A. S. Amarasekara, Acidic Ionic Liquids, *Chem. Rev.*, **2016**, 116, 6133–6183. DOI: 10.1021/acs.chemrev.5b00763.

[300] R. Sheldon, Catalytic reactions in ionic liquids, *Chem. Commun.*, **2001**, 2399–2407. DOI: 10.1039/b107270f.

[301] Z.-Z. Yang, L.-N. He, C.-X. Miao, S. Chanfreau, Lewis Basic Ionic Liquids-Catalyzed Conversion of Carbon Dioxide to Cyclic Carbonates, *Adv. Synth. Catal.*, **2010**, 352, 2233–2240. DOI: 10.1002/adsc.201000239.

[302] J. Choi, T. M. Benedetti, R. Jalili, A. Walker, G. G. Wallace, D. L. Officer, High Performance Fe Porphyrin/Ionic Liquid Co-catalyst for Electrochemical CO 2 Reduction, *Chem. - A Eur. J.*, **2016**, 22, 14158–14161. DOI: 10.1002/chem.201603359.

[303] Y. Oh, X. Hu, Ionic liquids enhance the electrochemical CO_2 reduction catalyzed by MoO_2, *Chem. Commun.*, **2015**, 51, 13698–13701. DOI: 10.1039/C5CC05263G.

[304] T. Li, X. Wang, W. Yuan, C. M. Li, Unique Co-Catalytic Behavior of Protic Ionic Liquids as Multifunctional Electrolytes for Water Splitting, *ChemElectroChem.*, **2016**, 3, 204–208. DOI: 10.1002/celc.201500458.

[305] E. Rafiee, M. Kahrizi, Mechanistic investigation of Heck reaction catalyzed by new catalytic system composed of Fe3O4@OA–Pd and ionic liquids as co-catalyst, *J. Mol. Liq.*, **2016**, 218, 625–631. DOI: 10.1016/j.molliq.2016.02.055.

[306] Š. Toma, R. Šebesta, in *Ionic Liquids in Biotransformations and Organocatalysis*, John Wiley & Sons, Inc., Hoboken, NJ, USA, **2012**, p. 331–359. DOI: 10.1002/9781118158753.ch9.

[307] A. Karakulina, A. Gopakumar, İ. Akçok, B. L. Roulier, T. LaGrange, S. A. Katsyuba, S. Das, P. J. Dyson, A Rhodium Nanoparticle-Lewis Acidic Ionic Liquid Catalyst for the Chemoselective Reduction of Heteroarenes, *Angew. Chemie Int. Ed.*, **2016**, 55, 292–296. DOI: 10.1002/anie.201507945.

[308] S. Wegner, C. Janiak, Metal Nanoparticles in Ionic Liquids, *Top. Curr. Chem.*, **2017**, 375, 65. DOI: 10.1007/s41061-017-0148-1.

[309] Z. He, P. Alexandridis, Nanoparticles in ionic liquids: interactions and organization, *Phys. Chem. Chem. Phys.*, **2015**, 17, 18238–18261. DOI: 10.1039/C5CP01620G.

[310] J. D. Scholten, B. C. Leal, J. Dupont, Transition Metal Nanoparticle Catalysis in Ionic Liquids, *ACS Catal.*, **2012**, 2, 184–200. DOI: 10.1021/cs200525e.

[311] Z. He, P. Alexandridis, Ionic liquid and nanoparticle hybrid systems: Emerging applications, *Adv. Colloid Interface Sci.*, **2017**, 244, 54–70. DOI: 10.1016/j.cis.2016.08.004.

[312] A.-V. Mudring, T. Alammar, T. Bäcker, K. Richter, in *ACS symposium series*, **2010**, vol. 1030, p. 177–188. DOI: 10.1021/bk-2009-1030.ch012.

[313] C. Janiak, Ionic Liquids for the Synthesis and Stabilization of Metal Nanoparticles, *Zeitschrift für Naturforsch. B.*, **2013**, 68, 1059–1089. DOI: 10.5560/znb.2013-3140.

[314] K. Richter, P. S. Campbell, T. Baecker, A. Schimitzek, D. Yaprak, A.-V. Mudring, Ionic liquids for the synthesis of metal nanoparticles, *Phys. status solidi.*, **2013**, 250, 1152–1164. DOI: 10.1002/pssb.201248547.

[315] M. Antonietti, D. Kuang, B. Smarsly, Y. Zhou, Ionic Liquids for the Convenient Synthesis of Functional Nanoparticles and Other Inorganic Nanostructures, *Angew. Chemie Int. Ed.*, **2004**, 43, 4988–4992. DOI:

10.1002/anie.200460091.

[316] P. Wasserscheid, T. Welton, Eds., *Ionic Liquids in Synthesis*, Wiley-VCH Verlag GmbH & Co. KGaA, Weinheim, Germany, **2007**.

[317] H.-P. Steinrück, P. Wasserscheid, Ionic Liquids in Catalysis, *Catal. Letters.*, **2015**, 145, 380–397. DOI: 10.1007/s10562-014-1435-x.

[318] V. I. Pârvulescu, C. Hardacre, Catalysis in Ionic Liquids, *Chem. Rev.*, **2007**, 107, 2615–2665. DOI: 10.1021/cr050948h.

[319] C. M. Gordon, New developments in catalysis using ionic liquids, *Appl. Catal., A.*, **2001**, 222, 101–117. DOI: 10.1016/S0926-860X(01)00834-1.

[320] C. Daguenet, P. J. Dyson, Switching the Mechanism of Catalyst Activation by Ionic Liquids Switching the Mechanism of Catalyst Activation by Ionic Liquids, *Organometallics.*, **2006**, 25, 5811–5816. DOI: 10.1021/om060728+.

[321] S. Kirchhecker, D. Esposito, Amino acid based ionic liquids: A green and sustainable perspective, *Curr. Opin. Green Sustain. Chem.*, **2016**, 2, 28–33. DOI: 10.1016/j.cogsc.2016.09.001.

[322] W. Bao, Z. Wang, Y. Li, Synthesis of Chiral Ionic Liquids from Natural Amino Acids, *J. Org. Chem.*, **2003**, 68, 591–593. DOI: 10.1021/jo020503i.

[323] J. Olchowka, M. Suta, C. Wickleder, Green Synthesis of A_2SiF_6 (A=Li-Cs) Nanoparticles using Ionic Liquids as Solvents and as Fluorine Sources: A Simple Approach without HF, *Chem. - A Eur. J.*, **2017**, 6, 12092–12095. DOI: 10.1002/chem.201702375.

[324] K. E. Gutowski, Industrial uses and applications of ionic liquids, *Phys. Sci. Rev.*, **2018**, 3, 1–10. DOI: 10.1515/psr-2017-0191.

[325] M. D. Morton, C. K. Hamer, Ionic liquids – The beginning of the end or the end of the beginning? – A look at the life of ionic liquids through patent claims, *Sep. Purif. Technol.*, **2018**, 196, 3–9. DOI: 10.1016/j.seppur.2017.11.023.

[326] M. Deetlefs, M. Fanselow, K. R. Seddon, Ionic liquids: the view from Mount Improbable, *RSC Adv.*, **2016**, 6, 4280–4288. DOI: 10.1039/C5RA05829E.

[327] M. Maase, in *Ionic Liquids in Synthesis*, Wiley-VCH Verlag GmbH & Co. KGaA, Weinheim, Germany, p. 663–687. DOI: 10.1002/9783527621194.ch9.

[328] T. J. Geldbach, D. Zhao, N. C. Castillo, G. Laurenczy, B. Weyershausen, P. J. Dyson, *Biphasic Hydrosilylation in Ionic Liquids: A Process Set for Industrial Implementation*, **2006**, vol. 128.

[329] A. Schönweiz, R. Franke, in *Supported Ionic Liquids*, Wiley-VCH Verlag GmbH & Co. KGaA, Weinheim, Germany, **2014**, p. 307–326. DOI: 10.1002/9783527654789.ch15.

[330] *Evonik demonstrates for the first time that SILP catalyst systems can be used commercially*, Evonik Industries Press Release, June 10, 2015, Essen, Germany.

[331] X. Shen, J. L. Shamshina, P. Berton, J. Bandomir, H. Wang, G. Gurau, R. D. Rogers, Comparison of Hydrogels Prepared with Ionic-Liquid-Isolated vs Commercial Chitin and Cellulose, *ACS Sustain. Chem. Eng.*, **2016**, 4, 471–480. DOI: 10.1021/acssuschemeng.5b01400.

[332] T. Trivedi1, A. Kumar1, 2, Utilization of Ionic Liquids for the Processing of Biopolymers, *Biomass and Biofuels.*, **2015**, 127–154. DOI: 10.1201/b18398-10.

[333] S. Zhang, J. Wang, X. Lu, Q. Zhou, Eds., *Structures and Interactions of Ionic Liquids*, Springer Berlin Heidelberg, Berlin, Heidelberg, **2014**, vol. 151.

[334] M. M. Jaworska, T. Kozlecki, A. Gorak, Review of the application of ionic liquids as solvents for chitin, *J. Polym. Eng.*, **2012**, 32, 67–69. DOI: 10.1515/polyeng-2011-0145.

[335] J. L. Shamshina, P. S. Barber, G. Gurau, C. S. Griggs, R. D. Rogers, Pulping of Crustacean Waste Using Ionic Liquids: To Extract or Not To Extract, *ACS Sustain. Chem. Eng.*, **2016**, 4, 6072–6081. DOI: 10.1021/acssuschemeng.6b01434.

[336] H. Xie, S. Li, S. Zhang, Ionic liquids as novel solvents for the dissolution and blending of wool keratin fibers, *Green Chem.*, **2005**, 7, 606. DOI: 10.1039/b502547h.

[337] H. Garcia, R. Ferreira, M. Petkovic, J. L. Ferguson, M. C. Leitão, H. Q. N. Gunaratne, K. R. Seddon, L. P. N. Rebelo, C. Silva Pereira, Dissolution of cork biopolymers in biocompatible ionic liquids, *Green Chem.*, **2010**, 12, 367. DOI: 10.1039/b922553f.

[338] W. E. S. Hart, J. B. Harper, L. Aldous, The effect of changing the components of an ionic liquid upon the solubility of lignin, *Green Chem.*, **2015**, 17, 214–218. DOI: 10.1039/C4GC01888E.

[339] R. P. Swatloski, S. K. Spear, J. D. Holbrey, R. D. Rogers, Dissolution of Cellose with Ionic Liquids, *J. Am. Chem. Soc.*, **2002**, 124, 4974–4975. DOI: 10.1021/ja025790m.

[340] I. Kilpeläinen, H. Xie, A. King, M. Granstrom, S. Heikkinen, D. S. Argyropoulos, Dissolution of Wood in Ionic Liquids, *J. Agric. Food Chem.*, **2007**, 55, 9142–9148. DOI: 10.1021/jf071692e.

[341] D. A. Fort, R. C. Remsing, R. P. Swatloski, P. Moyna, G. Moyna, R. D. Rogers, Can ionic liquids dissolve wood? Processing and analysis of lignocellulosic materials with 1-n-butyl-3-methylimidazolium chloride, *Green Chem.*, **2007**, 9, 63–69. DOI: 10.1039/B607614A.

[342] K. C. Badgujar, B. M. Bhanage, Factors governing dissolution process of lignocellulosic biomass in ionic liquid: Current status, overview and challenges, *Bioresour. Technol.*, **2015**, 178, 2–18. DOI: 10.1016/j.biortech.2014.09.138.

[343] A. Pinkert, K. N. Marsh, S. Pang, M. P. Staiger, Ionic Liquids and Their Interaction with Cellulose, *Chem. Rev.*, **2009**, 109, 6712–6728. DOI: 10.1021/cr9001947.

[344] H. Tadesse, R. Luque, Advances on biomass pretreatment using ionic liquids: An overview, *Energy Environ. Sci.*, **2011**, 4, 3913. DOI: 10.1039/c0ee00667j.

[345] A. George, A. Brandt, K. Tran, S. M. S. N. S. Zahari, D. Klein-Marcuschamer, N. Sun, N. Sathitsuksanoh, J. Shi, V. Stavila, R. Parthasarathi, S. Singh, B. M. Holmes, T. Welton, B. A. Simmons, J. P. Hallett, Design of low-cost ionic liquids for lignocellulosic biomass pretreatment, *Green Chem.*, **2015**, 17, 1728–1734. DOI: 10.1039/C4GC01208A.

[346] A. Brandt, M. J. Ray, T. Q. To, D. J. Leak, R. J. Murphy, T. Welton, Ionic liquid pretreatment of lignocellulosic biomass with ionic liquid–water mixtures, *Green Chem.*, **2011**, 13, 2489. DOI: 10.1039/c1gc15374a.

[347] A. Pinkert, D. F. Goeke, K. N. Marsh, S. Pang, Extracting wood lignin without dissolving or degrading cellulose: investigations on the use of food additive-derived ionic liquids, *Green Chem.*, **2011**, 13, 3124. DOI: 10.1039/c1gc15671c.

[348] N. Muhammad, Z. Man, M. I. A. Mutalib, M. A. Bustam, C. D. Wilfred, A. S. Khan, Z. Ullah, G. Gonfa, A. Nasrullah, Dissolution and Separation of Wood Biopolymers Using Ionic Liquids, *ChemBioEng Rev.*, **2015**, 2, 257–278. DOI: 10.1002/cben.201500003.

[349] S. Tang, G. A. Baker, S. Ravula, J. E. Jones, H. Zhao, PEG-functionalized ionic liquids for cellulose dissolution and saccharification, *Green Chem.*, **2012**, 14, 2922. DOI: 10.1039/c2gc35631g.

[350] Uju, Y. Shoda, A. Nakamoto, M. Goto, W. Tokuhara, Y. Noritake, S. Katahira, N. Ishida, K. Nakashima, C. Ogino, N. Kamiya, Short time ionic liquids pretreatment on lignocellulosic biomass to enhance enzymatic saccharification, *Bioresour. Technol.*, **2012**, 103, 446–452. DOI: 10.1016/j.biortech.2011.10.003.

[351] N. Kamiya, Y. Matsushita, M. Hanaki, K. Nakashima, M. Narita, M. Goto, H. Takahashi, Enzymatic in situ saccharification of cellulose in aqueous-ionic liquid media, *Biotechnol. Lett.*, **2008**, 30, 1037–1040. DOI: 10.1007/s10529-008-9638-0.

[352] R. M. Wahlström, A. Suurnäkki, Enzymatic hydrolysis of lignocellulosic polysaccharides in the presence of ionic liquids, *Green Chem.*, **2015**, 17, 694–714. DOI: 10.1039/C4GC01649A.

[353] A. M. da Costa Lopes, R. Bogel-Łukasik, Acidic Ionic Liquids as Sustainable Approach of Cellulose and Lignocellulosic Biomass Conversion without Additional Catalysts, *ChemSusChem.*, **2015**, 8, 947–965. DOI: 10.1002/cssc.201402950.

[354] F. Xu, J. Sun, N. V. S. N. M. Konda, J. Shi, T. Dutta, C. D. Scown, B. A. Simmons, S. Singh, Transforming biomass conversion with ionic liquids: process intensification and the development of a high-gravity, one-pot process for the production of cellulosic ethanol, *Energy Environ. Sci.*, **2016**, 9, 1042–1049. DOI: 10.1039/C5EE02940F.

[355] J. Sun, N. V. S. N. M. Konda, J. Shi, R. Parthasarathi, T. Dutta, F. Xu, C. D. Scown, B. A. Simmons, S. Singh, CO 2 enabled process integration for the production of cellulosic ethanol using bionic liquids, *Energy Environ. Sci.*, **2016**, 9, 2822–2834. DOI: 10.1039/C6EE00913A.

[356] S. Peleteiro, S. Rivas, J. L. Alonso, V. Santos, J. C. Parajó, Furfural production using ionic liquids: A review, *Bioresour. Technol.*, **2016**, 202, 181–191. DOI: 10.1016/j.biortech.2015.12.017.

[357] S. Peleteiro, V. Santos, G. Garrote, J. C. Parajó, Furfural production from Eucalyptus wood using an Acidic Ionic Liquid, *Carbohydr. Polym.*, **2016**, 146, 20–25. DOI: 10.1016/j.carbpol.2016.03.049.

[358] S. M. Sen, J. B. Binder, R. T. Raines, C. T. Maravelias, Conversion of biomass to sugars via ionic liquid hydrolysis: process synthesis and economic evaluation, *Biofuels, Bioprod. Biorefining.*, **2012**, 6, 444–452. DOI: 10.1002/bbb.1336.

[359] A. M. da Costa Lopes, R. M. Łukasik, Separation and Recovery of a Hemicellulose-Derived Sugar Produced from the Hydrolysis of Biomass by an Acidic Ionic Liquid, *ChemSusChem.*, **2018**, 11, 1099–1107. DOI: 10.1002/cssc.201702231.

[360] A. M. Socha, R. Parthasarathi, J. Shi, S. Pattathil, D. Whyte, M. Bergeron, A. George, K. Tran, V. Stavila, S. Venkatachalam, M. G. Hahn, B. a Simmons, S. Singh, Efficient biomass pretreatment using ionic liquids derived from lignin and hemicellulose, *Proc. Natl. Acad. Sci.*, **2014**, 111, E3587–E3595. DOI: 10.1073/pnas.1405685111.

[361] M. Olkiewicz, N. V. Plechkova, A. Fabregat, F. Stüber, A. Fortuny, J. Font, C. Bengoa, Efficient extraction of lipids from primary sewage sludge using ionic liquids for biodiesel production, *Sep. Purif. Technol.*, **2015**, 153, 118–125. DOI: 10.1016/j.seppur.2015.08.038.

[362] D. Z. Troter, Z. B. Todorović, D. R. Đokić-Stojanović, O. S. Stamenković, V. B. Veljković, Application of ionic liquids and deep eutectic solvents in biodiesel production: A review, *Renew. Sustain. Energy Rev.*, **2016**, 61, 473–500. DOI: 10.1016/j.rser.2016.04.011.

[363] Z. Zhang, J. Song, B. Han, Catalytic Transformation of Lignocellulose into Chemicals and Fuel Products in Ionic Liquids, *Chem. Rev.*, **2017**, 117, 6834–6880. DOI: 10.1021/acs.chemrev.6b00457.

[364] R. Ma, Y. Xu, X. Zhang, Catalytic Oxidation of Biorefinery Lignin to Value-added Chemicals to Support Sustainable Biofuel Production, *ChemSusChem.*, **2015**, 8, 24–51. DOI: 10.1002/cssc.201402503.

[365] I. Noshadi, B. W. Walker, R. Portillo-Lara, E. Shirzaei Sani, N. Gomes, M. R. Aziziyan, N. Annabi, Engineering Biodegradable and Biocompatible Bio-ionic Liquid Conjugated Hydrogels with Tunable Conductivity and Mechanical Properties, *Sci. Rep.*, **2017**, 7, 4345. DOI: 10.1038/s41598-017-04280-w.

[366] J. Zhang, J. Wu, J. Yu, X. Zhang, J. He, J. Zhang, Application of ionic liquids for dissolving cellulose and

fabricating cellulose-based materials: state of the art and future trends, *Mater. Chem. Front.*, **2017**, 1, 1273–1290. DOI: 10.1039/C6QM00348F.

[367] D. H. A. T. Gunasekera, S. Kuek, D. Hasanaj, Y. He, C. Tuck, A. K. Croft, R. D. Wildman, Three dimensional ink-jet printing of biomaterials using ionic liquids and co-solvents, *Faraday Discuss.*, **2016**, 190, 509–523. DOI: 10.1039/C5FD00219B.

[368] H. Mahmood, M. Moniruzzaman, S. Yusup, T. Welton, Ionic liquids assisted processing of renewable resources for the fabrication of biodegradable composite materials, *Green Chem.*, **2017**, 19, 2051–2075. DOI: 10.1039/C7GC00318H.

[369] M. Isik, H. Sardon, D. Mecerreyes, Ionic Liquids and Cellulose: Dissolution, Chemical Modification and Preparation of New Cellulosic Materials, *Int. J. Mol. Sci.*, **2014**, 15, 11922–11940. DOI: 10.3390/ijms150711922.

[370] L. Meli, J. Miao, J. S. Dordick, R. J. Linhardt, Electrospinning from room temperature ionic liquids for biopolymer fiber formation, *Green Chem.*, **2010**, 12, 1883. DOI: 10.1039/c0gc00283f.

[371] S. Livi, V. Bugatti, M. Marechal, B. G. Soares, G. M. O. Barra, J. Duchet-Rumeau, J.-F. Gérard, Ionic liquids–lignin combination: an innovative way to improve mechanical behaviour and water vapour permeability of eco-designed biodegradable polymer blends, *RSC Adv.*, **2015**, 5, 1989–1998. DOI: 10.1039/C4RA11919C.

[372] C. King, J. L. Shamshina, G. Gurau, P. Berton, N. F. A. F. Khan, R. D. Rogers, A platform for more sustainable chitin films from an ionic liquid process, *Green Chem.*, **2017**, 19, 117–126. DOI: 10.1039/C6GC02201D.

[373] X. Yang, C. Qiao, Y. Li, T. Li, Dissolution and resourcfulization of biopolymers in ionic liquids, *React. Funct. Polym.*, **2016**, 100, 181–190. DOI: 10.1016/j.reactfunctpolym.2016.01.017.

[374] T. Heinze, K. Schwikal, S. Barthel, Ionic Liquids as Reaction Medium in Cellulose Functionalization, *Macromol. Biosci.*, **2005**, 5, 520–525. DOI: 10.1002/mabi.200500039.

[375] H. Passos, M. G. Freire, J. A. P. Coutinho, Ionic liquid solutions as extractive solvents for value-added compounds from biomass, *Green Chem.*, **2014**, 16, 4786–4815. DOI: 10.1039/C4GC00236A.

[376] B. Tang, W. Bi, M. Tian, K. H. Row, Application of ionic liquid for extraction and separation of bioactive compounds from plants, *J. Chromatogr. B.*, **2012**, 904, 1–21. DOI: 10.1016/j.jchromb.2012.07.020.

[377] S. Dreyer, U. Kragl, Ionic liquids for aqueous two-phase extraction and stabilization of enzymes, *Biotechnol. Bioeng.*, **2008**, 99, 1416–1424. DOI: 10.1002/bit.21720.

[378] M. G. Freire, A. F. M. Cláudio, J. M. M. Araújo, J. A. P. Coutinho, I. M. Marrucho, J. N. C. Lopes, L. P. N. Rebelo, Aqueous biphasic systems: a boost brought about by using ionic liquids, *Chem. Soc. Rev.*, **2012**, 41, 4966. DOI: 10.1039/c2cs35151j.

[379] M. V. Quental, M. Caban, M. M. Pereira, P. Stepnowski, J. A. P. Coutinho, M. G. Freire, Enhanced extraction of proteins using cholinium-based ionic liquids as phase-forming components of aqueous biphasic systems, *Biotechnol. J.*, **2015**, 10, 1457–1466. DOI: 10.1002/biot.201500003.

[380] M. Taha, M. R. Almeida, F. A. e. Silva, P. Domingues, S. P. M. Ventura, J. A. P. Coutinho, M. G. Freire, Novel Biocompatible and Self-buffering Ionic Liquids for Biopharmaceutical Applications, *Chem. - A Eur. J.*, **2015**, 21, 4781–4788. DOI: 10.1002/chem.201405693.

[381] M. Moniruzzaman, K. Nakashima, N. Kamiya, M. Goto, Recent advances of enzymatic reactions in ionic liquids, *Biochem. Eng. J.*, **2010**, 48, 295–314. DOI: 10.1016/j.bej.2009.10.002.

[382] F. Van Rantwijk, R. a Sheldon, Biocatalysis in Ionic Liquids, *Chem. Rev.*, **2007**, 107, 2757–2785. DOI: 10.1021/cr050946x.

[383] M. Naushad, Z. A. ALOthman, A. B. Khan, M. Ali, Effect of ionic liquid on activity, stability, and structure of enzymes: A review, *Int. J. Biol. Macromol.*, **2012**, 51, 555–560. DOI: 10.1016/j.ijbiomac.2012.06.020.

[384] H. Weingärtner, C. Cabrele, C. Herrmann, How ionic liquids can help to stabilize native proteins, *Phys. Chem. Chem. Phys.*, **2012**, 14, 415–426. DOI: 10.1039/C1CP21947B.

[385] H. Zhao, Methods for stabilizing and activating enzymes in ionic liquids-a review, *J. Chem. Technol. Biotechnol.*, **2010**, 85, 891–907. DOI: 10.1002/jctb.2375.

[386] A. P. S. Brogan, L. Bui-Le, J. P. Hallett, Non-aqueous homogenous biocatalytic conversion of polysaccharides in ionic liquids using chemically modified glucosidase, *Nat. Chem.* DOI: 10.1038/s41557-018-0088-6.

[387] K. S. Egorova, E. G. Gordeev, V. P. Ananikov, Biological Activity of Ionic Liquids and Their Application in Pharmaceutics and Medicine, *Chem. Rev.*, **2017**, 117, 7132–7189. DOI: 10.1021/acs.chemrev.6b00562.

[388] W. L. Hough, M. Smiglak, H. Rodríguez, R. P. Swatloski, S. K. Spear, D. T. Daly, J. Pernak, J. E. Grisel, R. D. Carliss, M. D. Soutullo, J. H. Davis, Jr., R. D. Rogers, The third evolution of ionic liquids: active pharmaceutical ingredients, *New J. Chem.*, **2007**, 31, 1429. DOI: 10.1039/b706677p.

[389] N. Adawiyah, M. Moniruzzaman, S. Hawatulaila, M. Goto, Ionic liquids as a potential tool for drug delivery systems, *Medchemcomm.*, **2016**, 7, 1881–1897. DOI: 10.1039/C6MD00358C.

[390] R. Ferraz, L. C. Branco, C. Prudêncio, J. P. Noronha, Ž. Petrovski, Ionic Liquids as Active Pharmaceutical Ingredients, *ChemMedChem.*, **2011**, 6, 975–985. DOI: 10.1002/cmdc.201100082.

[391] J. L. Shamshina, P. S. Barber, R. D. Rogers, Ionic liquids in drug delivery, *Expert Opin. Drug Deliv.*, **2013**, 10, 1367–1381. DOI: 10.1517/17425247.2013.808185.

[392] A. Banerjee, K. Ibsen, T. Brown, R. Chen, C. Agatemor, S. Mitragotri, Ionic liquids for oral insulin delivery, *Proc. Natl. Acad. Sci.*, **2018**, 115, 7296–7301. DOI: 10.1073/pnas.1722338115.

[393] M. Koel, Ionic liquids in chemical analysis, *Crit. Rev. Anal. Chem.*, **2005**, 35, 177–192. DOI: 10.1080/10408340500304016.

[394] J. L. Anderson, D. W. Armstrong, G.-T. Wei, Ionic Liquids in Analytical Chemistry, *Anal. Chem.*, **2006**, 78, 2892–2902. DOI: 10.1021/ac069394o.

[395] H. N. Abdelhamid, Ionic Liquid-Assisted Laser Desorption/Ionization–Mass Spectrometry: Matrices, Microextraction, and Separation, *Methods Protoc.*, **2018**, 1, 23. DOI: 10.3390/mps1020023.

[396] A. Tholey, E. Heinzle, Ionic (liquid) matrices for matrix-assisted laser desorption/ionization mass spectrometry—applications and perspectives, *Anal. Bioanal. Chem.*, **2006**, 386, 24–37. DOI: 10.1007/s00216-006-0600-5.

[397] M. Zabet-Moghaddam, E. Heinzle, A. Tholey, Qualitative and quantitative analysis of low molecular weight compounds by ultraviolet matrix-assisted laser desorption/ionization mass spectrometry using ionic liquid matrices, *Rapid Commun. Mass Spectrom.*, **2004**, 18, 141–148. DOI: 10.1002/rcm.1293.

[398] T. D. Ho, C. Zhang, L. W. Hantao, J. L. Anderson, Ionic Liquids in Analytical Chemistry: Fundamentals, Advances, and Perspectives, *Anal. Chem.*, **2014**, 86, 262–285. DOI: 10.1021/ac4035554.

[399] P. Sun, D. W. Armstrong, Ionic liquids in analytical chemistry, *Anal. Chim. Acta.*, **2010**, 661, 1–16. DOI: 10.1016/j.aca.2009.12.007.

[400] M. C. García-Alvarez-Coque, M. J. Ruiz-Angel, A. Berthod, S. Carda-Broch, On the use of ionic liquids as mobile phase additives in high-performance liquid chromatography. A review, *Anal. Chim. Acta.*, **2015**, 883, 1–21. DOI: 10.1016/j.aca.2015.03.042.

[401] L. Brown, M. J. Earle, M. A. Gîlea, N. V. Plechkova, K. R. Seddon, Ionic Liquid–Liquid Chromatography: A New General Purpose Separation Methodology, *Top. Curr. Chem.*, **2017**, 375, 74. DOI: 10.1007/s41061-017-0159-y.

[402] T. K. F. Dier, D. Rauber, J. Jauch, R. Hempelmann, D. A. Volmer, Novel Mixed-Mode Stationary Phases for Chromatographic Separation of Complex Mixtures of Decomposed Lignin, *ChemistrySelect.*, **2017**, 2, 779–786. DOI: 10.1002/slct.201601673.

[403] M. L. Pusey, M. S. Paley, M. B. Turner, R. D. Rogers, Protein Crystallization Using Room Temperature Ionic Liquids, *Cryst. Growth Des.*, **2007**, 7, 787–793. DOI: 10.1021/cg060696t.

[404] X. Chen, J. Liu, J. Wang, Ionic liquids in the assay of proteins, *Anal. Methods.*, **2010**, 2, 1222. DOI: 10.1039/c0ay00342e.

[405] L. Gao, T. J. McCarthy, Ionic Liquids Are Useful Contact Angle Probe Fluids, *J. Am. Chem. Soc.*, **2007**, 129, 3804–3805. DOI: 10.1021/ja070169d.

[406] M. C. Buzzeo, C. Hardacre, R. G. Compton, Use of Room Temperature Ionic Liquids in Gas Sensor Design, *Anal. Chem.*, **2004**, 76, 4583–4588. DOI: 10.1021/ac040042w.

[407] Q. Ji, I. Honma, S.-M. Paek, M. Akada, J. P. Hill, A. Vinu, K. Ariga, Layer-by-Layer Films of Graphene and Ionic Liquids for Highly Selective Gas Sensing, *Angew. Chemie Int. Ed.*, **2010**, 49, 9737–9739. DOI: 10.1002/anie.201004929.

[408] M. J. A. Shiddiky, A. A. J. Torriero, Application of ionic liquids in electrochemical sensing systems, *Biosens. Bioelectron.*, **2011**, 26, 1775–1787. DOI: 10.1016/j.bios.2010.08.064.

[409] D. Wei, A. Ivaska, Applications of ionic liquids in electrochemical sensors, *Anal. Chim. Acta.*, **2008**, 607, 126–135. DOI: 10.1016/j.aca.2007.12.011.

[410] D. S. Silvester, Recent advances in the use of ionic liquids for electrochemical sensing, *Analyst.*, **2011**, 136, 4871. DOI: 10.1039/c1an15699c.

[411] T. Torimoto, T. Tsuda, K. Okazaki, S. Kuwabata, New Frontiers in Materials Science Opened by Ionic Liquids, *Adv. Mater.*, **2010**, 22, 1196–1221. DOI: 10.1002/adma.200902184.

[412] S. Zhang, K. Dokko, M. Watanabe, Carbon materialization of ionic liquids: from solvents to materials, *Mater. Horizons.*, **2015**, 2, 168–197. DOI: 10.1039/C4MH00141A.

[413] S. Kuwabata, T. Tsuda, T. Torimoto, Room-Temperature Ionic Liquid. A New Medium for Material Production and Analyses under Vacuum Conditions, *J. Phys. Chem. Lett.*, **2010**, 1, 3177–3188. DOI: 10.1021/jz100876m.

[414] T.-P. Fellinger, A. Thomas, J. Yuan, M. Antonietti, 25th Anniversary Article: "Cooking Carbon with Salt": Carbon Materials and Carbonaceous Frameworks from Ionic Liquids and Poly(ionic liquid)s, *Adv. Mater.*, **2013**, 25, 5838–5855. DOI: 10.1002/adma.201301975.

[415] J. S. Lee, X. Wang, H. Luo, S. Dai, Fluidic carbon precursors for formation of functional carbon under ambient pressure based on ionic liquids, *Adv. Mater.*, **2010**, 22, 1004–1007. DOI: 10.1002/adma.200903403.

[416] S. Zhang, K. Dokko, M. Watanabe, Direct Synthesis of Nitrogen-Doped Carbon Materials from Protic Ionic Liquids and Protic Salts: Structural and Physicochemical Correlations between Precursor and Carbon, *Chem. Mater.*, **2014**, 26, 2915–2926. DOI: 10.1021/cm5006168.

[417] J. P. Paraknowitsch, J. Zhang, D. Su, A. Thomas, M. Antonietti, Ionic Liquids as Precursors for Nitrogen-Doped Graphitic Carbon, *Adv. Mater.*, **2010**, 22, 87–92. DOI: 10.1002/adma.200900965.

[418] K. Goossens, K. Lava, C. W. Bielawski, K. Binnemans, Ionic Liquid Crystals: Versatile Materials, *Chem. Rev.*, **2016**, 116, 4643–4807. DOI: 10.1021/cr400334b.

[419] T. Ichikawa, T. Kato, H. Ohno, 3D Continuous Water Nanosheet as a Gyroid Minimal Surface Formed by Bicontinuous Cubic Liquid-Crystalline Zwitterions, *J. Am. Chem. Soc.*, **2012**, 134, 11354–11357. DOI:

10.1021/ja304124w.

[420] J. H. Lee, K. S. Han, J. S. Lee, A. S. Lee, S. K. Park, S. Y. Hong, J.-C. Lee, K. T. Mueller, S. M. Hong, C. M. Koo, Facilitated Ion Transport in Smectic Ordered Ionic Liquid Crystals, *Adv. Mater.*, **2016**, 28, 9301–9307. DOI: 10.1002/adma.201602702.

[421] A. Yildirim, P. Szymoniak, K. Sentker, M. Butschies, A. Bühlmeyer, P. Huber, S. Laschat, A. Schönhals, Dynamics and ionic conductivity of ionic liquid crystals forming a hexagonal columnar mesophase, *Phys. Chem. Chem. Phys.*, **2018**, 20, 5626–5635. DOI: 10.1039/C7CP08186C.

[422] M.-A. Néouze, J. Le Bideau, P. Gaveau, S. Bellayer, A. Vioux, Ionogels, New Materials Arising from the Confinement of Ionic Liquids within Silica-Derived Networks, *Chem. Mater.*, **2006**, 18, 3931–3936. DOI: 10.1021/cm060656c.

[423] S. A. M. Noor, P. M. Bayley, M. Forsyth, D. R. MacFarlane, Ionogels based on ionic liquids as potential highly conductive solid state electrolytes, *Electrochim. Acta.*, **2013**, 91, 219–226. DOI: 10.1016/j.electacta.2012.11.113.

[424] T. Echelmeyer, H. W. Meyer, L. van Wüllen, Novel Ternary Composite Electrolytes: Li Ion Conducting Ionic Liquids in Silica Glass, *Chem. Mater.*, **2009**, 21, 2280–2285. DOI: 10.1021/cm9005184.

[425] S. J. Craythorne, K. Anderson, F. Lorenzini, C. McCausland, E. F. Smith, P. Licence, A. C. Marr, P. C. Marr, The Co-Entrapment of a Homogeneous Catalyst and an Ionic Liquid by a Sol-gel Method: Recyclable Ionogel Hydrogenation Catalysts, *Chem. - A Eur. J.*, **2009**, 15, 7094–7100. DOI: 10.1002/chem.200801809.

[426] A. Vioux, L. Viau, S. Volland, J. Le Bideau, Use of ionic liquids in sol-gel; ionogels and applications, *Comptes Rendus Chim.*, **2010**, 13, 242–255. DOI: 10.1016/j.crci.2009.07.002.

[427] Y. Funasako, T. Mochida, T. Inagaki, T. Sakurai, H. Ohta, K. Furukawa, T. Nakamura, Magnetic memory based on magnetic alignment of a paramagnetic ionic liquid near room temperature, *Chem. Commun.*, **2011**, 47, 4475. DOI: 10.1039/c0cc05820c.

[428] K. D. Clark, O. Nacham, H. Yu, T. Li, M. M. Yamsek, D. R. Ronning, J. L. Anderson, Extraction of DNA by Magnetic Ionic Liquids: Tunable Solvents for Rapid and Selective DNA Analysis, *Anal. Chem.*, **2015**, 87, 1552–1559. DOI: 10.1021/ac504260t.

[429] M. Smiglak, A. Metlen, R. D. Rogers, The Second Evolution of Ionic Liquids: From Solvents and Separations to Advanced Materials - Energetic Examples from the Ionic Liquid Cookbook, *Acc. Chem. Res.*, **2007**, 40, 1182–1192. DOI: 10.1021/ar7001304.

[430] D. Chand, J. Zhang, J. M. Shreeve, Borohydride Ionic Liquids as Hypergolic Fuels: A Quest for Improved Stability, *Chem. - A Eur. J.*, **2015**, 21, 13297–13301. DOI: 10.1002/chem.201502059.

[431] Q. Zhang, P. Yin, J. Zhang, J. M. Shreeve, Cyanoborohydride-Based Ionic Liquids as Green Aerospace Bipropellant Fuels, *Chem. - A Eur. J.*, **2014**, 20, 6909–6914. DOI: 10.1002/chem.201402704.

[432] N. Jiao, Y. Zhang, L. Liu, J. M. Shreeve, S. Zhang, Hypergolic fuels based on water-stable borohydride cluster anions with ultralow ignition delay times, *J. Mater. Chem. A.*, **2017**, 5, 13341–13346. DOI: 10.1039/C7TA04038E.

[433] Q. Zhang, J. M. Shreeve, Ionic Liquid Propellants: Future Fuels for Space Propulsion, *Chem. - A Eur. J.*, **2013**, 19, 15446–15451. DOI: 10.1002/chem.201303131.

[434] R. A. Spores, in *51st AIAA/SAE/ASEE Joint Propulsion Conference*, American Institute of Aeronautics and Astronautics, Reston, Virginia, **2015**. DOI: 10.2514/6.2015-3753.

[435] Q. Berrod, F. Ferdeghini, J.-M. Zanotti, P. Judeinstein, D. Lairez, V. García Sakai, O. Czakkel, P. Fouquet, D. Constantin, Ionic Liquids: evidence of the viscosity scale-dependence, *Sci. Rep.*, **2017**, 7, 2241. DOI: 10.1038/s41598-017-02396-7.

[436] E. I. Izgorodina, D. R. MacFarlane, Nature of Hydrogen Bonding in Charged Hydrogen-Bonded Complexes and Imidazolium-Based Ionic Liquids, *J. Phys. Chem. B.*, **2011**, 115, 14659–14667. DOI: 10.1021/jp208150b.

[437] A. Knorr, R. Ludwig, Cation-cation clusters in ionic liquids: Cooperative hydrogen bonding overcomes like-charge repulsion, *Sci. Rep.*, **2015**, 5, 17505. DOI: 10.1038/srep17505.

[438] J. Dupont, On the solid, liquid and solution structural organization of imidazolium ionic liquids, *J. Braz. Chem. Soc.*, **2004**, 15, 341–350. DOI: 10.1590/S0103-50532004000300002.

[439] A. Podgoršek, J. Jacquemin, A. A. H. Pádua, M. F. Costa Gomes, Mixing Enthalpy for Binary Mixtures Containing Ionic Liquids, *Chem. Rev.*, **2016**, 116, 6075–6106. DOI: 10.1021/acs.chemrev.5b00379.

[440] O. Russina, A. Triolo, L. Gontrani, R. Caminiti, Mesoscopic Structural Heterogeneities in Room-Temperature Ionic Liquids, *J. Phys. Chem. Lett.*, **2012**, 3, 27–33. DOI: 10.1021/jz201349z.

[441] C. Hardacre, J. D. Holbrey, M. Nieuwenhuyzen, T. G. A. Youngs, Structure and Solvation in Ionic Liquids, *Acc. Chem. Res.*, **2007**, 40, 1146–1155. DOI: 10.1021/ar700068x.

[442] K. Fumino, S. Reimann, R. Ludwig, Probing molecular interaction in ionic liquids by low frequency spectroscopy: Coulomb energy, hydrogen bonding and dispersion forces, *Phys. Chem. Chem. Phys.*, **2014**, 16, 21903–21929. DOI: 10.1039/C4CP01476F.

[443] R. Ludwig, A Simple Geometrical Explanation for the Occurrence of Specific Large Aggregated Ions in Some Protic Ionic Liquids, *J. Phys. Chem. B.*, **2009**, 113, 15419–15422. DOI: 10.1021/jp907204x.

[444] A. Knorr, P. Stange, K. Fumino, F. Weinhold, R. Ludwig, Spectroscopic Evidence for Clusters of Like-Charged Ions in Ionic Liquids Stabilized by Cooperative Hydrogen Bonding, *ChemPhysChem.*, **2016**, 17, 458–462. DOI: 10.1002/cphc.201501134.

[445] K. Dong, S. Zhang, Hydrogen Bonds: A Structural Insight into Ionic Liquids, *Chem. - A Eur. J.*, **2012**, 18, 2748–2761. DOI: 10.1002/chem.201101645.

[446] O. Hollóczki, M. Macchiagodena, H. Weber, M. Thomas, M. Brehm, A. Stark, O. Russina, A. Triolo, B. Kirchner, Triphilic Ionic-Liquid Mixtures: Fluorinated and Non-fluorinated Aprotic Ionic-Liquid Mixtures, *ChemPhysChem.*, **2015**, 16, 3325–3333. DOI: 10.1002/cphc.201500473.

[447] A. J. L. Costa, M. R. C. Soromenho, K. Shimizu, J. M. S. S. Esperança, J. N. C. Lopes, L. P. N. Rebelo, Unusual LCST-type behaviour found in binary mixtures of choline-based ionic liquids with ethers, *RSC Adv.*, **2013**, 3, 10262. DOI: 10.1039/c3ra40327k.

[448] W. Jiang, Y. Wang, G. A. Voth, Molecular Dynamics Simulation of Nanostructural Organization in Ionic Liquid/Water Mixtures †, *J. Phys. Chem. B.*, **2007**, 111, 4812–4818. DOI: 10.1021/jp067142l.

[449] H. K. Kashyap, C. S. Santos, N. S. Murthy, J. J. Hettige, K. Kerr, S. Ramati, J. Gwon, M. Gohdo, S. I. Lall-Ramnarine, J. F. Wishart, C. J. Margulis, E. W. Castner, Structure of 1-Alkyl-1-methylpyrrolidinium Bis(trifluoromethylsulfonyl)amide Ionic Liquids with Linear, Branched, and Cyclic Alkyl Groups, *J. Phys. Chem. B.*, **2013**, 117, 15328–15337. DOI: 10.1021/jp403518j.

[450] B. A. Marekha, O. N. Kalugin, A. Idrissi, Non-covalent interactions in ionic liquid ion pairs and ion pair dimers: a quantum chemical calculation analysis, *Phys. Chem. Chem. Phys.*, **2015**, 17, 16846–16857. DOI: 10.1039/C5CP02197A.

[451] K. Ma, J. Forsman, C. E. Woodward, Influence of ion pairing in ionic liquids on electrical double layer structures and surface force using classical density functional approach, *J. Chem. Phys.*, **2015**, 142, 174704. DOI: 10.1063/1.4919314.

[452] B. A. D. Neto, E. C. Meurer, R. Galaverna, B. J. Bythell, J. Dupont, R. G. Cooks, M. N. Eberlin, Vapors from Ionic Liquids: Reconciling Simulations with Mass Spectrometric Data, *J. Phys. Chem. Lett.*, **2012**, 3, 3435–3441. DOI: 10.1021/jz301608c.

[453] J. P. Armstrong, C. Hurst, R. G. Jones, P. Licence, K. R. J. Lovelock, C. J. Satterley, I. J. Villar-Garcia, Vapourisation of ionic liquids, *Phys. Chem. Chem. Phys.*, **2007**, 9, 982–990. DOI: 10.1039/b615137j.

[454] Y. Marcus, G. Hefter, Ion Pairing, *Chem. Rev.*, **2006**, 106, 4585–4621. DOI: 10.1021/cr040087x.

[455] B. Kirchner, F. Malberg, D. S. Firaha, O. Hollóczki, Ion pairing in ionic liquids, *J. Phys. Condens. Matter.*, **2015**, 27, 463002. DOI: 10.1088/0953-8984/27/46/463002.

[456] H. Weingärtner, A. Knocks, W. Schrader, U. Kaatze, Dielectric Spectroscopy of the Room Temperature Molten Salt Ethylammonium Nitrate, *J. Phys. Chem. A.*, **2001**, 105, 8646–8650. DOI: 10.1021/jp0114586.

[457] T. Köddermann, C. Wertz, A. Heintz, R. Ludwig, Ion-Pair Formation in the Ionic Liquid 1-Ethyl-3-methylimidazolium Bis(triflyl)imide as a Function of Temperature and Concentration, *ChemPhysChem.*, **2006**, 7, 1944–1949. DOI: 10.1002/cphc.200600034.

[458] A. G. Avent, P. a Chaloner, M. P. Day, K. R. Seddon, T. Welton, Evidence for hydrogen bonding in solutions of 1-ethyl-3-methylimidazolium halides, and its implications for room-temperature halogenoaluminate(III) ionic liquids, *J. Chem. Soc. Dalt. Trans.*, **1994**, 3405. DOI: 10.1039/dt9940003405.

[459] G. W. Driver, Y. Huang, A. Laaksonen, T. Sparrman, Y.-L. Wang, P.-O. Westlund, Correlated/non-correlated ion dynamics of charge-neutral ion couples: the origin of ionicity in ionic liquids, *Phys. Chem. Chem. Phys.*, **2017**, 19, 4975–4988. DOI: 10.1039/C6CP05801A.

[460] M. A. Gebbie, H. A. Dobbs, M. Valtiner, J. N. Israelachvili, Long-range electrostatic screening in ionic liquids, *Proc. Natl. Acad. Sci.*, **2015**, 112, 7432–7437. DOI: 10.1073/pnas.1508366112.

[461] D. A. Turton, T. Sonnleitner, A. Ortner, M. Walther, G. Hefter, K. R. Seddon, S. Stana, N. V. Plechkova, R. Buchner, K. Wynne, Structure and dynamics in protic ionic liquids: A combined optical Kerr-effect and dielectric relaxation spectroscopy study, *Faraday Discuss.*, **2012**, 154, 145–153. DOI: 10.1039/C1FD00054C.

[462] H. Weingärtner, P. Sasisanker, C. Daguenet, P. J. Dyson, I. Krossing, J. M. Slattery, T. Schubert, The Dielectric Response of Room-Temperature Ionic Liquids: Effect of Cation Variation †, *J. Phys. Chem. B.*, **2007**, 111, 4775–4780. DOI: 10.1021/jp0671188.

[463] C. Daguenet, P. J. Dyson, I. Krossing, A. Oleinikova, J. Slattery, C. Wakai, H. Weingärtner, Dielectric Response of Imidazolium-Based Room-Temperature Ionic Liquids, *J. Phys. Chem. B.*, **2006**, 110, 12682–12688. DOI: 10.1021/jp0604903.

[464] M. Y. Lui, L. Crowhurst, J. P. Hallett, P. A. Hunt, H. Niedermeyer, T. Welton, Salts dissolved in salts: ionic liquid mixtures, *Chem. Sci.*, **2011**, 2, 1491. DOI: 10.1039/c1sc00227a.

[465] J. P. Hallett, C. L. Liotta, G. Ranieri, T. Welton, Charge Screening in the S N 2 Reaction of Charged Electrophiles and Charged Nucleophiles: An Ionic Liquid Effect, *J. Org. Chem.*, **2009**, 74, 1864–1868. DOI: 10.1021/jo802121d.

[466] Y. Zhang, E. J. Maginn, Direct Correlation between Ionic Liquid Transport Properties and Ion Pair Lifetimes: A Molecular Dynamics Study, *J. Phys. Chem. Lett.*, **2015**, 6, 700–705. DOI: 10.1021/acs.jpclett.5b00003.

[467] W. Zhao, F. Leroy, B. Heggen, S. Zahn, B. Kirchner, S. Balasubramanian, F. Müller-Plathe, Are There Stable Ion-Pairs in Room-Temperature Ionic Liquids? Molecular Dynamics Simulations of 1- n -Butyl-3-methylimidazolium Hexafluorophosphate, *J. Am. Chem. Soc.*, **2009**, 131, 15825–15833. DOI: 10.1021/ja906337p.

[468] P. A. Hunt, B. Kirchner, T. Welton, Characterising the Electronic Structure of Ionic Liquids: An Examination of the 1-Butyl-3-Methylimidazolium Chloride Ion Pair, *Chem. - A Eur. J.*, **2006**, 12, 6762–6775. DOI: 10.1002/chem.200600103.

[469] H. K. Stassen, R. Ludwig, A. Wulf, J. Dupont, Imidazolium Salt Ion Pairs in Solution, *Chem. - A Eur. J.*, **2015**, 21, 8324–8335. DOI: 10.1002/chem.201500239.

[470] P. Stange, K. Fumino, R. Ludwig, Ion Speciation of Protic Ionic Liquids in Water: Transition from Contact to Solvent-Separated Ion Pairs, *Angew. Chemie Int. Ed.*, **2013**, 52, 2990–2994. DOI: 10.1002/anie.201209609.

[471] C. E. S. Bernardes, M. E. Minas da Piedade, J. N. Canongia Lopes, The Structure of Aqueous Solutions of a Hydrophilic Ionic Liquid: The Full Concentration Range of 1-Ethyl-3-methylimidazolium Ethylsulfate and Water, *J. Phys. Chem. B.*, **2011**, 115, 2067–2074. DOI: 10.1021/jp1113202.

[472] R. LUDWIG, F. WEINHOLD, T. C. FARRAR, Quantum cluster equilibrium theory of liquids: molecular clusters and thermodynamics of liquid ethanol, *Mol. Phys.*, **1999**, 97, 465–477. DOI: 10.1080/00268979909482847.

[473] J. Ingenmey, M. von Domaros, E. Perlt, S. P. Verevkin, B. Kirchner, Thermodynamics and proton activities of protic ionic liquids with quantum cluster equilibrium theory, *J. Chem. Phys.*, **2018**, 148, 193822. DOI: 10.1063/1.5010791.

[474] S. Chen, S. Zhang, X. Liu, J. Wang, J. Wang, K. Dong, J. Sun, B. Xu, Ionic liquid clusters: structure, formation mechanism, and effect on the behavior of ionic liquids, *Phys. Chem. Chem. Phys.*, **2014**, 16, 5893–5906. DOI: 10.1039/C3CP53116C.

[475] W. Schroer, A. Triolo, O. Russina, Nature of Mesoscopic Organization in Protic Ionic Liquid–Alcohol Mixtures, *J. Phys. Chem. B.*, **2016**, 120, 2638–2643. DOI: 10.1021/acs.jpcb.6b01422.

[476] J. Bowers, C. P. Butts, P. J. Martin, M. C. Vergara-Gutierrez, R. K. Heenan, Aggregation Behavior of Aqueous Solutions of Ionic Liquids, *Langmuir.*, **2004**, 20, 2191–2198. DOI: 10.1021/la035940m.

[477] D. R. MacFarlane, A. L. Chong, M. Forsyth, M. Kar, R. Vijayaraghavan, A. Somers, J. M. Pringle, New dimensions in salt–solvent mixtures: a 4th evolution of ionic liquids, *Faraday Discuss.*, **2018**, 206, 9–28. DOI: 10.1039/C7FD00189D.

[478] D. F. Kennedy, C. J. Drummond, Large Aggregated Ions Found in Some Protic Ionic Liquids, *J. Phys. Chem. B.*, **2009**, 113, 5690–5693. DOI: 10.1021/jp900814y.

[479] F. C. Gozzo, L. S. Santos, R. Augusti, C. S. Consorti, J. Dupont, M. N. Eberlin, Gaseous Supramolecules of Imidazolium Ionic Liquids: 'Magic' Numbers and Intrinsic Strengths of Hydrogen Bonds, *Chem. - A Eur. J.*, **2004**, 10, 6187–6193. DOI: 10.1002/chem.200305742.

[480] R. Bini, O. Bortolini, C. Chiappe, D. Pieraccini, T. Siciliano, Development of Cation/Anion "Interaction" Scales for Ionic Liquids through ESI-MS Measurements, *J. Phys. Chem. B.*, **2007**, 111, 598–604. DOI: 10.1021/jp0663199.

[481] G. L. Burrell, N. F. Dunlop, F. Separovic, Non-Newtonian viscous shear thinning in ionic liquids, *Soft Matter.*, **2010**, 6, 2080. DOI: 10.1039/b916049n.

[482] C. J. Johnson, J. A. Fournier, C. T. Wolke, M. A. Johnson, Ionic liquids from the bottom up: Local assembly motifs in [EMIM][BF 4] through cryogenic ion spectroscopy, *J. Chem. Phys.*, **2013**, 139, 224305. DOI: 10.1063/1.4838475.

[483] G. L. Burrell, I. M. Burgar, Q. Gong, N. F. Dunlop, F. Separovic, NMR Relaxation and Self-Diffusion Study at High and Low Magnetic Fields of Ionic Association in Protic Ionic Liquids, *J. Phys. Chem. B.*, **2010**, 114, 11436–11443. DOI: 10.1021/jp105087n.

[484] A. Strate, T. Niemann, D. Michalik, R. Ludwig, When Like Charged Ions Attract in Ionic Liquids: Controlling the Formation of Cationic Clusters by the Interaction Strength of the Counterions, *Angew. Chemie Int. Ed.*, **2017**, 56, 496–500. DOI: 10.1002/anie.201609799.

[485] A. Strate, V. Overbeck, V. Lehde, J. Neumann, A.-M. Bonsa, T. Niemann, D. Paschek, D. Michalik, R. Ludwig, The influence of like-charge attraction on the structure and dynamics of ionic liquids: NMR chemical shifts, quadrupole coupling constants, rotational correlation times and failure of Stokes–Einstein–Debye, *Phys. Chem. Chem. Phys.*, **2018**, 20, 5617–5625. DOI: 10.1039/C7CP06454C.

[486] F. S. Menges, H. J. Zeng, P. J. Kelleher, O. Gorlova, M. A. Johnson, T. Niemann, A. Strate, R. Ludwig, Structural Motifs in Cold Ternary Ion Complexes of Hydroxyl-Functionalized Ionic Liquids: Isolating the Role of Cation–Cation Interactions, *J. Phys. Chem. Lett.*, **2018**, 9, 2979–2984. DOI: 10.1021/acs.jpclett.8b01130.

[487] D. Wakeham, P. Niga, C. Ridings, G. Andersson, A. Nelson, G. G. Warr, S. Baldelli, M. W. Rutland, R. Atkin, Surface structure of a "non-amphiphilic" protic ionic liquid, *Phys. Chem. Chem. Phys.*, **2012**, 14, 5106. DOI: 10.1039/c2cp23694j.

[488] C. Ridings, V. Lockett, G. Andersson, Effect of the aliphatic chain length on electrical double layer formation at the liquid/vacuum interface in the [Cnmim][BF4] ionic liquid series, *Phys. Chem. Chem. Phys.*, **2011**, 13, 17177. DOI: 10.1039/c1cp20910h.

[489] M. Casalegno, G. Raos, G. B. Appetecchi, S. Passerini, F. Castiglione, A. Mele, From Nanoscale to Microscale: Crossover in the Diffusion Dynamics within Two Pyrrolidinium-Based Ionic Liquids, *J. Phys. Chem. Lett.*, **2017**, 8, 5196–5202. DOI: 10.1021/acs.jpclett.7b02431.

[490] M. G. Del Pópolo, G. A. Voth, On the Structure and Dynamics of Ionic Liquids, *J. Phys. Chem. B.*, **2004**, 108, 1744–1752. DOI: 10.1021/jp0364699.

[491] Y.-L. Wang, Z.-Y. Lu, A. Laaksonen, Heterogeneous dynamics of ionic liquids in confined films with varied film thickness, *Phys. Chem. Chem. Phys.*, **2014**, 16, 20731–20740. DOI: 10.1039/C4CP02843K.

[492] R. Ludwig, The effect of dispersion forces on the interaction energies and far infrared spectra of protic ionic liquids, *Phys. Chem. Chem. Phys.*, **2015**, 17, 13790–13793. DOI: 10.1039/C5CP00885A.

[493] K. Fumino, E. Reichert, K. Wittler, R. Hempelmann, R. Ludwig, Low-Frequency Vibrational Modes of Protic

Molten Salts and Ionic Liquids: Detecting and Quantifying Hydrogen Bonds, *Angew. Chemie Int. Ed.*, **2012**, 51, 6236–6240. DOI: 10.1002/anie.201200508.

[494] K. Fumino, A. Wulf, R. Ludwig, The Cation–Anion Interaction in Ionic Liquids Probed by Far-Infrared Spectroscopy, *Angew. Chemie Int. Ed.*, **2008**, 47, 3830–3834. DOI: 10.1002/anie.200705736.

[495] K. Fumino, A. Wulf, R. Ludwig, Strong, Localized, and Directional Hydrogen Bonds Fluidize Ionic Liquids, *Angew. Chemie Int. Ed.*, **2008**, 47, 8731–8734. DOI: 10.1002/anie.200803446.

[496] M. Kohagen, M. Brehm, Y. Lingscheid, R. Giernoth, J. Sangoro, F. Kremer, S. Naumov, C. Iacob, J. Kärger, R. Valiullin, B. Kirchner, How Hydrogen Bonds Influence the Mobility of Imidazolium-Based Ionic Liquids. A Combined Theoretical and Experimental Study of 1- n -Butyl-3-methylimidazolium Bromide, *J. Phys. Chem. B.*, **2011**, 115, 15280–15288. DOI: 10.1021/jp206974h.

[497] D. F. Evans, S.-H. Chen, G. W. Schriver, E. M. Arnett, Thermodynamics of solution of nonpolar gases in a fused salt. Hydrophobic bonding behavior in a nonaqueous system, *J. Am. Chem. Soc.*, **1981**, 103, 481–482. DOI: 10.1021/ja00392a049.

[498] K. Dong, S. Zhang, D. Wang, X. Yao, Hydrogen Bonds in Imidazolium Ionic Liquids, *J. Phys. Chem. A.*, **2006**, 110, 9775–9782. DOI: 10.1021/jp054054c.

[499] J. J. Jodry, K. Mikami, New chiral imidazolium ionic liquids: 3D-network of hydrogen bonding, *Tetrahedron Lett.*, **2004**, 45, 4429–4431. DOI: 10.1016/j.tetlet.2004.04.063.

[500] P. A. Z. Suarez, S. Einloft, J. E. L. Dullius, R. F. de Souza, J. Dupont, Synthesis and physical-chemical properties of ionic liquids based on 1-n-butyl-3-methylimidazolium cation, *J. Chim. Phys. Physico-Chimie Biol.*, **1998**, 95, 1626–1639. DOI: 10.1051/jcp:1998103.

[501] C. Hardacre, J. D. Holbrey, S. E. J. McMath, D. T. Bowron, A. K. Soper, Structure of molten 1,3-dimethylimidazolium chloride using neutron diffraction, *J. Chem. Phys.*, **2003**, 118, 273–278. DOI: 10.1063/1.1523917.

[502] I. Skarmoutsos, D. Dellis, R. P. Matthews, T. Welton, P. A. Hunt, Hydrogen Bonding in 1-Butyl- and 1-Ethyl-3-methylimidazolium Chloride Ionic Liquids, *J. Phys. Chem. B.*, **2012**, 116, 4921–4933. DOI: 10.1021/jp209485y.

[503] A. Elaiwi, P. B. Hitchcock, K. R. Seddon, N. Srinivasan, Y. Tan, T. Welton, J. A. Zora, Hydrogen bonding in imidazolium salts and its implications for ambient-temperature halogenoaluminate(III) ionic liquids, *J. Chem. Soc. Dalt. Trans.*, **1995**, 3467. DOI: 10.1039/dt9950003467.

[504] P. B. Hitchcock, K. R. Seddon, T. Welton, Hydrogen-bond acceptor abilities of tetrachlorometalate(II) complexes in ionic liquids, *J. Chem. Soc. Dalt. Trans.*, **1993**, 2639. DOI: 10.1039/dt9930002639.

[505] Y.-L. Wang, B. Li, S. Sarman, A. Laaksonen, Microstructures and dynamics of tetraalkylphosphonium chloride ionic liquids, *J. Chem. Phys.*, **2017**, 147, 224502. DOI: 10.1063/1.4995003.

[506] G. Feng, S. Li, W. Zhao, P. T. Cummings, Microstructure of room temperature ionic liquids at stepped graphite electrodes, *AIChE J.*, **2015**, 61, 3022–3028. DOI: 10.1002/aic.14927.

[507] T. Cosby, Z. Vicars, M. Heres, K. Tsunashima, J. Sangoro, Dynamic and structural evidence of mesoscopic aggregation in phosphonium ionic liquids, *J. Chem. Phys.*, **2018**, 148, 193815. DOI: 10.1063/1.5009765.

[508] O. Russina, A. Triolo, New experimental evidence supporting the mesoscopic segregation model in room temperature ionic liquids, *Faraday Discuss.*, **2012**, 154, 97–109. DOI: 10.1039/C1FD00073J.

[509] O. Russina, F. Lo Celso, N. Plechkova, C. J. Jafta, G. B. Appetecchi, A. Triolo, Mesoscopic organization in ionic liquids, *Top. Curr. Chem.*, **2017**, 375, 58. DOI: 10.1007/s41061-017-0147-2.

[510] Y. Wang, G. A. Voth, Unique Spatial Heterogeneity in Ionic Liquids, *J. Am. Chem. Soc.*, **2005**, 127, 12192–12193. DOI: 10.1021/ja053796g.

[511] S. M. Urahata, M. C. C. Ribeiro, Structure of ionic liquids of 1-alkyl-3-methylimidazolium cations: A systematic computer simulation study, *J. Chem. Phys.*, **2004**, 120, 1855–1863. DOI: 10.1063/1.1635356.

[512] E. Bodo, L. Gontrani, A. Triolo, R. Caminiti, Structural Determination of Ionic Liquids with Theoretical Methods: C 8 mimBr and C 8 mimCl. Strength and Weakness of Current Force Fields, *J. Phys. Chem. Lett.*, **2010**, 1, 1095–1100. DOI: 10.1021/jz100146r.

[513] J. N. A. Canongia Lopes, A. A. H. P??dua, Nanostructural organization in ionic liquids, *J. Phys. Chem. B.*, **2006**, 110, 3330–3335. DOI: 10.1021/jp056006y.

[514] A. Triolo, O. Russina, B. Fazio, R. Triolo, E. Di Cola, Morphology of 1-alkyl-3-methylimidazolium hexafluorophosphate room temperature ionic liquids, *Chem. Phys. Lett.*, **2008**, 457, 362–365. DOI: 10.1016/j.cplett.2008.04.027.

[515] O. Russina, A. Triolo, L. Gontrani, R. Caminiti, D. Xiao, L. G. Hines Jr, R. A. Bartsch, E. L. Quitevis, N. Pleckhova, K. R. Seddon, Morphology and intermolecular dynamics of 1-alkyl-3-methylimidazolium bis{(trifluoromethane)sulfonyl}amide ionic liquids: structural and dynamic evidence of nanoscale segregation, *J. Phys. Condens. Matter.*, **2009**, 21, 424121. DOI: 10.1088/0953-8984/21/42/424121.

[516] D. Xiao, L. G. Hines, S. Li, R. A. Bartsch, E. L. Quitevis, O. Russina, A. Triolo, Effect of Cation Symmetry and Alkyl Chain Length on the Structure and Intermolecular Dynamics of 1,3-Dialkylimidazolium Bis(trifluoromethanesulfonyl)amide Ionic Liquids, *J. Phys. Chem. B.*, **2009**, 113, 6426–6433. DOI: 10.1021/jp8102595.

[517] W. Zheng, A. Mohammed, L. G. Hines, D. Xiao, O. J. Martinez, R. A. Bartsch, S. L. Simon, O. Russina, A. Triolo, E. L. Quitevis, Effect of Cation Symmetry on the Morphology and Physicochemical Properties of Imidazolium

Ionic Liquids, *J. Phys. Chem. B.*, **2011**, 115, 6572–6584. DOI: 10.1021/jp1115614.

[518] M. Macchiagodena, F. Ramondo, A. Triolo, L. Gontrani, R. Caminiti, Liquid Structure of 1-Ethyl-3-methylimidazolium Alkyl Sulfates by X-ray Scattering and Molecular Dynamics, *J. Phys. Chem. B.*, **2012**, 116, 13448–13458. DOI: 10.1021/jp306982e.

[519] M. Potangale, A. Das, S. Kapoor, S. Tiwari, Effect of anion and alkyl chain length on the structure and interactions of N -alkyl pyridinium ionic liquids, *J. Mol. Liq.*, **2017**, 240, 694–707. DOI: 10.1016/j.molliq.2017.05.036.

[520] A. Triolo, O. Russina, B. Fazio, G. B. Appetecchi, M. Carewska, S. Passerini, Nanoscale organization in piperidinium-based room temperature ionic liquids, *J. Chem. Phys.*, **2009**, 130, 164521. DOI: 10.1063/1.3119977.

[521] T. Pott, P. Méléard, New insight into the nanostructure of ionic liquids: a small angle X-ray scattering (SAXS) study on liquid tri-alkyl-methyl-ammonium bis(trifluoromethanesulfonyl)amides and their mixtures, *Phys. Chem. Chem. Phys.*, **2009**, 11, 5469. DOI: 10.1039/b901582e.

[522] H. K. Kashyap, J. J. Hettige, H. V. R. Annapureddy, C. J. Margulis, SAXS anti-peaks reveal the length-scales of dual positive–negative and polar–apolar ordering in room-temperature ionic liquids, *Chem. Commun.*, **2012**, 48, 5103. DOI: 10.1039/c2cc30609c.

[523] S. Li, J. L. Bañuelos, J. Guo, L. Anovitz, G. Rother, R. W. Shaw, P. C. Hillesheim, S. Dai, G. A. Baker, P. T. Cummings, Alkyl Chain Length and Temperature Effects on Structural Properties of Pyrrolidinium-Based Ionic Liquids: A Combined Atomistic Simulation and Small-Angle X-ray Scattering Study, *J. Phys. Chem. Lett.*, **2012**, 3, 125–130. DOI: 10.1021/jz2013209.

[524] J. J. Hettige, H. K. Kashyap, H. V. R. Annapureddy, C. J. Margulis, Anions, the Reporters of Structure in Ionic Liquids, *J. Phys. Chem. Lett.*, **2013**, 4, 105–110. DOI: 10.1021/jz301866f.

[525] C. S. Santos, H. V. R. Annapureddy, N. S. Murthy, H. K. Kashyap, E. W. Castner, C. J. Margulis, Temperature-dependent structure of methyltributylammonium bis(trifluoromethylsulfonyl)amide: X ray scattering and simulations, *J. Chem. Phys.*, **2011**, 134, 064501. DOI: 10.1063/1.3526958.

[526] H. K. Kashyap, C. S. Santos, H. V. R. Annapureddy, N. S. Murthy, C. J. Margulis, E. W. Castner, Jr, Temperature-dependent structure of ionic liquids: X-ray scattering and simulations, *Faraday Discuss.*, **2012**, 154, 133–143. DOI: 10.1039/C1FD00059D.

[527] L. Gontrani, O. Russina, F. Lo Celso, R. Caminiti, G. Annat, A. Triolo, Liquid Structure of Trihexyltetradecylphosphonium Chloride at Ambient Temperature: An X-ray Scattering and Simulation Study, *J. Phys. Chem. B.*, **2009**, 113, 9235–9240. DOI: 10.1021/jp808333a.

[528] A. Triolo, O. Russina, R. Caminiti, H. Shirota, H. Y. Lee, C. S. Santos, N. S. Murthy, E. W. Castner, Jr, Comparing intermediate range order for alkyl- vs. ether-substituted cations in ionic liquids, *Chem. Commun.*, **2012**, 48, 4959. DOI: 10.1039/c2cc31550e.

[529] K. Shimizu, C. E. S. Bernardes, A. Triolo, J. N. Canongia Lopes, Nano-segregation in ionic liquids: scorpions and vanishing chains, *Phys. Chem. Chem. Phys.*, **2013**, 15, 16256. DOI: 10.1039/c3cp52357h.

[530] K. Shimizu, M. F. Costa Gomes, A. A. H. Pádua, L. P. N. Rebelo, J. N. Canongia Lopes, Three commentaries on the nano-segregated structure of ionic liquids, *J. Mol. Struct. THEOCHEM.*, **2010**, 946, 70–76. DOI: 10.1016/j.theochem.2009.11.034.

[531] K. Fujii, R. Kanzaki, T. Takamuku, Y. Kameda, S. Kohara, M. Kanakubo, M. Shibayama, S. Ishiguro, Y. Umebayashi, Experimental evidences for molecular origin of low- Q peak in neutron/x-ray scattering of 1-alkyl-3-methylimidazolium bis(trifluoromethanesulfonyl)amide ionic liquids, *J. Chem. Phys.*, **2011**, 135, 244502. DOI: 10.1063/1.3672097.

[532] J. J. Hettige, J. C. Araque, C. J. Margulis, Bicontinuity and Multiple Length Scale Ordering in Triphilic Hydrogen-Bonding Ionic Liquids, *J. Phys. Chem. B.*, **2014**, 118, 12706–12716. DOI: 10.1021/jp5068457.

[533] J. C. Araque, J. J. Hettige, C. J. Margulis, Modern Room Temperature Ionic Liquids, a Simple Guide to Understanding Their Structure and How It May Relate to Dynamics, *J. Phys. Chem. B.*, **2015**, 119, 12727–12740. DOI: 10.1021/acs.jpcb.5b05506.

[534] H. V. R. Annapureddy, H. K. Kashyap, P. M. De Biase, C. J. Margulis, What is the Origin of the Prepeak in the X-ray Scattering of Imidazolium-Based Room-Temperature Ionic Liquids?, *J. Phys. Chem. B.*, **2011**, 115, 9507–9508. DOI: 10.1021/jp205051t.

[535] F. Castiglione, M. Moreno, G. Raos, A. Famulari, A. Mele, G. B. Appetecchi, S. Passerini, Structural Organization and Transport Properties of Novel Pyrrolidinium-Based Ionic Liquids with Perfluoroalkyl Sulfonylimide Anions, *J. Phys. Chem. B.*, **2009**, 113, 10750–10759. DOI: 10.1021/jp811434e.

[536] A. Martinelli, M. Maréchal, Å. Östlund, J. Cambedouzou, Insights into the interplay between molecular structure and diffusional motion in 1-alkyl-3-methylimidazolium ionic liquids: a combined PFG NMR and X-ray scattering study, *Phys. Chem. Chem. Phys.*, **2013**, 15, 5510. DOI: 10.1039/c3cp00097d.

[537] D. Merunka, M. Peric, M. Peric, Study of Nanostructural Organization of Ionic Liquids by Electron Paramagnetic Resonance Spectroscopy, *J. Phys. Chem. B.*, **2015**, 119, 3185–3193. DOI: 10.1021/jp512487y.

[538] K. Iwata, H. Okajima, S. Saha, H. Hamaguchi, Local Structure Formation in Alkyl-imidazolium-Based Ionic Liquid as Revealed by Linear and Nonlinear Raman, *Acc. Chem. Res.*, **2007**, 40, 1174–1181. DOI: 10.1021/ar700074c.

[539] D. A. Turton, J. Hunger, A. Stoppa, G. Hefter, A. Thoman, M. Walther, R. Buchner, K. Wynne, Dynamics of Imidazolium Ionic Liquids from a Combined Dielectric Relaxation and Optical Kerr Effect Study: Evidence for Mesoscopic Aggregation, *J. Am. Chem. Soc.*, **2009**, 131, 11140–11146. DOI: 10.1021/ja903315v.

[540] T. Burankova, G. Simeoni, R. Hempelmann, J. F. Mora Cardozo, J. P. Embs, Dynamic Heterogeneity and Flexibility of the Alkyl Chain in Pyridinium-Based Ionic Liquids, *J. Phys. Chem. B.*, **2017**, 121, 240–249. DOI: 10.1021/acs.jpcb.6b10235.

[541] M. Casalegno, G. Raos, G. B. Appetecchi, S. Passerini, F. Castiglione, A. Mele, From Nanoscale to Microscale: Crossover in the Diffusion Dynamics within Two Pyrrolidinium-Based Ionic Liquids, *J. Phys. Chem. Lett.*, **2017**, 8, 5196–5202. DOI: 10.1021/acs.jpclett.7b02431.

[542] M. Kofu, M. Nagao, T. Ueki, Y. Kitazawa, Y. Nakamura, S. Sawamura, M. Watanabe, O. Yamamuro, Heterogeneous Slow Dynamics of Imidazolium-Based Ionic Liquids Studied by Neutron Spin Echo, *J. Phys. Chem. B.*, **2013**, 117, 2773–2781. DOI: 10.1021/jp312608r.

[543] O. Russina, F. Lo Celso, M. Di Michiel, S. Passerini, G. B. Appetecchi, F. Castiglione, A. Mele, R. Caminiti, A. Triolo, Mesoscopic structural organization in triphilic room temperature ionic liquids, *Faraday Discuss.*, **2013**, 167, 499–513. DOI: 10.1039/c3fd00056g.

[544] P. Kirsch, *Modern Fluoroorganic Chemistry*, Wiley-VCH Verlag GmbH & Co. KGaA, Weinheim, Germany, **2013**.

[545] J. A. Gladysz, D. P. Curran, I. T. Horváth, Eds., *Handbook of Fluorous Chemistry*, Wiley-VCH Verlag GmbH & Co. KGaA, Weinheim, FRG, **2004**.

[546] O. Kysilka, M. Rybáčková, M. Skalický, M. Kvíčalová, J. Cvačka, J. Kvíčala, Fluorous imidazolium room-temperature ionic liquids based on HFPO trimer, *J. Fluor. Chem.*, **2009**, 130, 629–639. DOI: 10.1016/j.jfluchem.2009.04.006.

[547] L. P. Barthel-Rosa, J. A. Gladysz, Chemistry in fluorous media: a user's guide to practical considerations in the application of fluorous catalysts and reagents, *Coord. Chem. Rev.*, **1999**, 190–192, 587–605. DOI: 10.1016/S0010-8545(99)00102-2.

[548] C. L. Young, Upper critical solution temperature of perfluoro-n-alkane and n-alkane mixtures, *Trans. Faraday Soc.*, **1969**, 65, 2639. DOI: 10.1039/tf9696502639.

[549] R. H. Fish, Fluorous Biphasic Catalysis: A New Paradigm for the Separation of Homogeneous Catalysts from Their Reaction Substrates and Products, *Chem. - A Eur. J.*, **1999**, 5, 1677–1680. DOI: 10.1002/(SICI)1521-3765(19990604)5:6<1677::AID-CHEM1677>3.0.CO;2-X.

[550] T. Takamuku, M. Tobiishi, H. Saito, Solvation Properties of Aliphatic Alcohol–Water and Fluorinated Alcohol–Water Solutions for Amide Molecules Studied by IR and NMR Techniques, *J. Solution Chem.*, **2011**, 40, 2046–2056. DOI: 10.1007/s10953-011-9773-4.

[551] H. Fromme, S. A. Tittlemier, W. Völkel, M. Wilhelm, D. Twardella, Perfluorinated compounds – Exposure assessment for the general population in western countries, *Int. J. Hyg. Environ. Health.*, **2009**, 212, 239–270. DOI: 10.1016/j.ijheh.2008.04.007.

[552] S. Liu, Y. Lu, S. Xie, T. Wang, K. C. Jones, A. J. Sweetman, Exploring the fate, transport and risk of Perfluorooctane Sulfonate (PFOS) in a coastal region of China using a multimedia model, *Environ. Int.*, **2015**, 85, 15–26. DOI: 10.1016/j.envint.2015.08.007.

[553] A. B. Pereiro, J. M. M. Araújo, S. Martinho, F. Alves, S. Nunes, A. Matias, C. M. M. Duarte, L. P. N. Rebelo, I. M. Marrucho, Fluorinated Ionic Liquids: Properties and Applications, *ACS Sustain. Chem. Eng.*, **2013**, 1, 427–439. DOI: 10.1021/sc300163n.

[554] J. van den Broeke, F. Winter, B.-J. Deelman, G. van Koten, A Highly Fluorous Room-Temperature Ionic Liquid Exhibiting Fluorous Biphasic Behavior and Its Use in Catalyst Recycling, *Org. Lett.*, **2002**, 4, 3851–3854. DOI: 10.1021/ol026700l.

[555] A. R. R. Teles, H. Correia, G. J. Maximo, L. P. N. Rebelo, M. G. Freire, A. B. Pereiro, J. A. P. Coutinho, Solid–liquid equilibria of binary mixtures of fluorinated ionic liquids, *Phys. Chem. Chem. Phys.*, **2016**, 18, 25741–25750. DOI: 10.1039/C6CP05372F.

[556] A. B. Pereiro, J. M. M. Araújo, F. S. Teixeira, I. M. Marrucho, M. M. Piñeiro, L. P. N. Rebelo, Aggregation Behavior and Total Miscibility of Fluorinated Ionic Liquids in Water, *Langmuir.*, **2015**, 31, 1283–1295. DOI: 10.1021/la503961h.

[557] A. B. Pereiro, F. Llovell, J. M. M. Araújo, A. S. S. Santos, L. P. N. Rebelo, M. M. Piñeiro, L. F. Vega, Thermophysical Characterization of Ionic Liquids Based on the Perfluorobutanesulfonate Anion: Experimental and Soft-SAFT Modeling Results, *ChemPhysChem.*, **2017**, 18, 2012–2023. DOI: 10.1002/cphc.201700327.

[558] G. Vanhoutte, S. D. Hojniak, F. Bardé, K. Binnemans, J. Fransaer, Fluorine-functionalized ionic liquids with high oxygen solubility, *RSC Adv.*, **2018**, 8, 4525–4530. DOI: 10.1039/C7RA13403G.

[559] H. Matsumoto, H. Kageyama, Y. Miyazaki, Room temperature ionic liquids based on small aliphatic ammonium cations and asymmetric amide anions, *Chem. Commun.*, **2002**, 1726–1727. DOI: 10.1039/b204046h.

[560] M. B. Herath, T. Hickman, S. E. Creager, D. D. DesMarteau, A new fluorinated anion for room-temperature ionic liquids, *J. Fluor. Chem.*, **2011**, 132, 52–56. DOI: 10.1016/j.jfluchem.2010.11.005.

[561] S. L. I. Toh, J. McFarlane, C. Tsouris, D. W. DePaoli, H. Luo, S. Dai, Room-Temperature Ionic Liquids in Liquid–Liquid Extraction: Effects of Solubility in Aqueous Solutions on Surface Properties, *Solvent Extr. Ion Exch.*, **2006**, 24, 33–56. DOI: 10.1080/07366290500388400.

[562] S. K. Quek, I. M. Lyapkalo, H. V. Huynh, Synthesis and properties of N,N′-dialkylimidazolium bis(nonafluorobutane-1-sulfonyl)imides: A new subfamily of ionic liquids, *Tetrahedron.*, **2006**, 62, 3137–3145. DOI: 10.1016/j.tet.2006.01.015.

[563] N. S. M. Vieira, P. M. Reis, K. Shimizu, O. A. Cortes, I. M. Marrucho, J. M. M. Araújo, J. M. S. S. Esperança, J. N. C. Lopes, A. B. Pereiro, L. P. N. Rebelo, A thermophysical and structural characterization of ionic liquids with alkyl and perfluoroalkyl side chains, *RSC Adv.*, **2015**, 5, 65337–65350. DOI: 10.1039/C5RA13869H.

[564] N. Ignat'ev, U. Welz-Biermann, New ionic liquids with tris (perfluoroalkyl) trifluorophosphate (FAP) anions, *J. Fluor. …*, **2005**, 126, 1150–1159. DOI: 10.1016/j.jfluchem.2005.04.017.

[565] D. Bejan, N. Ignat'ev, H. Willner, New ionic liquids with the bis[bis(pentafluoroethyl)phosphinyl]imide anion, [(C2F5)2P(O)]2N−—Synthesis and characterization, *J. Fluor. Chem.*, **2010**, 131, 325–332. DOI: 10.1016/j.jfluchem.2009.11.004.

[566] Z.-B. Zhou, H. Matsumoto, K. Tatsumi, Low-Viscous, Low-Melting, Hydrophobic Ionic Liquids: 1-Alkyl-3-methylimidazolium Trifluoromethyltrifluoroborate, *Chem. Lett.*, **2004**, 33, 680–681. DOI: 10.1246/cl.2004.680.

[567] Z.-B. Zhou, H. Matsumoto, K. Tatsumi, Low-Melting, Low-Viscous, Hydrophobic Ionic Liquids: 1-Alkyl(Alkyl Ether)-3-methylimidazolium Perfluoroalkyltrifluoroborate, *Chem. - A Eur. J.*, **2004**, 10, 6581–6591. DOI: 10.1002/chem.200400533.

[568] J. Landmann, J. A. P. Sprenger, P. T. Hennig, R. Bertermann, M. Grüne, F. Würthner, N. V. Ignat'ev, M. Finze, Perfluoroalkyltricyanoborate and Perfluoroalkylcyanofluoroborate Anions: Building Blocks for Low-Viscosity Ionic Liquids, *Chem. - A Eur. J.*, **2018**, 24, 508–508. DOI: 10.1002/chem.201704533.

[569] V. R. Koch, L. A. Dominey, C. Nanjundiah, M. J. Ondrechen, The Intrinsic Anodic Stability of Several Anions Comprising Solvent-Free Ionic Liquids, *J. Electrochem. Soc.*, **1996**, 143, 798. DOI: 10.1149/1.1836540.

[570] K. M. Johansson, J. Adebahr, P. C. Howlett, M. Forsyth, D. R. MacFarlane, N -Methyl- N -Alkylpyrrolidinium Bis(perfluoroethylsulfonyl)amide ([NPf 2] –) and Tris(trifluoromethanesulfonyl)methide ([CTf 3] –) Salts: Synthesis and Characterization, *Aust. J. Chem.*, **2007**, 60, 57. DOI: 10.1071/CH06299.

[571] K. A. Kurnia, T. E. Sintra, Y. Danten, M. I. Cabaço, M. Besnard, J. A. P. Coutinho, A simple method for preparation of a novel hydrophobic ionic liquid with a per-fluoro-tert-butoxide anion, *New J. Chem.*, **2017**, 41, 47–50. DOI: 10.1039/C6NJ02575G.

[572] H. D. B. Jenkins, Ionic liquids – an overview, *Sci. Prog.*, **2011**, 94, 265–297. DOI: 10.3184/003685011X13138407794135.

[573] J. M. Pringle, J. Golding, K. Baranyai, C. M. Forsyth, G. B. Deacon, J. L. Scott, D. R. MacFarlane, The effect of anion fluorination in ionic liquids—physical properties of a range of bis(methanesulfonyl)amide salts, *New J. Chem.*, **2003**, 27, 1504–1510. DOI: 10.1039/B304072K.

[574] R. Hagiwara, Y. Ito, Room temperature ionic liquids of alkylimidazolium cations and fluoroanions, *J. Fluor. Chem.*, **2000**, 105, 221–227. DOI: 10.1016/S0022-1139(99)00267-5.

[575] M. G. Freire, C. M. S. S. Neves, I. M. Marrucho, J. A. P. Coutinho, A. M. Fernandes, Hydrolysis of Tetrafluoroborate and Hexafluorophosphate Counter Ions in Imidazolium-Based Ionic Liquids †, *J. Phys. Chem. A.*, **2010**, 114, 3744–3749. DOI: 10.1021/jp903292n.

[576] R. P. Singh, S. Manandhar, J. M. Shreeve, Mono- and Disubstituted PolyfluoroalkylimidazoliumQuaternary Salts and Ionic Liquids, *Synthesis (Stuttg).*, **2003**, 10, 1579–1585. DOI: 10.1055/s-2003-40515.

[577] C. M. S. S. Neves, M. L. S. Batista, A. F. M. Cláudio, L. M. N. B. F. Santos, I. M. Marrucho, M. G. Freire, J. A. P. Coutinho, Thermophysical Properties and Water Saturation of [PF 6]-Based Ionic Liquids, *J. Chem. Eng. Data.*, **2010**, 55, 5065–5073. DOI: 10.1021/je100638g.

[578] A. N. Tran, T. N. Van Do, L. P. M. Le, T. N. Le, Synthesis of new fluorinated imidazolium ionic liquids and their prospective function as the electrolytes for lithium-ion batteries, *J. Fluor. Chem.*, **2014**, 164, 38–43. DOI: 10.1016/j.jfluchem.2014.05.005.

[579] M. Tariq, P. J. Carvalho, J. A. P. Coutinho, I. M. Marrucho, J. N. C. Lopes, L. P. N. Rebelo, Viscosity of (C2–C14) 1-alkyl-3-methylimidazolium bis(trifluoromethylsulfonyl)amide ionic liquids in an extended temperature range, *Fluid Phase Equilib.*, **2011**, 301, 22–32. DOI: 10.1016/j.fluid.2010.10.018.

[580] S. Bansal, N. Kaur, G. R. Chaudhary, S. K. Mehta, A. S. Ahluwalia, Physiochemical Properties of New Formulations of 1-Ethyl-3-methylimidazolium Bis(trifluoromethylsulfonyl)imide with Tritons, *J. Chem. Eng. Data.*, **2014**, 59, 3988–3999. DOI: 10.1021/je500502a.

[581] F. Lo Celso, Y. Yoshida, F. Castiglione, M. Ferro, A. Mele, C. J. Jafta, A. Triolo, O. Russina, Direct experimental observation of mesoscopic fluorous domains in fluorinated room temperature ionic liquids, *Phys. Chem. Chem. Phys.*, **2017**, 19, 13101–13110. DOI: 10.1039/C7CP01971H.

[582] A. B. Pereiro, M. J. Pastoriza-Gallego, K. Shimizu, I. M. Marrucho, J. N. C. Lopes, M. M. Pi??eiro, L. P. N. Rebelo, On the formation of a third, nanostructured domain in ionic liquids, *J. Phys. Chem. B.*, **2013**, 117, 10826–10833. DOI: 10.1021/jp402300c.

[583] H. Weber, O. Hollóczki, A. S. Pensado, B. Kirchner, Side chain fluorination and anion effect on the structure of 1-butyl-3-methylimidazolium ionic liquids, *J. Chem. Phys.*, **2013**, 139, 084502. DOI: 10.1063/1.4818540.

[584] J. J. Tindale, C. Na, M. C. Jennings, P. J. Ragogna, Synthesis and characterization of fluorinated phosphonium ionic liquids, *Can. J. Chem.*, **2007**, 85, 660–667. DOI: 10.1139/v07-035.

[585] M. L. Ferreira, M. J. Pastoriza-Gallego, J. M. M. Araújo, J. N. Canongia Lopes, L. P. N. Rebelo, M. M. Piñeiro, K. Shimizu, A. B. Pereiro, Influence of Nanosegregation on the Phase Behavior of Fluorinated Ionic Liquids, *J. Phys. Chem. C.*, **2017**, 121, 5415–5427. DOI: 10.1021/acs.jpcc.7b00516.

[586] J. C. Bastos, S. F. Carvalho, T. Welton, J. N. Canongia Lopes, L. P. N. Rebelo, K. Shimizu, J. M. M. Araújo, A. B.

Pereiro, Design of task-specific fluorinated ionic liquids: nanosegregation versus hydrogen-bonding ability in aqueous solutions, *Chem. Commun.*, **2018**, 54, 3524–3527. DOI: 10.1039/C8CC00361K.

[587] Y. Shen, D. F. Kennedy, T. L. Greaves, A. Weerawardena, R. J. Mulder, N. Kirby, G. Song, C. J. Drummond, Protic ionic liquids with fluorous anions: physicochemical properties and self-assembly nanostructure, *Phys. Chem. Chem. Phys.*, **2012**, 14, 7981. DOI: 10.1039/c2cp40463j.

[588] F. Lo Celso, G. B. Appetecchi, C. J. Jafta, L. Gontrani, J. N. Canongia Lopes, A. Triolo, O. Russina, Nanoscale organization in the fluorinated room temperature ionic liquid: Tetraethyl ammonium (trifluoromethanesulfonyl)(nonafluorobutylsulfonyl)imide, *J. Chem. Phys.* DOI: 10.1063/1.5016236.

[589] F. Lo Celso, Y. Yoshida, R. Lombardo, C. Jafta, L. Gontrani, A. Triolo, O. Russina, Mesoscopic structural organization in fluorinated room temperature ionic liquids, *Comptes Rendus Chim.*, **2018**, 21, 757–770. DOI: 10.1016/j.crci.2018.02.001.

[590] T. L. Greaves, D. F. Kennedy, Y. Shen, A. Hawley, G. Song, C. J. Drummond, Fluorous protic ionic liquids exhibit discrete segregated nano-scale solvent domains and form new populations of nano-scale objects upon primary alcohol addition, *Phys. Chem. Chem. Phys.*, **2013**, 15, 7592–7598. DOI: 10.1039/c3cp44589e.

[591] A. M. Ferreira, P. D. O. Esteves, I. Boal-Palheiros, A. B. Pereiro, L. P. N. Rebelo, M. G. Freire, Enhanced tunability afforded by aqueous biphasic systems formed by fluorinated ionic liquids and carbohydrates, *Green Chem.*, **2016**, 18, 1070–1079. DOI: 10.1039/C5GC01610J.

[592] M. Alves, N. S. M. Vieira, L. P. N. Rebelo, J. M. M. Araújo, A. B. Pereiro, M. Archer, Fluorinated ionic liquids for protein drug delivery systems: Investigating their impact on the structure and function of lysozyme, *Int. J. Pharm.*, **2017**, 526, 309–320. DOI: 10.1016/j.ijpharm.2017.05.002.

[593] T. L. Merrigan, E. D. Bates, S. C. Dorman, J. H. Davis Jr., New fluorous ionic liquids function as surfactants in conventional room-temperature ionic liquids, *Chem. Commun.*, **2000**, 2051–2052. DOI: 10.1039/b005418f.

[594] N. S. M. Vieira, A. Luís, P. M. Reis, P. J. Carvalho, J. A. Lopes-da-Silva, J. M. S. S. Esperança, J. M. M. Araújo, L. P. N. Rebelo, M. G. Freire, A. B. Pereiro, Fluorination effects on the thermodynamic, thermophysical and surface properties of ionic liquids, *J. Chem. Thermodyn.*, **2016**, 97, 354–361. DOI: 10.1016/j.jct.2016.02.013.

[595] J. M. Breen, S. Olejarz, K. R. Seddon, Microwave Synthesis of Short-Chained Fluorinated Ionic Liquids and Their Surface Properties, *ACS Sustain. Chem. Eng.*, **2016**, 4, 387–391. DOI: 10.1021/acssuschemeng.5b01265.

[596] D. Almantariotis, A. S. Pensado, H. Q. N. Gunaratne, C. Hardacre, A. A. H. Pádua, J.-Y. Coxam, M. F. Costa Gomes, Influence of Fluorination on the Solubilities of Carbon Dioxide, Ethane, and Nitrogen in 1- n -Fluoro-alkyl-3-methylimidazolium Bis(n -fluoroalkylsulfonyl)amide Ionic Liquids, *J. Phys. Chem. B.*, **2017**, 121, 426–436. DOI: 10.1021/acs.jpcb.6b10301.

[597] A. M. A. Dias, M. Freire, J. A. P. Coutinho, I. M. Marrucho, Solubility of oxygen in liquid perfluorocarbons, *Fluid Phase Equilib.*, **2004**, 222–223, 325–330. DOI: 10.1016/j.fluid.2004.06.037.

[598] M. F. Costa Gomes, A. A. H. Pádua, Interactions of Carbon Dioxide with Liquid Fluorocarbons, *J. Phys. Chem. B.*, **2003**, 107, 14020–14024. DOI: 10.1021/jp0356564.

[599] M. J. Muldoon, S. N. V. K. Aki, J. L. Anderson, J. K. Dixon, J. F. Brennecke, Improving carbon dioxide solubility in ionic liquids, *J. Phys. Chem. B.*, **2007**, 111, 9001–9009. DOI: 10.1021/jp071897q.

[600] C. S. M. Kang, X. Zhang, D. R. MacFarlane, Synthesis and Physicochemical Properties of Fluorinated Ionic Liquids with High Nitrogen Gas Solubility, *J. Phys. Chem. C.*, **2018**, 122, 24550–24558. DOI: 10.1021/acs.jpcc.8b07752.

[601] S. Martinho, J. M. M. Araújo, L. P. N. Rebelo, A. B. Pereiro, I. M. Marrucho, (Liquid+liquid) equilibria of perfluorocarbons with fluorinated ionic liquids, *J. Chem. Thermodyn.*, **2013**, 64, 71–79. DOI: 10.1016/j.jct.2013.04.019.

[602] J. E. Bara, C. J. Gabriel, T. K. Carlisle, D. E. Camper, A. Finotello, D. L. Gin, R. D. Noble, Gas separations in fluoroalkyl-functionalized room-temperature ionic liquids using supported liquid membranes, *Chem. Eng. J.*, **2009**, 147, 43–50. DOI: 10.1016/j.cej.2008.11.021.

[603] A. B. Pereiro, L. C. Tomé, S. Martinho, L. P. N. Rebelo, I. M. Marrucho, Gas Permeation Properties of Fluorinated Ionic Liquids, *Ind. Eng. Chem. Res.*, **2013**, 52, 4994–5001. DOI: 10.1021/ie4002469.

[604] M. Honda, T. Iwamoto, T. Ohnogi, K.-K. Kunimoto, M. Segi, Synthesis of fluorous pyrrolidinium and piperidinium ionic liquids, *Tetrahedron Lett.*, **2017**, 58, 3191–3193. DOI: 10.1016/j.tetlet.2017.07.012.

[605] A. Tsurumaki, H. Ohno, Dissolution of oligo(tetrafluoroethylene) and preparation of poly(tetrafluoroethylene)-based composites by using fluorinated ionic liquids, *Chem. Commun.*, **2018**, 54, 409–412. DOI: 10.1039/C7CC08449H.

[606] J. J. Tindale, K. L. Mouland, P. J. Ragogna, Thiol appended, fluorinated phosphonium ionic liquids as covalent superhydrophobic coatings, *J. Mol. Liq.*, **2010**, 152, 14–18. DOI: 10.1016/j.molliq.2009.05.005.

[607] J. J. Tindale, P. J. Ragogna, Highly fluorinated phosphonium ionic liquids: novel media for the generation of superhydrophobic coatings, *Chem. Commun.*, **2009**, 1831–1833. DOI: 10.1039/b821174d.

[608] T. Alpers, M. Schmidtmann, T. W. T. Muesmann, O. Temme, J. Christoffers, Perfluorinated Pyridinium and Imidazolium Ionic Liquids, *European J. Org. Chem.*, **2017**, 2017, 4283–4290. DOI: 10.1002/ejoc.201700717.

[609] I. Newtom, *Philosophiae Naturalis Principia Mathematica*, Royal Society, London, **1687**.

[610] K. R. Harris, Scaling the transport properties of molecular and ionic liquids, *J. Mol. Liq.*, **2016**, 222, 520–534. DOI: 10.1016/j.molliq.2016.07.029.

[611] R. L. Gardas, J. A. P. Coutinho, Group contribution methods for the prediction of thermophysical and transport properties of ionic liquids, *AIChE J.*, **2009**, 55, 1274–1290. DOI: 10.1002/aic.11737.

[612] A. Noda, K. Hayamizu, M. Watanabe, Pulsed-Gradient Spin−Echo 1 H and 19 F NMR Ionic Diffusion Coefficient, Viscosity, and Ionic Conductivity of Non-Chloroaluminate Room-Temperature Ionic Liquids, *J. Phys. Chem. B.*, **2001**, 105, 4603–4610. DOI: 10.1021/jp004132q.

[613] K. R. Harris, M. Kanakubo, Self-diffusion, velocity cross-correlation, distinct diffusion and resistance coefficients of the ionic liquid [BMIM][Tf 2 N] at high pressure, *Phys. Chem. Chem. Phys.*, **2015**, 17, 23977–23993. DOI: 10.1039/C5CP04277A.

[614] M. A. González, B. Aoun, D. L. Price, Z. Izaola, M. Russina, J. Ollivier, M.-L. Saboungi, in *AIP Conference Proceedings*, **2018**, vol. 1969, p. 020002. DOI: 10.1063/1.5039291.

[615] T. Burankova, E. Reichert, V. Fossog, R. Hempelmann, J. P. Embs, The dynamics of cations in pyridinium-based ionic liquids by means of quasielastic- and inelastic neutron scattering, *J. Mol. Liq.*, **2014**, 192, 199–207. DOI: 10.1016/j.molliq.2014.03.007.

[616] K. R. Harris, M. Kanakubo, Revised and Extended Values for Self-Diffusion Coefficients of 1-Alkyl-3-methylimidazolium Tetrafluoroborates and Hexafluorophosphates: Relations between the Transport Properties, *J. Phys. Chem. B.*, **2016**, 120, 12937–12949. DOI: 10.1021/acs.jpcb.6b10341.

[617] K. R. Harris, M. Kanakubo, Self-Diffusion Coefficients and Related Transport Properties for a Number of Fragile Ionic Liquids, *J. Chem. Eng. Data.*, **2016**, 61, 2399–2411. DOI: 10.1021/acs.jced.6b00021.

[618] H. A. Every, A. G. Bishop, D. R. MacFarlane, G. Orädd, M. Forsyth, Transport properties in a family of dialkylimidazolium ionic liquids, *Phys. Chem. Chem. Phys.*, **2004**, 6, 1758–1765. DOI: 10.1039/B315813F.

[619] M. Gouverneur, J. Kopp, L. van Wüllen, M. Schönhoff, Direct determination of ionic transference numbers in ionic liquids by electrophoretic NMR, *Phys. Chem. Chem. Phys.*, **2015**, 17, 30680–30686. DOI: 10.1039/C5CP05753A.

[620] K. Oldiges, D. Diddens, M. Ebrahiminia, J. B. Hooper, I. Cekic-Laskovic, A. Heuer, D. Bedrov, M. Winter, G. Brunklaus, Understanding transport mechanisms in ionic liquid/carbonate solvent electrolyte blends, *Phys. Chem. Chem. Phys.*, **2018**, 20, 16579–16591. DOI: 10.1039/C8CP01485J.

[621] S. Seki, K. Hayamizu, S. Tsuzuki, K. Fujii, Y. Umebayashi, T. Mitsugi, T. Kobayashi, Y. Ohno, Y. Kobayashi, Y. Mita, H. Miyashiro, S. Ishiguro, Relationships between center atom species (N, P) and ionic conductivity, viscosity, density, self-diffusion coefficient of quaternary cation room-temperature ionic liquids, *Phys. Chem. Chem. Phys.*, **2009**, 11, 3509. DOI: 10.1039/b820343a.

[622] K. R. Harris, Can the Transport Properties of Molten Salts and Ionic Liquids Be Used To Determine Ion Association?, *J. Phys. Chem. B.*, **2016**, 120, 12135–12147. DOI: 10.1021/acs.jpcb.6b08381.

[623] K. Ueno, H. Tokuda, M. Watanabe, Ionicity in ionic liquids: correlation with ionic structure and physicochemical properties., *Phys. Chem. Chem. Phys.*, **2010**, 12, 1649–58. DOI: 10.1039/b921462n.

[624] C. Schreiner, S. Zugmann, R. Hartl, H. J. Gores, Temperature Dependence of Viscosity and Specific Conductivity of Fluoroborate-Based Ionic Liquids in Light of the Fractional Walden Rule and Angell's Fragility Concept †, *J. Chem. Eng. Data.*, **2010**, 55, 4372–4377. DOI: 10.1021/je1005505.

[625] D. R. MacFarlane, M. Forsyth, E. I. Izgorodina, A. P. Abbott, G. Annat, K. Fraser, On the concept of ionicity in ionic liquids, *Phys. Chem. Chem. Phys.*, **2009**, 11, 4962. DOI: 10.1039/b900201d.

[626] T. Welton, Ionic liquids: a brief history, *Biophys. Rev.*, **2018**, 10, 691–706. DOI: 10.1007/s12551-018-0419-2.

[627] B. Kirchner, F. Malberg, D. S. Firaha, O. Hollóczki, Ion pairing in ionic liquids, *J. Phys. Condens. Matter.*, **2015**, 27, 463002. DOI: 10.1088/0953-8984/27/46/463002.

[628] G. Feng, M. Chen, S. Bi, Z. A. H. Goodwin, E. B. Postnikov, M. Urbakh, A. A. Kornyshev, Kinetics of Ion Transport in Ionic Liquids: Two Dynamical Diffusion States, *arXiv Prepr. arXiv1805.00697*.

[629] O. Hollóczki, F. Malberg, T. Welton, B. Kirchner, On the origin of ionicity in ionic liquids. Ion pairing versus charge transfer, *Phys. Chem. Chem. Phys.*, **2014**, 16, 16880–16890. DOI: 10.1039/C4CP01177E.

[630] A. B. Patil, B. M. Bhanage, Assessing ionicity of protic ionic liquids by far IR spectroscopy, *J. Mol. Liq.*, **2018**, 252, 180–183. DOI: 10.1016/j.molliq.2017.12.131.

[631] S. K. Davidowski, F. Thompson, W. Huang, M. Hasani, S. A. Amin, C. A. Angell, J. L. Yarger, NMR Characterization of Ionicity and Transport Properties for a Series of Diethylmethylamine Based Protic Ionic Liquids, *J. Phys. Chem. B.*, **2016**, 120, 4279–4285. DOI: 10.1021/acs.jpcb.6b01203.

[632] S. E. Goodwin, D. E. Smith, J. S. Gibson, R. G. Jones, D. A. Walsh, Electroanalysis of Neutral Precursors in Protic Ionic Liquids and Synthesis of High-Ionicity Ionic Liquids, *Langmuir.*, **2017**, 33, 8436–8446. DOI: 10.1021/acs.langmuir.7b02294.

[633] K. R. Harris, T. Makino, M. Kanakubo, Viscosity scaling of the self-diffusion and velocity cross-correlation coefficients of two functionalised ionic liquids and of their non-functionalized analogues, *Phys. Chem. Chem. Phys.*, **2014**, 16, 9161–9170. DOI: 10.1039/C4CP00435C.

[634] H. K. Kashyap, H. V. R. Annapureddy, F. O. Raineri, C. J. Margulis, How Is Charge Transport Different in Ionic Liquids and Electrolyte Solutions?, *J. Phys. Chem. B.*, **2011**, 115, 13212–13221. DOI: 10.1021/jp204182c.

[635] H. J. Schoenert, Evaluation of velocity correlation coefficients from experimental transport data in electrolytic systems, *J. Phys. Chem.*, **1984**, 88, 3359–3363. DOI: 10.1021/j150659a045.

[636] T. Rüther, M. Kanakubo, A. S. Best, K. R. Harris, The importance of transport property studies for battery

electrolytes: revisiting the transport properties of lithium–N-methyl-N-propylpyrrolidinium bis(fluorosulfonyl)imide mixtures, *Phys. Chem. Chem. Phys.*, **2017**, 19, 10527–10542. DOI: 10.1039/C7CP01272A.

[637] D. W. McCall, D. C. Douglass, Diffusion in binary solutions, *J. Phys. Chem.*, **1967**, 71, 987–997. DOI: 10.1021/j100863a035.

[638] H. G. Hertz, K. R. Harris, R. Mills, L. A. Woolf, Velocity Correlations in Aqueous Electrolyte Solutions from Diffusion, Conductance, and Transference Data. Part 2, Applications to Concentrated Solutions of 1-1 Electrolytes, *Berichte der Bunsengesellschaft für Phys. Chemie.*, **1977**, 81, 664–670. DOI: 10.1002/bbpc.19770810708.

[639] R. W. Laity, INTERIONIC FRICTION COEFFICIENTS IN MOLTEN SALTS, *Ann. N. Y. Acad. Sci.*, **2006**, 79, 997–1022. DOI: 10.1111/j.1749-6632.1960.tb42770.x.

[640] K. R. Harris, M. Kanakubo, D. Kodama, T. Makino, Y. Mizuguchi, M. Watanabe, T. Watanabe, Temperature and Density Dependence of the Transport Properties of the Ionic Liquid Triethylpentylphosphonium Bis(trifluoromethanesulfonyl)amide, [P 222,5][Tf 2 N], *J. Chem. Eng. Data.*, **2018**, 63, 2015–2027. DOI: 10.1021/acs.jced.8b00011.

4. Scientific contributions

4.1. Publications of Daniel Rauber in peer-reviewed journals

(1) Viktor Misuk, Andreas Mai, Konstantinos Giannopoulos, Dominik Karl, Julian Heinrich, Daniel Rauber, Holger Löwe, Palladium-catalyzed carbon-carbon cross-coupling reactions in thermomorphous double emulsions, *J. Flow Chem.*, **2015**, 5 (1), 43-47. DOI: 10.1556/JFC-D-14-00040.

(2) Viktor Misuk, Andreas Mai, Zhao Yunning, Julian Heinrich, Daniel Rauber, Konstantinos Giannopoulos, Holger Löwe, Active mixing inside double emulsion segments in continuous flow, *J. Flow Chem.*, **2015**, 5 (2), 101-109. DOI: 10.1556/1846.2015.00011.

(3) Daniel Rauber, Florian Heib, Michael Schmitt, Rolf Hempelmann, Influence of perfluoroalkyl-chains on the surface properties of 1-methylimidazolium bis(trifluoromethanesulfonyl)imide ionic liquids, *J. Mol. Liq.*, **2016**, 216, 246-258. DOI: 10.1016/j.molliq.2016.01.011.

(4) Tobias K. F. Dier, Daniel Rauber, Johann Jauch, Rolf Hempelmann, Dietrich A. Volmer, Novel Mixed-Mode Stationary Phases for Chromatographic Separation of Complex Mixtures of Decomposed Lignin, *ChemistrySelect*, **2017**, 2 (2), 779-786. DOI: 10.1002/slct.201601673.

(5) Frederik Philippi, Daniel Rauber, Josef Zapp, Rolf Hempelmann, Transport properties and ionicity of phosphonium ionic liquids, *PCCP*, **2017**, 19, 23015-23023. DOI: 10.1039/C7CP04552B.

(6) Daniel Rauber, Peng Zhang, Volker Huch, Tobias Kraus, Rolf Hempelmann, Lamellar structures in fluorinated phosphonium ionic liquids: the roles of fluorination and chain length, *PCCP*, **2017**, 19, 27251-27258. DOI: 10.1039/C7CP04814A.

(7) Daniel Rauber, Frederik Philippi, Rolf Hempelmann, Catalyst retention utilizing a novel fluorinated phosphonium ionic liquid in Heck reactions under fluorous biphasic conditions, *J. Fluor. Chem.*, **2017**, 299, 115-122. DOI: 10.1016/j.jfluchem.2017.06.014.

(8) Daniel Rauber, Florian Heib, Tobias Dier, Dietrich A. Volmer, Michael Schmitt, Rolf Hempelmann, On the physicochemical and surface properties of 1-alkyl 3-methylimidazolium bis(nonafluorobutylsulfonyl ionic liquids, *Colloids Surf. A*, **2017**, 529, 169-177. DOI: 10.1016/j.colsurfa.2017.05.092.

(9) Tobias K. F. Dier, Daniel Rauber, Dan Durneata, Rolf Hempelmann, Dietrich A. Volmer, Sustainable Electrochemical Depolymerization of Lignin in Reusable Ionic Liquid, *Sci. Rep.*, **2017**, 7, 5041, 1-12. DOI: 10.1038/s41598-017-05316-x.

(10) Daniel Rauber, Tobias K. F. Dier, Dietrich A. Volmer, Rolf Hempelmann, Electrochemical Lignin Degradation in Ionic Liquids on Ternary Mixed Metal Electrode, Z. Phys. Chem., **2017**, 232 (2), 189-208. DOI: 10.1515/zpch-2017-0951.

(11) Daniel Rauber, Florian Heib, Michael Schmitt, Rolf Hempelmann, Trioctylphosphonium room temperature ionic liquids with perfluorinated groups – Physical properties and surface behavior in comparison with the nonfluorinated analogues, *Colloids Surf. A*, **2018**, 537, 116-125. DOI: 10.1016/j.colsurfa.2017.10.013.

(12) Daniel Rauber, Frederik Philippi, Josef Zapp, Guido Kickelbick, Harald Natter, Rolf Hempelmann, Transport properties of protic and aprotic guanidinium ionic liquids, *RSC Adv.*, **2018**, 8, 41639-41650. DOI: 10.1039/C8RA07412G.

(13) Tatsiana Burankova, Juan F. M. Cardozo, Daniel Rauber, Andrew Wildes, Jan P. Embs, Linking Structure to Dynamics in Protic Ionic Liquids: A Neutron Scattering Study of Correlated and Single-Particle Motions, *Sci. Rep.*, **2018**, 8, 16400. DOI: 10.1038/s41598-018-34481-w.

(14) Frederik Philippi, Daniel Rauber, Josef Zapp, Carsten Präsang, David Scheschkewitz, Rolf Hempelmann, Multiple Ether-Functionalized Phosphonium Ionic Liquids as Highly Fluid Electrolytes, *ChemPhysChem*, **2019**, *in press*. DOI: 10.1002/cphc.201800939.

(15) Frederik Philippi, Daniel Rauber, Michael Springborg, Rolf Hempelmann, Density Functional Theory Descriptors for Ionic Liquids and the Charge Transfer Interpretation of the Haven Ratio, *J. Phys. Chem. A*, **2019**, *in press*. DOI: 10.1021/acs.jpca.8b10827.

4.2. Contribution of Daniel Rauber to scientific conferences

(1) Viktor Misuk, *Andreas* Mai, Daniel Rauber, Konstantin Giannopoulos, Holger Löwe, C-C cross coupling reactions in thermomorphous double emulsions, *13th International Conference on Microreaction Technology IMRET*, **2014**.

(2) Daniel Rauber, Tobias K. F. Dier, Dietrich A. Volmer, Rolf Hempelmann, Electrochemical cleavage of lignin in recyclable ionic liquids for production of renewable aromatic compounds, *Jahrestagung der GdCH-Fachgruppe Nachhaltige Chemie*, **2016**.

(3) Daniel Rauber, Frederik Philippi, Josef Zapp, Rolf Hempelmann, Ionicity of ionic liquids determined by PFGSTE NMR, *116th General Assembly of the German Bunsen Society for Physical Chemistry*, **2017**.

(4) Daniel Rauber, Frederik Philippi, Harald Natter, Rolf Hempelmann, Transport Properties and Ionicity of Protic and Aprotic Guanidinium Ionic Liquids. *Electrochemistry 2018 - Electrochemical Surface Science: From Fundamentals to Application*, **2018**.

(5) Rolf Hempelmann, Daniel Rauber, Johannes Huwer, Ionische Flüssigkeiten in Experimenten für Schule und Schülerlabor, *Jahrestagung der GdCH-Fachgruppe Nachhaltige Chemie*, **2018**.

(6) Frederik Philippi, Daniel Rauber, Rolf Hempelmann, Tuning Phosphonium Ionic Liquids with ether chains, *27th EuCheMS Conference on Molten Salts and Ionic Liquids EuCheMSIL*, **2018**.

(7) Daniel Rauber, Frederik Philippi, Rolf Hempelmann, Transport properties and ionicity models of protic and aprotic tetramethyl-guanidinium ionic liquids, *27th EuCheMS Conference on Molten Salts and Ionic Liquids EuCheMSIL*, **2018**.

(8) Frederik Philippi, Daniel Rauber, Rolf Hempelmann, Pushing Fluidity to its Limits: Multiple Ether Functionalisation in Phosphonium Ionic Liquids, *Molten Salts Discussion Group Christmas Research Meeting*, **2018**.

4.3. Other publications

(1) Daniel Rauber, Johannes Huwer, Harald Natter, Rolf Hempelmann, *Nachhaltige Chemie mit Ionischen Flüssigkeitenin Experimenten für Schule und Schülerlabor*, Lernort Labor, Berlin **2018**, 184 pages. ISBN: 978-3-946709-04-6.